AD_____

Award Number: DAMD17-99-1-9571

TITLE: Molecular Mechanisms of Soft Tissue Regeneration and Bone Formation in Mice: Implications in Fracture Repair and Wound Healing in Humans

PRINCIPAL INVESTIGATOR: David J. Baylink, M.D.

CONTRACTING ORGANIZATION: Loma Linda Veterans Association for Research and Education
Loma Linda, California 92357

REPORT DATE: October 2000

TYPE OF REPORT: Annual

PREPARED FOR: U.S. Army Medical Research and Materiel Command
Fort Detrick, Maryland 21702-5012

REPORT DOCUMENTATION PAGE

Form Approved
OMB No. 074-0188

1. AGENCY USE ONLY (Leave blank)	2. REPORT DATE	3. REPORT TYPE AND DATES COVERED
	October 2000	Annual (1 Oct 99 - 30 Sep 00)

4. TITLE AND SUBTITLE
Molecular Mechanisms of Soft Tissue Regeneration and Bone Formation in Mice: Implications in Fracture Repair and Wound Healing in Humans

5. FUNDING NUMBERS
DAMD17-99-1-9571

6. AUTHOR(S)
David J. Baylink, M.D.

7. PERFORMING ORGANIZATION NAME(S) AND ADDRESS(ES)
Loma Linda Veterans Association for Research and Education
Loma Linda, California 92357

E-MAIL: baylid@lom.med.va.gov

8. PERFORMING ORGANIZATION REPORT NUMBER

9. SPONSORING / MONITORING AGENCY NAME(S) AND ADDRESS(ES)
U.S. Army Medical Research and Materiel Command
Fort Detrick, Maryland 21702-5012

10. SPONSORING / MONITORING AGENCY REPORT NUMBER

11. SUPPLEMENTARY NOTES

12a. DISTRIBUTION / AVAILABILITY STATEMENT
Approved for public release; Distribution unlimited

12b. DISTRIBUTION CODE

13. ABSTRACT *(Maximum 200 Words)*

The primary goal of the proposed work is to identify genes which play an anabolic role in bone and soft tissue function and to clarify the function of these genes. Three hypotheses have been proposed: 1) The high bone density gene in chromosome 1 in our CAST/B6 congenic mice can be cloned; 2) Genes that regulate soft- and hard-tissue regeneration can be identified by using appropriate mouse strains that exhibit differences in regeneration; and 3) ENU mutagenesis, applied to our mouse model, will lead to the identity of genes that regulate soft and hard tissue function. During the first twelve months of the funding period, we have proposed several specific objectives for each of the above-mentioned hypotheses. As disclosed in the progress report, we have successfully accomplished all of the specific objectives. Our work during the first year of the funding period has resulted in four manuscripts in press, four submitted manuscripts, one manuscript in preparation, and four abstracts. We believe that the successful accomplishment of the proposed studies will provide a better understanding of the molecular mechanisms involved in hard- and soft-tissue regeneration and will provide a framework for future development of therapies for hard and soft tissue injuries.

14. SUBJECT TERMS Soft- and hard-tissue regeneration; bone density; gene function; cDNA microarray analysis; congenic mice; QTL analysis; mouse genetics; musculoskeletal genes.

15. NUMBER OF PAGES
280

16. PRICE CODE

17. SECURITY CLASSIFICATION OF REPORT	18. SECURITY CLASSIFICATION OF THIS PAGE	19. SECURITY CLASSIFICATION OF ABSTRACT	20. LIMITATION OF ABSTRACT
Unclassified	Unclassified	Unclassified	Unlimited

NSN 7540-01-280-5500

Standard Form 298 (Rev. 2-89)
Prescribed by ANSI Std. Z39-18
298-102

Table of Contents

General Introduction

The primary goal of the project funded by the U.S. Army is to identify genes which play an anabolic role in bone tissue and soft tissue function, particularly during regeneration, and to clarify the function of these genes. To accomplish this goal, we have proposed 3 technical objectives during the first funding period. These 3 technical objectives are as follows:

1. Studies proposed in the first technical objective are designed to employ state-of-the-art molecular biotechniques to identify the gene located in mouse chromosome 1 that is involved in the regulation of peak bone density.

2. Our second technical objective has been focused on identifying the key genes that are involved in soft tissue repair/regeneration using inbred strains ofmice as model systems.

3. The goal of our third technical objective is to identify and characterize novel genes, using ENU mutagenesis techniques and to elucidate the function of known genes that play a key role in the metabolism of bone and soft tissue.

Our goals for the first 12-month funding period for each of the technical objectives, as well as our progress for each of the technical objectives, are described below. The progress report for each technical objective is organized according to the outline provided by the office of the U.S. Army Medical Research and Materiel Command.

In addition to completing all of the technical objectives required for the grant period, we are reporting progress on additional objectives accomplished above and beyond those contracted for. These are identified as "Additional Progress" in the first two objectives.

A. TECHNICAL OBJECTIVE 1 - To clone the gene regulating peak bone density on chromosome 1 in the CAST/B6 congenic mice.

1. Introduction

Our ultimate goal is to clone the gene regulating the peak bone density on chromosome 1 in the CAST/B6 congenic mice by the application of cDNA microarray followed by positional candidate gene functional studies. In the first year, we proposed to identify differentially expressed genes by applying and analysis of commercial microarray in order to identify potential candidate gene involved in regulation of peak BMD between B6 and CAST mice. To accomplish technical objective 1, we have proposed the following specific objectives for the first 12 months of this funding period.

1) Prepare total bone RNA from congenic and B6 mice and perform microarray analysis through a commercial facility.

2) Collect mouse cDNA/EST clones, which are differentially expressed in the commercial microarray assay and distinguish between those clones that are found inside and outside of the congenic region.

3) Identify and collect the cDNA/EST clones from the human syntenic region, 1q21-1q23.

4) Perform PCR amplification and purification of the cDNA clones.

5) Perform two-color simultaneous hybridization.

6) Perform temporal and spatial expression analysis to eliminate some of the differentially expressed genes.

7) Further narrowing down the QTL region by backcrossing the congenic mouse line with the recurrent parent mice.

We have now accomplished all of the above specific objectives. Our progress in each of the specific objectives is given below. In addition, we have performed additional studies on the development of BAC contig that covers the QTL region of chromosome 1 locus (page 9).

2. Body

a. Specific Objective 1: Prepare total bone RNA from congenic and B6 mice and perform microarray analysis through a commercial facility.

Microarray is a recently developed technology with high sensitivity to detect the levels of gene expression. cDNA microarray uniquely allows us to simultaneously screen thousands of genes for their differential expression. We opted to use commercial microarray in our initial studies because it allows us to rapidly select candidate genes within our QTL region. If we were to prepare our own array chips, there would have been a substantial delay in our research on this project. In our study, we used Incyte Genomics (Fremont, CA) for several reasons, including the cost and turnaround time. To accomplish our specific objective, we have conducted several related studies in order to optimize the microarray experiment. These studies include the determination of optimal time at which the genes that control the bone density are expressed; preparation of sufficient high quality RNA from the bone of the mice; and analysis of the results of commercial microarray experiment from Incyte Genomics. Given below are our accomplishments in these studies.

1) Evaluation of the Optimal Age of the Mice Used for Microarray Analysis. In order to identify the genes that control bone density by analysis of their expression with microarray technology, we need to take samples at the time when the genes that lead to the high bone density in the congenic mice are expressed. We had previously found that the bone density of congenic mice is significantly different from B6 mice at the age of 16 weeks. Accordingly, we expect differences in the expression of candidate gene(s) regulating bone density to occur either throughout the 16 week-period or a few weeks before the maximal difference in peak BMD is seen. In order to determine the optimal time for our gene expression study using microarray technology, we measured the bone density of 10- and 16-week old congenic mice and compared it to that of the B6 mice. Bone density of femurs was measured by peripheral quantitative computerized tomography (pQCT) with a Stratec XCT 960M (Norland Medical Systems, Ft. Atkinson, WI).

As shown in Table 1, neither the total bone density nor the total mineral content was significantly different between congenic and B6 mice at the age of 10 weeks. However, at 16 weeks, both the total bone density and total mineral content of congenic mice were significantly higher than that of B6 mice. This result indicated that the high bone density of the congenic mice was mainly achieved a few weeks before the age of 16 weeks. We, therefore, speculate that the genes that control the bone density differences between congenic and B6 mice are expressed during the time between 10 and 16 weeks. Therefore, we used the mice at 14 weeks of age for our microarray experiment.

2) Isolation of High Quality RNA from the Femurs of Mice for Microarray Experiment. The preparation of high-quality RNA (total RNA and messenger RNA) is the key to conduct microarray analysis. In order to correctly compare the expression of genes in congenic mice with that of the B6 mice, RNA at the same concentration and the same quality are needed from both the congenic and the B6. However, the extraction of high-quality RNA from bone has proven to be extremely difficult in the past. There is no published protocol

available for the extraction of RNA from the mouse femur. We, therefore, first developed an RNA extraction procedure for mouse femur using the Trizol reagent, which is a modification of the protocol from Life Technologies (Grand Island, NY). In our procedure, femurs were dissected from each mouse on ice within two minutes and immediately put in liquid nitrogen. Subsequently, femurs and Trizol reagent were ground together in a 6750 Freezer Mill machine from SPEX Centiprep, Inc. (Metuchen, NJ) and the RNA was purified twice with chloroform.

Table 1. Comparison of Bone Parameters Between B6 and the Congenic Strain

Parameter	1T Congenic	B6	Age (weeks)
Total content (mg/slice)	27.1±1.1	27.9±3.7	10
	29.0±1.1	23.6±3.7	16
Total density (mg/cm^3)	.617±.04	.588±.08	10
	.661±.04	.615±.08	16
Total volume (mm^3)	44.0±1.1	47.6±1.8	10
	43.9±1.1	38.3±1.8	16
Length (mm)	14.96±0.02	14.99±0.04	10
	15.17±0.17	14.85±0.42	16

The concentration and purity of the total RNA were checked by measuring 260/280 absorption ratio using a Spectronic Genesys spectrophotometer from Spectronic Instruments (Rochester, NY). Our measurement showed that the 260/280 absorption ratio of the total RNA was between 1.8 and 2, which indicates the high purity of the RNA. The quality of the total RNA was checked by electrophoresis on 1% agarose gel. As shown in Figure 1, the 28s and 18s ribosomal RNA are well preserved among the total RNA. We, therefore, conclude that our RNA was not degraded. mRNA was purified from the total RNA and was quantified on the Spectronic Genesys spectrophotometer. The 260/280 ratio of the mRNA is 1.8, which is exceeds the quality needed for microarray analysis.

Figure 1: Quality of the RNA checked on 1% agarose gel. Total RNA extracted from bone with Trizol reagent. Agarose gel was prepared with MOP buffer. Five μl of each RNA (about 1-5 μg) sample in formaldehyde loading buffer was loaded on each lane. RNA were separated by running at 100 voltage for 1.5 hours. The gel then was stained with Ethedium bromide and photographed under UV light. Arrows on the left point to the 28s and 18s ribosomal RNAs, indicating the intact of the RNA. The arrow on the right points to the band of 1353 bp of the standard marker.

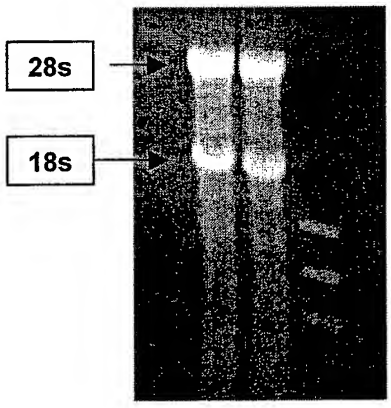

3) Microarray Hybridization. We used the Incyte Genomics commercial service for our probe labeling and microarray hybridization. We used the mRNA at the concentration of 50ng/μl for microarray hybridization. Samples from the congenic and B6 mice were sent to Incyte Genomics for microarray hybridization, where mRNA from congenic and B6 mice were labeled with Cy5 and Cy3, respectively, and hybridized onto the same microarray set, the Mouse GEM1 microarray. Detailed information of these clones and the hybridization procedure can be obtained from www.genomesystems.com.

4) Analysis of Gene Expression Data. The Mouse GEM1 microarray chip from Incyte Genomics contains 8,739 genes and ESTs selected from the NCBI's UniGene database. Incyte Genomics uses various measures to ensure that the total variability in measurement is limited to less than 15%. The major components of variability in differential expression results are from microarray scan setup and GEM microarray lot; each accounted for less than 5% of the total variance in differential expression data. As shown in Table 2, the relative signal intensity of empty wells can reach up to 200, while the spots containing 0.2X SSC (a mixture of NaCl, sodium citrate, and NaOH) buffer have a level between 28-48. In our study, we consider the samples that have a signal level higher than 800 as the valuable expression data for analysis. It is four times higher than that of the maximum value of the empty wells and ten times higher than that of the SSC buffer controls. Therefore, we feel confident that the result represents the real difference of gene expression between congenic and B6 mice.

Table 2. Variation of Expression Levels of Genes and ESTs in the B6

Full Name / No. of Genes	Expression Signal Level*
Positive control #1, 4 replicates	1488-2041
Positive control #2, 4 replicates	5555-8306
Positive control #3, 4 replicates	39465-48791
Negative control #1, 8 replicates, 0.2X SSC	28-48
Empty controls, 15 replicates	55-205
Positive control #4, 24 replicates	13631-29590
Mouse genes and ESTs: 2,736	<800
Mouse genes and ESTs: 5998	>800
Mouse genes and ESTs: 407	>5000
Mouse genes and ESTs: 93	>10,000

*The level of expression of a gene is measured by the relative intensity units of the signal level read by the scanner for the Cy3 channel.

We have found that 5,998 out of all 8,724 genes and ESTs have the expression levels that are higher than 800. By this criterion, about 75% of total genes are expressed in the femurs. Among these 5,998 genes and ESTs, most of them (5,633) have signal levels between 800 and 5000. Only a few of them (93) reached very high levels.

Among the 93 highly-expressed genes and ESTs, 27 are ESTs with neither known function nor similarity to known genes. The remaining 66 are genes or ESTs with similarity to known genes (see Appendix 1-1). As of July 25, 2000, literature searches from PubMed have produced a list of 30 genes with known functions related to bone or skeletal development. Thus, our microarray analysis data revealed that two-thirds of genes that are highly expressed in bone are either not being studied for their expression in the bone or have not been treated as the important genes in skeletal development.

Among the highly expressed genes, we found that most of them are structural (e.g., procollagen, type I, α1; hemoglobin-α, adult chain 1; and H3 histone, family 3A) and housekeeping genes (e.g., replication protein A2 eukaryotic translation elongation factor 1 α1; nuclear receptor binding factor 1). However, major growth factors are not among these highly expressed genes. Some of the important genes in bone, such as the bone morphogenetic protein (BMP), calcium binding protein, and insulin-like growth factor 1, have moderate expression levels. Their fluorescence absorption levels are around 1000 (see Appendix 1-1). It is quite common that some regulatory genes do not necessarily have a very high level of expression. Nevertheless, the genes that produce the most products during bone development are the important ones.

b. Specific Objective 2: Collect mouse cDNA/EST clones, which are differentially expressed in the commercial microarray assay, and distinguish between those clones that are found inside and outside of the congenic region.

To accomplish this specific objective, we need not only identify the cDNA/ESTs that are differentially expressed between congenic and B6 mice but, also, compare the genes with the current genetic map to locate the genes that are within the QTL region.

1) Comparison of Gene Expression Between Femurs of Congenic and B6 Mice. The expression patterns of most of the genes between congenic and B6 mice are similar. The difference in expression of the majority of genes (8,007) between these two strains is within the +1.5 to –1.5 folds. Among them, 254 genes and ESTs showed no detectable level of difference between these two strains. The expression levels of a total of 104 genes and ESTs have two-fold or higher difference between B6 and congenic mice. Two genes that exhibit the largest difference between B6 and congenic strains are the procollagen, type I, α1 (B6 vs Congenic: +3-fold) and an EST (B6 vs Congenic: -4.4-fold). Among these 104 genes and ESTs, most of them are expressed at moderate levels, with light intensity around 1,000, while twelve have an expression level higher than 5,000. Seventy-five of these differently expressed genes are ESTs that do not have a known function. Only 40 are known genes or ESTs with similar gene sequences (see Appendix 1-1).

There is no significant difference in expression levels of major growth factors that regulate bone formation between the two strains. Among them, transforming growth factor (TGF)-β is known as an important growth regulator and modulator in bone. BMPs, members of the TGF-β superfamily, are known to regulate proliferation, differentiation, and apoptosis of osteoblasts during bone development. Insulin-like growth factor-1 (IGF-1) and parathyroid hormone (PTH) receptor also play an important role in the regulation of bone formation.

2) Expression Levels of cDNA and ESTs Within the QTL Region. From the list of genes in the mouse genome database (www.rodentia.com/wmc/index.html), publications (1,2), and current available mouse genome sequences (www.ncbi.nlm.nih.gov/genome/seq/MmHome.html), we identified 18 genes and ESTs in the QTL region (Table 3). Among them, four candidates that are expressed differently between congenic and B6 are the CRP gene and three ESTs (AA184040, AA209869, AA437635).

CRP, the pretaxin related C-reactive protein, is located on chromosome 1, at the position of 94.2 cM. CRP has been reported as the protein produced by inflammatory response. We found that the RNA expression level in the congenic is two-fold higher than that of the B6. The other three ESTs have no reported function. They were matched to the genomic sequences in the QTL region. These candidates were further analyzed as described in Specific Objectives 5 and 6.

c. Specific Objective 3: Identify and collect the cDNA/EST clones from the human syntenic region, 1q21-1q23.

The QTL region of the mouse is homologous to the region of human 1q21-1q23, to which several homologous genes and loci have been mapped (www.ncbi.nlm.nih.gov/Homology). Incidentally, a QTL locus for bone density has also been located on the human 1q21-23 region (3), suggesting the possibility of homologous genes between humans and mice. We, therefore, examined the human 1q21-1q23 region to search for possible candidate genes.

1) ESTs from Human 1q21-1q23 Region. Because of the known syntenic relationship between these two regions, we found that most of the genes in the human 1q21-1q23 region have been mapped to mouse chromosome 1. Table 4 lists several ESTs which have been reported on the human homologous region and have been localized on the BAC clones of the mouse genome (1,2).

Table 3. Expression Levels of Genes Within the QTL Region

Gene Symbol	Full Name	Ratio B6/Congenic	B6 Expression Signal
Fcerg	Fc receptor IgE gamma	1.1	1592
Nhlhl	Nescient helix loop helix 1	1?	266
Atpla2	ATPase Na+/K+ transporting alpha-1	1.2	5057
Crp	C-reactive protein pretaxin related	-2.3	1341
ifi203	interferon activated gene 203 {IMAGE:620541}	1.1	862
ifi203	interferon activated gene 203 {IMAGE:618572}	1.4	2322
Olfr16	Olfactory receptor 16	0	145
Sap	Serum Amuloid P-component	-1.2	657
Pxf	Peroxisomal farnesylated protein	-1.2	2700
PLKr	Pyruvate kinase liver	1.2	2040
Tyro10	(Ntrkr3) neurotrophic tyrosine kinase	1.3	806
Dty	Duffy (promiscuous chemokine	1.1	667
Care2	nuclear receptor subfamily 1, group I, member 3	1	1342
MPZ	peripheral myelin protein	1.3	5417
Rxrg	retinoid X receptor gamma	1.2	1772
AA184040	EST	-2.9	1059
AA209869	EST	-3.3	2119
AA437635	EST	-3.9	1688

Table 4. Probes from Human Syntenic Region

Human ESTs	Mouse BAC clones containing the ESTs
ESTM33	m12-116*
ESTM32	p22-9, g15-16
ESTM28	h7-106
ESTM35	e5-132
ESTM38	j18-172
ESTM36	h7-106, c12-126
ESTM47	a19-191

*All BAC clones are from the RPCI-23 mouse BAC library from Roswell Park Cancer Institute. Labeling for the clones is in the order of column-row-plate #. Accordingly, a clone of m13-101 is from column M, row 13, on plate 101.

2) BAC Clones that Contain the Human Homologous ESTs. We took advantage of the availability of the mouse BAC clones library and screened the library for the human ESTs located in the QTL region. We designed a pair of primers for each of these ESTs. Then we hybridized the membranes that contain the BAC clones of the mouse library. Positive clones then were picked up and grown on LB culture over night. PCR was conducted using BAC DNA as a template with primers from each of the ESTs. Finally, we located these ESTs on the mouse BAC clones, as shown in Table 4. The localization of these ESTs in the BAC clones allows us to obtain the full-length gene, including intron, exon, and 5' and 3' untranslation

regions from the mouse genome. The availability of BAC clones containing the entire gene would allows us to search for polymorphisms in future studies.

d. Specific Objective 4: Perform PCR amplification and purification of the cDNA clones.

As we mentioned above, we successfully identified candidate genes from our initial study with commercial microarray and from human syntenic region. In order to confirm our findings, we need to study the expression of these genes at different time points and tissues using an in-house microarray system. In order to prepare the in-house microarray, we amplified and purified PCR products of these candidates.

We have amplified and purified PCR products of genes and ESTs:

a) We selected and purchased gene and EST clones from Incyte Genomics.
b) We grew these clones on LB medium overnight at 37°C.
c) We then used cells from each colony in our PCR amplification. Primers for all the clones are universal primers.
d) As shown in Figure 2, pure PCR products are run on 2% agarose gel electrophoresis and visualized under UV light after staining with ethidium bromide.
e) We purified the PCR products with the PCR purification kit from Qiagen (Valencia, CA). We successfully amplified and purified a total of 103 probes of genes and ESTs This list includes the ones that are differentially expressed in our microarray analysis, human syntenic region, ESTs with unknown chromosomal locations, and controls that are highly expressed in the mouse femurs.

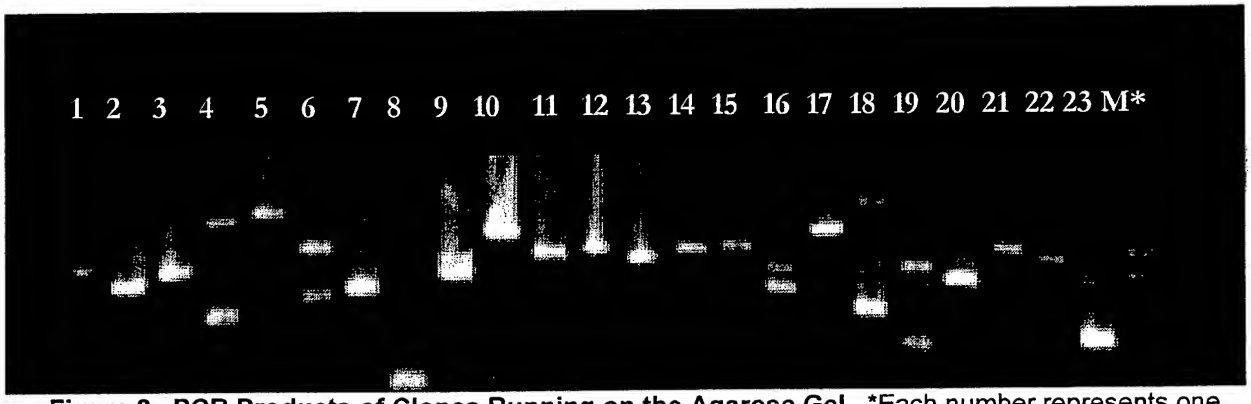

Figure 2. PCR Products of Clones Running on the Agarose Gel. *Each number represents one clone. M = molecular standard marker.

e. Specific Objectives 5 & 6: Perform two-color simultaneous hybridization and temporal and spatial expression analysis to eliminate some of the differentially expressed genes.

Specific objectives 5 and 6 were originally designed to eliminate some of the differentially expressed genes within the QTL region as candidate genes. Because we found that three ESTs and one gene within the QTL region were differentially expressed between congenic and B6 mice, we focused on their expression patterns during the follow-up microarray experiments.

To perform two-color simultaneous hybridization, we labeled the mRNA from congenic and B6 with different dyes, Cyanine 3 and Cyanine 5, and hybridized to probes on microarray chips simultaneously. To perform temporal expression analysis, we compared the difference of gene expression between congenic and B6 mice at 6 weeks and 14 weeks of age. To perform spatial expression analysis, we analyzed the gene expression of livers to evaluate if expression changes between congenic and B6 are unique to bone.

Our results indicated that the three ESTs and one gene, indeed, express differently in the femurs between the congenic and B6 strains at both 6 and 14 weeks of age (Table 5). We have not yet detected difference of expression of these candidates in the lever between congenic and B6. As indicated in our original proposal, our specific objectives in the next six months are to conduct in house microarray to further confirm these genes and to identify additional candidate genes.

Table 5. Candidate Genes Differentially Expressed Within the QTL Region

Gene symbol	Full Name	Ratio B6/congenic (14 wk/Femur)	Ratio B6/congenic (6 wk/Femur)
Crp	C-reactive protein pretaxin related	-2.3*	-2.7
AA184040	EST	-2.9	-2.8
AA209869	EST	-3.3	-2.6
AA437635	EST	-3.9	-2.9

* -2.3 means the expression level of this gene in congenic mice is 2.3 folds higher than that in B6 mice

f. Specific Objective 7: Further narrowing down of the QTL region by backcrossing the congenic mouse line with the recurrent parent mice.

In spite of the progress on the human and mouse genome projects, positional cloning of a QTL gene is still a challenge to molecular geneticists. This is partially because a QTL locus is located on a large region rather than a point on the chromosome. In an attempt to narrow down the QTL region of bone density on chromosome 1, we continued our effort in the subcongenic breeding.

Subcongenic breeding is the procedure to further break down the QTL region in congenic mice. Since a QTL locus is characterized as a region rather than a point on the chromosome, after the congenic strain is created and the QTL is confirmed, the QTL fragment of the chromosome in the congenic strain may still be too large to practically conduct positional cloning. However, if the 10 cM region is broken down into several different smaller fragments, such as 1-2 cM and, if one of these smaller fragments is confirmed to contain the QTL gene, then the positional cloning of the QTL gene becomes feasible.

To create subcongenic lines, the congenic mice are crossed with the recurrent parent, B6 mice. Recombinant individuals were selected based on molecular markers. Then the recombinants were further crossed to produce homozygous recombinants to serve as the subcongenic lines. The phenotype of each subcongenic line can then be measured to identify which one actually contains the QTL gene.

As shown in Figure 3, we have already obtained four subcongenic lines that contain smaller pieces of the chromosome within the QTL region. Of these four subcongenic lines, we have completed the phenotypic measurements in homozygous subcongenic line 3 mice and B6 control mice.

We have found that there is no significant difference between the bone density of subcongenic line 3 and B6 mice. We concluded that the QTL gene is not within the chromosomal region within this subline. Accordingly, the chromosomal region within this subline is excluded as part of our QTL region. Other subcongenic lines will be characterized during the next funding period.

3. **Additional Progress – Construction of BAC Contig:** In addition to accomplishing all of the specific objectives in our original proposal, we have initially constructed a contig that covers the peak region of the QTL locus.

In order to positional clone candidate gene(s) responsible for peak bone density on chromosome 1, it would be essential to have a physical map of this QTL. In this regard, a contig, which is a physical map that displays a set ofcontiguous overlapping and ordered clones along a specific region of a chromosome, would provide overlapping clones for a systematic searching of genomic sequences, which is essential for positional cloning of candidate genes. As an initial step, we have constructed a BAC contig that covers the peak region of the QTL locus.

The contig provides a template for mouse genome sequencing. As indicated in our attached manuscript (Appendix 1-2), this contig covers a 3 cM genome distance with 33 overlapping BAC clones. It is constructed with RPCI-23 mouse BAC library with detailed information of markers along the chromosome. Because of the high quality of the BAC clones in terms of coverage, size, and accuracy, BAC clones have been mainly used in the genome sequencing project. In addition, RPCI-23 mouse BAC library has been chosen as the template for the NIH mouse genome project. Therefore, the future availability of genome sequence information of this contig will facilitate the work in candidate gene searches of genetic loci within this region.

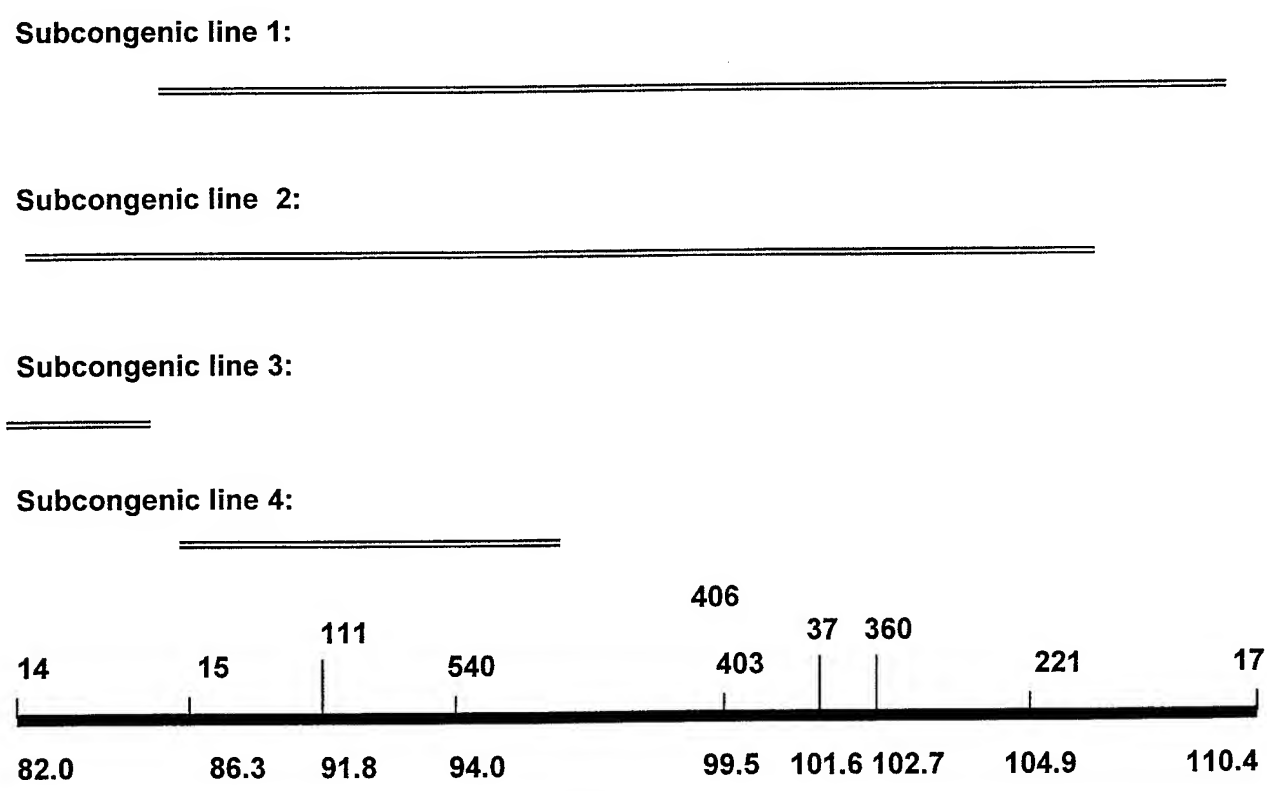

Figure 3. Subcongenic Lines of QTL Region. The double line represent the region covered by each of the subcongenic lines. The solid bar at the bottom represents the original region of the chromosome of CAST within the congenic strain. Numbers above the bar represent the position and names of D1mit microsatellite markers while the number under the bar represent the cM distance on the mouse chromosome 1.

4. Key Research Accomplishments

- Highly expressed genes in the femur of the mouse have been identified by commercial microarray.
- One candidate gene and three ESTs that are differentially expressed between the congenic and the control mice have been identified.
- Bone density measurement confirmed that the bone density in the congenic strain is higher than that of the control, B6.
- Four subcongenic strains that contain smaller pieces of QTL chromosomal regions have been bred. One of them has been excluded as the strain that contains the QTL gene.
- A BAC contig that covers a portion of the QTL locus has been constructed.

5. Reportable Outcomes

Abstracts:

1. WK Gu, XM Li, S Mohan, K-HW Lau, B Edderkaoui, LR Donahue, C Rosen, WG Beamer, DJ Baylink (2000) Identification of candidate genes that control peak bone density by combination of cDNA microarray analysis and physical mapping. Amer J of Human Gen, 67(4): #1409.
2. B Edderkaoui, S Mohan, K-HW Lau, XM Li, DD Strong, WK Gu and DJ Baylink. Physical mapping of a QTL locus that controls bone density on mouse chromosome 1. Presented at the First North American Scientific Meeting of Moroccan Association of Researchers and Scholars, June 23, 2000.
3. WK Gu, M Hellan, XM Li, H-CM Sheng, WG Beamer, JE Wergedal, K-HW Lau, S Mohan and DJ Baylink. Evaluation of the effect of a quantitative trait locus (QTL) on peak bone mineral density (BMD) using congenic mice. International Conference on Progress in Bone and Mineral Research, Vienna, Austria, November 30 – December 2, 2000.

Manuscripts:

1. WK Gu, XM Li, K-HW Lau, B Edderkaoui, LR Donahue, C Rosen, WG Beamer, S Mohan and DJ Baylink. Microarray analysis of gene expression of a congenic strain that contains a QTL locus of bone density in mice. In preparation, October 2000.
2. WK Gu, XM Li, B Edderkaoui, DD Strong, K-HW Lau, WG Beamer, LR Donahue, S Mohan and DJ Baylink. Physical mapping and genetic analysis of a 3 cM biologically significant region on mouse chromosome 1. Submitted to Mammalian Genome, October 2000.

Others:

1. Four mouse subcongenic strains have been developed.
2. A BAC contig has been constructed.
3. A functional molecular genetics laboratory with necessary equipment has been set up.
4. Three new employees have been recruited and trained in molecular genetics technology.

6. Conclusions

Our microarray study provides fundamental information on gene expression of high bone density of the QTL locus on mouse chromosome 1.

We have initially identified three candidate genes that are differentially expressed between the congenic and the control mice (C-reactive protein and 2 ESTs) by our combination approach of physical mapping and cDNA microarray analysis.

We have bred four subcongenic strains, which are going to be used to narrow down the QTL region.

Our contig is useful for mouse genomic sequencing. The future availability of genome sequence information of this contig will facilitate our work in candidate gene searches of genetic loci within this region.

7. References

1. Eddleston J, Murdoch JN, Copp AJ, Stanier P (1999) Physical and transcriptional map of a 3-Mb region of mouse chromosome 1 containing the gene for the neural tube defect mutant loop-tail (Lp). Genomics, 56(2):149-159.
2. Underhill DA, Mullick A, Groulx N, Beatty BG, Gros P (1999) Physical delineation of a 700-kb region overlapping the looptail mutation on mouse chromosome 1. Genomics, 55(2):185-193.
3. Koller DL, Econs MJ, Morin PA, Christian JC, Hui SL, Parry P, Curran ME, Rodriguez LA, Conneally PM, Joslyn G, Peacock M, Johnston CC and Foroud T (2000) Genome screen for QTLs contributing to normal variation in bone mineral density and osteoporosis. J Clin Endocrinol Metab, 85(9):3116-3120.

8. Appendices

Appendix 1-1:
WK Gu, XM Li, K-HW Lau, B Edderkaoui, LR Donahue, C Rosen, WG Beamer, S Mohan and DJ Baylink. Microarray analysis of gene expression of a congenic strain that contains a QTL locus of bone density in mice. In preparation, October 2000.

Appendix 1-2:
WK Gu, XM Li, B Edderkaoui, DD Strong, K-HW Lau, WG Beamer, LR Donahue, S Mohan and DJ Baylink. Physical mapping and genetic analysis of a 3 cM biologically significant region on mouse chromosome 1. Submitted to Mammalian Genome, October 2000.

Appendix 1-3
WK Gu, XM Li, S Mohan, K-HW Lau, B Edderkaoui, LR Donahue, C Rosen, WG Beamer, DJ Baylink (2000) Identification of candidate genes that control peak bone density by combination of cDNA microarray analysis and physical mapping. Amer J of Human Gen, 67(4): #1409.

Appendix 1-4:
B Edderkaoui, S Mohan, K-HW Lau, XM Li, DD Strong, WK Gu and DJ Baylink. Physical mapping of a QTL locus that controls bone density on mouse chromosome 1. Presented at the First North American Scientific Meeting of Moroccan Association of Researchers and Scholars, June 23, 2000.

Appendix 1-5:
WK Gu, M Hellan, XM Li, H-CM Sheng, WG Beamer, JE Wergedal, K-HW Lau, S Mohan and DJ Baylink. Evaluation of the effect of a quantitative trait locus (QTL) on peak bone mineral density (BMD) using congenic mice. International Conference on Progress in Bone and Mineral Research, Vienna, Austria, November 30 – December 2, 2000.

B. TECHNICAL OBJECTIVE 2 - To identify the key genes that are involved in the soft-tissue repair/regeneration in MRL/MpJ and SJL/J mice.

1. Introduction

Wound healing involves two major clinical issues: 1) the rate of healing; and 2) the quality of healing. The primary therapeutic goal of the treatment of a wound is to accelerate wound closure with minimal scar formation. However, the success of using therapeutic approaches to treat wounds depends heavily on understanding the molecular mechanisms underlying the wound healing process. The aim of this project is to identify the key genes and their cellular function that regulate the soft- and hard-tissue repair and regeneration in a mouse model. We have now achieved the two specific objectives we proposed during the first twelve months of this grant period: 1) To perform ear punch and vertebral fracture evaluations in 21 different inbred strains of mice; and 2) To determine the most appropriate mouse strain(s) for soft-tissue and hard-tissue regeneration studies. In addition to accomplishing the proposed specific objectives, we have also performed gene and protein expression studies in soft-tissue regeneration.

2. Body

This annual report is divided into two sections: The first section deals with the progress report on the two specific technical objectives we proposed for the first twelve months of this funding period. The second section is a report on our additional progress, which represents an extension of our soft-tissue regeneration study (page 13). For the convenience of this report, progress on soft-tissue and hard-tissue regeneration is presented separately.

a. Specific Objective 1: To perform ear punch experiment in different inbred strains of mice and determine the best mouse strain (s) for soft-tissue regeneration (see Appendix 21 for a detailed description)

Injury has been recognized as a major global public issue (1), but the genetics of wound healing is not well studied. In this study, we investigated the genetic variation for the rate of wound healing among 20 inbred strains of mice and explored the genetic basis underlying the difference using two segregating populations with different healing capacities.

Twenty inbred strains of mice were selected from a group of major inbred strains representing a diversified genetic origin. Three 4-week old female mice from each strain were obtained from The Jackson Laboratories (Bar Harbor, ME). A 2 mm through-and-through hole in diameter was made in the lower cartilaginous portion of each ear using a metal ear punch (Fisher Scientific, Pittsburgh, Catalog No. 01-337B). The hole closure (in diameter) was measured using a 7X magnifier at day 0, 5, 10, 15, 20, 25, and 30 after injury.

We have demonstrated that inbred strains of mice differ significantly in the rate of wound healing. Of the 20 strains tested, MRL/MpJ-Fas^{lpr} and LG/J/J mice were the most rapid and complete healers. They healed over 95% of the holes on the 30th day after wounding, in contrast to Balb/cByJ or SJL/J that only healed less than 25% of the holes at the same period of time. The overall wound-healing profile revealed three healing stages: 1) an initiation stage (day 0 to day 5) where there was no significant difference (P=0.01) in wound closure among all strains; 2) a fast-healing stage (day 6 to day 20) where most of the strains achieved their maximal wound closure and exhibited markedly different healing capacity among strains; 3) a slow-healing stage (day 21 to day 30) where most of the strains had no healing or very little healing. The fast healers, like MRL/MpJ-Fas^{lpr} and LG/J/J, had no slow healing stage. After initiation of healing, they closed the holes with a greater and constant rate. In contrast, slow healers, including Balb/cByJ and SJL/J, had no obvious fast healing stage. They remained at a slow healing stage until the healing is stopped

The genetic basis underlying the difference in the healing capacity was analyzed using F_2 populations of two different crosses. We showed that the rate of wound healing is a polygenically determined trait with an average estimated heritability of 86%. The modes of gene action for the two crosses are different. In the (MRL/MpJ × SJL/J) cross, the F_1 offspring exhibited intermediate values of the two parents and F_2 individuals exhibited a normal

distribution with an average value similar to that of F_1. In contrast, the average F_1 offspring in the (MRL/MpJ-Fas^{lpr} × CBA/J) cross had a similar value to one parent, CBA/J mice, and the phenotypic distribution of the F_2 offspring severely deviated from normality, being shifted toward the average value of the CBA/J parent. A χ^2 test showed that the MRL/MpJ-Fas^{lpr} type:CBA/J type ratio in the F_2 population did not differ significantly from 1:3. These results suggest that there is a dominant repressor gene in CBA/J mice which suppressed the additive action of fast-healing genes in MRL/MpJ-Fas^{lpr}.

In conclusion, the rate of ear wound healing differs significantly among strains. MRL/MpJ-Fas^{lpr} and LG/J/J are ideal strains for the study of soft-tissue repair/regeneration. Wound healing is a genetically controlled quantitative trait with a high heritability. The fast-healer genes exhibited an additive effect and the repressor gene showed a dominant effect. The healing capacity was a function of the number of fast-healer genes in the absence of the repressor gene and became a simple Mendelian trait (independent of the number of the fast-healer genes) in the presence of the repressor gene. These findings have been submitted to *Heredity* for publication (Appendix 2-1).

b. Specific Objective 2: To perform vertebral "drill-hole" experiments in different inbred strains of mice and determine the best mouse strain(s) for hard-tissue regeneration (see Appendix 2-2 for a detailed description).

Genetic variation in the bone regenerative capacity has not been studied in any animal model system. The lack of progress is due, in part, to technical difficulties associated with the creation and quantitative measurement of a reproducible injury. In a preliminary study, we found differences in the rate of vertebral fracture healing among strains using an Instron Mechanical Tester (Instron Corporation, Canton, MA) to create vertebral fractures. Due to the different biomechanical properties among the strains, it was difficult to introduce identical injury reproducibility and perform comparative analysis quantitatively. We, therefore, explored an alternative model, a drill-hole in the vertebra. This model effectively overcame the technical difficulties of the fracture model by introducing an injury of reproducible size and with a clearly defined boundary, making it possible to quantify and compare the rate of bone healing among strains.

Twelve inbred strains of mice were used for this study– the same number and strain as those of the soft-tissue regeneration study. A hole of 0.9 mm in diameter was produced in the third vertebra from the base of the tail using a Dremel Tool equipped with a 1/32-inch drill bit. The healing process was monitored up to 30 days at 10-day intervals using high resolution Faxitron X-ray images (MX-20 Specimen Radiography System, Illinois, USA) for qualitative evaluation and a ChemiImager™ 4000 Low Light Imaging System (Alpha Innotech Corporation, San Leandro, CA) for quantitative evaluation.

Using this approach, we have found significant variation in the bone regenerative capacity among strains. The difference approached three-fold between a fast regenerative strain and a slow regenerative strain. Of the twelve strains tested, Sencar was the most suitable model for the study of hard-tissue regeneration. It regained 73% of the bone removed by drill hole 30 days after injury, in contrast to a slow healer, CBA/J, which only recovered 25% of bone lost in the same period of time. The coefficient of variation across all strains was as high as 42%, suggesting a quantitative genetic regulation of the phenotype. Seventy-two percent of the variation could be attributed to genetic factors, providing a rationale for the mapping of loci critical to bone regeneration. In this regard, a (SENCAR X CBA/J) matting would be an ideal cross for the QTL mapping.

The most significant finding in this study was that bone regenerative capacity was not correlated to soft-tissue regenerative capacity but significantly correlated to bone density. A typical example of no correlation between the soft- and hard-tissue regenerative capacity is the CBA strain, which was a fast healer in ear repair/regeneration (a relative healing rate of 84%),

but a slow healer in bone regeneration (a relative healing rate of 25%). There are a number of potential explanations for the lack of correlation, including that the soft tissue consists of different cell types compared to the hard tissue; it has a much more severe inflammatory reaction than hard tissue in response to initial injury; and it does not form the callus characteristic of hard-tissue regeneration. It appears that, although they may share some common molecular pathways, hard-tissue healing involves a different regulatory program relative to soft-tissue healing. This finding will necessitate separate molecular investigations for soft- and hard-tissue regeneration. The significant association between bone regenerative capacity and bone density ($r=0.49$, $p<0.01$ with total BMD; $r=0.58$, $p<0.01$ with femur BMD; $r=0.49$, $p<0.01$ with forearm BMD; and $r=0.63$, $p<0.001$ with total BMC) suggests that high bone densities not only reduce the risk of bone fracture, but also promote the bone healing after injury. The genetic implication of this association is that some of the genes regulating bone density might also function in bone regeneration. Many candidate genes or QTL regions for high bone density in both humans and mice have been identified, and our QTL mapping programs for bone density genes are also in progress. Further studies of these candidate genes should disclose this intriguing genetic relationship and facilitate the identification of the genes regulating bone regeneration.

In conclusion, a significant genetic variation in bone regenerative capacity exists among inbred strains of mice. This variation provides a genetic basis for the molecular dissection of this highly inherited trait. The bone regenerative capacity did not correlate with soft-tissue repair/regeneration but exhibited a strong correlation with the total BMD. This correlation has significant genetic and practical implications in preventing bone fracture and accelerating bone healing in humans. The findings of this study have been submitted to *Bone* for publication (Appendix 2-2).

3. Additional Progress – Studies Related to Soft-Tissue Regeneration

a. Analysis of the differentially expressed genes between a regeneration strain, MRL, and a non-regeneration strain, B6, by commercial and in-house microarray hybridization (see Appendix 2-3 for a detailed description). Wound repair/regeneration is a complex process consisting of three stages: inflammation, tissue re-growth, and remodeling, which together involve the action of hundreds of genes. In order to identify and analyze the genes that are expressed at the inflammatory stage of repair (i.e., 24 hours after injury) and to evaluate the molecular basis of fast wound repair/regeneration in adult mammals, we examined the expression of 8,734 sequence-verified genes in response to ear punch in a fast wound repair/regeneration strain, MRL/MpJ-Fas^{lpr} mice, and a slow wound repair strain, C57BL/6J mice.

Three 2 mm through-and-through holes were made using a metal ear punch in both ears of the mice when animals reached 5 weeks of age. A 0.4 mm disc of ear-punched tissue was isolated 24 hours after ear punch from 10 animals from each strain. An equivalent amount of ear tissue at the corresponding region was also isolated from the non-ear-punched control mice. The ear-punched or control tissues from each strain were pooled. Total RNA was isolated using RNeasy Kit (QIAGEN) and mRNA was purified using Oligotex mRNA Kit (QIAGEN) based on the manufacturer's instructions. Incyte Genomics commercial service was used for probe labeling and microarray hybridization and in-house microarray facilities were used to validate the commercial results.

A comparison of the gene expression profile from the ear-punched and non-ear-punched control tissue revealed that the inflammatory stage of repair is associated with the altered mRNA expression of 2.5% of genes analyzed in both strains. Of the 8,734 mouse cDNA clones surveyed in the GEM1 microarray, 54 (0.6%) exhibited a greater than two-fold increase in expression levels in both MRL and B6 mice, 113 (1.3%) in MRL mice only, and 50 (0.6%) in B6 mice only. Many differentially expressed genes can be assigned to wound-repairing pathways

known to be active during the inflammatory phase, whereas others are involved in pathways not previously associated with wound repair. Many genes of unknown function (ESTs) exhibited a more than two-fold increase in MRL/MpJ-Fas^{lpr} or C57BL/6J mice, suggesting that current understanding of the molecular events at the inflammatory stage of repair is still limited. Some of the differentially expressed genes are localized to the wound healing QTL regions identified by McBrearty, et al (2). These genes include esterase 1, deubiquitinating enzyme, eIF-1A, keratin complex 2 gene 6A, lymphocyte antigen 6C, and metallothionein 1 and 2.

In conclusion, a comparison of the differential expression profiles between ear-punched MRL/MpJ-Fas^{lpr} and C57BL/6J tissue suggests that the expression profile in MRL mice exhibited a metabolic shift toward a lower inflammatory response and an enhanced tissue repair. The trigger for this shift may be pivotal for understanding rapid wound repair/regeneration in the MRL strain of mice. These results have been accepted for publication in *Mammalian Genome* (Appendix 2-3).

b. Analysis of the differentially expressed proteins between a regeneration strain, MRL, and a non-regeneration strain, B6, using the SELDI ProteinChip technology (see Appendix 2-4 for a detailed description). Systematic analysis of the function of genes can take place at the DNA or protein level. As a complementary approach to gene expression profiling on cDNA microarray, in this study we employed the SELDI ProteinChip technology to determine the differential protein expression profile between MRL and B6 in order to identify candidate genes regulating fast wound repair/regeneration in soft-tissue.

Three 2 mm through-and-through holes in diameter were made in both ears of mice at the age of 5 weeks using a metal ear punch (Fisher Scientific, Pittsburgh, Catalog No. 01-337B). A 4 mm square disc of ear tissue which contained the punched hole was isolated using scissors 1 day, 5 days, 10 days, or 20 days after ear punch. The equivalent amount of ear tissue was also isolated from the non-ear-punched control mice. Total proteins were extracted and the concentration was determined at OD_{595} using Bio-Rad Protein Assay reagent (Bio-RAD, Cat# 500-0006). Differential protein profile was examined using the SELDI ProteinChip array. The SELDI (Ciphergen Biosystems, Palo Alto, CA, USA) is able to determine molecular mass with deviations of less than 0.2% (200 ppm) to detect a few femtomoles of protein and to estimate the amount of hundreds of proteins simultaneously. These features have made it feasible to examine the protein profile from the crude protein extract in response to earpunch between MRL and B6.

Five candidate proteins were identified in which responses of MRL to the ear-punch were two- to four-fold different compared to those of B6. Their corresponding genes were predicted using an antigen-antibody assay validated mass-based approach. Most of the predicted genes are known to play a role or are likely to play a role in the wound repair/regeneration. Of the five candidate proteins, the amount of the 23560 Dalton protein in the ear-punched tissue was significantly correlated with the rate of ear healing in six representative strains of mice, making it a good candidate for fast wound repair/regeneration. We speculate that the increased concentration of the 23560 Dalton protein in the wound tissue could stimulate the expression of various growth-promoting proteins and, consequently, speed up the wound repair/regeneration processes.

In conclusion, we have demonstrated that examination of the protein expression profile using SELDI technology, coupled with database searches, is an alternative approach to search for candidate genes for wound repair/regeneration. This novel approach can be implemented in a variety of biological applications. These results have been accepted for publication in *Biochimica et Biophysica Acta* (Appendix 2-4).

4. Key Research Accomplishments

- Demonstrated that both soft-and hard-tissue regenerative capacities differ significantly among inbred strains of mice. These findings provide a genetic foundation for the therapeutic intervention of tissue regeneration.
- Identified a suitable regeneration strain, MRL/MpJ, and a non-regeneration strain, SJL/J, for the study of molecular mechanisms underlying soft-tissue regeneration.
- Discovered different gene actions in the soft-tissue regeneration, i.e., the fast-healer genes exhibited an additive effect and the repressor gene showed a dominant effect. This finding is fundamentally important in elucidating the molecular mechanisms of the wound healing process.
- Identified a suitable strain, Sencar, as a model system for the study of hard-tissue regeneration.
- Demonstrated that hard-tissue regenerative capacity is not correlated with soft-tissue regenerative capacity but significantly correlated with bone density. This finding implies that separate molecular investigations are necessary for soft- and hard-tissue regeneration and suggests that high bone densities not only reduce the risk of bone fracture but could also promote the bone healing after injury.
- Identified 44 genes and 135 ESTs that differentially expressed more than 2-fold between the regeneration strain, MRL, and non-regeneration strain, B6, using microarray hybridization. This information is important for subsequent genetic investigations of soft-tissue regeneration.
- Demonstrated that the expression profile in MRL mice exhibited a metabolic shift toward a lower inflammatory response and an enhanced tissue repair compared to that in B6 mice. This finding indicates that the clinic treatment of mammalian injury should target the enhancement of tissue repair as well as control of inflammation.
- Identified five differentially expressed proteins between the regeneration strain, MRL, and non-regeneration strain, B6, using SELDI technology. These proteins merit further investigation.
- Demonstrated that the amount of the 23560 Dalton protein in the ear-punched tissue was functionally correlated with the rate of ear healing in six representative strains of mice, making it a strong candidate for regulating soft-tissue repair/regeneration.

5. Reportable Outcomes

Publications:

1. Li X, Gu W, Masinde G, Hamilton-Ulland M, Xu S, Mohan S, Baylink DJ (2000) Genetic control of the rate of wound healing in mice. Submitted to Heredity.
2. Li X, Gu W, Masinde G, Hamilton-Ulland M, Mohan S, and Baylink DJ (2000) Genetic variation in the bone regenerative capacity among inbred strains of mice. Submitted to Bone.
3. Li X, Mohan S, Gu W and Baylink DJ (2000) Analysis of gene expression in the wound repair/regeneration process. Mammalian Genome. In press.
4. Li X, Mohan S, Gu W, Miyakoshi N and Baylink DJ (2000) Differential Protein Profile in the Ear-punched Tissue of Regeneration and Non-regeneration Strains of Mice: A Novel Approach to Explore the Candidate Genes for Soft-tissue Regeneration. Biochimica et Biophysica Acta. In press.
5. Li X, Mohan S, Gu W, Wergedal J and Baylink DJ (2000) Quantitative assessment of forearm muscle size, forelimb grip strength, forearm bone mineral density and forearm bone size in determining humerus breaking strength in ten inbred strains of mice. Calcified Tissue International. Accepted with minor revision.

Animal Models:

1. MRL and LG have been identified as model strains for the study of soft-tissue regeneration.
2. Sencar has been identified as a model strain for the study of hard-tissue regeneration.

Innovations:

1. Developed a "drill-hole" model in the tail vertebra of inbred strains of mice that allows us to reproducibly introduce an injury with a defined boundary and quantify the rate of bone healing using the combination of high resolution Faxitron X-ray images and a ChemiImager™ 4000 Low Light Imaging System.
2. Developed a protein mass-based, database-mediated novel approach to search for candidate genes using surface-enhanced laser desorption/ionization technology.

6. Conclusions

Using distantly related inbred strains of mice, we demonstrate that the soft- and hard-tissue repairing/regenerative capacities are highly inherited quantitative traits and differ significantly among inbred strains of mice. We have identified suitable inbred strains of mice for the study of soft- and hard-tissue regeneration. These findings provide a genetic foundation for the molecular dissection and therapeutic intervention of tissue regeneration. Using cDNA microarray and surface-enhanced laser desorption/ionization technologies, we have identified several genes whose expression levels are associated with soft-tissue repairing/regenerative capacity. *In vivo* functional studies are in progress to evaluate their therapeutic potential in the treatment of soft-tissue injury.

7. References

1. Satcher D (2000) Injury: an overlooked global health concern. JAMA 284:950.
2. McBrearty BA, Clark LD, Zhang XM, Blankenhorn EP, Heber-Katz E (1998) Genetic analysis of a mammalian wound-healing trait. Proc Natl Acade Sci, USA 95:11792-11797.

8. Appendices

Appendix 2-1:
Li X, Gu W, Masinde G, Hamilton-Ulland M, Xu S, Mohan S, Baylink DJ (2000) Genetic control of the rate of wound healing in mice. Submitted to Heredity.

Appendix 2-2:
Li X, Gu W, Masinde G, Hamilton-Ulland M, Mohan S, and Baylink DJ (2000) Genetic variation in the bone regenerative capacity among inbred strains of mice. Submitted to Bone.

Appendix 2-3:
Li X, Mohan S, Gu W and Baylink DJ (2000) Analysis of gene expression in the wound repair/regeneration process. Mammalian Genome. In press.

Appendix 2-4:
Li X, Mohan S, Gu W, Miyakoshi N and Baylink DJ (2000) Differential Protein Profile in the Ear-punched Tissue of Regeneration and Non-regeneration Strains of Mice: A Novel Approach to Explore the Candidate Genes for Soft-tissue Regeneration. Biochimica et Biophysica Acta. In press.

Appendix 2-5:
Li X, Mohan S, Gu W, Wergedal J and Baylink DJ (2000c) Quantitative assessment of forearm muscle size, forelimb grip strength, forearm bone mineral density and forearm bone size in determining humerus breaking strength in ten inbred strains of mice. Calcified Tissue International. Accepted with minor revision.

C. TECHNICAL OBJECTIVE 3 – To apply ENU mutagenesis to identify new genes that regulate soft- and hard-tissue regeneration in C3H strain of mice.

1. Introduction

The goal of this technical objective is to identify and characterize novel genes or to elucidate function for known genes that play a key role in the metabolism of bone and soft tissue using the ENU mutagenesis technique. Our initial studies are intended to perform dominant screening. During the first 12 months of the funding period, we have proposed the following specific objectives:

a. Determine the optimal ENU dosage;
b. Develop and optimize each of the proposed phenotypic screens;
c. Optimize each phenotypic screening method to allow for maximal reproducibility and sensitivity; and
d. Adapt each phenotypic screen to be applied to large populations of mice.

Our progress in each of the specific objectives is discussed below.

2. Body

a. Specific Objective 1: Determination of optimal dose of N-ethyl-N-nitrosourea (ENU).

1) Selection of C3H/HeJ (C3H) Mice for ENU Mutagenesis Study. Our main aim of using ENU mutagenesis in the mouse model is to identify genes that regulate bone density and soft-tissue regeneration in mice (and presumably in humans). We have earlier identified (1) that C3H mice have the highest bone mineral density (BMD) among 13 inbred strains. Since ENU mutagenesis is most likely to affect gene expression by disruptive mutations, it can be predicted that using a high-BMD mouse strain is ideal for identifying genes that effect bone density. In addition, we have observed that C3H is a good model for soft-tissue regeneration and fracture healing (see Appendix 2-2). Therefore, C3H mice offer an excellent model to study loss of function mutations on various phenotypes of interest to us. Furthermore, it has been reported (2) that C3H mice are one of the few strains that can tolerate ENU very well and are one of the most fertile strains after an initial recovery period. Consequently, a large number of mutants could be generated with similar amount of effort, as compared to other strains of mice that are relatively less fertile after ENU injections. An added advantage with the C3H strain is that spermatogonia from this strain can be frozen successfully for subsequent recovery of mutants. This is an essential feature for the success of our ENU program.

2) Injection of ENU in C3H Male Mice. Seven batches of 8- to 10-week-old C3H/HeJ (C3H) males were weighed individually and then injected with 85-250 mg/kg (body weight) ENU intra-peritoneally (for details of dose for each group see Table 1). All C3H male mice were purchased from The Jackson Laboratory (Bar Harbor, ME) and acclimatized for two weeks before ENU injections. ENU was purchased from Sigma Chemical Co. (St Louis, MO) in a 100mL serum bottle (ISOPAC, Cat # N3385, containing 1 g powder, and stored in-20°C in its original shipping container). To make the ENU solution, 5mL of 100% ethanol was injected in the ISOPAC ENU bottle and suspension was warmed in a 60°C water bath and, subsequently, diluted to 10 mg/mL using sterilized citrate/phosphate buffer. ENU concentration was finally

determined by measuring the absorbance at 395nm, where 0.7 OD was considered equivalent to 1.0 mg/mL.

Each mouse was individually weighed and ENU was administered by intra-peritoneal injections. After ENU injections, all mice were placed in the disposable animal cages (four mice per cage) and maintained for 48 hours in the fume hood where ENU is administered. Two days after the ENU injections, all mice were placed in the colony room with 12-hour day/night cycle and fed standard rodent diet for 10-12 weeks in groups of 2-4 mice/cage. For several groups, ENU injections were repeated 3 or 4 times at weekly intervals (for details see Table 1). ENU was handled with extreme care, since it is a powerful mutagen.

Table 1. Response of C3H/HeJ mice to different doses of ENU

Groups	Dose (number of weekly injections X dose)	Total Dose (mg/kg)	Number of Mice Injected/Survived	Number of Mice Fertile (14-week post ENU injections)	Number of F1 Offspring Produced
Batch # 1	4 × 90 mg/kg	360	15/1	None	None
Batch # 2	3 × 90 mg/kg	270	15/13	7	141
Batch # 3	3 × 85 mg/kg	255	15/14	8	101
Batch # 4	1 × 250 mg/kg	250	20/18	1	18
Batch # 5	3 × 85 mg/kg	255	45/45	24	196
Batch # 6	4 × 85 mg/kg	340	15/15	Data not yet available	Data not yet available
Batch # 7	3 × 100 mg/kg	300	15/15	Data not yet available	Data not yet available

F1 offspring are currently being screened for various phenotypes.

3) Breeding Strategy. Since ENU is mutagenic or cytotoxic to all stages of spermatogenic cells, causing cessation of cell division and cell death, successfully mutagenized mice are rendered temporarily sterile after existing post-meiotic cells have completed spermatogenesis to become mature spermatozoa, which takes about 4 weeks after ENU injection. In a typical case, new rounds of spermatogenesis will cease for 10-12 weeks following injection; during this period surviving mutagenized stem cell spermatogonia repopulate the testis. In the case of C3H mice, we observed that C3H males regained fertility only after a 14-week period after the final ENU injection. Mortality and fertility were closely monitored and recorded at this stage. The dose of ENU for future experiments will be chosen based on the percent of mice that regain fertility after ENU treatment and the frequency of mutations at the various ENU doses.

4) Mating Scheme. To insure enough progeny are produced in the life span of a male, each ENU-treated C3H male was mated with two 8- to 10-week-old C3H females. The

pregnant females are moved to isolator cages for delivery of the offspring. A new female is introduce to the ENU male to replace the pregnant female. After an 8-10 week period, the males are rotated back to the original group of females to start the cycle over again. C3H females were replaced with younger mice (10 weeks) after 6 months and the males were replaced with new ENU-treated mice after three months.

To insure that repeat mutations are not frequently obtained, only 50 progeny will be generated and screened for each male injected with ENU.

5) Maintenance and Identification of F1 Progeny. All ENU male mice were identified by the use of an ear tag. A unique number marked by a tattoo in the tail identifies all female mice. ENU male and female mice involved in breeding are fed breeder diet and checked twice a week for pregnancies. Once a female is pregnant and is ready for delivery, she is moved to micro-isolator cages. Female mice will remain in the micro-isolator cage until weaning. All F1 progeny were housed in the micro-isolator cages and fed irradiated diet and sterile water. For screening purposes, mice were taken out from the micro-isolator cages in a Laminar flow workstation.

b. Specific Objective 2: Develop and optimize each of the proposed phenotypic screens.

In any search for mutations, the yield would depend on the sensitivity and reproducibility of the phenotypic screen. Since the phenotypic screen for ENU studies involves a large number of animals, we must be able to perform them in an efficient manner. The following section describes our progress in the development and validation of various phenotypic screens, which are divided into four categories as shown below:

1) Markers of bone turnover
   a) C-telopeptide
   b) Osteocalcin
   c) Skeletal alkaline phosphatase
2) Growth screens
   a) Body weight
   b) IGF-I
   c) Muscle mass by PIXImus
3) Bone phenotype screens
   a) Bone density (DEXA) by PIXImus
   b) X-ray images by Faxitron
4) Soft tissue regeneration screen using ear punch healing

We have selected a wide range of biochemical tests that can detect changes in bone formation as well as resorption. A major focus of the biochemical screen is to identify genes affecting bone turnover. A brief description of all the assays used in the screening is described in this section. All biochemical assays have been developed and validated for application to the mouse model.

1) C-telopeptide of Type-I Collagen. During osteoclastic resorption, carboxyl and amino terminal fragments of type-I collagen were released into the circulation where its concentration correlates with indices of bone resorption in a human, as well as in mouse, model. We have developed a C-telopeptide (of type-I alpha 1 collagen) ELISA to measure bone resorption in mouse serum. The ELISA procedure utilizes an affinity-purified polyclonal antibody, which was generated against a linear synthetic peptide sequence DFSFLPQPPQEKAHDGGR (3). The C-telopeptide ELISA has been validated for *in vivo* usefulness in the mouse model by assessing several skeletal perturbations that are known to effect bone resorption. The sensitivity of the ELISA is 0.5 ng/ml, and it requires 10μL of mouse serum for measurements of C-telopeptide. The ELISA exhibited intra- and inter-assay (n=3) variations of coefficient of variance (CV) <9% and <13%, respectively. Our work dealing with

the development and validation of C-telopeptide for mouse serum has been accepted for publication in *Bone* (see Appendix 3-1).

2) Osteocalcin. Osteocalcin is a bone specific protein (46 amino acids) secreted by osteoblasts. It comprises 1-2 % of the total bone protein. A fraction of newly synthesized intact osteocalcin (about 15%) is released into the circulation, where its concentration reflects osteoblastic activity and bone formation. We have developed a synthetic peptide-based osteocalcin radioimmunoassay (4) and validated its *in vivo* utility in the mouse model. For application to ENU screening, the RIA was modified into an ELISA format, which showed analytical and clinical performance identical to RIA. The sensitivity of the ELISA is 6 ng/ml and it requires 10 µL of serum. The assay showed an average intra- (n=9) and inter-assay coefficient of variation of CV<14%. Our work dealing with the development and validation of synthetic peptide based RIA for mouse serum has been published in *Calcified Tissue International* (Appendix 3-2).

3) Alkaline Phosphatase. Measurement of bone specific alkaline phosphatase (sALP) has been shown to provide an index of the rate of bone formation. Alkaline phosphatase can be measured in serum by kinetic methods using p-nitrophenylphosphate as substrate. In the mouse, the major isoform of alkaline phosphatase (ALP) that can interfere in the serum measurements of sALP is the intestinal alkaline phosphatase. However, activity of this intestinal isoenzyme is more sensitive to inhibition by L-phenylalanine. By the addition of 15 mM L-phenylalanine, up to 90% of intestinal alkaline phosphatase can be inhibited without significantly affecting the skeletal isoenzyme activity (5). The L-phenylalanine inhibition assay exhibited intra-assay (n=10) and inter-assay (n=8) variation (CV) between 1.9% and 3.8%. The assay can detect <10 mU/ml of alkaline phosphatase in mouse serum.

4) Insulin-like Growth Factor-1 (IGF-I). It is well known that growth hormone effects on bone and other tissues are mediated via IGF-I. In addition, IGF-I is an important autocrine and paracrine regulator of bone formation. It has been shown that IGF-I concentration in mouse serum correlates highly with bone mineral density. Therefore, measurement of IGF-I provides important insight into growth and normal bone development. We have developed an RIA for the measurement of IGF-I in mouse serum using polyclonal antibodies generated against recombinant human IGF-I in chickens. Human recombinant IGF-I (GroPep, Australia) was used as a tracer and calibrator. Since the IGF-I concentration is regulated by multiple components of the IGF-I regulatory system, including IGF binding proteins (IGFBPs), removal of this protein is necessary for the precise and meaningful estimation of IGF-I concentrations. In our assay, IGF-I was separated from binding proteins by using acid-ethanol extraction protocol described previously (6). The cross reactivity with IGF-II was <0.5%. The sensitivity of the IGF-I measurement was <50 pg/ml, and the intra- and inter-assay CV was <12%.

5) Bone Mineral Density and Lean Body Mass. *In vivo* measurements of total bone mineral density (BMD), bone mineral content (BMC), and lean body mass were determined by dual energy X-ray absorptiometry (DEXA) using the PIXImus instrument (Lunar Corporation, Madison, WI). Data was analyzed by using PIXI software 1.45. Whole body scan was performed and the skull was omitted from final analysis by region of interest (ROI) placement. The fat mass and lean mass were also determined by PIXImus software. The manufacturers described reproducibility of BMD and BMC measurements is CV <2%.

6) Soft Tissue Regeneration Screen. We have developed a methodology to screen for the capacity of an animal to repair or regenerate soft tissue. This methodology is described in detail in Specific Objective 1 of Technical Objective 2. This method has been successfully used as a tool to identify differences in the regenerative capacity of various strains of mice. A similar procedure will be followed for screening F1 offspring obtained from ENU injected male mice.

c. **Specific Objective 3:** Optimize each phenotypic screening method to allow for maximal reproducibility and sensitivity.

We have proposed to use population-based reference values for biochemical markers and bone density measurements to identify mutants with abnormal bone phenotype. However, the utility of these conventional population-based values remains unknown unless the data on biological variation are available and the factors affecting biological variations are minimized. In the mouse model, data on biological variation in biochemical markers is scarce and published data on biological variations indicates differences in circadian variation in different strains. As a result, optimization of all screening procedures to maximize sensitivity and discriminatory power is essential to obtain full benefits of our ENU screens. One of the important parameters for biochemical measurements is to establish the appropriate sampling time for optimal use of biochemical markers to reflect bone turnover changes. To establish the optimal sampling time, we evaluated three main components of biological variation in C3H/HeJ mice, the strain used in the ENU mutagenesis: 1) the circadian changes; 2) within-subject (longitudinal) variation; and 3) between-subject (population) variation. Our data on biological variation in biochemical marker assays are summarized below.

1) **Circadian Variation.** Biological variation studies were performed for three mouse bone turnover assays, namely osteocalcin, C-telopeptide (Type-I collagen alpha-1 chain), and skeletal alkaline phosphatase. The diurnal variation was studied over a 24-hour period covering a 12-hour light/dark cycle. To determine whether the circadian rhythm is intrinsically regulated or influenced by restricted food intake, circadian rhythm was also studied in male and female C3H mice by collecting blood after a 12-hour fasting period.

The serum levels of skeletal alkaline phosphatase, C-telopeptide, and osteocalcin in female and male C3H/HeJ mice, determined at 8 different time intervals spread over a 24-hour period, are shown in the manuscript submitted for publication (see Appendix 3-3). Briefly, results of this study demonstrated significant circadian variations in osteocalcin and C-telopeptide levels with a peak value between 0900 and 1200 hours during daytime and a nadir between 1500 and 1800 hours. The peak levels of C-telopeptide and osteocalcin were 26% to 66% higher as compared to the 24-hour mean values. The pattern of the circadian variation of C-telopeptide and osteocalcin was similar in female and male animals and was not significantly affected by restricted food intake. The sALP activity showed little or no change during the 24-hour period. Only the non-fasting female group showed a circadian type rhythm. In this group, the sALP levels were significantly higher for the 0900-hour samples ($p<0.05$) compared to all other time points. Apart from this group, the serum sALP activity indicated non-existence of a definite 24-hour rhythm in serum activity of sALP. Notably, fasting significantly reduced the sALP activity in the male group throughout the 24-hour period, as compared to the non-fasting male group. On the other hand, fasting had no significant effect on sALP levels of female mice.

2) **Longitudinal Variation.** Longitudinal variation was studied over a 7-day period. Two studies were performed: 1) blood samples were collected in the morning on day 1, day 3, and day 7; and 2) blood samples were collected as described in study one, but in the afternoon. The longitudinal variation expressed as coefficient of variance (CV) in osteocalcin, C-telopeptide, and sALP concentrations were 17%, 14%, and 16%, respectively. The longitudinal variations were not significantly influenced by the time of blood collection in sALP and osteocalcin levels, whereas C-telopeptide levels showed significantly higher within-subject day-to-day variation in morning samples. For details, please see Appendix 3-2.

3) **Population Variation.** Between-subject variations were calculated from samples collected on three different days and mean value of population CV (from three days) are shown in the attached manuscript (Appendix 3-2).

The average between-subject (n=12) CV for C-telopeptide was 60% higher for morning blood collection as compared to afternoon samples ($p<0.05$). The differences in population CV

of sALP and osteocalcin levels for morning and afternoon blood collection were statistically not significant.

4) Strategy for Biochemical Screening and Evaluation. The above results highlight the importance of the timing of sample collection for appropriate interpretation of the bone marker data. Based on our data, we have formulated the following strategy for biochemical and other phenotype screening in our ENU study:

a) All blood samples will be strictly collected between 1500 – 1600 hours. We have chosen this time because we observed comparatively lower between-subject variation in C-telopeptide and sALP levels. To avoid the effect of circadian variation, all blood samples will be invariably collected between the same time periods.

b) The blood samples will be collected by retro-orbital sinus puncture under anesthesia. Once anesthesia is administered, animals are sedated for less than 30 minutes. During this period, DEXA measurements will be performed using PIXImus. This will avoid repeated administration of anesthesia and reduce the risk of fatality.

c) Since there are age- and sex-related differences in biochemical marker levels, a separate reference range will be obtained and utilized to identify abnormal values. A separate reference range is required for repeat measurements performed at 7.5 weeks of age. In addition to a normal reference range, comparison with littermates will also be used to define abnormal bone phenotype.

d) Abnormal values are defined as 3SD (standard deviation) lower or higher than the age and sex matched normal reference range. We have chosen 3SD criteria because of the large between-subject differences in marker levels, and 5-10% values fall outside 2SD criterion.

Using the above guidelines, we have generated normal range data for 6-week-old (42-days) male and female C3H mice (with n=25 for each group). Weights were recorded using an electronic balance with measurement errors <0.01% at 25 g. All biochemical measurements were performed in blood collected between 1500-1600 hours. Serum samples were assayed in duplicate in single run to avoid the effect of between-run variation. Total BMD measurements were performed by DEXA using PIXImus. For soft-tissue regeneration (STR), a hole was punched in normal 3-week-old mice and the size of hole was measured after 1, 2, and 3 weeks. Details of all normal range data are given in Table 2. These data are critical for deciding whether a given offspring from an ENU treated male is mutant or normal.

Table 2. Normal Reference Range for Bone Density, STR, Muscle Mass, Weight, and Biochemical Markers.

Phenotype	Sex	Mean (n)	99% Confidence intervals
Weight (g)	Female	16.6 (25)	13.8 – 19.4
	Male	20.5 (25)	16.8 – 24.2
BMD (g/cm^2)	Female	0.04140 (25)	0.03489 – 0.04791
	Male	0.04161 (25)	0.03693 – 0.04629
Muscle mass (g)	Female	8.4 (25)	6 – 10.8
	Male	10.4 (25)	8.8 – 12
STR (mm)	Female	1.3 (14)	0.9 – 1.7
	Male	1.3 (23)	0.8 – 1.8

sALP (IU/L)	Female	180 (25)	120 – 240
	Male	148 (25)	98.8 - 197.2
Osteocalcin (ng/ml)	Female	176.5 (25)	91.9 - 261.1
	Male	180.7 (25)	132.2 - 229.2
C-telopeptide (ng/ml)	Female	9.2 (25)	3.8 - 14.6
	Male	21.2 (25)	8 - 34.4
IGF-I (ng/ml)	Female	253 (18)	119-387
	Male	282.4 (23)	203-362

d. Specific Objective 4: Adapt each phenotypic screen to be applied to large populations of mice.

To identify new dominant mutations, screening was carried out on the F1 offspring to identify bone and soft tissue phenotypes. Our main biochemical and bone density screens will be performed at 6 weeks of age. The rationale for selecting this age group was to screen for genes that affect bone density after pubertal growth phase when peak bone density is attained. In addition, any changes in bone turnover observed at this stage will have a long-term effect on bone density; therefore, mice with abnormal bone turnover can be followed up for an extended period (up to 12 months). Furthermore, age is critical in terms of housing cost of the mice, as it will affect the maximum number of mice that are housed at a given time. Our estimates indicate that primary screening performed at 6 weeks of age will substantially save the housing cost, as compared to 8-12 weeks of age, without significantly compromising the effectiveness of phenotype screens.

Our screening strategy incorporates body growth, soft-tissue regeneration, and bone density. The following screening strategy has been formulated for identifying the above-mentioned phenotypes:

1) At days 1-21:

To systematically screen for anomalies identifiable at birth and during weaning, cages will be inspected daily for litters. The following observations will be recorded: a) stillbirths; b) litter size; c) deaths between birth and weaning; and d) each animal will also be examined for obvious visible anomalies.

Size of littermates (weight, length, and size of head & limbs), weight, and length of each offspring is recorded on day 7. Weight and length are compared with two littermates to identify abnormal values.

2) At day 21:

All F1 offspring are ear tagged for identification. F1 males and females are housed in separate cages in groups of 4 mice per cage. A hole is punched (2-mm) in each ear for STR monitoring.

3) At day 31:

The size of the ear hole is measured to monitor STR.

4) At day 42:

The size of the ear hole is measured to monitor STR. Between 1500-1600 hours, animals are sedated by injectable anesthesia and 200-250 μl blood is collected by retro-orbital sinus

puncture. Blood is transferred to small tubes (1.0-ml capacity) with clot activating gel and stored at 4°C until the serum has separated. Serum is aliquoted in 2-3 aliquots and stored at–70°C for biochemical analysis. BMD and muscle mass measurements are performed during this period using PIXImus. Animals are kept warm and frequently recover within 30 to 60 minutes.

5) At day 56:

In order to confirm a bone phenotype, blood is collected when the animals are 52-56 days old. Blood is collected, as described above, and bone density measurements repeated at this time using PIXImus. Biochemical tests were performed on the serum and compared with age- and sex-matched normal range data, and with at least two littermates, to confirm the phenotype. After confirmations of biochemical test, all animals are back crossed with wild type C3H male or female animals.

6) Aging phenotypes:

Mice with abnormal bone turnover will be kept for extended periods (12-18 months), during which period bone density measurements will be repeated several times to detect long-term effects of altered bone turnover on changes in BMD or BMC.

7) Data Processing:

All results on phenotype screens are currently entered in Excel spreadsheets and pictures of mice with dismorphologic features are stored on CD-ROM. For mouse colony maintenance and phenotype data management, a network based computer program COLONY (Locus Technology, Inc., Orland, ME) is currently procured. The software can be used for storage and retrieval of phenotype and genotype data, list of animal characteristics, breeding record, weaning dates, litter history, storing images, etc. Data currently stored in the Excel spreadsheets will be transferred to the COLONY database.

We have, thus far, generated 456 F1 offspring. Phenotypic screens are in progress as planned. The data on mutant phenotypes will be reported in the next progress report.

3. Key Research Accomplishments

- Optimal ENU dosage and time of sterile/fertile period have been determined in C3H/HeJ mice.
- Bone phenotypic screens were developed and validated for mouse model.
- Optimum timing of blood collection was determined for biochemical measurements to allow for maximal reproducibility and sensitivity.
- A screening strategy was developed to identify bone in a large population of F1 progeny.
- We have generated 456 F1 offspring that are being screened for bone and soft tissue phenotype abnormalities.

4. Reportable Outcomes

a) Srivastava AK, Bhattacharyya S, Castillo G, Miyakoshi N, Mohan S and Baylink DJ (2000) Development and evaluation of C-telopeptide enzyme-linked immunoassay for measurement of bone resorption in mouse serum. Bone 27(4).
b) Srivastava AK, Castillo G, Wergedal JE, Mohan S and Baylink DJ (2000) Development and application of a synthetic peptide-based osteocalcin assay for the measurement of bone formation in mouse serum. Bone, volume 67, In press.

c) Srivastava AK, Bhattacharyya S, Li X, Mohan S and Baylink DJ (2000) Circadian and longitudinal variation of serum C-telopeptide, osteocalcin, and skeletal alkaline phosphatase in C3H/HeJ mice. Submitted to Bone.
d) Paper presented at the 22nd Annual American Society for Bone and Mineral Research Meeting in Toronto, Canada.

5. Conclusions

We have developed, validated, and adapted all biochemical screens for mouse model. In addition, we have determined, through an extensive biological variation study, the optimal sampling time for biochemical measurements. We have then synchronized the phenotype screens by performing bone density and biochemical screens under one episode of anesthesia. Consequently, we have achieved our primary objective of developing, validating, and optimizing the phenotype screening procedure.

We have tested six different doses of ENU on seven different batches of male C3H mice. Although these experiments are still under progress, our preliminary results strongly suggest that three weekly injections of 90 mg/kg ENU is highly effective in producing a large number of mutants. This will accomplish our second main objective of identifying the optimum ENU dosage.

Finally, we have developed a screening strategy, which will effectively screen body growth, soft tissue, and bone phenotypes, in F1 progeny.

6. References

1. Beamer, W. G., Donahue, L. R., Rosen, C. J. and Baylink, D. J. Genetic variability in adult bone density among inbred strains of mice. Bone 18(5): 397-403; 1996.
2. Justice, M. J., Carpenter, D. A., Favor, J., Klaus, N. A., Angelis, M. H., et al. Effect of ENU dosage on mouse strains. Mammalian Genome, 11:484-488; 2000.
3. Srivastava, A. K., Bhattacharyya, S., Castillo, G., Wergedal, J., Mohan, S. and Baylink, D. J. Development and application of a serum C-telopeptide and osteocalcin assay to measure bone turnover in ovariectomized rat model. Calcif Tissue Int 60:435-442; 2000.
4. Srivastava, A. K., Castillo, G., Wergedal, J. E., Mohan, S. and Baylink, D. J. Development and application of a synthetic peptide-based osteocalcin assay for the measurement of bone formation in mouse serum. Calcif Tissue Int 66; 2000 (In press).
5. Farley, J.R., Hall, S.L., Herring, S., and Tarbaux, N.M. Two biochemical indices of mouse bone formation are increased, in vivo, in response to calcitonin. Calcif Tissue Int 50(1):67-73; 1992.
6. Mohan, S., and Baylink, D. J. Development of a simple valid method for the complete removal of insulin-like growth factor (IGF)-binding proteins from IGFs in human serum and other biological fluids: comparison with acid-ethanol treatment and C18 Sep-Pak separation. J Clin Endocrinol Metab 80:637-47; 1995.

7. Appendices

Appendix 3-1:
Srivastava AK, Bhattacharyya S, Castillo G, Miyakoshi N, Mohan S and Baylink DJ (2000) Development and evaluation of C-telopeptide enzyme-linked immunoassay for measurement of bone resorption in mouse serum. Bone 27(4).

Appendix 3-2:
Srivastava AK, Castillo G, Wergedal JE, Mohan S and Baylink DJ (2000) Development and application of a synthetic peptide-based osteocalcin assay for the measurement of bone formation in mouse serum. Bone, volume 67, In press.

Appendix 3-3:
Srivastava AK, Bhattacharyya S, Li X, Mohan S and Baylink DJ (2000) Circadian and longitudinal variation of serum C-telopeptide, osteocalcin, and skeletal alkaline phosphatase in C3H/HeJ mice. Submitted to Bone.

Appendix 3-4:
Srivastava AK, Bhattacharyya S, Castillo G, Li X and Baylink DJ (2000) Circadian rhythms of serum C-telopeptide, osteocalcin, and skeletal alkaline phosphatase. Presented at 22nd Annual American Society for Bone and Mineral Research meeting, Toronto, Canada, September 22-26th.

Microarray analysis of gene expression of a congenic strain that contains a QTL locus of bone density in mice

W.K. Gu[1], X.M. Li[1], K-H.W. Lau[1], B. Edderkaoui[1], L. R. Donahae[2], C. Rosen[3], W.G. Beamer[2], S. Mohan[1], D. J. Baylink[1]

[1] Musculoskeletal Disease Center, JL Pettis VA Medical Center and Loma Linda University, Loma Linda, CA. [2] The Jackson Laboratory, Bar Harbor, ME. [3]St. Joseph Hospital, Banger, ME. USA

Running head: Gene expression of high bone density QTL locus

Corresponding Author: David J Baylink, MD., Musculoskeletal Disease Center, JL Pettis VA Medical Center, 11201 Benton Street (151), Loma Linda, CA 92357, USA

Tel: (909) 422-3101
Fax: (909) 796-1680
E-Mail: David.Baylink@med.va.gov

Abstract

Osteoporosis is a debilitating bone disease that afflicts 30 million people in the U.S. Peak bone density is an important determining factor of future osteoporosis. We have previously identified a QTL locus on mouse chromosome 1 that contributes to approximately 40% of the total variation of bone density between C57BL/6J (B6) and CAST/EiJ (CAST) strains. We have also produced a congenic strain in which the chromosome 1 fragment containing this QTL locus has been transferred from CAST (donor) to the congenic mouse strain of B6 background. In order to analyze the mechanism controlling the bone density and to identify candidate genes of the QTL locus, we have conducted microarray analysis with the RNA from both congenic and control mice, B6. The isolated mRNA from femurs of both congenic and B6 strains were labeled with different dyes and hybridized onto the same microarray chip containing 8734 genes and ESTs of GEM1 from Incyte genomic inc. This analysis revealed that 134 genes and ESTs showed at least 2-fold difference between the congenic and the B6 strain. Among these candidates, 32 are known genes and 13 are ESTs with similar known genes, and 89 are ESTs without known similar genes or function. Analysis of the 45 known candidates indicated that expression level of several important genes of bone formation in B6 is higher than that of congenic. In contract, genes inhibiting bone resorption have a higher level of expression in congenic mice. Based on these results, a model of low rate of bone turnover of the congenic mice is proposed. This study provides a fundamental information on the mechanism of high bone density of the QTL locus on mouse chromosome 1. The information is useful to us for searching candidate genes of the QTL locus during positional cloning and for biological function testing of genes and drugs using B6 and congenic mice.

Introduction

Osteoporosis is one of the most prevalent diseases affecting millions of people worldwide. Peak bone density is considered as one of the strongest determinants of subsequent osteoporotic fractures. More than 70% of the variability in human bone density has been attributed to genetic factors. Therefore, understanding the genetic mechanism of the bone density is essential for prediction and treatment of the osteoporosis.

Using mouse model, we have identified 6 QTL loci of the peak bone density using a F2 population from C57BL/6J (B6) X CAST/EiJ (CAST) (Beamer et al., 1999). Dissection of individual QTL locus revealed different effect on the bone density of each such locus. However, none of molecular base of any locus has been known. Recently, we developed several congenic strains that contain each individual QTL region. In particular, we have a congenic strain containing the QTL region on chromosome 1. The QTL locus contributes to approximately 40% of the total variation of bone density between CAST and B6, and it has the LOD score of 8, which is the strongest of 6 QTL loci. To further dissect and narrow down this QTL locus, we transferred a fragment on chromosome 1 that contains the QTL locus from CAST (donor) to the B6 (recipient) background. Accordingly, only the QTL region of the congenic strain differs from the control, e. g. the B6 mouse.

The congenic strain not only provides us a suitable strain to confirm the phenotype of this particular QTL locus, but also give us the opportunity to study the molecular bases of this QTL locus. Theoretically, any difference of the gene expression that is related to bone density between congenic and B6 is caused by the QTL locus. However, because it is most likely that the QTL

gene will cause changes of expression of a series of genes in its pathway which include down and up regulated genes. In reality, we expect the change of expression level will happen to a group of genes rather than a particular gene. Therefore, analysis of the profile of gene expression between congenic and B6 mice will provide information which may be used to predict the functional mechanism of the QTL gene and the possible pathway of the high bone density, and finally, to search and select candidate genes.

DNA microarrays, which are microscopic and physically ordered arrays of thousands of DNAs of known sequences attached to solid surfaces, are most suitable to analysis of gene expression between B6 and congenic mice. Microarrays have been used for a wide scope of applications, including sequencing, detection of mutations or polymorphisms, identification of drug targets, and gene expression profiling (reviewed by Wilgenbus and Lichter 2). The latter application has gained wide use for monitoring differences in gene expression patterns in normal versus pathological conditions. Particularly, the use of two-color simultaneously analysis of profiles of gene expressions from two samples provides us a unique opportunity to the mechanism of the high bone density in the congenic mice.

This study is to analyze the molecular mechanism of the QTL on chromosome 1 using microarray analysis to address several questions: which genes are highly expressed in the femurs, which genes are expressed differently between the congenic and B6 mice, and what molecular mechanism in congenic leads to the high bone density.

Materials and methods

Animals

Mice from congenic strain, C-T, which contains the QTL locus for bone density on chromosome 1 and the control strain, C57BL/6J (B6), were used for this study. For the phenotypic measurement, both congenic and B6 mice were produced and maintained in the research colony under 14:10 hr. light:dark cycle in The Jackson Laboratory (JAX). Autoclaved diet NIH-31 with 6% fat and HCI acidified water (pH 2.8-3.2) were provided ad libitum. For the microarray experiment, Both congenic and B6 strains were housed at the Animal Research Facility, JLP VA Medical Center, under the same condition as in JAX.

Bone density measurement

According to our previous study (W. Beamer 1999), the biggest difference between the high and low bone density of different mouse strains achieved at the age of 4 months. Therefore, bone measurement of congenic and B6 strains was conducted with femurs from mice at 4 months of age. Before measurement of the phenotype, genotype of the congenic strain was confirmed with the microsatellite markers along the QTL region (Beamer et al 1999). Bone density of femurs was measured by peripheral quantitative computerized tomography (pQCT) with a Stratec XCT 960M (Norland Medical Systems, Ft. Atkinson, WI). Total bone density of congenic mice then was compared to that of B6 strain.

RNA preparation

RNA was extracted from femurs of congenic and B6 mice of both 14 and 6 weeks of age. We extracted RNA from femurs with a modified procedure of Life Technologies using Trizol reagent. In our procedure, femurs and Trizol reagent were first ground in a 6750 Freezer Mill machine from SPEX Centtiprep Inc (Metuchen, NJ). The concentration and the quality of the total RNA were checked by measuring 260/280 absorption ratio using a Spectronic Genesys spectrophotometer from Spectronic Instruments (Rochester, NY), and by electrophoresis on 1% agarose gel. Then we followed the recommend procedure from Incyte to isolate polyA RNA from high qualified total RNA. To purify the mRNA, we double passed the mRNA over OligoTex mRNA isolation columns from Qiagen. After the elution of the polyA RNA, we conducted an ethanol precipitation, so the final product is brought up in TE in an Ambion Siliconized RNase-Free Microfuge Tubes 1.5ml size. Finally, we quantified mRNA on the Spectronic Genesys spectrophotometer.

Microarray hybridization

We used the Incyte commercial service for our probe labeling and microarray hybridization. We used the mRNA at the concentration of 50ng/μl for microarray hybridization. Samples from the congenic and B6 mice are sent to Incyte Genomic Inc. for microarray hybridization, where mRNA from congenic and B6 mice were labeled with Cy5 and Cy3 respectively and hybridized on to the same microarray set, the Mouse GEM1 microarray. The Mouse GEM1 microarray chips contians containing 8739 genes and ESTs selected from the NCBI's UniGene database. Detailed information of these clones and the hybridization procedure can be obtained from *www.genomesystems.com*.

Microarray data analysis

Data from microarray experiment was analyzed with software GEMTools (Version 2.4. 1a) from Incyte genomic Inc. The relative strength of the signal of both samples are balanced according to the overall signal area and the strength. Based on the reproducibility study of the GEM1 microarray (Incyte technical survey, Incyte genomic Inc., 1999), the reliable level of differential expression ratio is 1.75. In this study, The balanced differential ratio more than 2 folds is initially chosen as the threshold for considering as real difference of the expression between the congenic and B6.

Data search for gene expression and function: We search through the PubMed (www.ncbi.nlm.nih.gov/entrez/query.fcgi?db=PubMed) for literature reports on the expression and function of genes that are interested in this study. To search if a gene is expressed in the bone, we retrieved the publications that are contain key words: "(gene name) and bone and expression" in title/abstract words. To search the function of a gene, we used the key words "(gene name), bone, formation/resorption, and function.

Result

Bone density between B6 and congenic mice.

Total of 13 congenic and 15 B6 controls at 4 months of age were used for the measurement of bone density. As indicated in the table 1, there is no significantly difference on the body weight and the length of the femur between the congenic and the B6 mice. While the total bone density and the cortical density of femurs from congenic mice are significantly higher than that of the B6 (0.536±0.007 vs 0.496±0.006 and 0.657+0.006 vs 0.631+0.004, respectively). The increased bone density in the congenic mice appears due to the increased size of the bone, as indicated by the larger periosteal circumference.

Microarray analysis

We first conducted the microarray experiment with the RNA from mice of 14 weeks. Then a second experiment using RNA from mice of 6 weeks was to confirm the different expression of genes and ESTs in the first experiment. Therefore, our analysis is mainly based on the first experiment, and whenever necessary, we use the second to confirm the result. By using vary measures, Incyte Genomic Inc. has ensured that the total variability in measurement is limited to less than 15%. As shown in table 2, the relative signal intensity of empty wells in the first experiment can reach up to 200 while the spots contains 0.2X SSC have level between 28-48. In our study, we consider the samples that have the signal level higher than 800 as the valuable expression data for analysis. This criterion is 4 times higher than that of the maximum value of the empty wells and ten times higher than that of the SSC controls. Accordingly, using B6 of 14 weeks as the standard sample in the experiment, we counted that 5998 out of all 8724 genes and ESTs have the expression levels that are higher than 800. According to this data, about 75% of total genes in this study are expressed in the femurs. Among these 5998 genes and ESTs, most of them (5633) have the signal levels between 800 and 5000. Only few of them (93) reached very high level.

Among the 93 highly expressed genes and ESTs in the B6, 27 are ESTs without known function or similar genes. The rest 66 are genes or ESTs with known similar sequences of genes (Table 3). By literature searching, as date of July 25, 2000 from the PubMed, 30 are known related to bone or skeletal development. Based on this data, our microarray analysis revealed two third of

new genes that are either not being studied for their expression in the bone, or have not been treated as the important/highly expressed genes in the skeletal development. Among highly expressed genes, we found that most of them are structural (such as procollagen, type I, alpha 1, hemoglobin alpha, adult chain 1, and H3 histone, family 3A) and house-keeping genes (such as replication protein A2 eukaryotic translation elongation factor 1 alpha 1, nuclear receptor binding factor 1). However, major growth factors are not among these highly expressed genes. Some of important genes in the bone, such as the bone morphological genes (BMPs), calcium binding protein, and insulin-like growth factor 1 have moderate expression levels. Their fluorescence absorption levels are around 1000 (Data not shown in Table 2). It is quite common that some regulatory genes are not necessary have a very high level of expression, nevertheless, the gene the produces the most products during bone development is the important one.

Comparison of gene expression between femurs of congenic and B6 mice.

The expression patterns of most of the genes between congenic and B6 mice are similar. Statistical comparison of gene expression of total 8734 genes and ESTs between B6 and congenic mice using Analysis of Variance (ANOVA) indicated that they have the similar pattern (P= 0.468207) (Figure 1). The difference on the expression of majority genes (8007) between these two strains is within the +1.5 to –1.5 folds. The expression levels of a total of 134 genes and ESTs have 2 (some are ~1.8 or higher) folders or higher difference between B6 and congenic mice (data not shown). The two genes that have the largest difference between B6 and congenic strains are the procollagen, type I, alpha 1 (B6 vs Congenic: +3) and an EST (B6 vs Congenic: -4.4). Among these 134 samples, most of them are expressed at moderately level, with light intensity around 1000. While 12 have the expression level higher than 5000. 89 of these

differently expressed samples are ESTs that do not have known function. Only 45 are known genes or ESTs with similar gene sequences (Table 3), The expression of these genes was also analyzed with the mice of 6 weeks. Comparison of the result of these two experiments using ANOVA (single factor), we found that they are highly similar, P= 0.949757.

Several evidence indicated that bone turnover activity in congenic mice is lower than that in B6 mice.

As indicated in table 4, several important genes for bone formation have higher expression levels in B6 than that in congenic mice. 1) Osteoblast specific factor 2, a direct indicator of the activity of the osteoblast, is expressed three times higher in B6 than that in congenics. 2) An important enzyme to the activity of osteoblast, catenin beta is expressed almost three folds higher in B6 than in congenic. 3) Several genes playing important roles in the pathway of bone formation are expressed highly in B6, such as Ras related protein RAB-6, secreted phosphoprotein 1. 4) As the result, expressions of major collagen genes are higher in B6 than in congenic (Table 4). The high expression level of myosin light chain 2 reflects the co-effect of the high bone formation on muscle in the B6 mouse.

Bone resorption in B6 is also higher than that in congenic (Table 5). The fibronectin 1, an important regulator and stimulate of the osteoclast, is highly expressed in B6. The negative regulators of the osteoclast, the SHP1, tyrosine phosphatase, Ras-binding protein SUR-8, cytochrome P450, and transforming growth factor beta binding protein 1 have a lower expression level in B6. These results indicated that the bone resorption activity in the B6 is higher than that in congenic mice.

There is no significant difference at expression levels of major growth factors that regulate the bone formation between the two strains. Table 5 lists their expression ratio between B6 and congenic mice. Among them, transforming growth factor (TGF) beta is known as an important growth regulator and modulator in bone. Bone morphogenetic BMPs, members of TGF-beta superfamily, are known to regulate proliferation, differentiation, and apoptosis of osteoblasts during bone development. Insulin-like growth factor 1 (IGF1) and parathyroid hormone (PTH) receptor are also important regulator and stimulator of bone formation. Protein alkaline phosphatase (ALP) is a bone formation marker.

Discussion

Our data indicated that the high bone density in the congenic mice is a result of low bone turnover rate. Bone is a dynamistic tissue in which the bone formation and resorption are constantly conducted. Accumulation of the bone is a result of net income between the bone formation and resorption. Therefore, high bone density can be achieved by a higher rate of bone formation, lower rate of bone resorption, and low rate of bone turnover. In this study, we found that the expressions of important genes of bone formation in the B6 are higher than that of congenics. Particularly, the procollagen, type I, alpha 1, which is a clear indicator of the bone formation rate, expressed highly in B6 mice. We therefore conclude that the high bone density in the congenic mice is not gained through the high bone formation rate. When we examine the genes that regulate the bone resorption, we found the evidence indicating that the bone resorption in the congenic is lower than that in B6. Several bone resorption inhibitors are highly expressed

in the congenic mice. An example is the (TGF-beta) binding protein, which binds the TGF and influence its availability in bone and other connective tissues, is two folders higher in the congenic than that in the B6. While the expression level of TGF-beta is similar between the congenic and B6 (Table 4). Accordingly, we propose that the higher bone density of the congenic mouse is obtained through the decreased bone turnover in which the bone resorption is actively regulated. The QTL gene trige the pathway that decreases the activity of the osteoclast (Figure 2). The lower activity of the osteoblast is a passive response to the decreased activity of the osteoclast. As the result, the net gain of the bone from this procedure is higher than a high bone turnover model.

The gene expression profiles between B6 and congenic mice provide us important information for candidate gene search. Parallel to this study, we have already constructed a contig of the QTL peak region using BAC library. The contig is currently being sequenced by by the Advanced Center for Genome Technology at University of Oklahoma (ACGTUO). The information in this study will be very useful for us to analyze the genes from the genomic sequences of the contig. First, it allows us to focus on the genes that regulate the bone resorption. At present, we do not find any known gene to be particular interested candidate within the QTL region. This means that we will search a quite large number of candidates when the genomic sequence of the QTL region is available. With the information of microarray analysis, we will eliminate a large number of the genes from our priority list. By sequence comparison and analysis, we will first group the genes according to their possible function. Then we can eliminate growth factors that regulate bone formation, house keeping, and structure genes from list of candidates. Secondly, the level of expression of those genes in the microarray analysis that expressed differently between the B6 and congenic mice may be used as the molecular markers

for the *in vitro* function study during our candidate gene screening. Thirdly, with more information in the future, we will be able to further establish a complete biopathway of the gene that regulates the bone turnover.

Our data supports the theory that derived from human study that high bone turnover is a risk factor for spinal fracture and osteoporosis. In the mouse study to compare the bone density of 12 different strains, Beamer et al (1997) found that B6 has the lowest bone density, which may equivalent to the lower bone density population of humans, which have high risk to develop osteoporosis in the late stage of life. In order to address the importance of bone turnover in human population, Garnero et al. (1996) measured a battery of new sensitive and specific markers of bone turnover in a population-based study of 653 healthy women. They found that high bone turnover is associated with a greater rate of bone loss. In a study of rheumatoid arthritis (RA), Gough et al. (1998), reported that the osteoclastic activation, rather than suppression of bone formation, is the dominant process leading to bone loss in early RA. In the study of a group of 366 healthy, white postmenopausal women, aged 50-81 years, Ravn et al. (1997) found a strong association among high bone turnover, low bone mass, and prevalence of spinal fracture.

Considering the similar difference between the B6/congenic mice and the low/high bone density human population, the B6 and congenic strains may be an ideal pair of mouse model to study the treatment of osteoporosis. Though more than 15 QTL loci of bone density have been identified using mouse model, the mechanism of these loci have not been described. To our knowledge, this is the first report on the molecular basis of the bone density of a particular QTL locus, which represents the difference between two normal population groups rather than a mutation or a deletion. Furthermore, there are several characters that make this pair to be a very

useful one. The difference of bone density between the two strains is not dramatically but detectable. This situation is most common in human populations. The genetic background between the two strains is identical except the QTL locus. Therefore experimental error can be minimized. Because of the heterozygosity and the large environmental, the effects of drugs on treatment and prevent of osteoporosis using human population have been complicated. In addition, the rate of bone formation, resorption, and turnover can be precisely detected with known molecular markers from the microarray analysis. Considering all above, they may be ideal pair for drug testing.

In spit of the important information provided from this study, we recognize that our study still has some limitation. 1). Though we analyzed more than 8000 genes in this study, they are sill a small portion of the total mouse genome. Our interpretation on the mechanism of the difference of bone density between these two strains is limited to the information from these genes. 2). Due to the expenses of the experiment, we only repeated once to confirm the expression of some important genes. 3). We also realized that difference between expression level of a gene is not correlated to activity and impact of function of a gene. Furthermore, some times, the transcription level may not represent the actual translation level of a gene. However, we only used the expression level as the measurement of activity, which may mislead us in some cases.

In summary, we have analyzed the molecular bases of the high and low bone density between the B6 strain and the congenic strain that contains a QTL locus that cause the high bone density. The information of this study will be greatly helpful in the identification of candidate genes of high bone density and function study of candidate and other genes.

Table 1. Phenotypic comparison between congenic and B6 at 4 months of age.

Strain	Body weight (g)	Femur length (mm)	Total density[b] (mg/.mm3)	Cortical density[a] (mg/mm3)	Periosteal circumfer-ence[b] (mm)	Endosteal circumfer-ence (mm)
Congenic (13)	20.7+0.5	15.5+0.1	0.536+0.007	0.657+0.006	4.841+0.041	2.751+0.033
B6 (15)	21.8+0.8	15.4+0.2	0.496+0.006	0.631+0.004	4.580+0.116	2.671+0.074

a=<0.05; b=<0.01

Table 2. Variation of expression levels of genes and ESTs in the B6

Full Name / # of genes	Expression signal level*
Positive control #1, 4 replicates	1488-2041
Positive control #2, 4 replicates	5555-8306
Positive control #3, 4 replicates	39465-48791
Negative control #1, 8 replicates, 0.2X SSC	28-48
Empty controls, 15 replicates	55-205
Positive control #4, 24 replicates	13631-29590
Mouse genes and ESTs: 2736	<800
Mouse Genes and ESTs: 5998	>800
Mouse Genes and ESTs: 407	>5000
Mouse Genes and ESTs: 93	>10,000

*The level of expression of a gene is measured by the relative intensity of the signal level read by the scanner for the Cy3 channel

Table 3. Highly expressed genes detected from the femurs of the mice

Signal level	Gene names and Image #	Expression in bone
37381	procollagen, type I, alpha 1 {IMAGE:536306}	Bone formation
33877	Mus musculus mRNA for N-acetylglucosamine-6-O-sulfotransferase, complete cds {IMAGE:920327}	X
32419	lactotransferrin {IMAGE:874383}	Bone marrow
29700	CD24a antigen {IMAGE:421150}	bone marrow and liver
28359	ESTs, Highly similar to HYPOTHETICAL 44.2 KD PROTEIN IN SCO2-MRF1 INTERGENIC REGION [Saccharomyces cerevisiae] {IMAGE:524792}	X
27466	ESTs, Highly similar to MATERNAL EFFECT PROTEIN STAUFEN [Drosophila melanogaster] {IMAGE:533314}	X
26834	ESTs, Moderately similar to PTD017 [H.sapiens] {IMAGE:481469}	X
24486	hemoglobin alpha, adult chain 1 {IMAGE:571819}	fetal liver, spleen, and bone marrow
22923	H3 histone, family 3A {IMAGE:776614}	X
22792	nuclear receptor binding factor 1 {IMAGE:735186}	Bone ?
21600	heparin cofactor II {IMAGE:693170}	X
21503	glyceraldehyde-3-phosphate dehydrogenase {IMAGE:579715}	Bone
20392	solute carrier family 4 (anion exchanger), member 1 {IMAGE:422440}	X
19642	carbonic anhydrase 2 {IMAGE:579391}	Osteoclast
19615	tubulin alpha 4 {IMAGE:329726}	bone marrow stromal cells
19485	histocompatibility 2, L region {IMAGE:920425}	T cell
19215	interferon gamma receptor {IMAGE:920516}	Bone marrow
18314	solute carrier family 4 (anion exchanger), member 1 {IMAGE:407275}	X
17889	histocompatibility 2, L region {IMAGE:694651}	bone marrow
16708	secreted phosphoprotein 1 {IMAGE:571759}	Bone
16004	ESTs, Moderately similar to PHOSPHATIDYLINOSITOL [Homo sapiens] {IMAGE:761041}	Osteoclast
15396	S100 calcium binding protein A8 (calgranulin A) {IMAGE:669813}	bone/teeth
15338	eukaryotic translation elongation factor 1 alpha 1 {IMAGE:735225}	X
15169	ESTs, Highly similar to DRIM protein [H.sapiens] {IMAGE:616975}	X
14295	interferon dependent positive acting transcription factor 3 gamma {IMAGE:747655}	bone resorption?
14264	hemoglobin alpha, adult chain 1 {IMAGE:696858}	bone marrow and fetal liver
13781	aquaporin 1 {IMAGE:656654}	X
13709	ribosomal protein l3 {IMAGE:570533}	*
13270	glucose phosphate isomerase 1 complex {IMAGE:776210}	X
12963	Mus musculus mRNA for Zinc finger protein s11-6, complete cds {IMAGE:331386}	Osteobalst
12861	lipocalin 2 {IMAGE:493658}	bone
12601	Bcl-associated death promoter {IMAGE:423721}	X
12549	peptidylprolyl isomerase A {IMAGE:920055}	X

12501	vesicle-associated membrane protein 3 {IMAGE:818971}	X
12472	uncoupling protein 2, mitochondrial {IMAGE:748112}	X
12419	CCAAT/enhancer binding protein (C/EBP), alpha {IMAGE:738252}	Osteoblast
12403	ESTs, Weakly similar to /prediction {IMAGE:525168}	X
12376	myeloperoxidase {IMAGE:367693}	hematopoietic cells, Bone marrow
12283	RAD21 homolog (S. pombe) {IMAGE:959708}	X
12070	Mus musculus endothelial monocyte-activating polypeptide I mRNA, complete cds {IMAGE:669969}	osteoblast
12044	beta-2 microglobulin {IMAGE:572542}	bone
11909	RAB11B, member RAS oncogene family {IMAGE:733701}	bone
11803	hexokinase 1 {IMAGE:318642}	X
11580	ADP-ribosylation factor 1 {IMAGE:720444}	X
11386	coproporphyrinogen oxidase {IMAGE:734795}	X
11356	calponin 2 {IMAGE:695687}	muscle
11311	tubulin, beta 5 {IMAGE:333325}	Bone marrow bone marrow, spleen, developing liver and lung
11297	RNA binding motif protein 3 {IMAGE:467238}	*
11202	aminolevulinic acid synthase 2, erythroid {IMAGE:439199}	X
11193	myeloperoxidase {IMAGE:465816}	myeloid cells
11056	enolase 3, beta muscle {IMAGE:316967}	muscle?
11009	replication protein A2 {IMAGE:717102}	*
10991	ATPase-like vacuolar proton channel {IMAGE:776055}	osteoclast
10982	neuroblastoma ras oncogene {IMAGE:333030}	X
10942	cathelin-like protein {IMAGE:334755}	host defense and wound repair
10890	Mus musculus heterogenous nuclear ribonucleoprotein A2/B1 (hnRNP A2/B1) mRNA, complete cds {IMAGE:315740}	*
10864	ESTs, Highly similar to SUCCINATE DEHYDROGENASE [Homo sapiens] {IMAGE:776319}	X
10788	ESTs, Highly similar to ARP2/3 COMPLEX 16 KD SUBUNIT [H.sapiens] {IMAGE:355211}	X
10738	Mus musculus mRNA for cathepsin Z precursor (ctsZ gene) {IMAGE:330668}	X
10587	thioredoxin peroxidase 1 {IMAGE:579867}	X
10503	Mus musculus mRNA for synaptotagmin XI, complete cds {IMAGE:752465}	X
10451	Mus musculus myosin light chain 2 mRNA, complete cds {IMAGE:466382}	muscle
10268	Mus musculus Btk locus, alpha-D-galactosidase A (Ags), ribosomal protein (L44L), and Bruton's tyrosine kinase (Btk) genes, complete cds {IMAGE:437469}	B cell
10247	calpactin I heavy chain {IMAGE:420429}	X
10206	Mus musculus mRNA for heterogeneous nuclear ribonucleoprotein H {IMAGE:426163}	*
10032	ESTs, Moderately similar to CHLORINE CHANNEL PROTEIN P64 [Bos taurus] {IMAGE:317868}	X

Table 4. Known genes differently expressed between B6 and congenic mice

Name	Expression ratio B6/congenic* (14 weeks)	Expression ratio B6/congenic*(6 weeks)	Possible function in bone formatoin/resorption
EST, Moderately similar to putative pheromone receptor	-2.1	-4.4	expression in the vomeronasal epithelium cells related to the Ca2+-sensing receptor mediates an adaptive response to pheromone olfactory epithelium (MOE) and the vomeronasal organ (VNO).
cytochrome P450, 2j6	-2.1	-1.6	involved in the oxidation of fatty acids (**Ma et al., 1998**)
ESTs, Highly similar to CYTOCHROME P450 IVF3	-2.2	-2.7	Cytochrome P-450 inhibition blocks bone resorption in vitro and in vivo. Otolaryngol
cytochrome P450, 2b19 {IMAGE:473877}	-1.8	-2.3	125 vitamin D biosynthesis (**Miller& Portale, 1999**)
cytochrome P450, steroid inducible 3a11 {IMAGE:748318}	-1.8	-4.1	elevated 1,25(OH)2D levels, acting through the vitamin D receptor, were responsible for the observed accumulation of osteoid (**St-Arnaud** et al., 2000)
ESTs, Moderately similar to HYPOTHETICAL 97.6 KD PROTEIN IN SHP1-SEC17 INTERGENIC REGION	-2.6	-2.0	Cytokine signaling SHPI up, TNF alpha down.
tumor necrosis factor (ligand), Superfamily 13b {IMAGE:803594}	-2.1	-1.9	Non soluble (B-cell activating factor)
ESTs, Moderately similar to ZINC FINGER PROTEIN	-2.4	-2.1	to prevent the expression of neuronal genes in non-neuronal cell types or in inappropriate neuronal subtypes
Mus musculus mRNA for Zinc finger protein s11-6, complete cds {IMAGE:722568}	-1.9	-1.7	
ESTs, Weakly similar to LATENT TRANSFORMING GROWTH FACTOR BETA BINDING	-3.9	-2.6	bind latent transforming growth factor beta (TGF-beta) and influence its availability in bone

PROTEIN 1 PRECURSOR [Rattus norvegicus] {IMAGE:424525}			and other connective tissues.
ESTs, Weakly similar to Ras-binding protein SUR-8 [M.musculus] {IMAGE:681010}	-2.1	-1.7	enhances MAP kinase activation and forms a complex with Ras and Raf. activity by Ras(DN) overexpression rapidly induced the apoptosis of osteoclast-like cells (OCLs) formed in vitro
mitogen activated protein kinase kinase 7 {IMAGE:750360}	-2.1	-2.3	Many of the biological activities of FGF-2 have been found to depend on its receptor's intrinsic tyrosine kinase activity and second messengers such as the mitogen activated protein kinases
hyaluronan mediated motility receptor (RHAMM) {IMAGE:424197}	-2.6	-2.0	to play a fundamental role in locomotion of ras-transformed cells as well as functioning in signal transduction role for RHAMM in malignant invasion and metastatic growth
immunity-associated protein, 38 kDa {IMAGE:748015}	-3.0	-2.6	-
ESTs, Moderately similar to betaine homocysteine methyl transferase [M.musculus]	-2.8	-2.5	catalyzes the second pathway in methionine and S-adenosylmethionine (SAM) biosynthesis
ESTs, Moderately similar to CGI-83 protein [H.sapiens] {IMAGE:777403}	-3.1	-2.8	The balance between free CGI and that bound to Tamm-Horsfall protein may be important in the overall balance of urinary macromolecules that affect calcium oxalate nephrolithiasis.
ESTs, Weakly similar to envelope polyprotein [M.musculus] {IMAGE:621991}	-3.1	-2.1	-
Murine (DBA/2) mRNA fragment for gag related peptide {IMAGE:717197}	-2.7	-2.8	component of palate (**Foreman** et al., 1991)
sulfotransferase, hydroxysteroid preferring 2 {IMAGE:748540}	-3.7	-2.5	specific on nonpeptide hormones such as estogen, corticoid.
transcription termination factor 1 {IMAGE:442415}	-2.9	-2.4	Involving VD3 pathway?

			(Haussler et al., 1997)
C-reactive protein, petaxin related	-2.3	-2.7	-
protein phosphatase, EF hand calcium-binding domain 2 {IMAGE:482001}	-1.9	-2.1	May related to reduction of bone formation (Goad et al., 1992)
coproporphyrinogen oxidase {IMAGE:570602}	-1.8	-2.2	the sixth enzyme in the biosynthetic heme pathway
coproporphyrinogen oxidase {IMAGE:419503}	-1.9	-2.1	-
solute carrier family 27 (fatty acid transporter), member 1 {IMAGE:482059}	-1.8	-1.9	-
carbonic anhydrase 5, mitochondrial {IMAGE:464556}	-1.8	-1.8	-
proteolipid protein (myelin) {IMAGE:426510}	-1.9	-1.9	
fibronectin 1 {IMAGE:597005}	1.8	1.8	fimbria-stimulated bone resorption is inhibited by human fibronectin
protein tyrosine phosphatase, receptor type, C {IMAGE:639168}	1.9	1.9	regulates osteoclast formation and function
ESTs, Highly similar to RAS-RELATED PROTEIN RAB-6 [Homo sapiens] {IMAGE:466099}	1.9	2.2	involvement of Ras/Raf/AP-1 in the BMP-4 signaling pathway.
DEAD (aspartate-glutamate-alanine-aspartate) box polypeptide 5 {IMAGE:680475}	2.0	1.7	-
eukaryotic translation elongation factor 1 alpha 1 {IMAGE:735225}	2.0	2.5	-
metallothionein 2 {IMAGE:643725}	2.0	1.9	-
capping protein alpha 1 {IMAGE:779754}	2.0	2.9	binds to the barbed ends of actin filaments in vitro and controls actin assembly and cell motility in vivo (Hart et al., 1997)
pyruvate dehydrogenase E1alpha subunit {IMAGE:820409}	2.0	2.3	Defects in the pyruvate dehydrogenase (PDH) complex are an important cause of primary lactic acidosis (Lissens et al., 2000)
ESTs, Highly similar to MATERNAL PUMILIO PROTEIN [Drosophila melanogaster] {IMAGE:803681}	2.0	1.6	-
ESTs, Moderately similar to tpr	2.1	1.7	nuclear pore complex

protein [H.sapiens] {IMAGE:789711}			associated
ESTs, Highly similar to FRUCTOSE-1,6-BISPHOSPHATASE	2.1	1.5	glycolysis and gluconeogenesis
Mus musculus myosin light chain 2 mRNA, complete cds {IMAGE:466382}	2.3	3.0	expression of the cardiac myosin light chain 2 (MLC2) gene is repressed in skeletal muscle as a result of the negative regulation
catenin beta	+2.2	+2.9	Important to actitivity of osteoblast
osteoblast specific factor 2	+2.9	+2.7	associated with the bone extracellular matrix after secretion by osteoblasts and participate in cell adhesion and/or cell communication
procollagen, type I, alpha 1	+3.1	+1.6	Bone formation
procollagen, type V	+2.5	+1.8	-
procollagen, type XI	+2.4	+1.7	stablize cartilage fibrils
procollagen, type III	+2.2	+1.8	-
secreted phosphoprotein 1	+2.2	+2.0	osteopontin Bone formation marker

* "+" = the expression level of B6 > congenic, "-" = expression level of B6 <congenic.
** This is the third highest value of differences between B6 and congenics among all tested genes and ESTs. ANOVA analysis B6 vs Congenic: P = 0.949757012

Table 5. Express of bone related genes between B6 and congenic mice.

Name	Expression ratio B6/congenic*	Expression ratio B6/congenic*
bone morphogenetic protein 5 {IMAGE:737934}	-1.1	-1.0
parathyroid hormone receptor {IMAGE:467172}	1.1	1.3
transformation related protein 53 {IMAGE:464741}	1.1	1.1
alkaline phosphatase 2, liver {IMAGE:465052}	1.1	1.1
alkaline phosphatase 2, liver {IMAGE:535409}	-1.1	1.4
transformation related protein 53 {IMAGE:464741}	1.2	-1.3
ATPase, Ca++ transporting, cardiac muscle, slow twitch 2 {IMAGE:695695}	1.3	1.6
CBFA2T3 identified gene homolog (human) {IMAGE:439477}	-1.1	-1.1
ESTs, Highly similar to PROBABLE CALCIUM-BINDING PROTEIN PMP41 [Mus musculus] {IMAGE:572282}	1.3	1.2
ESTs, Highly similar to 100 kDa thyroid hormone receptor associated protein [M.musculus] {IMAGE:577821}	1.2	1.2
ESTs, Weakly similar to RAS-LIKE PROTEIN 2 [Rhizomucor racemosus] {IMAGE:573845}	1.1	1.0
ESTs, Highly similar to thyroid hormone receptor-associated protein complex component TRAP150 [H.sapiens] {IMAGE:670557}	1.1	1.2
c-src tyrosine kinase {IMAGE:420269}	1.1	1.2

Figure legends:

Fig. 1. Distribution of the genes that are expression at different level. Each triangle and square represent one gene or EST. Triangles represent the genes or ESTs of congenic mice while squares represent genes and ESTs of B6 mice. The label on the left is the relative light absorption level; Label on the bottom is the number of genes and ESTs at that level.

Fig. 2. Schematic representation of the sequential pathway in the congenic mice during the bone development.

Figure 1. Signal comparison between B6 and congenic mice

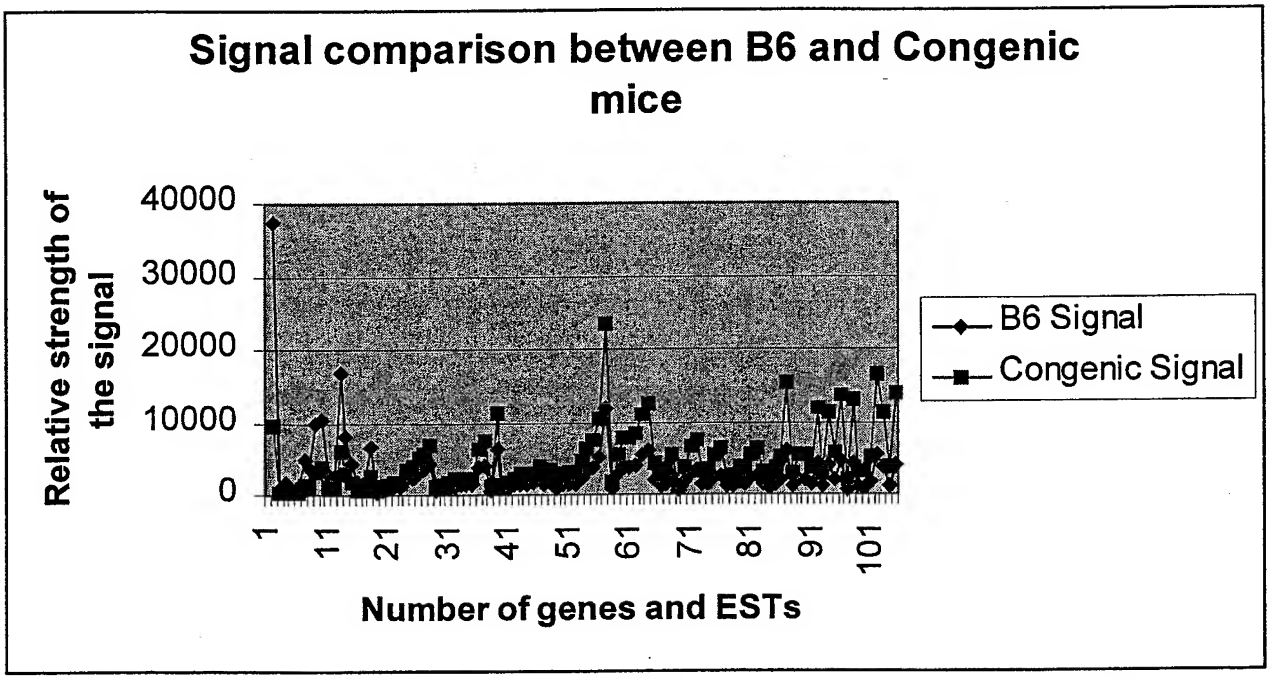

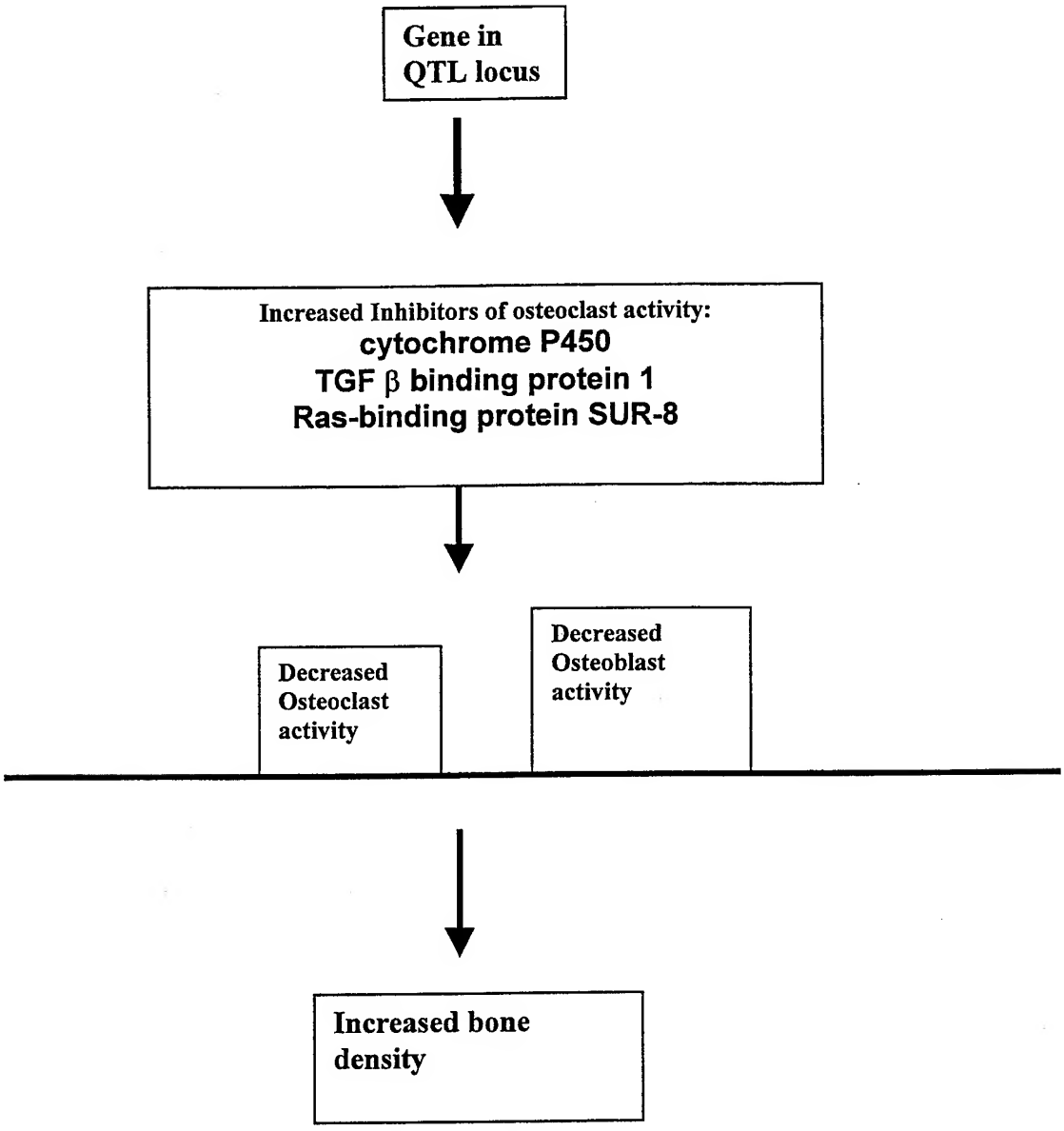

Figure 2. Model of mechanism of the high bone density in the congenic strain.

References:

In the study of patients with ankylosing spondylitis, Yilmaz and Ozaslan (2000) did not find a correlation between markers of disease activity [ESR and C-reactive protein (CRP)] and bone turnover markers was not observed

Goad et al (1992) investigated the consequences of persistent protein phosphorylation on bone resorption in neonatal mouse calvariae using okadaic acid (OA) and calyculin-A, two inhibitors of protein phosphatase-1 and -2A. They reported that the protein dephosphorylation plays a functionally important role in the modulation of bone resorption

It has been reported that various cytokines, including **tumor necrosis factor-alpha, interleukin-1beta,** and **interferon-gamma,** used alone and in combination, are powerful inducers of bone resorption **(Young & Chole, 1999)**

Increased adipogenesis and myelopoiesis in the bone marrow of SAMP6, a murine model of defective osteoblastogenesis and low turnover osteopenia.
J Bone Miner Res. 1997 Nov;12(11):1772-9.

Ravn P, Rix M, Andreassen H, Clemmesen B, Bidstrup M, Gunnes M High bone turnover is associated with low bone mass and spinal fracture in postmenopausal women.
Calcif Tissue Int. 1997 Mar;60(3):255-60.

Garnero P, Sornay-Rendu E, Chapuy MC, Delmas PD. Increased bone turnover in late postmenopausal women is a major determinant of osteoporosis. J Bone Miner Res 1996;11:337-49.

Hansen MA, Overgaard K, Riis BJ, Christiansen C. Role of peak bone mass and bone loss in postmenopausal osteoporosis: 12 year study. BMJ 1991;303:961-4.

Jaiswal RK, Jaiswal N, Bruder SP, Mbalaviele G, Marshak DR, Pittenger MF. Adult human mesenchymal stem cell differentiation to the osteogenic or adipogenic lineage is regulated by mitogen-activated protein kinase.
J Biol Chem. 2000 Mar 31;275(13):9645-52.
PMID: 10734116; UI: 20200462

Yamazaki M, Majeska RJ, Yoshioka H, Moriya H, Einhorn TA. Spatial and temporal expression of fibril-forming minor collagen genes (types V and XI) during fracture healing.
J Orthop Res. 1997 Sep;15(5):757-64.
PMID: 9420607; UI: 98082177

Lukinmaa PL, Vaahtokari A, Vainio S, Sandberg M, Waltimo J, Thesleff I. Transient expression of type III collagen by odontoblasts: developmental changes in the distribution of pro-alpha 1(III)

and pro-alpha 1(I) collagen mRNAs in dental tissues.
Matrix. 1993 Nov;13(6):503-15.

Kasugai S, Todescan R Jr, Nagata T, Yao KL, Butler WT, Sodek J. Expression of bone matrix proteins associated with mineralized tissue formation by adult rat bone marrow cells in vitro: inductive effects of dexamethasone on the osteoblastic phenotype.
J Cell Physiol. 1991 Apr;147(1):111-20.
PMID: 2037618; UI: 91244876

Nagata T, Goldberg HA, Zhang Q, Domenicucci C, Sodek J. Biosynthesis of bone proteins by fetal porcine calvariae in vitro. Rapid association of sulfated sialoproteins (secreted phosphoprotein-1 and bone sialoprotein) and chondroitin sulfate proteoglycan (CS-PGIII) with bone mineral.
Matrix. 1991 Apr;11(2):86-100.
PMID: 1649377; UI: 91304343

References for gene function

1. Barsh GS, Byers PH. Reduced secretion of structurally abnormal type I procollagen in a form of osteogenesis imperfecta.
Proc Natl Acad Sci U S A. 1981 Aug;78(8):5142-6.

2. Uchimura K, Muramatsu H, Kaname T, Ogawa H, Yamakawa T, Fan QW, Mitsuoka C, Kannagi R, Habuchi O, Yokoyama I, Yamamura K, Ozaki T, Nakagawara A, Kadomatsu K, Muramatsu T. Human N-acetylglucosamine-6-O-sulfotransferase involved in the biosynthesis of 6-sulfo sialyl Lewis X: molecular cloning, chromosomal mapping, and expression in various organs and tumor cells. J Biochem (Tokyo). 1998 Sep;124(3):670-8.

3. **Bowman KG, Hemmerich S, Bhakta S, Singer MS, Bistrup A, Rosen SD, Bertozzi CR** Identification of an N-acetylglucosamine-6-0-sulfotransferase activity specific to lymphoid tissue: an enzyme with a possible role in lymphocyte homing.
Chem Biol. 1998 Aug;5(8):447-60.

4. **Lee JK, Bhakta S, Rosen SD, Hemmerich S** Cloning and characterization of a mammalian N-acetylglucosamine-6-sulfotransferase that is highly restricted to intestinal tissue.
Biochem Biophys Res Commun. 1999 Sep 24;263(2):543-9.

5. Moscinski LC, Prystowsky MB Identification of a series of differentiation-associated gene sequences from GM-CSF stimulated bone marrow.
Oncogene. 1990 Jan;5(1):31-7.

6. Lavabre-Bertrand T, Duperray C, Brunet C, Poncelet P, Exbrayat C, Bourquard P, Lavabre-Bertrand C, Brochier J, Navarro M, Janossy G. Quantification of CD24 and CD45 antigens in parallel allows a precise determination of B-cell maturation stages: relevance for the study of B-cell neoplasias.
Leukemia. 1994 Mar;8(3):402-8.

7. D'Surney SJ, Popp RA Changes in alpha-globin gene expression in mice of two alpha-globin haplotypes during development. Biochem Genet. 1990 Oct;28(9-10):445-57.

8. Haussler MR, Haussler CA, Jurutka PW, Thompson PD, Hsieh JC, Remus LS, Selznick SH, Whitfield GK

The vitamin D hormone and its nuclear receptor: molecular actions and disease states. J Endocrinol. 1997 Sep;154 Suppl:S57-73. Review.

9. **Backup P, Westerlind K, Harris S, Spelsberg T, Kline B, Turner R** Spaceflight results in reduced mRNA levels for tissue-specific proteins in the musculoskeletal system. Am J Physiol. 1994 Apr;266(4 Pt 1):E567-73.

10. **Lehenkari P, Hentunen TA, Laitala-Leinonen T, Tuukkanen J, Vaananen HK** Carbonic anhydrase II plays a major role in osteoclast differentiation and bone resorption by effecting the steady state intracellular pH and Ca2+. Exp Cell Res. 1998 Jul 10;242(1):128-37.

11. **Lisignoli G, Toneguzzi S, Monaco MC, Bertollini V, Facchini A** Immunohistochemical analysis of extracellular matrix components and cytoskeletal products of bone marrow stromal cells.

12. **Villa-Verde DM, Mello-Coelho V, Lagrota-Candido JM, Chammas R, Savino W** The thymic nurse cell complex: an in vitro model for extracellular matrix-mediated intrathymic T cell migration.
Braz J Med Biol Res. 1995 Aug;28(8):907-12. Review.

13. **Car BD, Eng VM, Schnyder B, Ozmen L, Huang S, Gallay P, Heumann D, Aguet M, Ryffel B** Interferon gamma receptor deficient mice are resistant to endotoxic shock. J Exp Med. 1994 May 1;179(5):1437-44.

14. **Nakamura I, Takahashi N, Sasaki T, Tanaka S, Udagawa N, Murakami H, Kimura K, Kabuyama Y, Kurokawa T, Suda T, et al** Wortmannin, a specific inhibitor of phosphatidylinositol-3 kinase, blocks osteoclastic bone resorption. FEBS Lett. 1995 Mar 13;361(1):79-84.

15. **Chen J, Zhang Q, McCulloch CA, Sodek J** Immunohistochemical localization of bone sialoprotein in foetal porcine bone tissues: comparisons with secreted phosphoprotein 1 (SPP-1, osteopontin) and SPARC (osteonectin). Histochem J. 1991 Jun;23(6):281-9.

16. **Duarte WR, Kasugai S, Iimura T, Oida S, Takenaga K, Ohya K, Ishikawa I** cDNA cloning of S100 calcium-binding proteins from bovine periodontal ligament and their expression in oral tissues. J Dent Res. 1998 Sep;77(9):1694-9.

17. **Lanyon WG, Ottolenghi S, Williamson R** Human globin gene expression and linkage in bone marrow and fetal liver. Proc Natl Acad Sci U S A. 1975 Jan;72(1):258-62.

18. **Subramaniam M, Harris SA, Oursler MJ, Rasmussen K, Riggs BL, Spelsberg TC** Identification of a novel TGF-beta-regulated gene encoding a putative zinc finger protein in human osteoblasts. Nucleic Acids Res. 1995 Dec 11;23(23):4907-12.

19. **Cermelli S, Zerega B, Carlevaro M, Gentili C, Thorp B, Farquharson C, Cancedda R, Cancedda FD** Extracellular fatty acid binding protein (Ex-FABP) modulation by inflammatory agents: "physiological" acute phase response in endochondral bone formation. Eur J Cell Biol. 2000 Mar;79(3):155-64.

20. **Umayahara Y, Billiard J, Ji C, Centrella M, McCarthy TL, Rotwein P** CCAAT/enhancer-binding protein delta is a critical regulator of insulin-like growth factor-I gene transcription in osteoblasts.

21. **Austin GE, Lam L, Zaki SR, Chan WC, Hodge T, Hou J, Swan D, Zhang W, Racine M, Whitsett C, et al** Sequence comparison of putative regulatory DNA of the 5' flanking region of the myeloperoxidase gene in normal and leukemic bone marrow cells.
Leukemia. 1993 Sep;7(9):1445-50.

22. **Kasperk CH, Borcsok I, Schairer HU, Schneider U, Nawroth PP, Niethard FU, Ziegler R** . Endothelin-1 is a potent regulator of human bone cell metabolism in vitro.

Calcif Tissue Int. 1997 Apr;60(4):368-74.

23. **Evans DB, Thavarajah M, Kanis JA** Immunoreactivity and proliferative actions of beta 2 microglobulin on human bone-derived cells in vitro. Biochem Biophys Res Commun. 1991 Mar 29;175(3):795-803.

24. **Fan K** Heterogeneous subpopulations of human prostatic adenocarcinoma cells: potential usefulness of P21 protein as a predictor for bone metastasis. J Urol. 1988 Feb;139(2):318-22.

25. **Yoshikawa H, Taniguchi SI, Yamamura H, Mori S, Sugimoto M, Miyado K, Nakamura K, Nakao K, Katsuki M, Shibata N, Takahashi K** Mice lacking smooth muscle calponin display increased bone formation that is associated with enhancement of bone morphogenetic protein responses. Genes Cells. 1998 Oct;3(10):685-95.

26. **Wang D, Villasante A, Lewis SA, Cowan NJ** The mammalian beta-tubulin repertoire: hematopoietic expression of a novel, heterologous beta-tubulin isotype. J Cell Biol. 1986 Nov;103(5):1903-10.

27. **Tsuruta T, Tani K, Hoshika A, Asano S** Myeloperoxidase gene expression and regulation by myeloid cell growth factors in normal and leukemic cells. Leuk Lymphoma. 1999 Jan;32(3-4):257-67. Review.

28. **Toyomura T, Oka T, Yamaguchi C, Wada Y, Futai M** Three subunit a isoforms of mouse vacuolar H(+)-ATPase. Preferential expression of the a3 isoform during osteoclast differentiation. J Biol Chem. 2000 Mar 24;275(12):8760-5.

29. **Gallo RL, Kim KJ, Bernfield M, Kozak CA, Zanetti M, Merluzzi L, Gennaro R.** Identification of CRAMP, a cathelin-related antimicrobial peptide expressed in the embryonic and adult mouse. J Biol Chem. 1997 May 16;272(20):13088-93.

30. **Buckingham M, Alonso S, Barton P, Cohen A, Daubas P, Garner I, Robert B, Weydert A** Actin and myosin multigene families: their expression during the formation and maturation of striated muscle. Am J Med Genet. 1986 Dec;25(4):623-34.

31. **Hata D, Kawakami Y, Inagaki N, Lantz CS, Kitamura T, Khan WN, Maeda-Yamamoto M, Miura T, Han W, Hartman SE, Yao L, Nagai H, Goldfeld AE, Alt FW, Galli SJ, Witte ON, Kawakami T** Involvement of Bruton's tyrosine kinase in FcepsilonRI-dependent mast cell degranulation and cytokine production. J Exp Med. 1998 Apr 20;187(8):1235-47.

Function of differentially expressed genes

Monti-Bloch L, Grosser BI . Effect of putative pheromones on the electrical activity of the human vomeronasal organ and olfactory epithelium. J Steroid Biochem Mol Biol. 1991 Oct;39(4B):573-82.

Dulac C, Axel R A novel family of genes encoding putative pheromone receptors in mammals.
Cell. 1995 Oct 20;83(2):195-206.

Hammerland LG, Krapcho KJ, Garrett JE, Alasti N, Hung BC, Simin RT, Levinthal C, Nemeth EF, Fuller FH Domains determining ligand specificity for Ca2+ receptors.
Mol Pharmacol. 1999 Apr;55(4):642-8.

Miyazaki T, Katagiri H, Kanegae Y, Takayanagi H, Sawada Y, Yamamoto A, Pando MP, Asano T, Verma IM, Oda H, Nakamura K, Tanaka S Reciprocal role of ERK and NF-kappaB pathways in survival and activation of osteoclasts. *J Cell Biol* 2000 Jan 24;148(2):333-42

Choo MJ, Chole RA Cytochrome P-450 inhibition blocks bone resorption in vitro and in vivo. Otolaryngol Head Neck Surg. 1999 Jan;120(1):84-91.

Dallas SL, Keene DR, Bruder SP, Saharinen J, Sakai LY, Mundy GR, Bonewald LF.Role of the latent transforming growth factor beta binding protein 1 in fibrillin-containing microfibrils in bone cells in vitro and in vivo. J Bone Miner Res. 2000 Jan;15(1):68-81.

Schoenherr CJ, Anderson DJ Silencing is golden: negative regulation in the control of neuronal gene transcription. Curr Opin Neurobiol. 1995 Oct;5(5):566-71. Review.

Nugent MA, Iozzo RV. Fibroblast growth factor-2. Int J Biochem Cell Biol. 2000 Feb;32(2):115-20. Review.

Turley EA, Belch AJ, Poppema S, Pilarski LM Expression and function of a receptor for hyaluronan-mediated motility on normal and malignant B lymphocytes. Blood. 1993 Jan 15;81(2):446-53.

Barak AJ, Beckenhauer HC, Tuma DJ Betaine, ethanol, and the liver: a review. Alcohol. 1996 Jul-Aug;13(4):395-8. Review.

Lopez M, Nakagawa Y, Coe FL, Tsai C, Michael AF, Scheinman JI Immunochemistry of urinary calcium oxalate crystal growth inhibitor (CGI). Kidney Int. 1986 Apr;29(4):829-33.

Worcester EM, Blumenthal SS, Beshensky AM, Lewand DL The calcium oxalate crystal growth inhibitor protein produced by mouse kidney cortical cells in culture is osteopontin. J Bone Miner Res. 1992 Sep;7(9):1029-36.

Dhar M, Mascareno EM, Siddiqui MA Two distinct factor-binding DNA elements in cardiac myosin light chain 2 gene are essential for repression of its expression in skeletal muscle. Isolation of a cDNA clone for repressor protein Nished. J Biol Chem. 1997 Jul 18;272(29):18490-7.

Manning DR, Stull JT Myosin light chain phosphorylation-dephosphorylation in mammalian skeletal muscle. Am J Physiol. 1982 Mar;242(3):C234-41.

Iwao K, Miyoshi Y, Nawa G, Yoshikawa H, Ochi T, Nakamura Y Frequent beta-catenin abnormalities in bone and soft-tissue tumors. Jpn J Cancer Res. 1999 Feb;90(2):205-9.

Cheng SL, Lecanda F, Davidson MK, Warlow PM, Zhang SF, Zhang L, Suzuki S, St John T, Civitelli R Human osteoblasts express a repertoire of cadherins, which are critical for BMP-2-induced osteogenic differentiation. J Bone Miner Res. 1998 Apr;13(4):633-44.

Sugiura T, Takamatsu H, Kudo A, Amann E Expression and characterization of murine osteoblast-specific factor 2 (OSF-2) in a baculovirus expression system. Protein Expr Purif. 1995 Jun;6(3):305-11.

Takeshita S, Kikuno R, Tezuka K, Amann E Osteoblast-specific factor 2: cloning of a putative bone adhesion protein with homology with the insect protein fasciclin I. Biochem J. 1993 Aug 15;294 (Pt 1):271-8.

Nagata T, Bellows CG, Kasugai S, Butler WT, Sodek J Biosynthesis of bone proteins [SPP-1 (secreted phosphoprotein-1, osteopontin), BSP (bone sialoprotein) and SPARC (osteonectin)] in association with mineralized-tissue formation by fetal-rat calvarial cells in culture. Biochem J. 1991 Mar 1;274 (Pt 2):513-20.

Iraburu MJ, Dominguez-Rosales JA, Fontana L, Auster A, Garcia-Trevijano ER, Covarrubias-Pinedo A, Rivas-Estilla AM, Greenwel P, Rojkind M Tumor necrosis factor alpha down-regulates expression of the

alpha1(I) collagen gene in rat hepatic stellate cells through a p20C/EBPbeta- and C/EBPdelta-dependent mechanism. Hepatology. 2000 May;31(5):1086-93.

Hernandez-Munoz I, de la Torre P, Sanchez-Alcazar JA, Garcia I, Santiago E, Munoz-Yague MT, Solis-Herruzo JA Tumor necrosis factor alpha inhibits collagen alpha 1(I) gene expression in rat hepatic stellate cells through a G protein. Gastroenterology. 1997 Aug;113(2):625-40.

Omura T, Morohashi K Gene regulation of steroidogenesis. J Steroid Biochem Mol Biol. 1995 Jun;53(1-6):19-25. Review.

Xiao G, Jiang D, Thomas P, Benson MD, Guan K, Karsenty G, Franceschi RT MAPK pathways activate and phosphorylate the osteoblast-specific transcription factor, Cbfa1. J Biol Chem. 2000 Feb 11;275(6):4453-9.

Dallas SL, Keene DR, Bruder SP, Saharinen J, Sakai LY, Mundy GR, Bonewald LF Role of the latent transforming growth factor beta binding protein 1 in fibrillin-containing microfibrils in bone cells in vitro and in vivo. J Bone Miner Res. 2000 Jan;15(1):68-81.

Damoulis PD, Hauschka PV Nitric oxide acts in conjunction with proinflammatory cytokines to promote cell death in osteoblasts. J Bone Miner Res. 1997 Mar;12(3):412-22.

Kwon BS, Wang S, Udagawa N, Haridas V, Lee ZH, Kim KK, Oh KO, Greene J, Li Y, Su J, Gentz R, Aggarwal BB, Ni J TR1, a new member of the tumor necrosis factor receptor superfamily, induces fibroblast proliferation and inhibits osteoclastogenesis and bone resorption. FASEB J. 1998 Jul;12(10):845-54.

Nanes MS, McKoy WM, Marx SJ Inhibitory effects of tumor necrosis factor-alpha and interferon-gamma on deoxyribonucleic acid and collagen synthesis by rat osteosarcoma cells (ROS 17/2.8). Endocrinology. 1989 Jan;124(1):339-45.

Kawata Y, Iwasaka H, Kitano S, Hanazawa S Porphyromonas gingivalis fimbria-stimulated bone resorption is inhibited through binding of the fimbriae to fibronectin. Infect Immun. 1997 Feb;65(2):815-7.

Xu RH, Dong Z, Maeno M, Kim J, Suzuki A, Ueno N, Sredni D, Colburn NH, Kung HF Involvement of Ras/Raf/AP-1 in BMP-4 signaling during Xenopus embryonic development. Proc Natl Acad Sci U S A. 1996 Jan 23;93(2):834-8.

Umeda S, Beamer WG, Takagi K, Naito M, Hayashi S, Yonemitsu H, Yi T, Shultz LD Deficiency of SHP-1 protein-tyrosine phosphatase activity results in heightened osteoclast function and decreased bone density. Am J Pathol. 1999 Jul;155(1):223-33.

Schmidt A, Rutledge SJ, Endo N, Opas EE, Tanaka H, Wesolowski G, Leu CT, Huang Z, Ramachandaran C, Rodan SB, Rodan GA Protein-tyrosine phosphatase activity regulates osteoclast formation and function: inhibition by alendronate. Proc Natl Acad Sci U S A. 1996 Apr 2;93(7):3068-73.

Young N, Chole R Cytokine-mediated bone resorption is cytochrome P-450 dependent. Student Research Award 1998. Otolaryngol Head Neck Surg. 1999 Dec;121(6):708-12.

Ma J, Ramachandran S, Fiedorek FT Jr, Zeldin DC Mapping of the CYP2J cytochrome P450 genes to human chromosome 1 and mouse chromosome 4. Genomics. 1998 Apr 1;49(1):152-5.

Miller WL, Portale AA Genetic disorders of vitamin D biosynthesis. Endocrinol Metab Clin North Am. 1999 Dec;28(4):825-40, x. Review.

Foreman DM, Sharpe PM, Ferguson MW Comparative biochemistry of mouse and chick secondary-palate development in vivo and in vitro with particular emphasis on extracellular matrix molecules and the effects of growth factors on their synthesis. Arch Oral Biol. 1991;36(6):457-71.

Haussler MR, Haussler CA, Jurutka PW, Thompson PD, Hsieh JC, Remus LS, Selznick SH, Whitfield GK The vitamin D hormone and its nuclear receptor: molecular actions and disease states. J Endocrinol. 1997 Sep;154 Suppl:S57-73. Review.

Gough A, Sambrook P, Devlin J, Huissoon A, Njeh C, Robbins S, Nguyen T, Emery P Osteoclastic activation is the principal mechanism leading to secondary osteoporosis in rheumatoid arthritis. J Rheumatol. 1998 Jul;25(7):1282-9.

Yilmaz N, Ozaslan J Biochemical bone turnover markers in patients with ankylosing spondylitis. Clin Rheumatol. 2000;19(2):92-8.

Goad DL, Meurer EA, Voelkel EF, Petrou CP, Tashjian AH Protein phosphatase inhibitors and bone resorption: inhibition by okadaic acid and biphasic actions of calyculin-A. Endocrinology. 1992 Jun;130(6):3402-10.

Hart MC, Korshunova YO, Cooper JA Mapping of the mouse actin capping protein alpha subunit genes and pseudogenes. Genomics. 1997 Feb 1;39(3):264-70.

Lissens W, De Meirleir L, Seneca S, Liebaers I, Brown GK, Brown RM, Ito M, Naito E, Kuroda Y, Kerr DS, Wexler ID, Patel MS, Robinson BH, Seyda A Mutations in the X-linked pyruvate dehydrogenase (E1) alpha subunit gene (PDHA1) in patients with a pyruvate dehydrogenase complex deficiency. Hum Mutat. 2000;15(3):209-19. Review.

St-Arnaud R, Arabian A, Travers R, Barletta F, Raval-Pandya M, Chapin K, Depovere J, Mathieu C, Christakos S, Demay MB, Glorieux FH Deficient mineralization of intramembranous bone in vitamin D-24-hydroxylase-ablated mice is due to elevated 1,25-dihydroxyvitamin D and not to the absence of 24,25-dihydroxyvitamin D. Endocrinology. 2000 Jul;141(7):2658-66.

3. Baynes RD, Bezwoda WR. Lactoferrin and the inflammatory response. Adv Exp Med Biol. 1994;357:133-41. Review.

Figure 1. Signal comparison between B6 and congenic mice

Physical mapping and genetic analysis of a 3 cM biologically significant region of mouse chromosome 1

W.K. Gu[1], X.M. Li[1], B. Edderkaoui[1], D. D. Strong[1], K-H.W. Lau[1], W.G. Beamer[2], L. R. Donahae[2], S. Mohan[1], & D. J. Baylink[1]

[1] Musculoskeletal Disease Center, JL Pettis VA Medical Center and Loma Linda University, Loma Linda, CA. [2] The Jackson Laboratory, Bar Harbor, ME. USA

Running head: Physical mapping and analysis of a 3 cM region on mouse chromosome 1

Corresponding Author: David J Baylink, MD., Musculoskeletal Disease Center, JL Pettis VA Medical Center, 11201 Benton Street (151), Loma Linda, CA 92357, USA

Tel: (909) 422-3101
Fax: (909) 796-1680
E-Mail: David.Baylink@med.va.gov

Abstract. One QTL and several mutation loci have been localized in the region between 92 cM and 95 cM of mouse chromosome 1. The QTL locus contributes to approximately 40 % of the variation of the peak bone density between C57BL/6J (B6) and CAST/EiJ (CAST) strains. Other loci located in this chromosomal region include a neural tube defect mutant loop-tail (*Lp*), a lymphocyte-stimulating determinant (*Lsd*), and the Transgelen 2(*TAGLN 2*). The human chromosome region that is homologous to this region is 1q21-23, which also contains a QTL locus for high bone mineral density (BMD). Furthermore, it has been reported that this region may have duplicated several times in the mouse genome. Therefore, genomic sequencing of this region will provide important information for mouse genome structure, for positional cloning of mouse genes, and for the study of syntenic human genes. In order to provide a suitable template for genomic sequencing by the NIH sponsored genomic centers, we have constructed a BAC contig of this region with the RPCI-23 library. We have also identified the currently available mouse genomic sequences that are localized onto the BAC clones of the contig. Further analysis of these sequences and BAC clones indicated that there is a high frequency of repetitive sequences among these BAC clones. This region also contains L1 retrotrasposon sequences, providing a potential mechanism for the repetitive sequences described in the literature.

Introduction

Genomic sequencing of the whole mouse genome is the next goal of national and international genome centers. In terms of the priority for sequencing the mouse genome, sequencing biologically significant regions has received considerable priority. The biologically significant region of a chromosome is defined as a region that contains clusters of genetic loci responsible for clinical diseases or phenotypes of interest. One such region of interest is chromosome 1 between 92-95 cM, for the reasons mentioned below.

First, several important loci have been mapped on this region of the chromosome (www.rodentia.com/wmc/index.html). The neural tube defect mutant loop-tail (*Lp*), which is a semidominant mouse gene that, in homozygous mutants, causes the severe neural tube defect (*NTD*) phenotype, cranio-rachischisis. Linkage analysis in a large intraspecific backcross mapped the *Lp* locus to 93.7 cM on mouse chromosome 1 (Eddleston et al., 1999). *LSD*, a new lymphocyte-stimulating determinant (Lsd) controlled by a single gene, is located on the 93.1 cM on chromosome 1 (www.rodentia.com/wmc/index.html). Transgelen 2 (*TAGLN 2*) is one of the earliest markers of differentiated smooth muscle, being expressed exclusively in the smooth muscle cells of adult tissues and transiently in embryonic skeletal and cardiac tissues. It has been reported that the *TAGLN 2* is linked to Fcgr2, which is located at the 92.3cM of the mouse chromosome 1(Stanier et al., 1998). Furthermore, a bone mineral density (BMD) QTL has recently been mapped to this region (Beamer et al., 1999). This QTL locus is one of the 6 QTL loci identified using a F2 population from C57BL/6J (B6) X

CAST/EiJ (CAST) intercross matings. The chromosome 1 BMD QTL has been shown to account for the largest proportion of genetic variance between the BMD of the two strains (Beamer et al., 1999). Second, this region is homologous to the region of human 1q21-q23, to which several homologous genes and loci have been mapped (www.ncbi.nlm.nih.gov/Homology). Incidentally, a QTL locus for bone density has also been located on the human 1q21-23 region (Koller et al., 1999), suggesting the possibility of homologous genes between human and mice. Third, it has been reported that this region of the mouse chromosome has been duplicated several times during evolution (Lundin 1993; Katsanis et al., 1996). Finally, genomic information will be important for the analysis of chromosomal structure of the mouse genome. Based on these features, it is obvious that the availability of genomic sequences of this region should facilitate positional cloning of important genes that are relevant to clinical diseases of interest.

The genomic sequencing of a chromosomal region requires construction of a contig from a high quality BAC library. In this region, two contigs have been previously constructed for the physical mapping of the LP locus (Eddleston et al., 1999; Underhill et al., 1999). One contig was constructed using the yeast artificial chromosome (YAC). The other covered a smaller (700kb) region within the YAC contig and was constructed using both YAC and bacterial artificial chromosome (BAC). However, these two contigs were constructed mainly using YAC clones, which are not suitable for sequencing. Our first goal in this study was to construct a sequencing-ready BAC contig covering the 92-95 cM region on mouse chromosome 1 using the RPCI-23 library, which has been designated for mouse genome sequencing. Our second goal was to analyze the genetic components within the BAC clones of the contig using available genomic sequences in

the GenBank.

Materials and Methods

Probes. Probes are mainly collected from three sources: publications (Eddleston et al., 1999; Underhill et al., 1999), The mouse genome database for molecular markers and probes (www.rodentia.com/wmc/index.html), current available mouse genome sequences for new probes (www.ncbi.nlm.nih.gov/genome/seq/MmHome.html). A total of 80 probes (Table 1), including genes, Ests, STS markers, and microsatellite markers were used in our screening. Probes were amplified by PCR or RT-PCR. The amplified products then were used as templates for ^{32}P labeling of the probes.

BAC library screening. We used the RPCI-23 mouse BAC library from Roswell Park Cancer Institute (RPCI) for our contig construction. It was made from the kidney and brain genomic DNA of the female B6 mouse. We first screened the high-density filters with pooled probes. We then constructed secondary filters with positive clones and conducted secondary screening with individual probes. Clones finally were connected to each other with the hybridization information.

For hybridization of high-density filters of the BAC library using pooled probes, we followed the procedure provided by RPCI (www.chori.org/bacpac). The purified PCR products then were labeled with ^{32}P. Pooled probes between 10 and 20 were used to hybridize the high-density filters at 65 ^{o}C over night. Filters then were exposed at different time points (1-5 days) to ensure the proper background, such that the positive clones and the corresponding grids could be clearly read. In case too many clones were

positive, positive clones were divided into strong, medium, and weakly positive groups. A portion of clones from each group was initially used for the next experiment.

Selected positive clones were then used to make secondary filters. Clones were picked up from the library and grown on LB medium over night. A 384-well pin tool was used to transfer the selected clones on new Nylon membrane filters. The new filters were then hybridized using individual probes. Finally, the positive clones for each probe were identified.

Connection of contig. Clones that were hybridized by more than one probe or were amplified by more than one marker were used to construct the contig. Clones containing the same probes or markers were considered to contain the same sequences at or around the marker/probe. Accordingly, if two clones contained at least one identical marker/probe as well as other different markers/probes, they were considered to be neighboring clones with overlapping sequences. Eventually, a contig was constructed with the overlapping markers/probes among all the neighboring clones.

GenBank searching of genomic sequences. To search for possible genomic sequences in the BMD QTL region, especially within the BAC contig, we conducted a limited search through the Genebank. We did our search through the Entrez at the websit of National Center for Biotechnology Information (NCBI) (http://www.ncbi.nlm.nih.gov/Entrez/). We searched the nucloetide database using the key words: 1q21, 1q22, 1q23, 1q21-22, 1q21-23, and "Mus musculus and chromosome 1, limited to genomic DNA/RNA", and excluded "ESTs/STSs". The list of all accession numbers from this search then were

examined and the accessions that contained mouse genomic sequences were further analyzed.

Localization of genomic sequences on BAC clones. Primers were designed from the selected mouse genomic sequences from mouse chromosome 1. The primers then were used for two experiments: 1) to amplify PCR products to hybridize the BAC library. 2) to conduct PCR amplification using the BAC clones as templates and the mouse genomic DNA as positive control.

BLAST searching of genomic sequences. After we located the known genomic sequences from GenBank on to BAC clones within the contig, we conducted a BLAST search (www.ncbi.nlm.nih.gov/BLAST) to identify similar/repetitive sequences and possible genes within the sequences. DNA sequences of each accession were divided into fragments of 500-800 bp. Each fragment then was deposited into GenBank for the Basic BLAST search. We first eliminated some sequences by discarding retrieved sequences that had a similarity score of less than 100. At this level, the identity of the sequences between the retrieved and the input sequence is usually less than 40 percent, and the length of the sequence is less than 100 nucleotides. The sequences with higher similarity scores were further examined for their identity as cDNA or genomic DNA. If the sequence from the BAC clones matched a cDNA sequence in the GenBank, the sequence was considered as a possible coding region/gene. If a sequence matched an intron region or a non-coding repetitive element, it was considered a non-coding region.

Contamination detection test. Contamination of BAC clones was suspected when one pair of primers amplified from multiple BAC clones. In case we found that one pair of primers amplified the same PCR product from a large number of BAC clones, an experiment was done to rule out the problem of contamination among these clones. Six BAC clones were used for this experiment. Each clone was spread on a LB plate and grown overnight at 37 °C. Five individual colonies from each plate were taken for PCR amplification with the same pair of primers under identical conditions. Three pairs of primers were used for PCR with each of the five colonies from each of the six BAC clones. Only when all of the colonies of five BAC clones amplified the same product with the same pair of primers was the clone considered not to be contaminated.

Results

BAC contig. Seven hundred positive clones were identified from the total library in the initial screening using pooled probes, which were subsequently grown to make secondary filters. The secondary filters were hybridized with individual probes. By examining the overlapping markers in the neighboring clones, we selected 37 BAC clones for further analyses. These BAC clones were then subjected to PCR amplification with the original probes and microsatellite markers. Figure 1 shows the positive clones that contained probes, which included 14 known genes, 6 ESTs, 4 microsatellite and 14 STS markers, for the QTL region of interest in mouse chromosome 1. In general, the order of the markers in this contig agrees with previous publications with few exceptions, such as ESTM36 and B17, which differ from that of Eddleston et al. and Underhill et al., respectively. The availability of genomic sequences would help us to clarify this

inconsistency.

Comprehensive physical map of the QTL region. A BAC contig that covers a 3 cM genome distance was constructed with 33 overlapping BAC clones as shown in figure 2. From the positions of microsatellite markers, D1mit112 and D1mit354, we estimated that the contig covers a region from 92 to 95 cM of the mouse chromosome 1.

BAC clones within the contig are currently being sequenced at the Advanced Center for Genome Technology at University of Oklahoma (ACGTUO). The result of these sequences can be obtained through the web page /www.genome.ou.edu/. Because the contig is being sequenced, sizes of the BAC clones were not further analyzed.

Genomic sequences of mouse chromosome 1 *identified from GenBank.* We searched the GenBank for mouse genomic sequences that are located in the contig and found a total of 11 unique accessions that contain the mouse genome sequences of chromosome 1 (Table 2). Four accessions, AC005992, AC007049, AC006944, AC008100, are from the mouse chromosome region that is syntenic to the human chromosome 1q21-23 region. Another seven accessions were labeled as they were from chromosome 1, but positions on the chromosome are not given. They are also labeled as a currently "working draft" sequence, each containing several unordered sequences. Further analysis of these seven accessions indicated that they were not located in the contig region (data not shown).

Among the four accessions that are homologous to the human 1q21-23 region, AC008100 is characterized as a "working draft" sequence. We conducted a BLAST search using 5 DNA fragments of about 700 bp that were randomly taken from the

Accession AC008100. To our surprise, all five fragments matched the sequences in accession AC006944, demonstrating 98-100% sequence identity. In addition, two of these fragments also matched both AC005992 and AC007049. These results suggest that at least a large portion, if not all, of the accession AC008100 contains the sequences either overlapping or sharing sequence similarity with the other three accessions in the 1q21-23 region. Further comparison of the genomic sequences of the other three accessions in the 1q21-23 region revealed that some sequences overlapped each other. In particular, comparison with the program "BLAST TWO SEQUENCES" (www.ncbi.nlm.nih.gov/gorf/bl2.html) indicated that the AC005992 (151218 bp) contains the entire sequences of AC007049 (85931 bp) and two other unconnected pieces of genomic sequences.

In an effort to determine if any of these accessions are located in our contig, primers were designed from these sequences to amplify PCR products from BAC clones of the contig. Primers (BESQ3, 5, 7) from AC005992, AC006944, and AC007049 amplified PCR products of the expected size from the same BAC clone, f23-30, which is at one end of the contig (Figure 1). Blast searching of sequences of AC007049 indicated that it contained the cluster of musculus interferon activated genes, which have been mapped to 95.2 cM according to the MGD database.

Repetitive sequences within the known genomic sequences. Initially, we used the accession AC007049 as the representative sequence of the three overlapping sequences, AC007049, AC006944 and AC005992, to conduct a BLAST search in GenBank. During the search of the similar sequences in GenBank, we found that AC007049 contains a

large number of repetitive sequences. Within the total of 85931 bp of this accession, we found that, in addition to other repetitive sequences, it contains seven regions of sequences, each of which matched at least one L1 retrotransposon sequence. Furthermore, unlike other genomic sequences, the sizes of these repetitive regions are large (2~3 kb). Between these L1 retrotransposon sequences are clusters of interferon activated genes. More importantly, in a detailed search, we found that sequences from 26321 to 32180 in AC005992 contains the entire sequences of the L1 element except the non coding sequences at 5' end.

L1 *retrotransposon sequence within the contig.* In order to determine if any of the other BAC clones within the contig contain L1 retrotransposon, we designed a pair of primers (BEQS 7) within the L1 retrotransposon sequence of AC007049 and conducted PCR with all the clones in the contig. We found that 16 out of the total 37 clones (Figure 1) produced the DNA fragment of expected size, indicating that these clones contain the same repetitive sequences (Figure 1).

Other repetitive sequences reside within the contig. In addition to the L1 retrotransposon sequences within the contig, we also found duplications of other non-repetitive sequences within the contig. During the construction of the contig, we found that three primer pairs, b2, CD51, and EST38, amplified the expected PCR products from a large number of BAC clones within the contig (Figure 1). The b2 primers are from the end sequence of a clone previously described by Underhill et al. (1999). Primers for CD51 and EST38 were designed according to Eddleston et al. (1999), both of which are outside of the contig.

All of these primers are different from known repetitive sequences. However, their distribution among the BAC clones is not random. They are either within the clones which contain the L1 retrotransposon or within the same clones that other repetitive sequences are in (Figure 1). In order to rule out the possibility of contamination among these clones, we conducted a PCR test as described in the Material and Methods section. In the test, five individual colonies from each of six BAC clones were randomly picked as templates in the PCR amplification. Each colony was used in the PCR with each of three pairs of primers. In this case, if the BAC clones were contaminated, there would be some contaminated and some non-contaminated colonies among all the 30 colonies derived from the original 6 clones. PCR products of the contaminated and non-contaminated colonies will give the different PCR products. However, our result showed that every individual colony in this study amplified the same expected fragment. We therefore speculated that these BAC clones contain repetitive sequences that might exist only within this region.

Discussion

The contig that we have constructed provides a template that is suitable for mouse genome sequencing. The contig covers a similar region of the YAC contig reported by Eddleston et al., (1999), which is larger than that of Underhill et al., (1999). Because this contig is constructed completely using the RPCI-23 mouse BAC library, which has been chosen as the template for the NIH mouse genome project, it provides a suitable template for mouse genome sequencing. The future availability of genomic sequence information

of this contig will facilitate candidate gene searches by various approaches.

The sequencing information from this contig will also be useful in identifying the syntenic gene for humans. A QTL locus for high bone density in humans is also located on the 1q21-23 region. Considering the syntenic relationship between the human and mouse genome and the location of the QTL loci in this region from both human and mouse studies, it is possible that the same gene causes high bone density in both humans and in mice. Therefore, if a QTL gene is identified from the mouse that is responsible for high bone density, the syntenic human gene is likely to have the same function, and vice versa.

This contig also provides the mouse sequences for detailed comparison between the human and mouse genome. In general, the major portion of this region of the mouse is assigned to the human 1q21-23, such as the QTL locus for bone density. However, the order of some genes along the chromosome is different between humans and mouse (www.ncbi.nlm.nih.gov/Homology). Furthermore, at least 8 genes within the human 1q21-23 are located on mouse chromosome 3. The detailed comparison of DNA structure between human and mouse chromosomes can be obtained when the mouse genomic sequences of this region are available.

The detection of large pieces of L1 retrotransposon sequences from this region raises several interesting issues. First, according to the current published information on the human genome, it can be predicted that the more repetitive sequences there are, the fewer genes that will be located in the corresponding region of the chromosome. In this regard, our data agree with the previous reports that this is a gene-poor region

(Kingsmore et al., 1989; Oakey et al., 1992; Eddleston et al., 1999). Secondly, like the human 1q21-23 region, it has been reported that genes and fragments of this region of mouse chromosome 1 have been duplicated in some of the other chromosomes (Lundin LG, 1993; Katsanis et al., 1996; Stanier et al., 1998). Because the large pieces of L1 retrotransposons, particularly an entire L1 element, was found in this region, we speculate that the duplication of this region in the other chromosomes of the mouse genome is due to the activity of the retrotransposons (Kazazian, 2000). In addition, it is also possible that the retrotransposons may cause mutations in this region (Kingsmore et al., 1994).

Analysis of human genomic sequences reveals that L1 repetitive sequences are a common component of human genome. In general, most of the L1 retrotranspons have tunacked 5' end and therefore have lost their translocational activity. However, there are several reports indicating that some of retrotransposons are actually actively expressed and regulate other genes (Kingsmore et al., 1994; Casteels et al., 1995; Moran et al., 1996; Sassaman et al., 1997; Palmer et al., 1998). Particularly, Sassaman et al. found that two human L1 elements (L1.2 and LRE2) could act as retrotransposons in cultured mammalian cells. Kingsmore et al. (1994) reported that the Glycine receptor beta-subunit (*Glrb*) gene mutation in the *spastic* mouse is associated with a LINE-1 element insertion. It has been reported that the activity of the L1 element *in vitro* is correlated to the size of the elements (Farley et al., 2000). Because we found an entire L1 sequence within the AC005992, it is possible that the L1 element in this region may still be active. Consistent with this idea is the finding that the AC007949 and AC005992 contains a cluster of musculus interferon activated genes with retrotransposons that are located in

between these genes. These findings raise the possibility that the duplications of the interferon genes were caused by the activity of retrotransposons. In addition, we found that some sequences have been repeated among these BAC clones (PCR amplification with primers from b2, CD51, and EST38), but these sequences are not the part of the known repetitive elements, indicating that they are repeated only within this chromosomal region. Furthermore, the above repetitive sequences were found to be present in most of the clones that also contained L1 retrotransposons (Figure 1). This suggests that the repetitive sequences could have moved together with the L1 retrotransposons. Further studies are needed to evaluate if retrotransposons is the cause for duplication and/or the mutation of this region.

In conclusion, we have constructed a contig that covers several important genetic loci on mouse chromosome 1. The future availability of genomic sequence information of this contig will facilitate the work in candidate gene search of genetic loci within this region and analysis of the genome structure of the mouse. In addition, we analyzed genetic information of BAC clones of the contig, particularly, the L1 retrotransposon sequences within the BACs. Our study provides preliminary but important evidence on the potential mechanism of the mutation/polymorphism and duplication of this region in the mouse genome. Further study of the organization and the number of these repetitive sequences in this region will help us to examine in detail the effect of L1 retrotransposon sequences on the expression and function of the mouse genes.

Acknowledgments

This work was supported by Assistance Award No. DAMD17-99-1-9571. The U.S. Army Medical Research Acquisition Activity, 820 Chandler Street, Fort Detrick MD 21702-5014, is the awarding and administering acquisition office. The information contained in this publication does not necessarily reflect the position or the policy of the Government and no official endorsement should be inferred

References

Beamer WG, Shultz KL, Churchill GA, Frankel WN, Baylink DJ, Rosen CJ, Donahue LR (1999) Quantitative trait loci for bone density in C57BL/6J and CAST/EiJ inbred mice. Mamm Genome Nov;10(11), 1043-9.

Bertling WM (1989) Full length L1 retroposons contain tRNA-like sequences near the 5' termini--hypothesis on the replication mechanism of retroposons. J Theor Biol May 22;138(2), 185-94.

Casteels D, Poirier C, Guenet JL, Merregaert J (1995) The mouse Fau gene: genomic structure, chromosomal localization, and characterization of two retropseudogenes. Genomics Jan 1;25(1, 291-4.

Crabbe JC (1998) Provisional mapping of quantitative trait loci for chronic ethanol withdrawal severity in BXD recombinant inbred mice. J Pharmacol Exp Ther Jul;286(1):263-71.

Eddleston J, Murdoch JN, Copp AJ, Stanier P (1999) Physical and transcriptional map of a 3-Mb region of mouse chromosome 1 containing the gene for the neural tube defect mutant loop-tail (Lp). Genomics Mar 1;56(2):149-59.

Farley AH, Luning Park ET, and Kazazian Jr HH (2000) L1 insertion length is correlated with retrotransposition activity in a cultured cell assay. 50th Annual Meeting of the American Society of Human Genetics. p23.

Genant HK, Engelke K, Fuerst T, Gluer CC, Grampp S, Harris ST, Jergas M, Lang T, Lu Y, Majumdar S, Mathur A, and Takada M (1996) Noninvasive assessment of bone mineral and structure: state of the art. [Review] [273 refs] Journal of Bone & Mineral Research. 11(6), 707-30

Hunter KW, Ontiveros SD, Watson ML, Stanton VP Jr, Gutierrez P, Bhat D, Rochelle J, Graw S, Ton C, Schalling M, et al (1994) Rapid and efficient construction of yeast artificial chromosome contigs in the mouse genome with interspersed repetitive sequence PCR (IRS-PCR): generation of a 5-cM, > 5 megabase contig on mouse chromosome 1. Mamm Genome Oct;5(10):597-607.

Jouanny P, Guillemin F, Kuntz C, Jeandel C, and Pourel J (1995) Environmental and genetic factors affecting bone mass. Similarity of bone density among members of healthy families. Arthritis & Rheumatism 38(1), 61-67.

Kazazian HH Jr Genetics. L1 retrotransposons shape the mammalian genome. Science. 2000 Aug 18;289(5482):1152-3.

Katsanis N, Fitzgibbon J, Fisher EMC (1996) Paralogy mapping: identification of a region in the human MHC triplicated onto human chromosomes 1 and 9 allows the prediction and isolation of novel PBX and NOTCH loci. Genomics Jul 1;35(1):101-8.

Kingsmore SF, Giros B, Suh D, Bieniarz M, Caron MG, Seldin MF (1994) Glycine receptor beta-subunit gene mutation in spastic mouse associated with LINE-1 element insertion. Nat Genet Jun;7(2):136-41.

Koller DL, Econs MJ, Morin PA, Christian JC, Hui SL, Parry P. Curran ME Rodriguez LA, Conneally PM, Joslyn G, Peacock M, Johnston CC, Christian JC, Foroud T(1999) Strategies for fine mapping of QTLs contributing to variation in peak bone density. 49th Annual Meeting of the American Society of Human Genetics. p523.

Kuhn A, Deppert U, Grummt I A (1990) 140-base-pair repetitive sequence element in the mouse rRNA gene spacer enhances transcription by RNA polymerase I in a cell-free system. Proc Natl Acad Sci U S A Oct;87(19), 7527-31.

Lundin LG . Evolution of the vertebrate genome as reflected in paralogous chromosomal regions in man and the house mouse. Genomics. 1993 Apr;16(1):1-19. Review.

Moran JV, Holmes SE, Naas TP, DeBerardinis RJ, Boeke JD, Kazazian HH Jr (1996) High frequency retrotransposition in cultured mammalian cells. Cell Nov 29;87(5), 917-927.

Nouvel P (1994) The mammalian genome shaping activity of reverse transcriptase. Genetica. 93(1-3), 191-201. Review.

Palmer DB, McVey JH, Purohit R, Picard J, Dyson PJ (1998) Characterization of a recent retroposon insertion on mouse chromosome 2 and localization of the cognate parental gene to chromosome 11. Mamm Genome Feb;9(2), 103-6.

Pan Y, Decker WK, Huq AH, Craigen WJ (1999) Retrotransposition of glycerol kinase-related genes from the X chromosome to autosomes: functional and evolutionary aspects. Genomics Aug 1;59(3), 282-90.

Pantazidis A, Labrador M, Fontdevila A (1999) The retrotransposon Osvaldo from Drosophila buzzatii displays all structural features of a functional retrovirus. Mol Biol Evol Jul;16(7), 909-21.

Peterfy M, Gyuris T, Antonio L, Takacs L (1998) Characterization and chromosomal mapping of two pseudogenes of the mouse Pafaha/Lis1 gene: retrointegration hotspots in

the mouse genome. Gene Aug 31;216(2), 225-31.

Sassaman DM, Dombroski BA, Moran JV, Kimberland ML, Naas TP, DeBerardinis RJ, Gabriel A, Swergold GD, Kazazian HH Jr (1997) Many human L1 elements are capable of retrotransposition. Nat Genet May;16(1), 37-43.

Stanier P, Abu-Hayyeh S, Murdoch JN, Eddleston J, Copp AJ (1998) Paralogous sm22alpha (Tagln) genes map to mouse chromosomes 1 and 9: further evidence for a paralogous relationship. Genomics. Jul 1;51(1), 144-7.

Underhill DA, Mullick A, Groulx N, Beatty BG, Gros P (1999) Physical delineation of a 700-kb region overlapping the looptail mutation on mouse chromosome 1. Genomics Jan 15;55(2), 185-93.

Vidal F, Mougneau E, Glaichenhaus N, Vaigot P, Darmon M, Cuzin F (1993) Coordinated posttranscriptional control of gene expression by modular elements including Alu-like repetitive sequences. Proc Natl Acad Sci U S AJan 1;90(1), 208-12.

Zhao Y, Greene-Till R, Hardies SC (1998) Mus spretus LINE-1s in C57BL/6J map to at least two different chromosomes. Mamm Genome Aug;9(8), 679-80.

Table 1. Probes for contig construction

Marker	Type/ Name	Sources/References
MilT454	microsatellite marker	www. odentia.com/wmc/index.html
MIT112	microsatellite marker	www. odentia.com/wmc/index.html
MIT111	microsatellite marker	www. odentia.com/wmc/index.html
MIT356	microsatellite marker	www. odentia.com/wmc/index.html
MIT354	microsatellite marker	www. odentia.com/wmc/index.html
MIT114	microsatellite marker	www. odentia.com/wmc/index.html
Fcerg	Fc receptor IgE gamma	Eddleston et al., 1999
APOa	apolipoprotein A1	Eddleston et al., 1999
Cd48	CD48 antigen	Eddleston et al., 1999
Ly9	Lymphocyte Antigen 9	Eddleston et al., 1999
Nhlhl	nescient helix loop helix 1	Eddleston et al., 1999
Atpla2	ATPase Na+/K+ transporting alpha-1 polypeptide	Eddleston et al., 1999
Crp	C-reactive protein pretaxin related	Eddleston et al., 1999
Olfr16	Olfactory receptor 16	Eddleston et al., 1999
Sap	Serum Amuloid P-component	Eddleston et al., 1999
Fcer1a	Fc Receptor IgE- gamma	Eddleston et al., 1999
Spna1	Alpha spectrin 1 erythroid	Eddleston et al., 1999
D1Sta01	DNA Segment	www. odentia.com/wmc/index.html
D1Sta02	DNA Segment	www. odentia.com/wmc/index.html
D1Sta03	DNA Segment	www. odentia.com/wmc/index.html
D1Sta04	DNA Segment	www. odentia.com/wmc/index.html
D1Sta06	DNA Segment	www. odentia.com/wmc/index.html
D1Sta07	DNA Segment	www. odentia.com/wmc/index.html
D1Sta08	DNA Segment	www. odentia.com/wmc/index.html
D1Sta09	DNA Segment	www. odentia.com/wmc/index.html
D1Sta10	DNA Segment	www. odentia.com/wmc/index.html
D1Sta13	DNA Segment	www. odentia.com/wmc/index.html
Pea15	Phosphoprotein enriched in astrocytes 15	Eddleston et al., 1999
Kenj10	potassium inwardly-rectifying channel, subfamily J, member 10	Eddleston et al., 1999
Kenj9	potassium inwardly-rectifying channel, subfamily J, member 9	Eddleston et al., 1999
Pxf-F	peroxisomal farnesylated protein	Eddleston et al., 1999
D1Ucla4	DNA Segment	www. odentia.com/wmc/index.html
ESTM33	Expressed Sequence Tagged Mouse Sequences (EST)	www. odentia.com/wmc/index.html
Copa	coatomer protein complex subunit alpha	Eddleston et al., 1999
ESTM32	EST	www. odentia.com/wmc/index.html

ESTM30	EST	www. odentia.com/wmc/index.html
Usf1	Upstream transcription factor 1	Eddleston et al., 1999
ESTM28	EST	www. odentia.com/wmc/index.html
ESTM29	EST	www. odentia.com/wmc/index.html
ESTM34	EST	www. odentia.com/wmc/index.html
Tagln2	Transgelin octoplacental cone	Eddleston et al., 1999
ESTM35	EST	www. odentia.com/wmc/index.html
U-PS	Hydroxymethylbilane synthase	Eddleston et al., 1999
ESTM44	EST	Eddleston et al., 1999
ESTM43	EST	www. odentia.com/wmc/index.html
ESTM41	EST	Eddleston et al., 1999
ESTM42	EST	Eddleston et al., 1999
ESTM40	EST	Eddleston et al., 1999
ESTM38	EST	Eddleston et al., 1999
Cd51	CD5 antigen-like	Eddleston et al., 1999
ESTM36	EST	www. odentia.com/wmc/index.html
ESTM37	EST	www. odentia.com/wmc/index.html
PLKr	Pyruvate kinase liver	Eddleston et al., 1999
Arnt	aryl hydrocarbon receptor nuclear translocator	Eddleston et al., 1999
ESTM46	EST	Eddleston et al., 1999
B1	STS genomic sequence	Underhill et al. 1999
B2	STS genomic sequence	Underhill et al. 1999
B3	STS genomic sequence	Underhill et al. 1999
B15	STS genomic sequence	Underhill et al. 1999
B16	STS genomic sequence	Underhill et al. 1999
B17	STS genomic sequence	Underhill et al. 1999
B18	STS genomic sequence	Underhill et al. 1999
B19	STS genomic sequence	Underhill et al. 1999
B9	STS genomic sequence	Underhill et al. 1999
B25	STS genomic sequence	Underhill et al. 1999
B20	STS genomic sequence	Underhill et al. 1999
B25	STS genomic sequence	Underhill et al. 1999
bseq9	BAC sequence	www.genome.ou.edu
bseq5	BAC sequence	www.genome.ou.edu
bseq6	BAC sequence	www.genome.ou.edu
bseq7	BAC sequence	www.genome.ou.edu
bseq3	BAC sequence	www.genome.ou.edu
bseq4	BAC sequence	www.genome.ou.edu
bseq2	BAC sequence	www.genome.ou.edu
Tyro10	(Ntrkr3) neurotrophic tyrosine kinase receptor 3 related	Eddleston et al., 1999
Dty	Duffy (promiscuous chemokine recrptor	Eddleston et al., 1999
NMrk	non-MHC restricted killing associated	Eddleston et al., 1999
Care2	marker	Eddleston et al., 1999
MPZ	Peripheral myelin protein	Eddleston et al., 1999
Rxrg-R	retinoid X receptor gamma	Eddleston et al., 1999

Table 2. List of genomic sequences of mouse chromosome 1 from GenBank

Searching key words	Total number of accessions	Mouse genomic accession #	Position of the clones	Repetitive sequences	Library/position
1q21	484	AC005992* AC007049* AC006944* AC008100*	- - - -		mouse ES cell BAC libraries I and II:129X1/SvJ ES cell line RW4
1q22	146	0	N/A		N/A
1q23	182	0	N/A		N/A
1q21-22	7	0	N/A		N/A
1q21-23	4	AC005992* AC007049* AC006944* AC008100*	- - - -		mouse ES cell BAC libraries I and II:129X1/SvJ ES cell line RW4
Mus musculus AND chromosome 1	307	AC024069 AC034109 AC024915 AC068906 AC034108 AC058787 AC024068	78m21 88k7 212g20 240p23 70m05 202p02 86n23		RPCI mouse BAC library 23:C57BL/6J RPCI mouse BAC library 22:129S6/SvEv Tac
Total	1130	11			N/A

* Searches with 1q21 and 1q23 separately retrieved the same accessions of mouse genomic DNA.

Figure legends:

Fig. 1. Physical and transcriptional map of the QTL peak region. All BAC clones are from the RPCI-23 mouse BAC library from Roswell Park Cancer Institute. Labeling for the clones is in the order of column-row-plate #. Accordingly, a clone of m134-101 is from the column M, row 134, on plate 101. Other notations are: B= positive confirmed by both hybridization and PCR; Y= positive according to PCR amplification; H= positive according to hybridization result; X= possibility of chimeric clones or the non-specific hybridization and/or PCR amplification. A full-description of probes has been given in Table 1. Clones that contain the repetitive or retrotransposon sequences are indicated by one asterisk *. Each of these last five probes amplified the PCR product of the same size from a large number of clones, which indicates that these clones contain the same repetitive sequences. These probes are indicated by two asterisks **.

Fig. 2. Schematic representation of BAC clones across the QTL peak region. The lower panel indicates the names of 33 BAC clones that were selected as non-chimeric clones covering the region in order. In the up panel, the dotted lines indicate the coverage and the shape of the QTL locus and the LOD score along the mouse chromosome 1. The position of the chromosome is indicated by the cM of the chromosome and MIT microsatellite markers along the chromosome. The center panel indicates the probes of the contig which are listed in order according to their positions in the contig.

Figure 1.

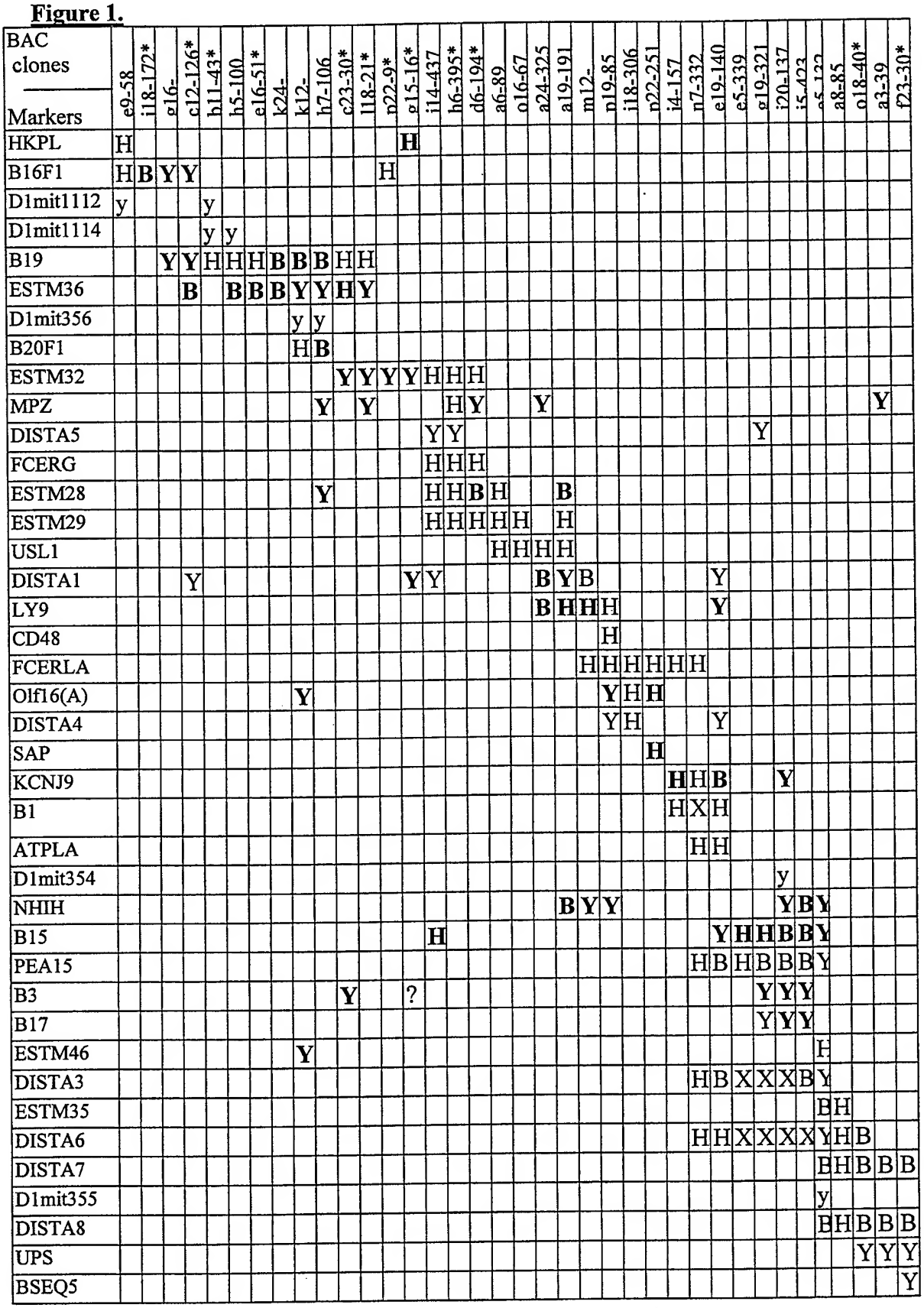
BAC clones
Markers
e9-58
i18-172*
g16-
c12-126*
h11-43*
h5-100
e16-51*
k24-
k12-
h7-106
c23-30*
l18-21*
n22-9*
g15-16*
i14-437
h6-395*
d6-194*
a6-89
o16-67
a24-325
a19-191
m12-
n19-85
i18-306
n22-251
i4-157
n7-332
e19-140
e5-339
g19-321
i20-137
i5-423
a8-85
o18-40*
a3-39
f23-30*
HKPL
B16F1
D1mit1112
D1mit1114
B19
ESTM36
D1mit356
B20F1
ESTM32
MPZ
DISTA5
FCERG
ESTM28
ESTM29
USL1
DISTA1
LY9
CD48
FCERLA
Olf16(A)
DISTA4
SAP
KCNJ9
B1
ATPLA
D1mit354
NHIH
B15
PEA15
B3
B17
ESTM46
DISTA3
ESTM35
DISTA6
DISTA7
D1mit355
DISTA8
UPS
BSEQ5

BSEQ3**		**Y**	**B**	**Y**	H		**Y**		**Y**	**Y**		**B**	**Y**	H																			**Y**
BSEQ7**		B	B	**Y**	B		Y	Y	Y		Y	Y	B	Y		H	Y					Y											Y		Y
B2**			Y	Y	Y		Y		Y	Y	Y	Y	Y	Y						Y	Y	Y	Y			Y		H	B	Y	B	Y	Y	Y	Y
CD51**				Y	Y		Y		Y	Y	Y	Y	Y	Y								Y	Y								Y		Y	Y	Y
EST38**		Y		Y							Y	Y	Y	Y									Y	Y							Y		Y	Y	Y

Figure 2

Representative BAC clones that cover the QTL peak region of the mouse chromosome 1.

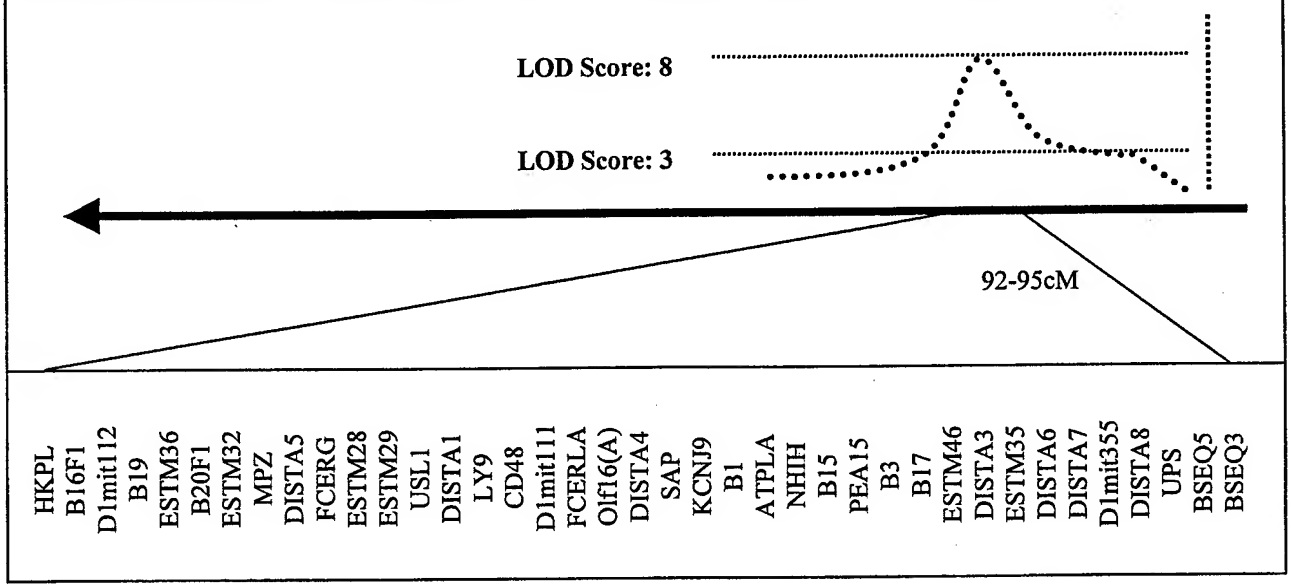

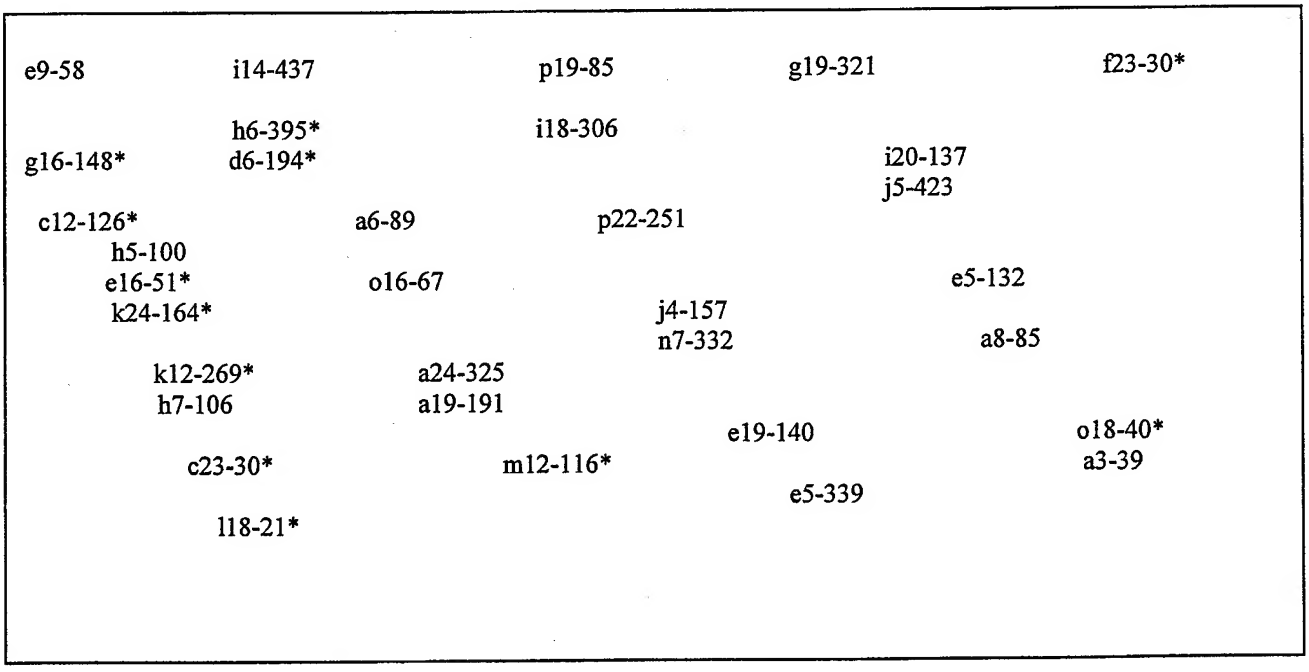

ed and newer versions of the sequence have been generated.

The American Journal of Human Genetics
Volume 67, Number 4, October 2000

1409

Identification of candidate genes that control the peak bone density by combination of cDNA microarray analysis and physical mapping. *W.K. Gu[1], X.M. Li[1], S. Mohan[1], K-H.W. Lau[1], B. Edderkaoui[1], L.R. Donahue[2], C. Rosen[3], W.G. Beamer[2], D.J. Baylink[1].* 1) Musculoskeletal Disease Ctr, Loma Linda Univ & JL Pettis VAMC, Loma Linda, CA; 2) The Jackson Lab., Bar Harbor, ME; 3) St. Joseph Hosp., Banger, ME.

Osteoporosis is a debilitating bone disease that afflicts 30 millions people in the U.S. Peak bone density is an important determining factor of future osteoporosis risks. Genetic factors determine up to 80% of variation in peak bone density. Our previous study has identified a QTL locus on mouse chromosome 1 that contributes to 40% of the total peak bone density difference between C57BL/6J (B6) and CAST/EiJ (CAST) mouse strains. We have produced congenic mice in which the chromosome 1 fragment containing this QTL locus has been transferred from CAST to the congenic mouse strain of B6 background. To identify candidate genes within this QTL locus, we have developed an approach in which we combined physical mapping and cDNA microarray analysis to select candidate gene(s) based on their relative expression level and chromosomal locations. In this study, we constructed a BAC contig that contains 40 BAC clones and covers the peak region of this QTL locus (92 to 94 cM) on mouse chromosome 1. cDNA microarray analysis was conducted by Incyte Genome Systems. The isolated mRNA from femur of both the congenic and B6 strains were labeled with different dyes and hybridized onto the same microarray chip containing 8,739 genes and ESTs. This analysis revealed that 104 genes and ESTs showed at least 2-fold difference between the two strains. Among these candidate genes, 19 are known genes and 85 are ESTs. Among the known genes, 10 have functions relevant to bone. Only one (petaxin-related C-reactive protein) is located within the chromosome 1 QTL region. Among the ESTs, three are matched to the QTL locus of chromosome 1 and two are located within our BAC contig. In summary, we have identified 3 peak bone density candidate genes (C-reactive protein and 2 ESTs) in mice by our combination approach of physical mapping and cDNA microarray analysis. [This work was supported by USAMRAA through Assistance Award No. DAMD17-99-1-9571].

1411

YAC/BAC contig and STS mapping of the human $GABA_A$ receptor subunit gene cluster on chromosome 4. *J. Du, S.A. Karim, K.J. Johnson, M.E.S. Bailey.* Division of Molecular Genetics, I.B.L.S., University of Glasgow, Glasgow, U.K.

The GABA (γ-aminobutyric acid) type A receptor is a ligand-gated ion channel complex that is important in inhibitory neurotransmission in the vertebrate brain. Each of the 19 distinct related subunits known in mammals, which are classified into seven subclasses (α, β, γ, δ, ε, θ, π and ρ), is encoded by a separate GABR gene. A cluster of

Oral presentation on the First North American Scientific Meeting of Moroccan Association of Researchers and Scholars:

06-23-2000

Physical mapping of a QTL locus that controls bone density on mouse chromosome 1

B. Edderkaoui, S. Mohan, K-H.W. Lau, X.M. Li, D. Strong, W.K. Gu, & D. J. Baylink
Musculoskeletal Disease Center, JL Pettis VA Medical Center and Loma Linda University, Loma Linda, CA

We have previously identified a QTL locus that controls peak bone density in the mouse using the F2 population of C57BL/6J (B6) X CAST/EiJ (CAST) strains of mice. This QTL is located on mouse chromosome 1 and contributes approximately 40 % of the variation of the peak bone density between these two strains. In order to positional clone candidate gene(s) responsible for peak bone density, it would be essential to have a physical map of this QTL. In this regard, a contig, which is a physical map that displays a set of contiguous overlapping and ordered clones along a specific region of a chromosome, would provide overlapping clones for a systematic searching of genomic sequences, which is essential for positional cloning of candidate genes. Consequently, the present objective was to construct a contig that covers this QTL locus in mouse chromosome 1 using a bacterial artificial chromosomal (BAC) library.

The RPCI-23 BAC library was used to construct the contig. Information from the mouse genome database and publications was used to design PCR primers for generating our probes. The probes were used to hybridize the high-density filters of RPCI-23 BAC library according to the procedure developed by Rosewell Park Cancer Institute. The high-density filters were initially screened with pooled probes. Positive clones were isolated and used to prepare secondary screening filters. The secondary filters were then screened with individual probes. The hybridization results were used as our basis to connect various BAC clones together to form the contig. With this approach, we have constructed a BAC contig that covers the peak area of the chromosomal QTL locus that controls peak bone density in the mouse. Clones within the contig were confirmed by PCR amplification using our primers that were used for the hybridization probes. The contig consisted of 40 BAC clones that overlap with each other among neighboring clones without gaps. This contig is currently being sequence. Sequence information will be used to identify candidate genes. In conclusion, we have constructed a contig that covers the peak region of the QTL locus within mouse chromosome 1 that controls the peak bone density in mouse. The future availability of genomic sequence information of this contig will facilitate our work in candidate gene search by various approaches.

*This work was supported by USAMRAA, through Assistance Award No. DAMD17-99-1-9571.

Abstract Form

Appendix 1–5

International Conference on
Progress in Bone and Mineral Research 2000 and
8. Österreichisches Osteoporoseforum
Vienna, Austria, November 30 – December 2, 2000

Name(s) and initial(s) of the author(s) W.K. GU, M. HELLAN, X.M. LI,
(presenting author underlined)
H-C.M. SHENG, W.G. BEAMER, J. WERGEDAL, K-H.W. LAU,
S. MOHAN, D.J. BAYLINK

Full address of presenting author MUSCULOSKELETAL DISEASE CENTER (151)
JERRY L. PETTIS VAMC and LOMA LINDA UNIVERSITY
11201 BENTON STREET, LOMA LINDA, CA 92357, USA

Organization of the Abstract:
(in camera ready format, Font: 11 Pt or larger)
Titel in Capital Letters
Author(s)
Institution, City, State
Text (Purpose, Methods, Results, Conclusion)

Sessions Classification
(please check)

	A	B
Session 1	☒	☐
Session 2	☐	☐
Session 3	☐	☐
Session 4	☐	☐
Session 5	☐	☒
Session 6	☐	☐
Osteoporoseforum	☐	☐

Mark with "A" your first choice, with "B" your second choice. This will determine for the Session in which your poster might be chosen for oral presentation as well as the location of the abstract in the booklet.

Abstract Fee: ATS 500,–
☐ I made a bank transfer
☐ I enclose a cheque
☐ Please charge my credit card:
☒ VISA ☐ Eurocard/Mastercard
☐ Diners Club
Card no.: 4024 2120 1080 0220
Expiry Date: 11. 2001
Name of the Cardholder: MINIA HELLAN

Date: 26.6.00 Signature: Minia Hellan

Please mail this Abstract Form (only the original form can be used) plus two photocopies together with the Acknowledgement-Receipt Card and with ATS 500,– Abstract fee, so that it is in our hands not later than June 30, 2000 to:
Vienna Medical Academy (Wiener Medizinische Akademie)
Alser Strasse 4, A-1090 Vienna, Austria

Type abstract here – stay strictly within border!

EVALUATION OF THE EFFECT OF A QUANTITATIVE TRAIT LOCUS (QTL) ON PEAK BONE MINERAL DENSITY (BMD) USING CONGENIC MICE *

W.K. Gu[1], M. Hellan[1], X.M. Li[1], H-C.M. Sheng[1], W.G. Beamer[2], J. Wergedal[1], K-H.W. Lau[1], S. Mohan[1], & D.J. Baylink[1]
1) Musculoskeletal Disease Center, JL Pettis VA Medical Center and Loma Linda University, Loma Linda, CA. 2) The Jackson Laboratory, Bar Harbor, ME.

Peak bone mineral density (BMD) is one of the strongest determinants of subsequent osteoporotic fracture risk. More than 70% of variance in peak BMD is determined by genetic factors. Our previous genetic studies of regulation of peak BMD indicated that peak BMD difference between CAST/EiJ (CAST) and C57BL/6J (B6) mouse strains, which exhibit high and low peak BMD, respectively, is controlled by 6 quantitative trait loci (QTL) located on different chromosomes. Subsequently, we focused on the relative contribution of CAST chromosome 1 QTL to the peak BMD difference because of the high LOD score and its location on the syntenic region of human chromosome 1Q21-23, a region implicated in peak BMD regulation in humans. To determine whether chromosome 1 QTL contained biologically active gene/s that contribute to significant peak BMD difference between CAST and B6 strains, we generated congenic strains by transferring CAST chromosome 1 QTL region (donor) into the B6 strain (recipient) with 6 cycles of backcrossing (N6F1). CAST 1 chromosomal segments were identified by following flanking polymorphic SSLP markers during the backcrossing procedure. N6F2 littermate mice were produced by crossing N6F1 X N6F1 and progenies genotyped to identify homozygotes carrying CAST 1 QTL prior to bone phenotypic analysis. BMD of congenic mice of different ages (6, 10 and 16 weeks) was determined by pQCT and compared to respective age-matched B6 mice. We found that volumetric BMD at the mid diaphysis of the femur was significantly higher in the congenic mice compared to age-matched B6 mice at 16 weeks of age (685±34 vs 638±41 mg/cm^3; $P<0.05$). The periosteal circumference but not the endosteal circumference was significantly greater in the congenic mice compared to B6 mice at 16 weeks of age. Conclusion: Our data demonstrate through congenic mice that CAST chromosome 1 QTL contains biologically active gene/s that regulates femoral peak BMD in part by increasing periosteal circumference.

*This work was supported by USAMRAA, through Assistance Award No. DAMD17-99-1-9571.

Genetic Control of the Rate of Wound Healing in Mice

Xinmin Li[1], Weikuan Gu[1], Godfred Masinde[1], Melanie Hamilton-Ulland[1], Shizhong Xu[2], Subburaman Mohan[1], David J Baylink[1]

[1]Molecular Genetics Division, Musculoskeletal Disease Center, JL Pettis VA Medical Center and Loma Linda University, Loma Linda, CA 92357, USA

[2]Department of Botany and Plant Sciences, University of California, Riverside, CA 92521-0124, USA

Corresponding author: David J Baylink, MD., Musculoskeletal Disease Center, JL Pettis VA Medical Center, 11201 Benton Street (151), Loma Linda, CA 92357, USA

Tel: (909) 422-3101

Fax: (909) 796-1680

E-mail: David.Baylink@med.va.gov

Keywords: wound healing, inbred mouse, heritability, quantitative trait, genetic variability, segregating population

Running title: inheritance of wound healing

Summary

There have been few studies of the inheritance of the rate of wound healing in mammals, although the subject is fundamentally important in wound healing research. In this study, we demonstrate that inbred strains of mice differ significantly in the rate of wound healing. Of the 20 strains tested, MRL/MpJ-Fas^{lpr} and LG/J/J mice were the most rapid and complete healers, while Balb/cByJ was the poorest healer (healed less than 25%). The genetic basis underlying the difference in the healing capacity was analyzed using F_2 populations of two different crosses. We show that the rate of wound healing is a polygenically determined quantitative trait with an average estimated heritability of 86%. The modes of gene action for the two crosses are different. In the (MRL/MpJ × SJL/J) cross, the F_1 offspring exhibited intermediate values of the two parents and F_2 individuals exhibited a normal distribution with an average value similar to that of F_1. In contrast, the average of F_1 offspring in the (MRL/MpJ-Fas^{lpr} × CBA/J) cross had a similar value to one parent, CBA/J mice, and the phenotypic distribution of the F_2 offspring severely deviated from normality, being shifted toward the average value of the CBA/J parent. A χ^2 test showed that the MRL/MpJ-Fas^{lpr} type:CBA/J type ratio in the F_2 population did not differ significantly from 1:3. These results suggest that there is a dominant repressor gene in CBA/J mice which suppressed the additive action of fast-healing genes in MRL/MpJ-Fas^{lpr}. Information gained from this investigation provides a foundation for further study of molecular mechanisms underlying the rate of wound healing in mammals.

Introduction

Wound healing is a complex process requiring the joint effort of many different genes (Kunimoto, 1999). The clinical endpoints of mammalian wound repair involve the quality of healing (tissue regeneration) and the rate of healing (Goss, 1992; Martin, 1997; Singer & Clark, 1999). *In vivo* animal models have been developed to study the mechanisms of wound healing in both normal states and impaired states (Rothe & Falanga, 1992). Studies have shown that topological application of cod liver oil ointment, vitamin A, deoxyribonucleosides, and some proteins can accelerate wound healing (Shan *et al.*, 1995; Chen *et al.*, 1999; Terkelsen *et al.*, 2000). However, up to now we know very little about the inheritance of the rate of wound healing and the mode of its inheritance.

In 1998, Clark *et al.* accidentally found that the MRL/MpJ-Fas^{lpr} (MRL-F) strain of mice could completely heal an ear-punched hole (2 mm in diameter) with normal tissue architecture within 4 weeks in contrast to the control mice, B6, which only healed 30% of the original hole with scar tissue at the same period of time. Using (MRL-F × B6) F_2 and backcross populations, it was demonstrated for the first time that rapid wound healing in MRL-F mice is a genetically-controlled quantitative trait (McBrearty *et al.*, 1998). This study led to an opportunity to search for fast-healer genes in mammals and also raised several fundamental questions related to genetic variability and heritability of wound healing that will be addressed in this study.

The objectives in this study are: (1) to investigate the genetic variability in the rate of wound healing in the genetically distantly-related inbred strains of mice; (2) to determine from which progenitor strain the rapid-wound-healing phenotype in MRL-F

mice was derived; (3) to explore the mode of gene action using different genetic backgrounds; and (4) to estimate the broad-sense heritability of the rate of wound healing.

Materials and methods

Animals

Twenty inbred strains of mice (see Fig. 1 for the strains) were selected from a group of major inbred strains representing a diversified genetic origin. Four-week old female mice were obtained from The Jackson Laboratories (Bar Harbor, ME) and housed at the Animal Research Facility, JL Pettis VA Medical Center, Loma Linda, CA, under the standard condition of 14 h light, 10 h darkness, ambient temperature of 20°C, and relative humidity of 30-60%. All F_1 and F_2 mice including (MRL/MpJ-Fas^{lpr} × LG/J/J), (MRL/MpJ-Fas^{lpr} × CBA/J/J), and (MRL/MpJ × SJL/J/J) crosses were bred at the Animal Research Facility. The experimental protocols were in compliance with the animal welfare regulation and approved by the JL Pettis VA Medical Center, Loma Linda, CA.

MRL/MpJ-Fas^{lpr} and MRL/MpJ strains

MRL/MpJ-Fas^{lpr} mouse is a mutant derived from MRL/MpJ colony. The mutation is the direct result of a retrotransposon insertion into the second intron of the *fas* gene in the Mrl/MpJ strain (Adachi *et al.*, 1993). It has been shown that the mutation is not related to

the rapid and complete wound closure in MRL mice (McBrearty *et al.*, 1998). However, for an unidentified reason, MRL/MpJ-Fas^{lpr} mice have a slightly better healing capacity than MRL-MpJ mice (McBrearty *et al.*, 1998 and our observation in this study).

Ear punch and measurement

One week after the animals arrived, a 2 mm through-and-through hole in diameter was made in the lower cartilaginous part of each ear using a metal ear punch (Fisher Scientific, Pittsburgh, Catalog No. 01-337B). The hole closure was measured using a 7X magnifier at day 0, 5, 10, 15, 20, 25, and 30 for the 20 inbred strains of mice and at day 0, 15, 21, and 25 for the parents, F_1 and F_2 crosses. Each hole was measured twice (horizontal and vertical measurement) from the back of the ear (less hair at the back) and the average value for each time point was calculated from four measurements of two ears. The precision of hole measurement, determined by repeatedly measuring the same hole for 10 times, was 2.4% when the average size was 1.4 mm in diameter and 4.6% when the average size was 0.96 mm in diameter.

Statistical analysis

Two methods were used for estimation of the genetic variance for wound healing. The first method involved data from the 20 inbred strains only. We used a one-way ANOVA with strains treated as groups. Three individuals were measured for wound healing within each inbred strain. The mean square within strains (MS_W) reflects the environmental

variance (σ_W^2), while the mean square between strains (MS_B) is determined by both the genetic variance between strains (σ_B^2) and the environmental variance. The expectations of MS_W and MS_B are $E(MS_W) = \sigma_W^2$ and $E(MS_B) = \sigma_W^2 + r\sigma_B^2$, respectively, where $r = 3$ is the replicate within each strain. Letting the expected mean squares equal the observed mean squares, we get the estimated broad-sense heritability:

$$\hat{H}^2 = \frac{\hat{\sigma}_B^2}{\hat{\sigma}_B^2 + \hat{\sigma}_W^2} = \frac{MS_B - MS_W}{MS_B + (r-1)MS_W}$$

The second method of estimation used the difference between variances of different populations. The F_1, P_1 and P_2 are non-segregating populations whose variances (V_{F_1}, V_{P_1} and V_{P_2}) are purely due to environment. The F_2, however, is a segregating population whose variance (V_{F_2}) is determined by the sum of genotypic and environmental effect. Therefore, $V_{F_2} - (\frac{1}{2}V_{F_1} + \frac{1}{4}V_{P_1} + \frac{1}{4}V_{P_2})$ is an estimate of the genotypic variance. The broad-sense heritability is then estimated from:

$$\hat{H}^2 = \frac{V_{F_2} - (\frac{1}{2}V_{F_1} + \frac{1}{4}V_{P_1} + \frac{1}{4}V_{P_2})}{V_{F_2}}$$

Results

Genetic variability in the rate of wound healing among inbred strains

The change in the hole diameter is the measurement of the rate of wound healing. Fig. 1 shows the wound healing profiles for the 20 representative strains of mice. Each strain has a certain capacity for wound repair, but the rate of wound healing can be several-fold

different. LG/J healed over 95% of the holes on the 30th day after wounding, in contrast to Balb/cByJ or SJL/J that only healed less than 25% of the holes at the same period of time. The overall wound-healing profile revealed three healing stages: a) an initiation stage (day 0 to day 5) where there was no significant difference (P=0.01) in wound closure among all strains; b) a fast-healing stage (day 6 to day 20) where most of the strains achieved their maximal wound closure and exhibited markedly different healing capacity among strains; c) a slow-healing stage (day 21 to day 30) where most of strains had no healing or very little healing. Based on the rates of healing at day 30 after wounding, 20 strains were clustered into three groups (Fig. 2). The first group contained the fast healers, including MRL-F and LG/J mice. Strains in this group did not have an obvious slow-healing stage and closed the holes with a greater and more constant rate after initiation of healing. The second group included the intermediate healers that exhibited three distinct healing stages. The third group contained the poor healers, including Balb/cByJ and SJL/J. Strains in this group did not have an obvious fast-healing stage. The CBA/J strain was between the intermediate and fast-healer group (Fig. 1). It had a similar rapid-healing rate to the MRL-F and LG/J strain up to day 20 but stopped afterward, while MRL-F and LG/J continued their active healing process.

Genes regulating the rapid wound healing in MRL-F derived from LG/J mice

MRL-F mouse is a synthetic strain derived from the interbreeding of four progenitor inbred lines: LG/J (75%), AKR (12.6%), C3H (12.1%) and B6 (0.3%). Fig. 3 shows that LG/J completely healed the holes 30 days after wounding and had the same healing rate

as that of MRL-F, while the other three progenitor strains (AKR, C3H, and B6) healed less or about 50% of the holes. This result phenotypically suggests that the major fast-healer genes in MRL-F were likely derived from LG/J rather than other progenitor strains. However, different sets of genes could code for a similar phenotype. In order to genetically clarify the issue, we examined the rate of healing in a (MRL-F × LG/J) F_2 population. If the fast-healer genes in LG/J were different from those in MRL-F (i.e., the fast-healer genes in MRL-F were largely derived from other progenitor strains), it was expected to observe a wide range of phenotypic variation with a normal distribution (under the assumption of additive gene effect) and some individuals that healed even faster than both parents due to transgressive segregation in F_2 population. Conversely, Fig. 4 shows that the ranges of healing rate in F_1 and F_2 mice were not significantly different from those of their parents, and super-healers were not identified when the observation was made on the 15th day after wounding (data not shown). These results suggest that genes regulating the fast-healing phenotype in MRL-F mice were mainly derived from LG/J mice.

The modes of inheritance for the rate of wound healing in segregating populations

The genetic basis underlying the different rate of wound healing was analyzed in two F_2 populations derived from crosses (Mrl-MpJ × SJL/J) and (MRL-F × CBA/J), respectively. Strain SJL/J is a slow healer while CBA/J is a relatively good healer with a unique healing profile (Fig. 1). In the (Mrl-MpJ × SJL/J) cross, the average healing rate of F_1 at day 21 after wounding showed an intermediate value between the two parents,

and F_2 individuals exhibited a normal distribution, typical of a quantitative trait with additive gene effects (see Fig. 5A). A certain degree of transgressive segregation was observed. However, the (MRL-F × CBA/J) cross revealed a different healing profile, where F_1 mice had a healing capacity similar to its CBA/J parent, and the majority of F_2 mice exhibited a healing range similar to that of F_1 or CBA/J parent (Fig. 5B). When the F_2 mice were classified into the two groups based on the rate of healing observed in the parental strains and F_1, namely, $X \leq 0.3$ (MRL-F type), $X>0.3$ (F_1 and CBA/J type), the ratio of segregation was 1:2.9, which is not significantly different from the expected ratio of 1:3 under the hypothesis of a single dominant gene ($\chi^2= 0.017$, $0.90<P<0.95$). The average healing rates at three different time points after wounding are summarized in Table 1, which shows similar healing profiles. These parental phenotype-dependent F_2 distributions demonstrate the inherited nature of the rate of wound healing.

The rate of wound healing has a high broad-sense heritability

Table 2 shows the estimated broad-sense heritability using variance of analysis of 20 strains. The average heritability of the three time points (15 days, 20 days, and 30 days after wounding) is 0.84. When the segregating populations are used, the average estimated broad-sense heritability (15 days, 21 days, and 25 days after wounding) is 0.88 from the cross (MRL-MpJ × SJL/J) and 0.86 from the cross (MRL-F × CBA/J), respectively (see Table 3).

Discussion

We investigated the genetic variation for the rate of wound healing among 20 inbred strains of mice and explored the genetic basis underlying the difference using two segregating populations with different healing capacities. The salient findings of this study are: 1) the capacity for wound healing significantly differs among strains; 2) the fast-healer genes in MRL-F mice were most likely derived from LG/J strain; 3) the action of fast-healer genes is additive in the (MRL-MpJ × SJL/J) cross and the repressor gene in the CBA/J strain is dominant in the (MRL-F X CBA/J) cross; and (4) the healing rate has an estimated heritability of about 0.86. We will sequentially discuss these findings below.

Ear punching has been traditionally used as a means of identification of mice kept in colonies. The rate of healing of this hole (normally 2 mm in diameter) has never been systematically studied among inbred strains. In this study, we found dramatic variation in the rate of healing among strains. The difference could be up to 27 times between a good healer (LG/J) and a poor healer (Balb/cByJ). The healing capacity appears not related to their genealogy (Beck *et al.*, 2000). CBA/J and Balb/cByJ are all derived from Caste's mice, but CBA/J healed the holes 5 times faster than Balb/cByJ mice. B6 (C57-related strains), FVB (Swiss mice) and NZB (Castle's mice) have different genealogical origins but have almost identical healing capacity.

The healing profile revealed three healing stages: initiation stage, fast-healing stage, and slow-healing stage. The difference in healing primarily occurred in the fast-healing stage. The rate of fast healing and the time period of fast healing will determine

overall healing performance. Therefore, elucidation of molecular mechanisms underlying the healing capacity should target the fast-healing stage.

The MRL-F mouse is the best healer among 20 strains studied. To investigate the potential origin of the fast-healer genes, we examined the healing capacity of four progenitor strains of MRL-F mice and determined that LG/J is the most likely donor for the fast-healing phenotype of MRL-F. This conclusion is reinforced by overlapping phenotypic distribution in the parental, (MRL-F × LG/J)F_1 and F_2 populations. The LG/J mouse was developed by Goodale with selection for large body size (Chai, 1961). Fast-healing capacity in LG/J is unlikely associated with the body size, because SENCAR with a large body size (39.6 ± 3.9g) has an average healing rate while CBA/J, with a small body size (24.6 ± 1.2g), is a good healer. The coefficient of correlation between body weight and healing rate 30 days after wounding is –0.26 (P=0.191). It would be interesting to investigate where these fast-healer genes came from and how they were maintained during the selection of body size. There are two substrains, LG/J and LG/Ckc, which were separated at F_{27}. Further examination of the healing capacity in the LG/Ckc mice should provide insight into the evolutionary origin of these fast-healer genes.

To examine the mode of inheritance of these genes, two segregation populations were produced: (MRL-MpJ × SJL/J) and (MRL-F × CBA/J). The rationale for selecting the (MRL-MpJ × SJL/J) cross was based on their extreme phenotype in the rate of ear healing. We did not select the MRL-F strain for this particular cross, which was used in the (MRL-F × CBA/J) cross, because this cross will be used for bone density screening as well and MRL-F mice are highly susceptible to autoimmune disease and their health

conditions will deteriorate with age that will affect the measurement of bone density. A normal distribution profile in the (MRL-MpJ × SJL/J)F_2 mice indicates that the genes regulating fast healing have an additive effect and no major gene with dominant inheritance exists in this segregation population, although we could not rule out the action of semi-dominant genes because segregation populations tend to shift toward MRL-MpJ parent (Fig. 5A). Transgressive segregation, which is a common phenomenon in segregating hybrid populations (Rieseberg *et al.*, 1999), was observed in the F_2 population. The primary cause could be the action of complementary genes or/and epistasis.

We hypothesized that the (MRL-F × CBA/J) F_2 cross should produce superhealers with the ability to heal the hole faster than MRL-F, because both strains are good healers and have a different genetic origin (Beck *et al.*, 2000). Surprisingly, the healing capacity of F_1 individuals fell into the range of CBA/J mice and F_2 population fits the ratio of 3:1 (CBA/J type:MRL-F type), suggesting that a dominant repressor gene is present in CBA/J mice, which suppressed the action of the additive fast-healer genes derived from MRL-F. Because CBA/J itself is a good healer, the repressor most likely works in conjunction with the fast-healer genes, i.e., the fast-healer genes still function but are limited to a certain degree due to the presence of the repressor. Twenty-five percent of F_2 mice did not carry CBA/J-derived repressor gene. Under the assumption of additive gene effect, these mice should exhibit a continuous variation between the two parents. Consistent with this expectation, we observed a distribution peak within the range of $0.2 < X \leq 0.3$ between MRL-F and CBA/J parents (Fig. 5B).

Estimated heritabilities using variance of analysis and two segregating populations at different time points consistently show that the rate of healing is a highly inherited trait (average $H^2 = 86\%$). Little environmental contribution to the phenotypic variation suggests that the rate of healing is mainly controlled by genetic factors. This makes the identification and isolation of fast-healer genes feasible and the genetic manipulation of wound healing process possible.

In conclusion, the rate of wound healing is a genetically controlled quantitative trait with high heritability. The fast-healer genes exhibited an additive effect and the repressor gene showed a dominant effect. The healing capacity was a function of the number of fast-healer genes in the absence of the repressor gene and became a simple Mendelian trait (independent of the number of the fast-healer genes) in the presence of the repressor gene.

Acknowledgements

This work was supported by Assistance Award No. DAMD17-99-1-9571. The U.S. Army Medical Research Acquisition Activity, 820 Chandler Street, Fort Detrick MD 21702-5014, is the awarding and administering acquisition office. The information contained in this publication does not necessarily reflect the position or the policy of the Government and no official endorsement should be inferred. The authors wish to thank the JL Pettis VA Medical Center for their support.This work was also supported by funding from Veteran and Administration. The authors would also thank Heather Davidson for her excellent technical support.

References

ADACHI, M., WATANABE-FUKUNAGA, R. AND NAGATA, S. 1993. Aberrant transcription caused by the insertion of an endogenous retrovirus in an apoptosis gene. Proc. Natl. Acad. Sci., **90**, 1756-1760.

BECK, J. A., LLOYD, S., HAFEZPARAST, M., LENNON-PIERCE, M., EPPIG, J. T., FESTING, M.F. AND FISHER, E. M. 2000. Genealogies of mouse inbred strains. Nat. Genet., **24**, 23-25.

CHAI, C. K. 1961. Analysis of quantitative inheritance of body size in mice. IV an attempt to isolate polygenes. Genet. Res., **2**, 25-32.

CHEN, E. A., ZHAO, L., BAMAT, M., VON BORSTEL, R. AND MUSTOE, T. 1999. Acceleration of wound healing with topically applied deoxyribonucleosides. Arch. Surg., **134**, 520-525.

CLARK, L. D., CLARK, R. K., HEBER-KATZ, E. 1998. A new murine model for

mammalian wound repair and regeneration. Clin. Immunol. Immunopathol. **88**, 35-45.

GOSS, R. J. 1992. The evolution of regeneration. Adaptive or inherent? J. Theor. Biol., **159**, 241-260.

KUNIMOTO, B. T. 1999. Growth factors in wound healing: the next great innovation? Ostomy/Wound Management, **45**, 56-64.

MARTIN, P. 1997. Wound healing-aiming for perfect skin regeneration. Science, **276**, 75-81.

MCBREARTY, B. A., CLARK, L. D., ZHANG, X. M., BLANKENHORN, E. P., HEBER-KATZ, E. 1998. Genetic analysis of a mammalian wound-healing trait. Proc. Natl. Acad. Sci., **95**, 11792-11797.

RIESEBERG, L. H., ARCHER, M. A. AND WAYNE, R. K. 1999. Transgressive segregation, adaptation and speciation. Heredity, **83**, 363-72.

ROTHE, M. AND FALANGA, V. 1992. Growth factors and wound healing. Clinics in Dermatology. **9**, 553-559.

SHAN, M., FOREMAN, D. M., FERGUSON, M. W. J. 1995. Neutralisation of TGF-β_1 and TGF-β_2 or exogenous addition of TGF ... cutaneous rat wounds reduces scarring. J. Cell Sci. **108**, 985-1002.

SINGER, A. J. AND CLARK, R. A. F. 1999. Cutaneous wound healing. The New England J. Med. **341**, 738-746.

TERKELSEN, L. H., ESKILD-JENSEN, A., KJELDSEN, H., BARKER, J.H., HJORTDAL, V.E. 2000. Topical application of cod liver oil ointment accelerates

wound healing: an experimental study in wounds in the ears of hairless mice. Scand. J. Plast. Reconstr. Surg. Hand Surg. **34**, 15-20.

Figure legends:

Fig. 1 Rates of healing of a 2 mm ear hole in 20 inbred strains of mice. The healing process can be divided into three phases: initiation phase (I), rapid healing phase (II), and slow healing phase (III).

Fig. 2 Tree diagram for 20 inbred strains of mice. Cluster analysis was performed using the residual hole-size on the 30^{th} day after wounding. The X-axis represents single linkage Euclidean distance. When the tree is divided into three groups, the fast and complete healers fall into one group indicated by the solid dark lines, the poor healers fall into another group indicated by dashed lines, and intermediate healers fall into the third group.

Fig. 3 The ear-healing profiles of MRL-F and its four progenitor strains over 40 days after wounding.

Fig. 4 The histogram of frequencies of residual hole size on the 21^{st} day after wounding in parental, (MRL-F X LG/J)F_1 and F_2 populations. The numbers of mice used for MRL-F, LG/J, F_1, and F_2 populations are 11, 6, 11, and 65, respectively.

Fig. 5 The histogram of frequencies of residual hole size on the 21st day after wounding in parental, F_1 and F_2 populations. A. (MRL-MpJ X SJL/J) cross; B. (MRL-F X CBA/J) cross. See Table 1 for the numbers of mice used for the parental, F_1, and F_2 populations.

Table 1 Measurement of average hole-size (mm in diameter) at different time points after wounding in the parental, F_1 and F_2 mice (mean ± SD)

	MRL-MpJ	MRL-MpJ X SJL/J			MRL-F	MRL-F X CBA/J		
		SJL/J	F_1	F_2		CBA/J	F_1	F_2
Number of mice	19	20	36	500	11	8	9	78
Day 15	0.70±0.10	1.27±0.12	0.97±0.09	0.90±0.30	0.42±0.06	0.78±0.10	N/A	0.72±0.20
Day 21	0.44±0.10	1.10±0.10	0.71±0.11	0.69±0.32	0.07±0.08	0.53±0.09	0.42±0.05	0.46±0.19
Day 25	0.33±0.12	1.01±0.10	0.61±0.12	0.60±0.32	0.01±0.02	0.46±0.09	N/A	0.38±0.20

Table 2 Analysis of variance of the healing rate at different time points using 20 inbred strains of mice

Variable	SS effect	Df effect	MS effect	SS error	Df error	MS error	F	P	H^2
Day 15	3.78	19	0.199	0.929	40	0.023	8.57	>0.001	0.72
Day 20	6.92	19	0.364	0.418	40	0.01	34.8	>0.001	0.92
Day 30	9.13	19	0.481	0.857	40	0.021	22.4	>0.001	0.88

H^2 is estimated broad-sense heritability. SS: sum of squares; Df: degree of freedom; MS: mean squares.

Table 3 Estimated broad-sense heritabilities at different time points using variances of the parental, F_1 and F_2 populations

Time	Variance (MRL-MpJ X SJL/J)				H^2	Variance (MRL-F X CBA/J)				H^2
	MRL-MpJ	SJL/J	F_1	F_2		MRL-F	CBA/J	F_1	F_2	
Day 15	0.01	0.015	0.0085	0.0916	**0.88**	0.0039	0.01	N/A	0.0416	**0.83***
Day 21	0.01	0.009	0.0118	0.1014	**0.89**	0.0064	0.0073	0.0029	0.0366	**0.87**
Day 25	0.015	0.011	0.014	0.103	**0.87**	0.0004	0.0089	N/A	0.0408	**0.89***

*Environmental variances were estimated from the average of two parents. Estimated heritabilities are bold.

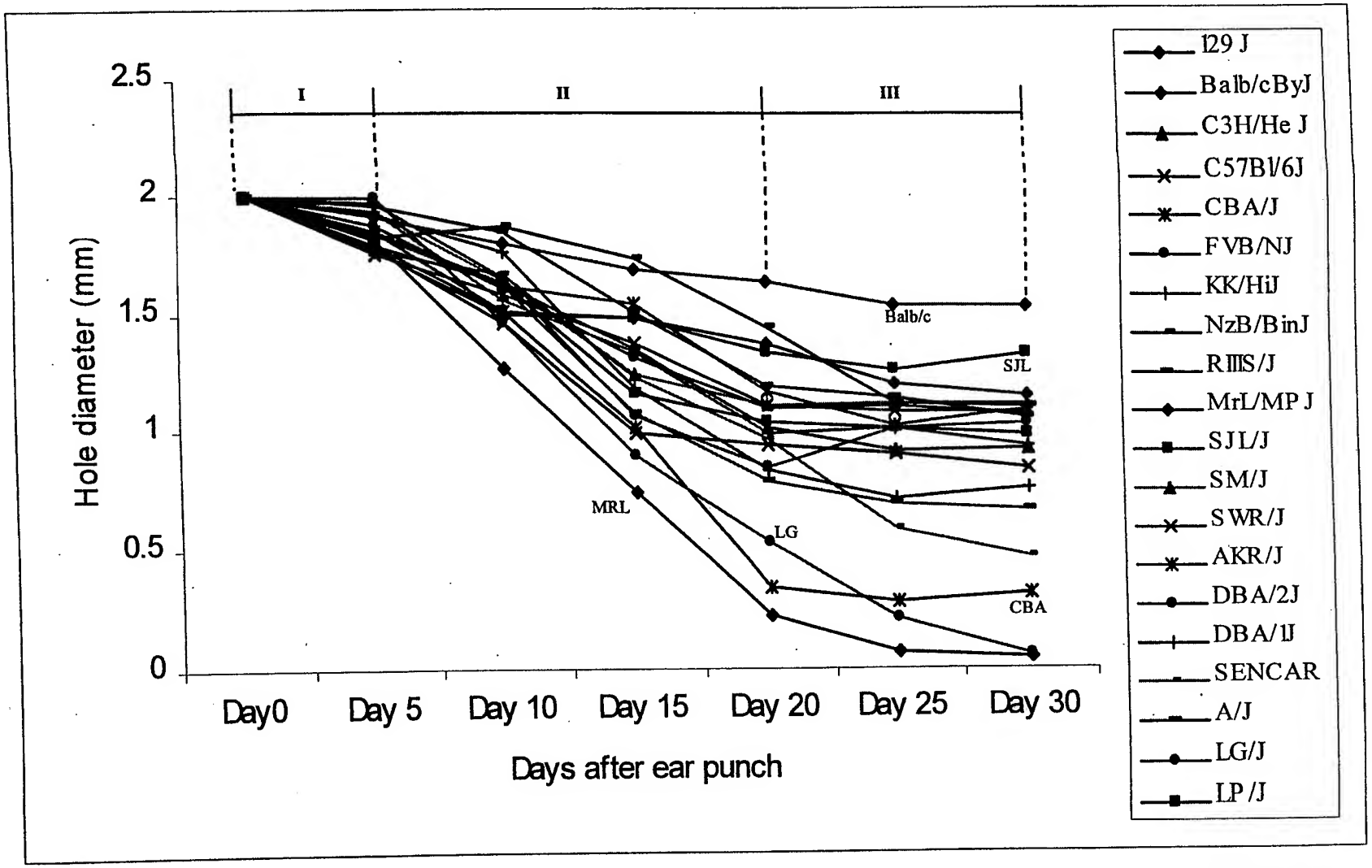
2.5
2
1.5
1
0.5
0
Hole diameter (mm)
I
II
III
Balb/c
SJL
MRL
LG
CBA
Day0
Day 5
Day 10
Day 15
Day 20
Day 25
Day 30
Days after ear punch
129 J
Balb/cByJ
C3H/He J
C57Bl/6J
CBA/J
FVB/NJ
KK/HiJ
NzB/BinJ
RIIIS/J
MrL/MP J
SJL/J
SM/J
SWR/J
AKR/J
DBA/2J
DBA/1J
SENCAR
A/J
LG/J
LP/J

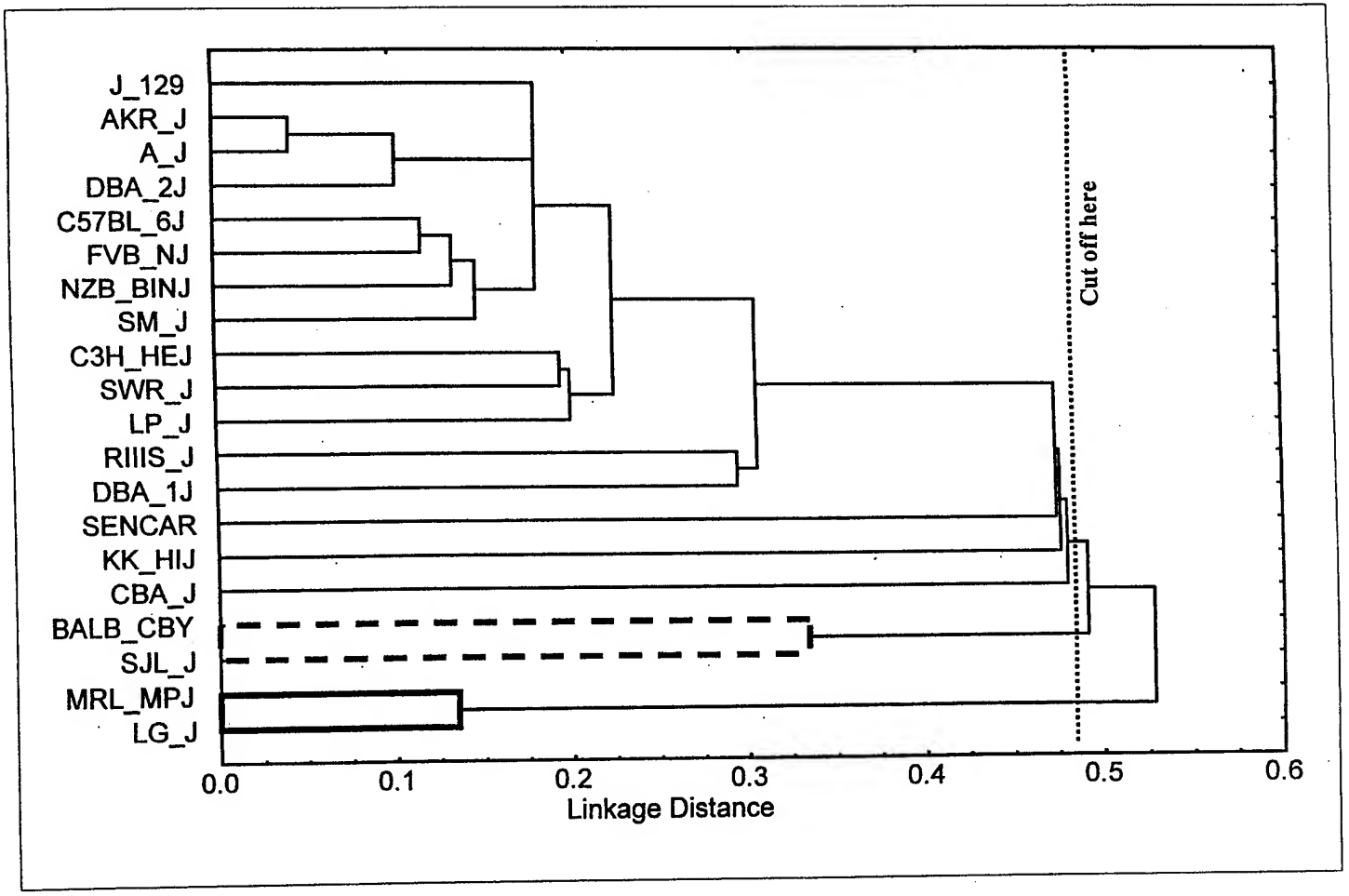
J_129
AKR_J
A_J
DBA_2J
C57BL_6J
FVB_NJ
NZB_BINJ
SM_J
C3H_HEJ
SWR_J
LP_J
RIIIS_J
DBA_1J
SENCAR
KK_HIJ
CBA_J
BALB_CBY
SJL_J
MRL_MPJ
LG_J
Cut off here
0.0
0.1
0.2
0.3
0.4
0.5
0.6
Linkage Distance

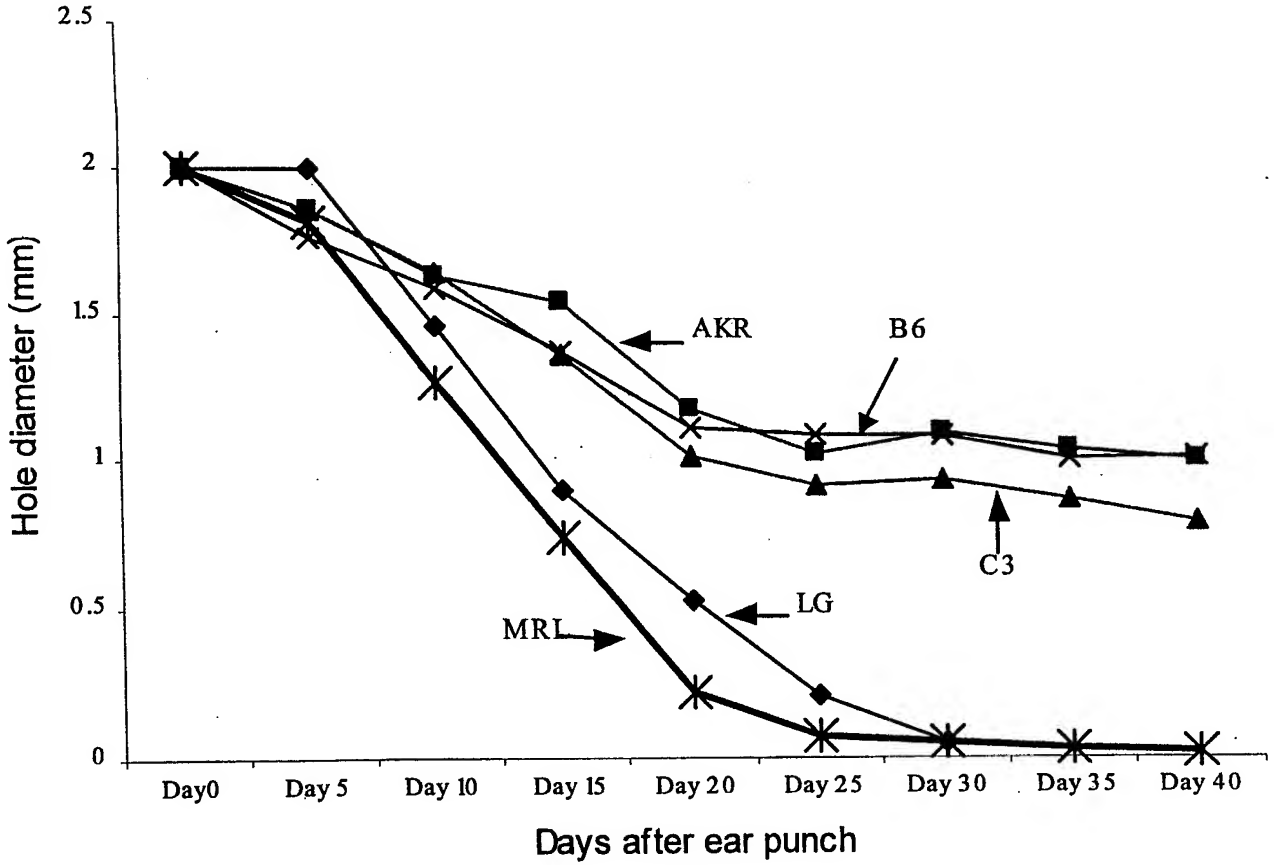
2.5
2
1.5
1
0.5
0
Hole diameter (mm)
AKR
B6
C3
LG
MRL
Day0
Day 5
Day 10
Day 15
Day 20
Day 25
Day 30
Day 35
Day 40
Days after ear punch

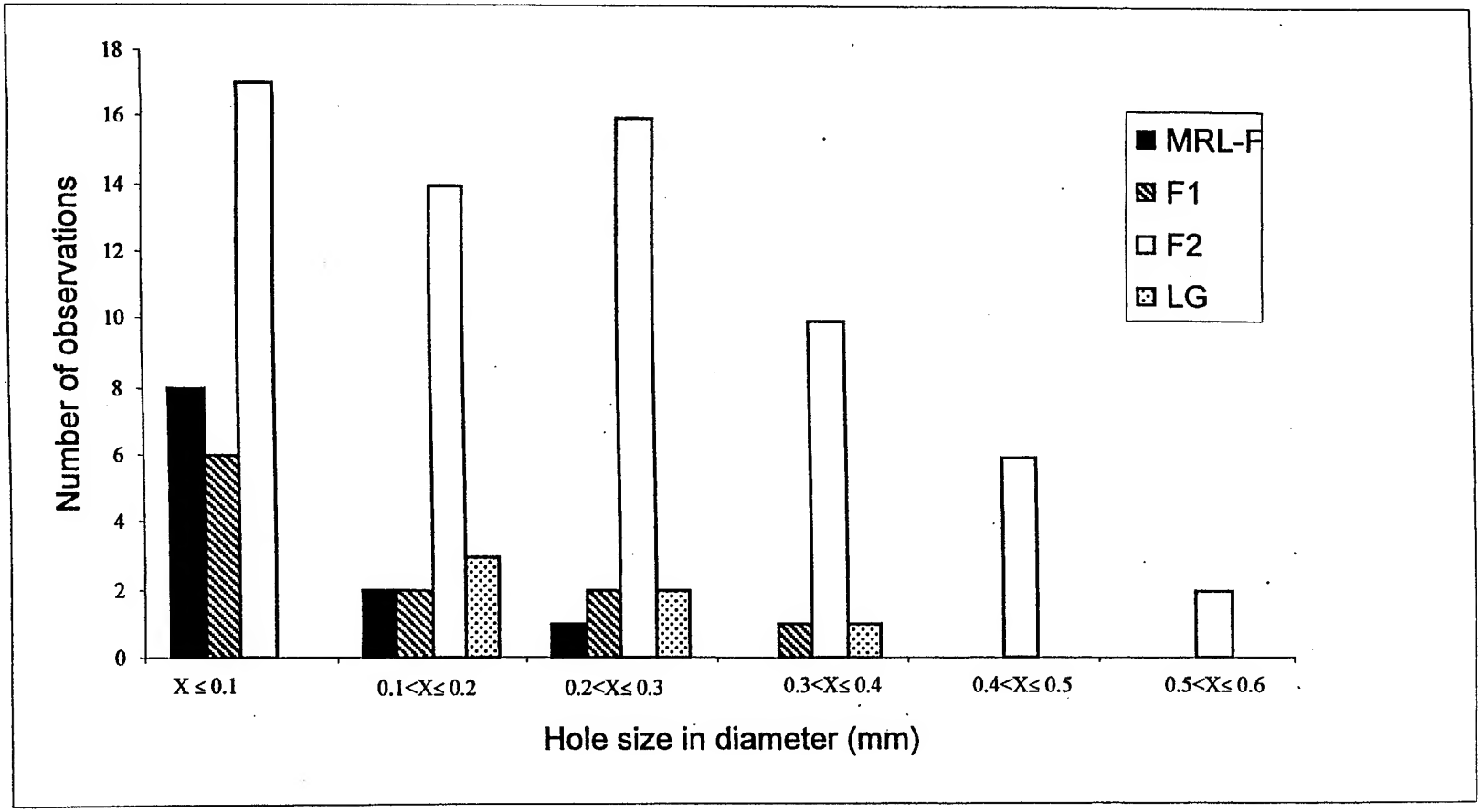
Number of observations
18
16
14
12
10
8
6
4
2
0
MRL-F
F1
F2
LG
X ≤ 0.1
0.1<X≤ 0.2
0.2<X≤ 0.3
0.3<X≤ 0.4
0.4<X≤ 0.5
0.5<X≤ 0.6
Hole size in diameter (mm)

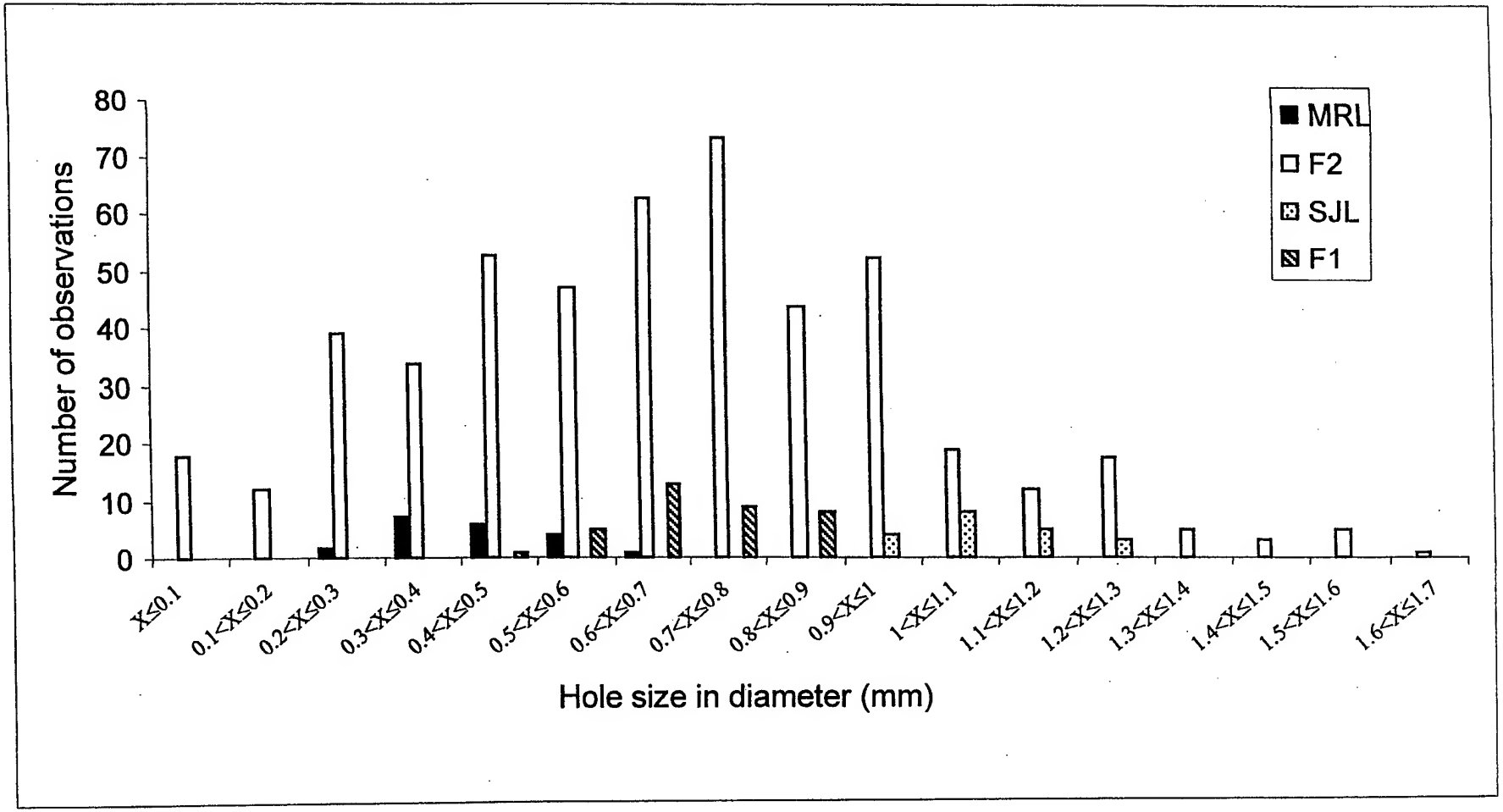
Number of observations
80
70
60
50
40
30
20
10
0
MRL
F2
SJL
F1
X≤0.1
0.1<X≤0.2
0.2<X≤0.3
0.3<X≤0.4
0.4<X≤0.5
0.5<X≤0.6
0.6<X≤0.7
0.7<X≤0.8
0.8<X≤0.9
0.9<X≤1
1<X≤1.1
1.1<X≤1.2
1.2<X≤1.3
1.3<X≤1.4
1.4<X≤1.5
1.5<X≤1.6
1.6<X≤1.7
Hole size in diameter (mm)

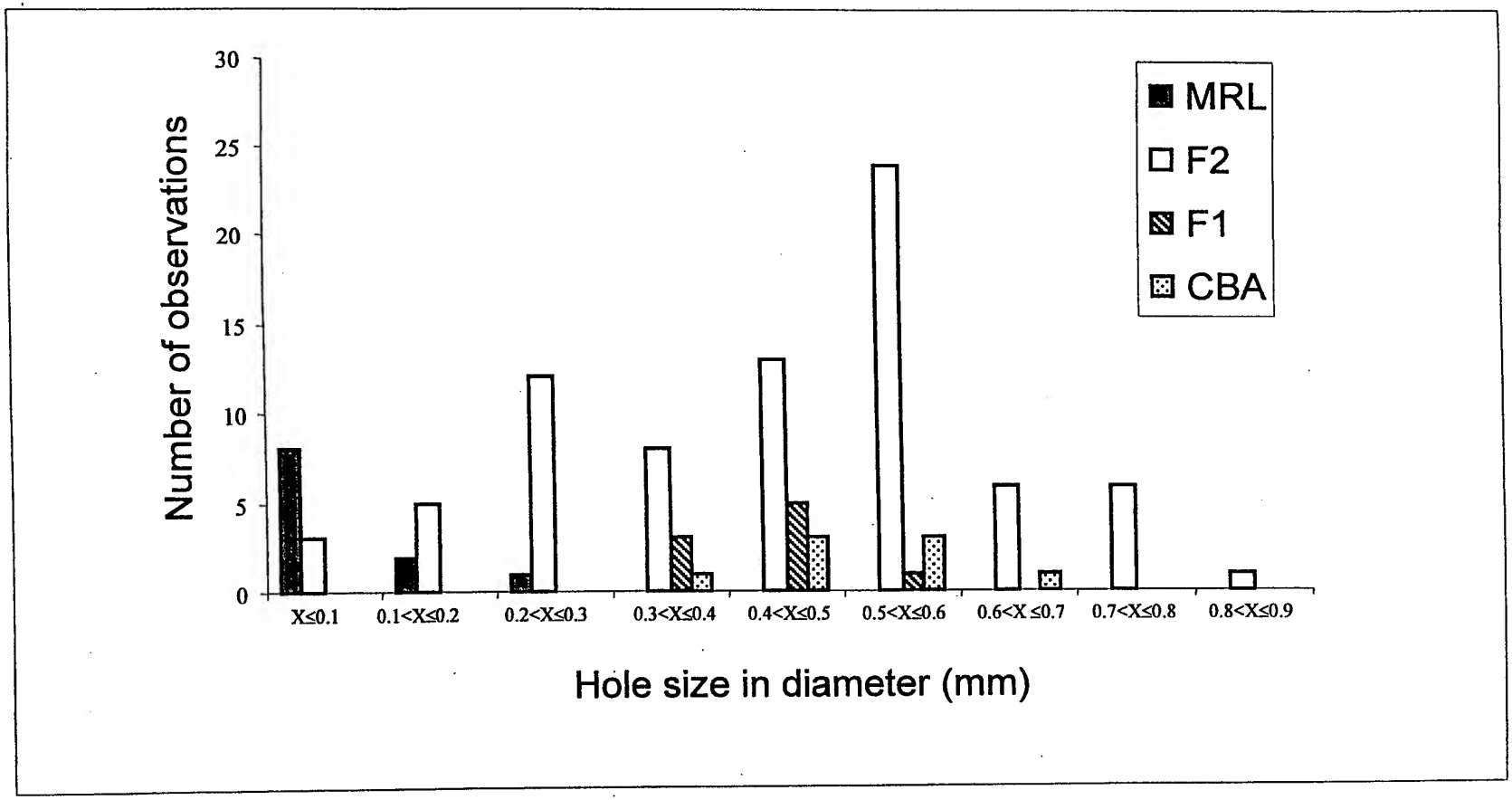
30
25
20
15
10
5
0
Number of observations
MRL
F2
F1
CBA
X≤0.1
0.1<X≤0.2
0.2<X≤0.3
0.3<X≤0.4
0.4<X≤0.5
0.5<X≤0.6
0.6<X ≤0.7
0.7<X≤0.8
0.8<X≤0.9
Hole size in diameter (mm)

Genetic variation in the bone regenerative capacity among inbred strains of mice

X. Li, W. Gu, G. Masinde, M. Hamilton-Ulland, C. H. Rundle, S. Mohan, D. J. Baylink

Molecular Genetics Division, Musculoskeletal Disease Center, JL Pettis VA Medical Center and Loma Linda University, Loma Linda, CA 92357, USA

Running title: Variation in bone healing

Corresponding author: David J Baylink, MD, Musculoskeletal Disease Center, JL Pettis VA Medical Center, 11201 Benton Street (151), Loma Linda, CA 92357, USA

Tel: (909) 422-3101

Fax: (909) 796-1680

E-mail: David.Baylink@med.va.gov

Abstract Genetic variation in bone regenerative capacity has not been studied in any animal model system. We have developed a "drill-hole" model in the tail vertebra of inbred strains of mice that allows us to reproducibly introduce an injury with a defined boundary and quantify the rate of bone healing using the combination of high resolution Faxitron X-ray images and a ChemiImager™ 4400 Low Light Imaging System. Using this model, we have demonstrated that bone regenerative capacity is a genetically controlled trait with an estimated heritability of 72% and it differs significantly among the inbred strains of mice. Of the 12 inbred strains tested, Sencar has been identified as a suitable model for the study of hard-tissue regeneration. It regained 73% of the bone loss 30 days after injury, in contrast to the slow healer, CBA/J, which only recovered 25% of bone loss at the same period of time. The bone regenerative capacity was not correlated with the soft-tissue regenerative capacity, suggesting that different sets of genes may regulate soft- and hard-tissue regeneration. It was, however, significantly correlated with the total bone mineral density ($R=0.49$, $p<0.01$), indicating that a high bone density is associated not only with prevention of bone fracture, but also with promotion of bone regeneration.

Key words: Wound healing; Bone regenerative capacity; Inbred mouse; Heritability; Quantitative analysis; Genetic variation.

Introduction

The ability of mammals to regenerate tissues is limited[7]. Bone is one of the few tissues able to regenerate in response to injury and, thus, is an excellent model for the study of the molecular mechanisms of tissue regeneration in mammals. To this end, a number of growth factors have been identified that play a role in the bone formation and repair cascades[3,13]. These include fibroblast growth factors (FGFs), platelet-derived growth factors (PDGFs), insulin-like growth factors (IGFs), transforming growth factor βs (TGF-βs) and the bone morphogenic proteins (BMPs). Several therapeutic approaches have applied these growth factors to enhance bone fracture healing[2,8].

In contrast to the existing knowledge on the role of individual growth factors in the bone healing process[1,10,11,15], the genetics of bone regenerative capacity as a whole is less well studied. Very little is known about the inheritance of bone regeneration, its genetic variability among populations, and its relationship to bone density. This lack of progress is due in part to technical difficulties associated with the creation and quantitative measurement of a reproducible injury. Addressing these fundamental questions is important in understanding the genetic complexity of bone regeneration and will contribute to the molecular dissection of this complex process.

Inbred strains of mice offer a rich genetic resource for experimentally defining the variation in the rate of bone regeneration. We have developed a "drill-hole" model that allows us to introduce a reproducible injury with a clearly defined boundary to the

tail vertebral body of the mouse and subsequently quantify the rate of bone healing among inbred strains of mice. Because previous studies have established that many genes have the potential to initiate and accelerate bone fracture healing[13], we hypothesized that the bone regenerative capacity is genetically controlled and varies among strains. Here we present data to show: 1) the genetic variation in bone regeneration among the 12 inbred strains of mice; 2) the characteristic temporal healing profiles in two commonly studied strains[12], C3H/HeJ (C3) and C57BL/6J (B6); and 3) the relationship among bone mineral density, hard-tissue regeneration and soft-tissue healing.

Materials and Methods

Experimental Animals

Twelve inbred strains of mice (129J, CBA/J, FVB/NJ, LG/J, LP/J, NZB/BINJ, RIIIS/J, SENCAR/PtJ, KK/HiJ, C3H/HeJ, C57Bl/6J, DBA/1J) were selected from subgroups of the major inbred strains representing a diversified genetic origin[6]. Three female mice of each of these strains and 10 female mice of C3 and B6 strains were obtained from The Jackson Laboratory (Bar Harbor, ME). The animals were housed at the Animal Research Facility, VA Medical Center, Loma Linda under conditions of 14 h light, 10 h darkness, an ambient temperature of 20° C, and a relative humidity of 30-60%. The animals were six months old in 12 representative strains and four weeks old in the C3 and B6 strains when the experiments were performed. All experimental protocols were in compliance

with the Animal Welfare Act and were approved by the Institutional Animal Care and Use Committee (IACUC) of the JL Pettis VA Medical Center, Loma Linda, CA.

"Drill-hole" procedure and measurement of bone healing

A hole of 0.9 mm in diameter was produced in the third vertebra from the base of tail using a Dremel Tool equipped with a 1/32 inch drill bit. Before the operation, mice were anesthetized using a dose of 50/10 mg/kg Ketamine/xylazine solution delivered intraperitoneally. The healing process was monitored up to 30 days at 10-day intervals using Faxitron X-ray (MX-20 Specimen Radiography System, lllinois USA) for qualitative evaluation. The Faxitron X-ray System was calibrated to obtain a flat field image for daily measurement. The third vertebra of the tail was positioned on the platform along with a 1cm X 2cm metal plate with a standard hole (0.9 mm in diameter) on it. This standard hole was used as a reference for later quantitative analysis. X-ray images were taken under constant conditions (26kVp, 6 seconds exposure and 5 x magnifications) using the Kodak XTL2 X-ray film (Kodak, Rochester, NY) so that the healing process could be quantitatively analyzed from different X-ray images.

The quantitative analysis was performed using the ChemiImager^{TM} 4400 Low Light Imaging System (Alpha Innotech Corporation, CA). The system can quantify DNA or RNA concentration from the ethidium bromide stained gels by measuring the light pixels. The value is expressed as the Integrated Density Value (IDV). We developed a procedure using this system to quantitatively evaluate the bone healing process from the X-ray images where the more bone is regenerated at the wound site, the higher the IDV

will be. The measurement procedures are illustrated in **Figure 1**. A template circle identical to the size of a standard drill hole on the X-ray film was made using the spot densitometery tool (software Version 5.5) and was moved next to the wounded vertebra (but not overlapping with the vertebra) for a local background reading. It was then superimposed over the original hole made on the third vertebra for the IDV reading. Two additional IDV readings were obtained by placing the circle over the position on the second and fourth vertebra equivalent to the hole position on the third vertebra. The absolute bone regenerative capacity was defined as "the hole IDV (step 3) – background IDV (step 2)". The relative bone regenerative capacity was defined as "the hole IDV ÷ [0.5 × (IDV from the second vertebra + IDV from the fourth vertebra)]".

Measurement of BMD

A PIXIMUS^{TM} Densitometer (LUNAR Corporation, Madison, WI) was used for the measurement of BMD. It is a rapid (5-minute image acquisition) and precise small animal densitometer with the precision of 1% CV for total skeletal BMD and 1.5% CV for femur region of interest (ROI) BMD. Calibration was performed daily with a defined standard (phantom) before measurement. Anesthetized mice were placed on a specimen tray and then inserted into the PIXI imaging area for analysis. After a measurement was completed, the PIXI software automatically recorded the data as a Microsoft Excel file.

Ear punch and measurement

A 2 mm diameter through-and-through hole was made in the lower cartilaginous portion of each ear using a metal ear punch (Fisher Scientific, Pittsburgh, Catalog No. 01-337B). The hole closure (in diameter) was measured 30 days after ear punch using a 7X magnifier. Each hole was measured horizontally and vertically from the back of the ear (less hair), and the average value was calculated from the four measurements in two ears. The precision of hole measurement, determined by repeatedly measuring the same hole 10 times, was 2.4% when the average hole size was 1.4 mm in diameter and 4.6% when the average hole size was 0.96 mm in diameter.

Statistical analysis

Results are reported as mean ± SD for 3 animals per strain. ANOVA and correlation analysis were performed using commercially available statistical software (STATISTICA, StatSoft Inc., Tulsa, OK). Results were considered significantly different for $P<0.05$. Heritability was estimated from the analysis of variance. We used a one-way ANOVA with strains treated as groups. Three individuals were measured for bone regeneration within each inbred strain at day 30 after operation. The mean square within strains (MS_W) reflects the environmental variance (σ_W^2), while the mean square between strains (MS_B) is determined by both the genetic variance between strains (σ_B^2) and the environmental variance. The expectations of MS_W and MS_B are $E(MS_W) = \sigma_W^2$ and $E(MS_B) = \sigma_W^2 + r\sigma_B^2$, respectively, where $r = 3$ is the replicate within each strain. Letting the expected mean squares equal the observed mean squares, we calculate the estimated broad-sense heritability as:

$$\hat{H}^2 = \frac{\hat{\sigma}_B^2}{\hat{\sigma}_B^2 + \hat{\sigma}_W^2} = \frac{MS_B - MS_W}{MS_B + (r-1)MS_W}$$

Results

Precision and validation of quantitative evaluation of bone regeneration

We used the ChemiImager™ 4400 Low Light Imaging System to quantitatively determine the rate of bone regeneration from high-resolution X-ray images. The precision of the measurement was tested to validate its suitability for the proposed study. Potential sources of variation between images include the X-ray film quality, exposure and development. We determined this image variation to be 2%, by measuring the same hole of 10 successive X-ray images taken from the same mouse (Table 1). Additional variation could occur between the actual image measurements, such as positioning the X-ray film on the light box of the ChemiImager™ 4400 Low Light Imaging System cabinet and superimposing the defined circle over the wounded site of the third vertebra. By 10 successive measurements of the same hole, this precision was determined to be 11% when CBA (slow healer) was measured and 2% when C3 (fast healer) was measured 30 days after injury (Table 1).

The validity of this comparative analysis also depends on the linear relationship between the bone regenerative capacity and IDV measurement. The ChemiImager™ 4400 Low Light Imaging System has a built-in mechanism to check the linearity (i.e., a capacity to examine the data saturation). When the data (image) becomes saturated, the bone regenerative capacity loses its linear relationship with the IDV reading. We

examined the images of all our measurements and established that they were not saturated. We further tested the linearity between the standard images and IDV readings using an aluminum mammographic step wedge (Pacific Northwest X-ray Inc., Gresham, OR). The correlation coefficient between the thickness of the step wedge and the corresponding IDV was 0.99 (**Figure 2**).

Qualitative and quantitative assessment of bone regeneration at day 30 after injury in 12 inbred strains of mice

The absolute bone regenerative capacity measures the net gain in bone after injury, while relative bone regenerative capacity reflects a percentage of bone recovery in relation to the original bone content. Because both of these measurements showed a high correlation ($R=0.86$, $p<0.0001$), we used the absolute bone regenerative capacity for subsequent comparisons.

The rate of tail vertebral regeneration varied significantly among strains. Based upon the rate of healing, we have classified the 12 strains into three groups, namely fast, intermediate or slow healers. **Figure 3** shows three representative strains of each group. Fast healers almost completely healed the 0.9 mm hole within 30 days, in contrast to the slow healers that healed very little in the same period of time. ANOVA analysis showed that the rate of bone healing is significantly different ($F=8.7$, $p<0.0001$) among strains. Sencar was the most suitable hard-tissue regeneration model among the strains tested (**Table 2**). The rate of healing was 3 times faster (70.7 ± 13) than that of the slow healer,

CBA (23.6±5.5). The estimate of broad-sense heritability was 0.72 for the absolute bone regenerative capacity and 0.82 for the relative regenerative capacity.

Temporal assessment of bone regeneration in C3 and B6 strains of mice

Because the C3 and B6 strains are commonly used in bone research, and have about 50% difference in bone mineral density[4] and more than 100% difference in bone regenerative capacity, as demonstrated in this study, we selected these two inbred strains for a comparison of the temporal healing profile. C3 mice progressively healed the hole over 30 days, while B6 mice healed very little. Perhaps because of the inability to heal, vertebra from B6 mice became deformed 10 days after injury (**Figure 4**). Deformation of wounded vertebra was a characteristics of B6 mice at four weeks of age. Nine of the 10 B6 mice had a deformed vertebra, while the C3 mice had none. Because of the deformation, we could not quantitatively compare the rate of bone healing between C3 and B6 mice.

Capacity for the hard-tissue regeneration is not correlated to that for soft-tissue healing but significantly correlated with total BMD

We have previously demonstrated that soft-tissue repair/regeneration varied significantly among inbred strains of mice, with a heritability estimate of 0.82. This study used the same individuals as those of the soft-tissue regeneration study, and we could, therefore, compare the regenerative ability in hard tissue with soft tissue. **Figure 5A** shows that the

bone regeneration is not correlated to the ear repair/regeneration. A typical example of lack of correlation between the hard-and soft-tissue regeneration is the CBA strain, which was a fast healer in ear repair/regeneration (a relative healing rate of 84%), but a slow healer in bone regeneration (a relative healing rate of 25%). The bone regeneration was significantly correlated to BMD (**Figure 5**B) and total BMC (**Figure 5**C). The correlation coefficient was 0.49 ($p<0.01$) with total BMD and 0.63 ($p<0.001$) with total BMC. In addition, the bone regenerative capacity at the tail vertebra also showed a significant correlation with femur BMD ($r=0.58$ $p<0.01$) and forearm BMD ($r=0.49$ $p<0.01$).

Discussion

Bone injury is a prominent clinical issue, but the genetic contributions to bone regeneration have not been well studied. We developed a novel approach to quantitatively determine the genetic variation in bone regenerative capacities among 12 inbred strains of mice and compared them with their respective soft-tissue repair/regeneration capacities and BMD. Our findings in this study are as follows: 1) the "drill-hole" model is a feasible approach to quantify the bone regeneration after injury; 2) inbred strains of mice harbor remarkable differences in the rate of bone healing; 3) SENCAR is the best strain for molecular dissection of the bone regeneration phenotype; and 4) hard-tissue regeneration is significantly correlated to bone density but not to soft-tissue repair/regeneration.

In a preliminary study, we found differences in the rate of vertebral fracture healing among strains using an Instron Mechanical Tester (Instron Corporation, Canton,

MA) to create vertebral fractures. Due to the different biomechanical properties among the strains, it was difficult to introduce identical injury reproducibility and perform comparative analysis quantitatively. We therefore explored an alternative model, a drill-hole in the vertebra. This model effectively overcame the technical difficulties of the fracture model by introducing an injury of reproducible size and with a clearly defined boundary that made quantitative analysis possible. We subsequently examined the precision and linearity of the measurements to verify the feasibility of this approach. We established that the variation of the measurements (2-11%) was far less than the genetic variation (42%) in the rate of bone healing among strains, and the bone regenerative capacity had a linear relationship with the measured IDV within the range of our data set ($r=0.99$, $p<0.001$). We concluded that the bone healing process can be quantitatively evaluated directly on high-resolution x-ray images using the ChemiImager^{TM} 4400 Low Light Imaging System.

Using this approach, we have found that there was a dramatic variation in the bone regenerative capacity among strains. The difference approached 3-fold between a fast regenerative strain and a slow regenerative strain. The coefficient variation across all strains was as high as 42%, suggesting a quantitative genetic regulation of the phenotype. Seventy-two percent of the variation could be attributed to genetic factors, providing a rationale for the mapping of loci critical to bone regeneration. In this regard, a (SENCAR X CBA/J) matting would be an ideal cross for the QTL mapping. These two strains exhibit extreme phenotypes in bone regenerative capacity (IDV of 70.7 for SENCAR and 23.6 for CBA/J), and the cross between the two will most likely produce a desirable wide range of phenotypic segregation in the F_2 population. The different genetic origins of

these two strains[6] should also promote the identification of a large number of polymorphic markers for construction of a dense genetic map, which is important for a high-resolution QTL mapping.

We attempted to identify the time point when the difference in the rate of bone healing occurs between a fast healer, C3, and a slow healer, B6, by comparing their temporal healing profiles. This information is essential for collecting samples at the optimum times for gene expression study. It was unexpectedly found that B6 vertebra had collapsed by the first observation at day 10, which prevented us from further quantitative comparison. We speculated that the density of the vertebrae may be related to the number of trabeculae (C3 mice have a 50% higher bone density than B6 mice). One possible explanation for the collapse is that B6 mice may have less trabeculae compared to C3 mice and, subsequently, have less trabecular struts to initiate healing. The cause of the collapse could be a combination of a low bone density and a reduced healing capacity. Histological comparison of the trabecular organization between a fast healer and a slow healer might elucidate contributions of trabecular number to the rate of bone healing.

The most significant finding of this study, from a practical standpoint, was the association of bone regenerative capacity with bone density. This association suggests that high bone densities not only reduce the risk of bone fracture but also promote bone healing after injury. The genetic implication of this association is that some of the genes regulating bone density might also function in bone regeneration. Many candidate genes or QTL regions for high bone density in both humans and mice have been identified[5, 9, 14, 16], and our QTL mapping programs for bone density genes are also in progress. Further

studies of these candidate genes should disclose this intriguing genetic relationship and facilitate the identification of the genes regulating bone regeneration.

It is not surprising that hard-tissue regeneration was not correlated with soft-tissue repair/regeneration. Both tissues undergo three similar stages (inflammation, repair/regeneration and remodeling) during wound healing. However, there are a number of differences in the response to injury at the cellular level. The soft tissue consists of different cell types compared to the hard tissue, and it has a much more severe inflammatory reaction than hard tissue in response to initial injury and does not form the callus characteristic of hard tissue regeneration. It appears that, although they may share some common molecular pathways, hard-tissue healing involves a different regulatory program relative to soft-tissue healing. This finding will necessitate separate molecular investigations for soft- and hard-tissue regeneration.

In conclusion, a significant genetic variation in bone regenerative capacity exists among inbred strains of mice. This variation provides a genetic basis for the molecular dissection of this highly inherited trait. The bone regenerative capacity has no correlation with soft-tissue repair/regeneration but has a sound correlation with the total BMD. This correlation has significant genetic and practical implications in preventing bone fracture or accelerating bone healing in humans.

Acknowledgements:

This work was supported by Assistance Award No. DAMD17-99-1-9571. The U.S. Army Medical Research Acquisition Activity, 820 Chandler Street, Fort Detrick MD 21702-5014, is the awarding and administering acquisition office. The information contained in this publication does not necessarily reflect the position or the policy of the Government and no official endorsement should be inferred. The authors wish to thank the JL Pettis VA Medical Center for their support. The authors would also thank Heather Davidson for her excellent technical support.

References

1. Bax, B. E., Wozney, J. M., Ashhurst, D. E. Bone morphogenetic protein-2 increases the rate of callus formation after fracture of the rabbit tibia. Calcif Tissue Int 65: 83-89; 1999.
2. Baltzer, A. W., Lattermann, C., Whalen, J. D., Braunstein, S., Robbins, P. D., Evans, C. H. A gene therapy approach to accelerating bone healing. Evaluation of gene expression in a New Zealand white rabbit model. Knee Surg Sports Traumatol Arthrosc 7: 197-202;1999.
3. Baylink, D. J., Finkelman, R. D., Mohan, S. Growth factors to stimulate bone formation. J Bone Miner Res 8 (Suppl): 565-572; 1993.
4. Beamer, W. G., Donahue, L. R., Rosen, C. J., Baylink, D. J. Genetic variability in adult bone density among inbred strains of mice. Bone 18: 397-403; 1996.
5. Beamer, W. G., Shultz, K. L., Churchill, G. A., Frankel, W. N, Baylink, D. J, Rosen, C. J, Donahue, L. R. Quantitative trait loci for bone density in C57BL/6J and CAST/EiJ inbred mice. Mammalian Genome 10: 1043-1049; 1999.
6. Beck ,J. A., Lloyd, S., Hafezparast, H, Lennon-pierce, M., Eppig, J. T, Festing, M. F, Fisher, E. M. Genealogies of mouse inbred strains. Nat Genet 24: 23-25;2000.
7. Chernoff, E. A. G., Stocum, D. L. Developmental aspects of spinal cord and limb regeneration. Develop Growth Differ 37: 133-147; 1995.
8. Goldstein, S. A., Bonadio, J. Potential role for direct gene transfer in the enhancement of fracture healing. Clin Orthop 355 (Suppl): 154-162; 1998.

9. Livshits, G., Karasik, D., Pavlovsky, O., Kobyliansky, E. Segregation analysis reveals a major gene effect in compact and cancellous bone mineral density in 2 populations. Human Biology 71: 155-172; 1995.

10. Murakami, S., Noda, M. Expression of indian hedgehog during fracture healing in adult rat femora. Calcif Tissue Int 66: 272-276; 2000.

11. Ohta, S., Muramatsu, H., Senda, T., Zou, K., Iwata, H., Muramatsu, T. Midkine is expressed during repair of bone fracture and promotes chondrogenesis. J Bone Miner Res 14: 1132-1144; 1999.

12. Rosen, C. J., Dimai, H. P., Vereault, D., Donahue, L. R., Beamer, W. G., Farley, J., Linkhart, S., Linkhart, T., Mohan, S., Baylink, D. J. Circulating and skeletal insulin-like growth factor-I (IGF-I) concentration in two inbred strains of mice with different bone mineral density. Bone 21: 217-223; 1997.

13. Rosen, V. R. and Thies, R. S. The cellular and molecular basis of bone formation and repair. Springer-Verlag, Heidelberg; 1995.

14. Sambrook, P. and Nguyen, T Bone mineral density and gene-environment interactions in the search for osteoporosis genes (Editorial). Environmental Health Perspectives 107: A130-131; 1999.

15. Yamagiwa, H., Tokunaga, K., Hayami, T., Hatano, H., Uchida, M., Endo, N., and Takahashi, H. E. Expression of metalloproteinase-13 (Collagenase-3) is induced during fracture healing in mice. Bone 25: 197-203; 1999.

16. Xu, T., Bianco, P., Fisher, L. W., Longenecker, G., Smith, E., Goldstein, S., Bonadio, J., Boskey, A., Heegaard, A. M., Sommer, B., Satomura, K., Dominguez, P., Zhao, C., Kulkarni, A. B., Robey, P. G., Young, M. F. Targeted disruption of the biglycan

gene leads to an osteoporosis-like phenotype in mice. Nature Genetics 20: 78-82; 1998.

Figure legends:

Figure 1. Outline of measurement procedures. Step 1 determines circle size based on the standard hole. Steps 2 and 3 measure background and hole IDVs, respectively, for the calculation of the absolute bone regeneration at the injured site. Steps 4 and 5 measure normal bone IDV at the equivalent position to the injured site for the calculation of the relative bone regeneration.

Figure 2. Relationship between the integrated density value and thickness of the mammographic step wedge.

Figure 3. Rates of healing of a 0.9 mm vertebral hole in 9 representative strains of mice. Top panel: fast healers (from the left to right, Sencar, 129/J and DBA/1J); Middle panel: intermediate healers (NZB/BinJ, LP/J and RIIIS/J); Bottom panel: slow healers (CBA/J, C57Bl/6J and FVB/NJ).

Figure 4. Temporal bone-regeneration profiles in C3 and B6 mice. Top panel: a representative C3 mouse; Bottom panel: a representative B6 mouse. The X-ray images were taken immediately (A and E), 10 days (B and F), 20 days (C and G) and 30 days (D and H) after injury.

Figure 5. Relationship between the absolute bone regenerative capacity and ear healing capacity, total BMD or total BMC. A: no correlation between bone healing and ear healing 30 days after injury; B: a moderate, significant correlation between bone healing and total BMD; C: a good correlation between bone healing and total BMC.

Table 1. Precision of measurements of bone regenerative capacity

# of measurement	Measurement A[1](relative density unit)	Measurement B[2] (relative density unit)		
		Hole #1	Hole #2	Hole#3
1	56	58	44	26
2	54	58	46	26
3	53	56	45	32
4	53	55	43	36
5	55	57	48	26
6	55	58	45	27
7	55	56	45	32
8	53	58	43	32
9	55	55	41	29
10	54	55	41	28
Average	54.3	56.6	44.1	29.4
STD	1.06	1.35	2.18	3.44
CV%	**2**	**2**	**5**	**11**

[1]Measurements of the same hole from different X-ray images taken from the same animal. [2]Repeated measurements of the same hole from one X-ray image. Hole #1, 2 and 3 represent three different X-ray images.

Table 2. Measurements of bone and ear phenotypes among inbred strains of mice[a]

Strains	Absolute bone regenerative capacity (relative density unit)	Relative bone regenerative capacity	Ear hole residue in diameter (mm)	Total BMD (g/cm^2)
KK/HiJ	50.0±6.2	0.35±0.05	0.96±0.33	0.070±0.008
C3H/HeJ	57.3±15.0	0.56±0.13	0.93±0.11	0.064±0.001
C57Bl/6J	25.0±2.6	0.29±0.02	1.1±0.11	0.057±0.001
RIIIS/J	29.7±8.7	0.32±0.04	0.68±0.12	0.057±0.003
CBA/J	23.6±5.5	0.25±0.03	0.33±0.07	0.065±0.004
SENCAR	70.7±13.0	0.73±0.14	0.48±0.26	0.066±0.005
FVB/NJ	24.3±6.6	0.27±0.01	1.12±0.12	0.059±0.002
NzB/BinJ	42.3±11.0	0.49±0.04	1.13±0.18	0.064±0.001
129/J	58.3±6.5	0.65±0.03	1.18±0.17	0.064±0.003
LG/J	53.3±15.2	0.40±0.01	0.08±0.08	0.070±0.002
All strains	43.5±18.32	0.43±0.17	0.80±0.40	0.063±0.005
F value	8.69	15.09	14.11	4.08
p	<0.0001	<0.0001	<0.0001	<0.01
Heritability	0.72	0.82	0.82	0.57
LP/J*	35	0.44	0.925	0.059
DBA/1J*	68	0.53	0.9	0.050

[a]Data are presented as mean±SD. The bone and ear healing capacity was measured 30 days after injury. *Only one animal was available when the bone regeneration analysis was performed and these animals were not included in the statistical analysis.

FIGURE 1

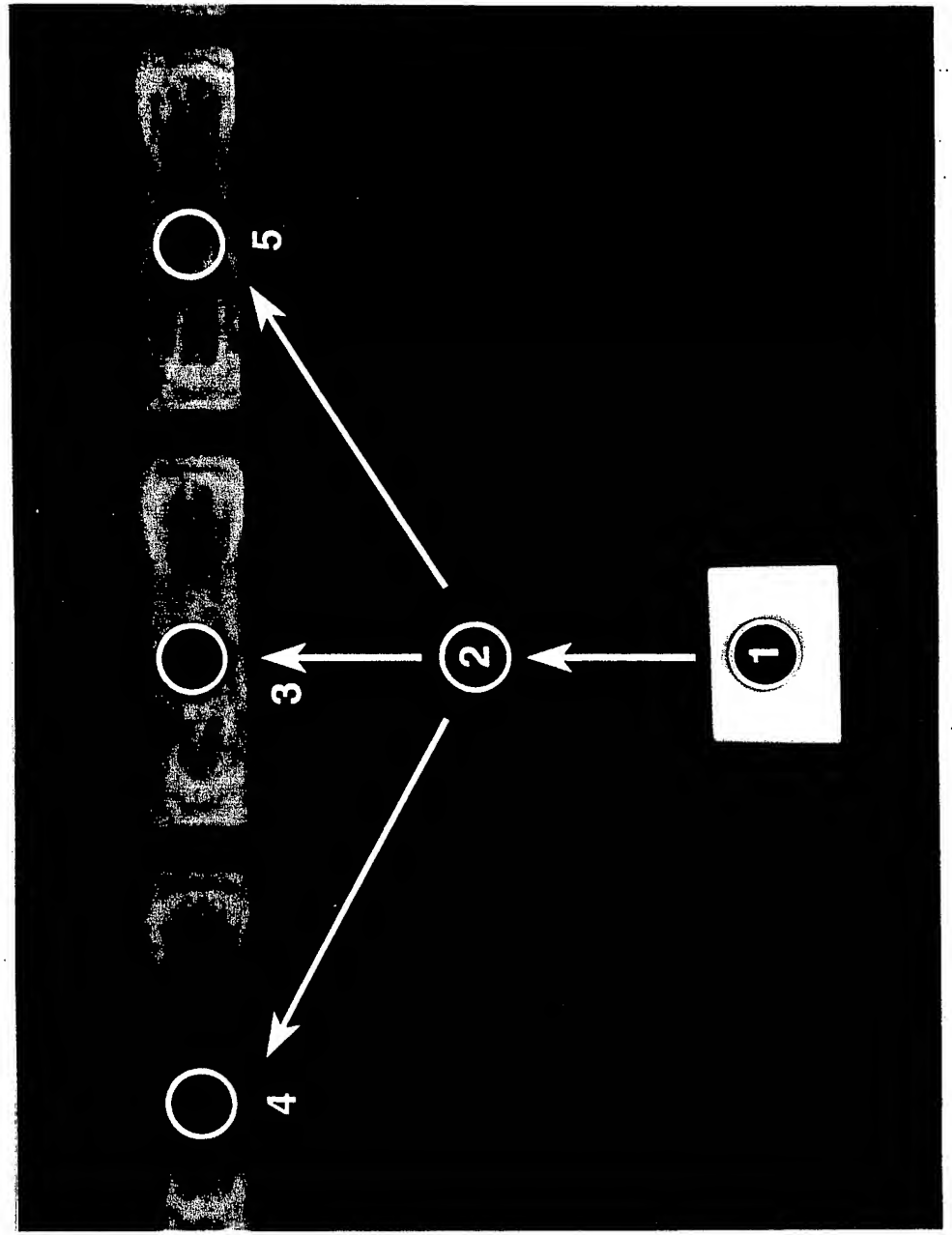

FIGURE 2

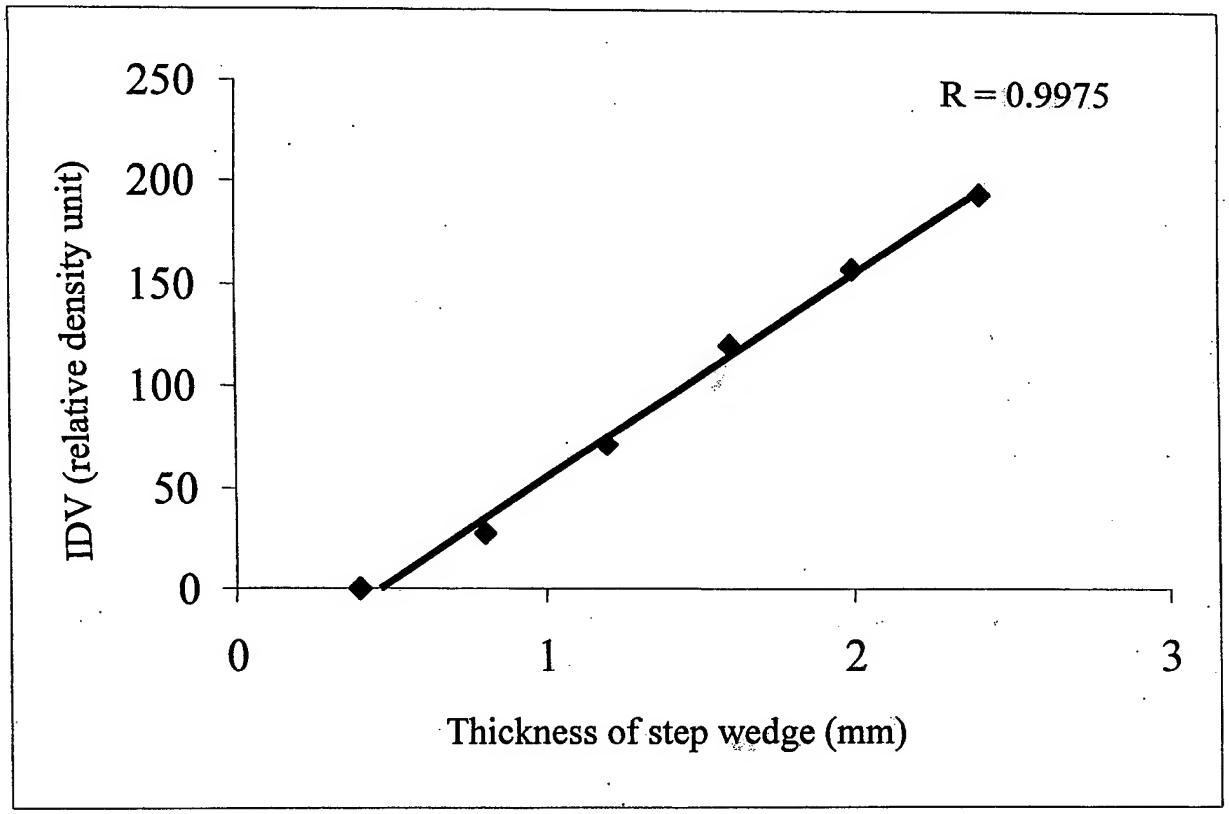
R = 0.9975
IDV (relative density unit)
250
200
150
100
50
0
0
1
2
3
Thickness of step wedge (mm)

FIGURE 3

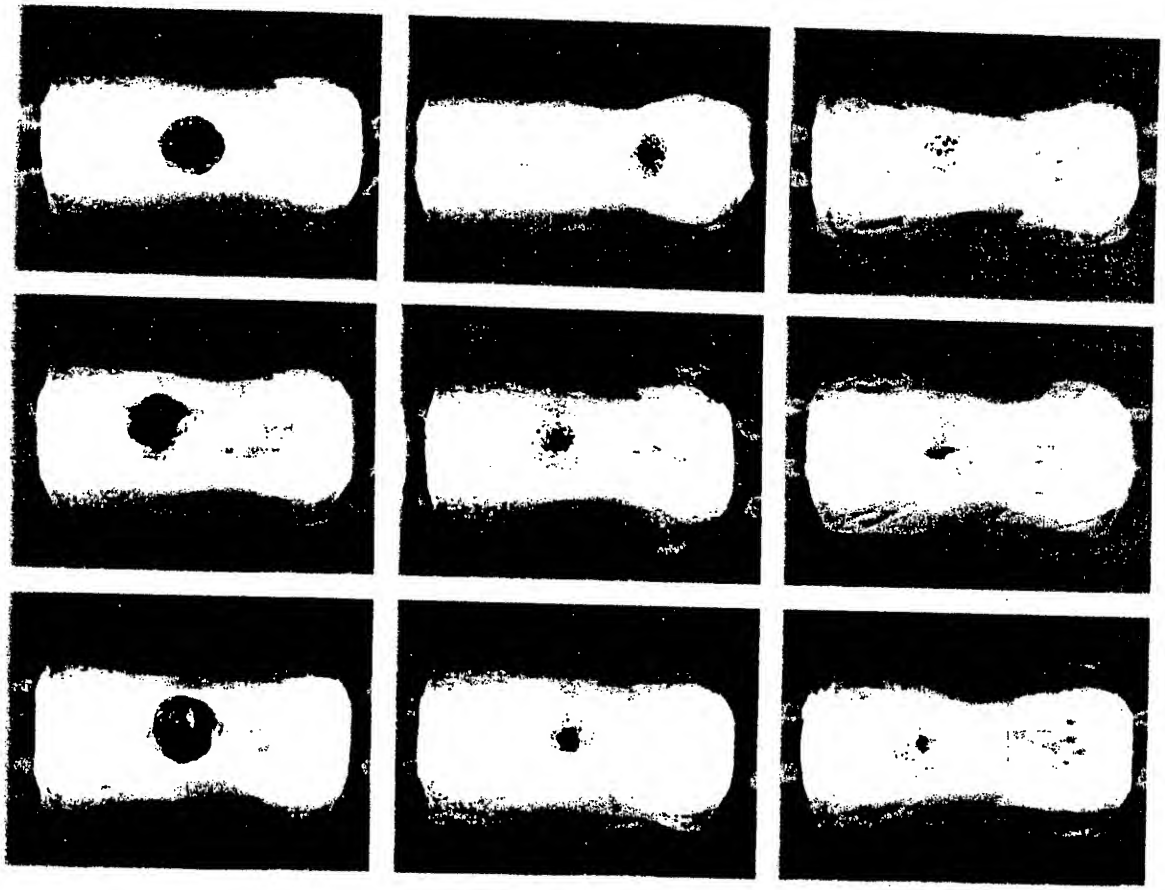

FIGURE 4

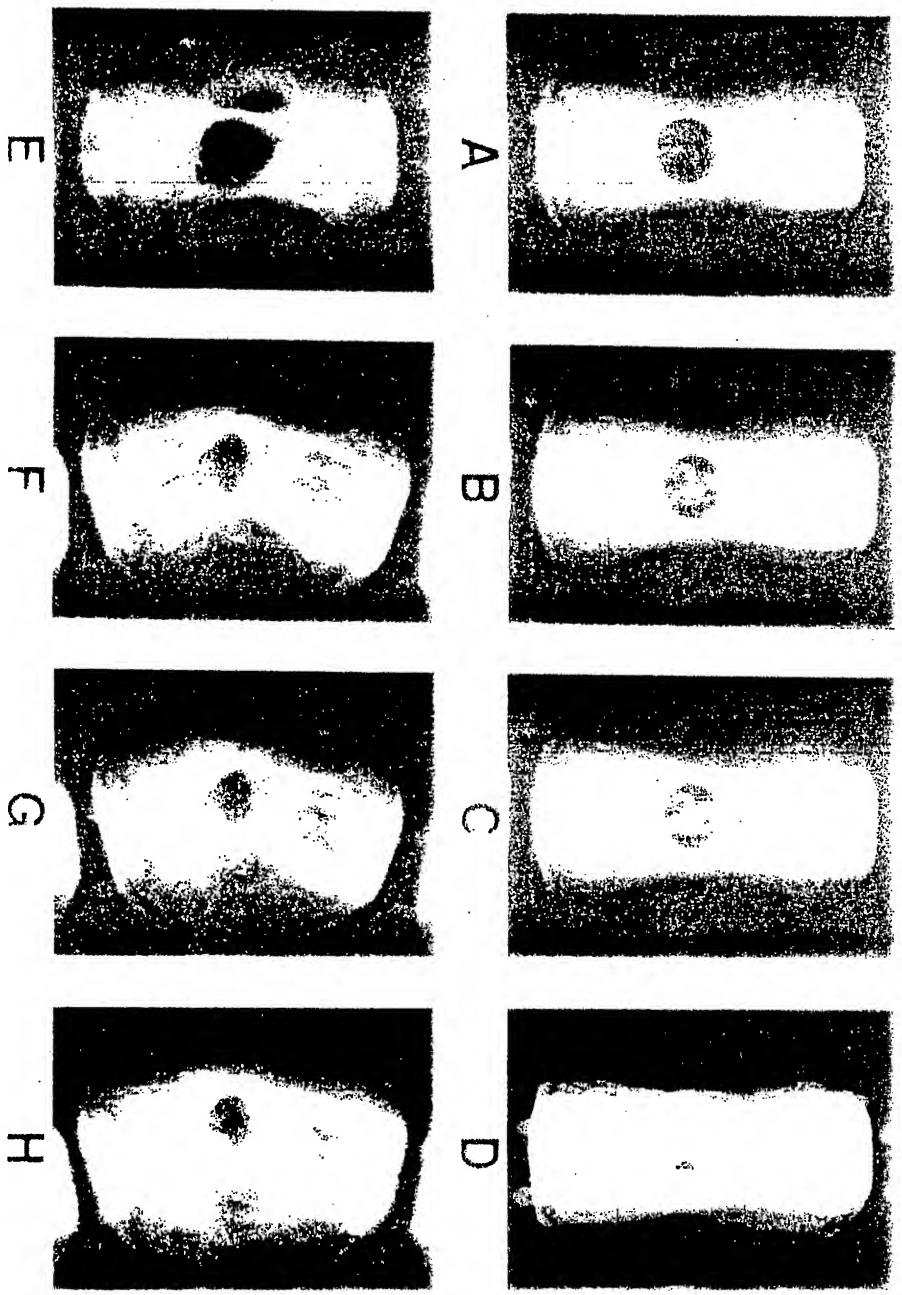

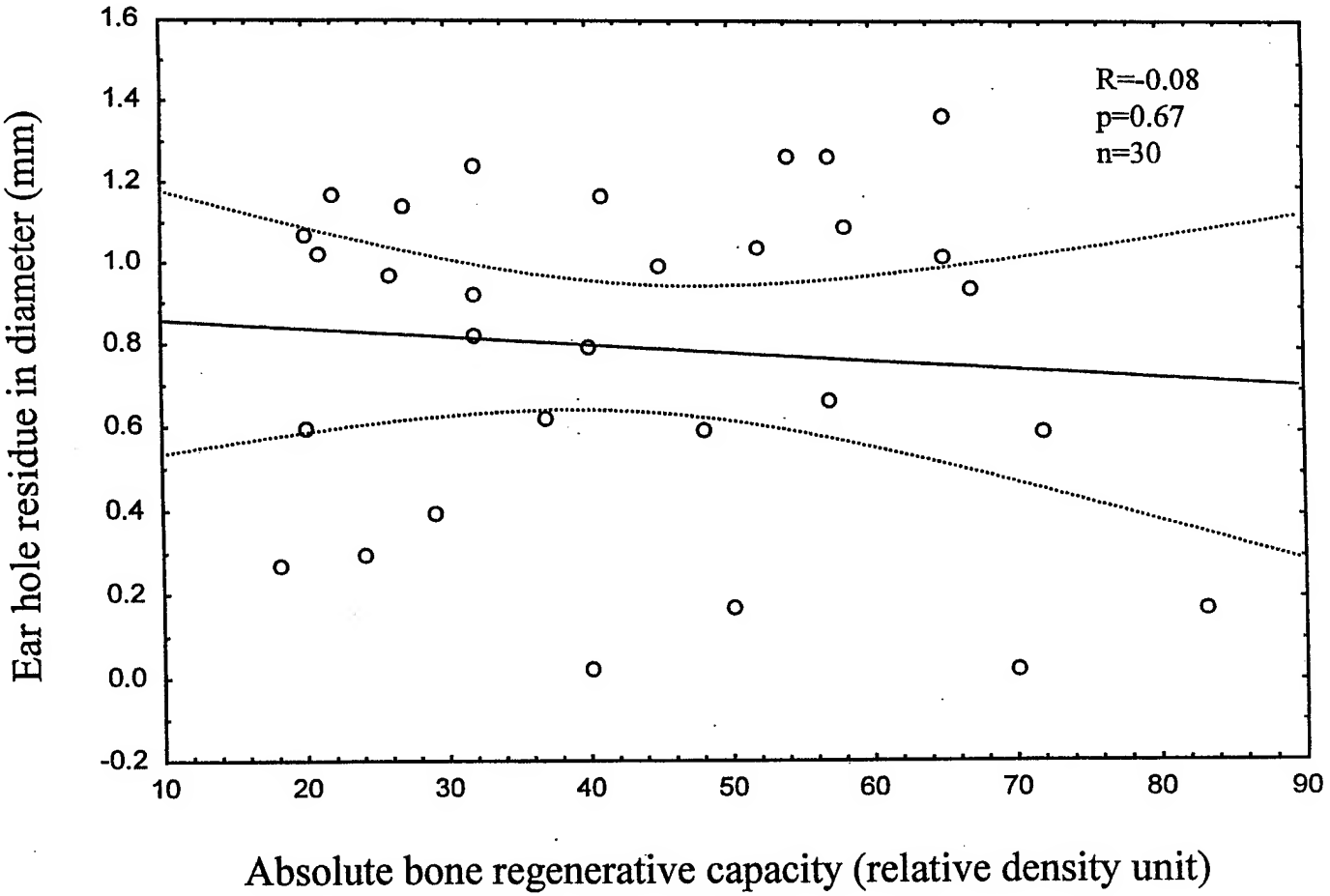
R=-0.08
p=0.67
n=30
Ear hole residue in diameter (mm)
Absolute bone regenerative capacity (relative density unit)
1.6
1.4
1.2
1.0
0.8
0.6
0.4
0.2
0.0
-0.2
10
20
30
40
50
60
70
80
90

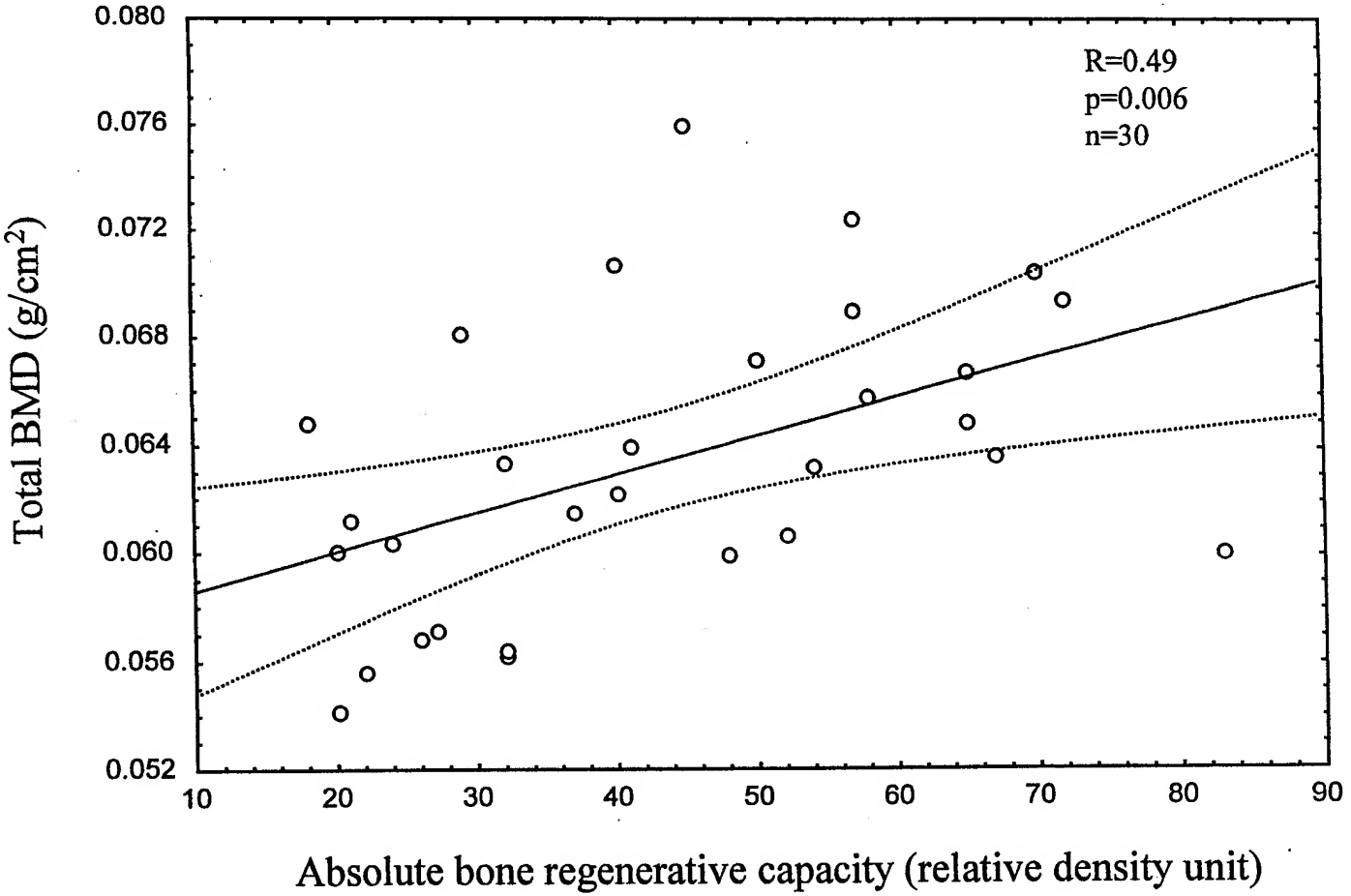
R=0.49
p=0.006
n=30
Total BMD (g/cm²)
0.080
0.076
0.072
0.068
0.064
0.060
0.056
0.052
10
20
30
40
50
60
70
80
90
Absolute bone regenerative capacity (relative density unit)

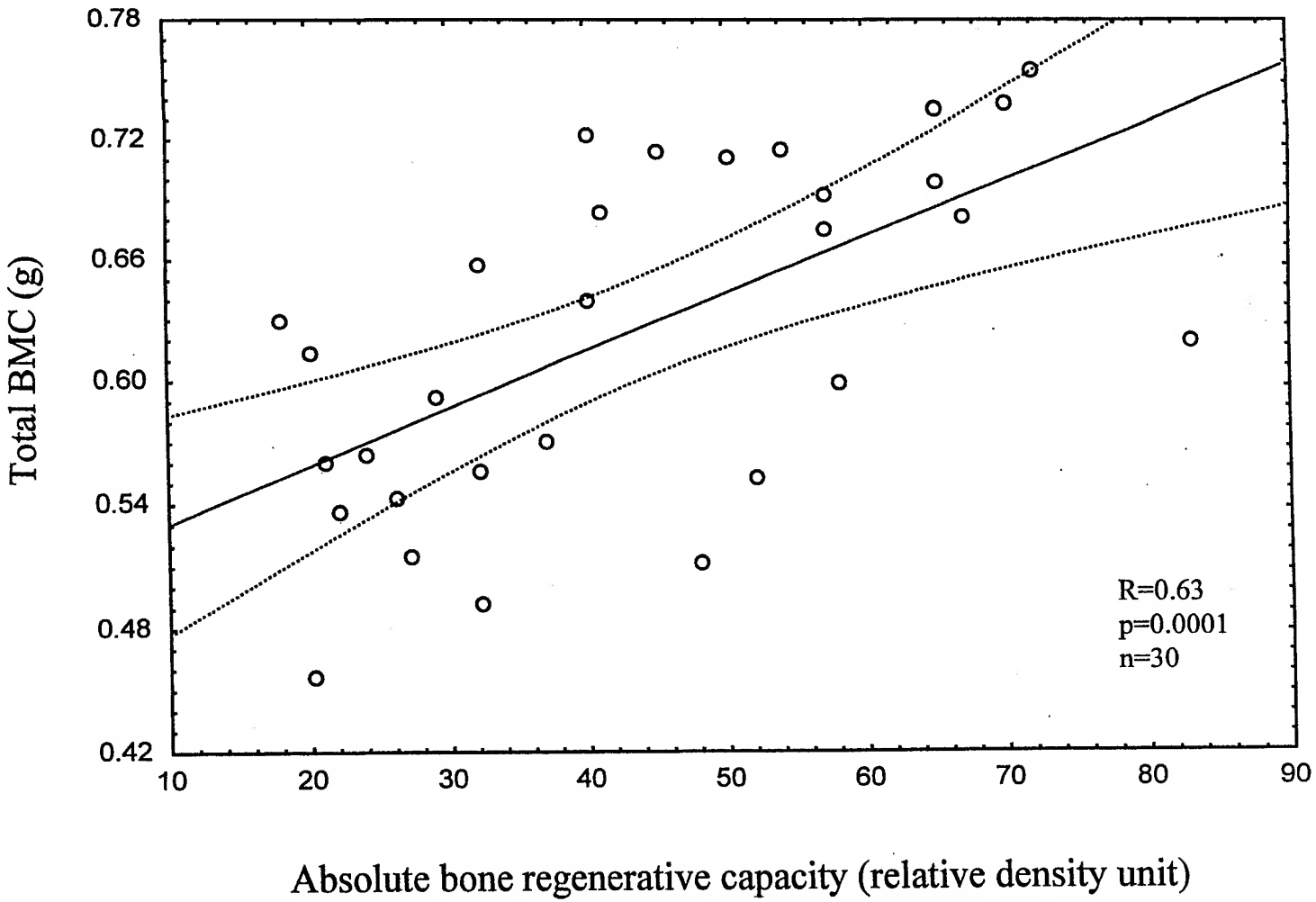
0.78
0.72
0.66
0.60
0.54
0.48
0.42
Total BMC (g)
10
20
30
40
50
60
70
80
90
R=0.63
p=0.0001
n=30
Absolute bone regenerative capacity (relative density unit)

Analysis of gene expression in the wound repair/regeneration process

Xinmin Li, Subburaman Mohan, Weikuan Gu, David J Baylink

Molecular Genetics Division, Musculoskeletal Disease Center, JL Pettis VA Medical Center and Loma Linda University, Loma Linda, CA 92357, USA

Running head: Analysis of gene expression in wound repair

Corresponding author: David J Baylink, MD., Musculoskeletal Disease Center, JL Pettis VA Medical Center, 11201 Benton Street (151), Loma Linda, CA 92357, USA

Tel: (909) 422-3101

Fax: (909) 796-1680

E-mail: David.Baylink@med.va.gov

Abstract. Wound repair/regeneration is a complex process consisting of three stages: inflammation, tissue re-growth, and remodeling, which together involve the action of hundreds of genes. In order to1) identify and analyze the genes that are expressed at the inflammatory stage of repair (i.e., 24 hours after injury), and 2) evaluate the molecular basis of fast-wound repair/regeneration in adult mammals, we examined the expression of 8734 sequence-verified genes in response to ear punch in a fast-wound repair/regeneration strain, MRL/MpJ-Fas^{lpr} mice, and a slow-wound repair strain, C57BL/6J mice. Many differentially expressed genes can be assigned to wound-repairing pathways known to be active during the inflammatory phase, whereas others are involved in pathways not previously associated with wound repair. Many genes of unknown function (ESTs) exhibited a more than 2-fold increase in MRL/MpJ-Fas^{lpr} or C57BL/6J mice, suggesting that current understanding of the molecular events at the inflammatory stage of repair is still limited. A comparison of the differential expression profiles between MRL/MpJ-Fas^{lpr} and C57BL/6J mice suggests that fast-wound repair in MRL/MpJ-Fas^{lpr} mice is mediated by a metabolic shift toward a low inflammatory response and an enhanced tissue repair.

Introduction

Wound healing is a genetically-controlled, complex process requiring the cooperation of cells involved in hemostasis, inflammation, immune defense, vascularization, fibroplasia,

and epithelialization (Kunimoto 1999). Each of these steps could affect this interactive process and lead to an altered healing process. Recent advances in cellular and molecular biology have greatly expanded our understanding of the biological processes involved in wound repair and tissue regeneration (Singer et al. 1999). A number of wound-repair-related genes have been identified (Rothe and Falanga 1992). However, due to the limitations inherent in the methods used in the wound-repair/regeneration studies, the key genetic events underlying the initiation and progression of wound repair are less clear. Studies using the large-scale genome analysis techniques suggest that the number of such genes may be large, and many important wound-repair-related genes remain to be discovered (Iyer et al. 1999).

Wound repair involves two major clinical issues: the rate of healing - a prominent problem in the elderly population, and the quality of healing - a major concern relating to cosmetic appearance, particularly in the young population. Therefore, the primary therapeutic goal of the treatment of wounds involves rapid wound closure with minimal scar formation. In order to achieve this goal, it is necessary to identify the genetic basis for wound-repair/regeneration using appropriate animal models. A recent study and our own research have shown that MRL/MpJ-Fas^{lpr} strain of mice could completely heal an ear-punched hole (2 mm in diameter) with normal tissue architecture within 4 weeks in contrast to the control mice, B6, which only healed about 40% of the original hole with scar tissue at the same period of time (Clark et al. 1998). Further study has demonstrated that this healing capacity is a heritable trait in inbred mice (McBrearty et al. 1998). The characteristics of rapid wound closure and no scar formation in MRL mice have provided

an ideal model to study the molecular mechanisms that underlie wound-repair/regeneration in mammals.

The high density cDNA microarray technology, with its capacity for two-color simultaneous monitoring of thousands of genes, provides a unique opportunity for high-throughput gene expression analysis (Schena et al. 1995). DNA microarrays have been particularly useful for analyzing gene expression profiles in single-celled organisms and in tissue culture (White et al. 1999). Here we report the application of cDNA microarray technology to analyze gene expression in the multi-cellular ear-punched tissue of a regeneration strain, MRL mouse, and that of a non-regeneration strain, B6 mouse, using Mouse GEM1 microarry that contains 8734 Incyte sequence-verified IMAGE Consortium mouse cDNA clones. This study focused on the inflammatory stage of wound repair. The aims of this study were to evaluate the genes whose expression levels change during wound healing processes in general, and the genes whose expression levels are different in response to ear punch in MRL vs B6 mice. Our results indicate that high-throughput *in vivo* gene expression analysis should be of value in elucidating the genetic events associated with wound repair/regeneration in mammals.

Materials and methods

Animals. Four-week old MRL/MpJ-Fas^{lpr} and C57BL/6 female mice were obtained from the Jackson Laboratories (Bar Harbor, ME) and housed at the Animal Research Facility, Pettis VA Medical Center, Loma Linda, CA under conditions of 14 h light, 10 h darkness, ambient temperature of 20^0 C, and relative humidity of 30-60%. Experimental

animal procedures performed in this study have been approved by the Animal Studies Subcommittee of the Jerry L Pettis Memorial VA Medical Center, Loma Linda, CA.

Ear punch and measurement. One week after the animals arrived, a 2 mm through-and-through hole was made in the center of the cartilaginous part of both ears of three mice from each strain using a metal ear punch (Fisher Scientific, Pittsburgh, Catalog No. 01-337B). The holes were measured at the time of wounding (Day 0) and 5, 10, 15, 20, 25, and 30 days after wounding using a 7 X Magnifier. The precision of the Magnifier for ear hole measurement has been determined, by repeated measurement of the same ear hole 10 times, to be 2.4%.

Tissue collection and RNA purification. Three 2 mm through-and-through holes were made using a metal ear punch in both ears of the mice when animals reached 5-week of age. A 0.4 mm disc of ear-punched tissue was isolated 24hrs after ear punch from 10 animals of each strain. The equivalent amount of ear tissue at the corresponding region was also isolated from the non-ear-punched control mice. The ear-punched or control tissues from each strain were pooled and immediately put into liquid nitrogen until use. Total RNA was isolated using RNeasy Kit (GIAGEN) and mRNA was purified using Oligotex mRNA Kit (QIAGEN) based on the manufacture's instruction.

Commercial Microarray Hybridization. Incyte commercial service was used for probe labeling and microarray hybridization. The Mouse GEM1 microarray contains 8734 Incyte sequence-verified IMAGE Consortium clones mapped to NCBI's UniGene

database. The detailed technical and hybridization control procedures can be found at Incyte's web site (http://www.genomesystems.com/). Three hybridizations were performed: MRL ear-punched sample vs MRL control sample, B6 ear-punched sample vs B6 control sample, and MRL control sample vs B6 control sample, so that the comparison could be made between the MRL ear-punched sample and B6 ear-punched sample.

Commercial Microarray data analysis. After passing various quality control processes performed by Incyte (http://www.genomesystems.com/), data were directly downloaded to the image analysis software GEMTools Version 2.4.1 (Incyte). The GEMTools normalized the two different hybridizations, subtracted background, located, calculated, and stored each cDNA spot intensity from each file and simultaneously compared two different normalized images. The differential expression ratios were obtained for each cDNA. Based on the GEM^{TM} microarray reproducibility study, the coefficient of variation for differential expression derived from the Incyte GEM microarray hybridization is approximately 15%, and the level of detectable differential expression ratio is 1.75 (Incyte technical survey, Incyte Pharmaceuticals, Inc. 1999). For this study, we used a threshold value of >2-fold to define differential gene expression to minimize false-positive elements.

In-house microarray hybridization and data analysis Ten cDNA clones were randomly selected and purchased from the Incyte Genomics (St. Louis, Missouri). These clones exhibited more than 2-fold change in expression by Incyte hybridization. The insert was

amplified by PCR with the following universal primers: 5'-GTGCTGCAAGGCGATTAAG-3' and 5'-GGAATTGTGAGCGGATAAC-3'. The PCR product was purified using QIAquick PCR Purification Kit (QIAGEN), concentrated and resuspended in 3 X SSC at a concentration of 0.25μg/μl, and then printed on the amino-silane coated microscope slides (Corning, NY) using a GMS 417 Arrayer (Genetic MicroSystems). Ten replicates of the individual cDNA clone were printed on each slide. DNA was fixed by baking the slides at 80°C for three hours.

Fluorescently labeled cDNA with either Cy3 (MRL ear-punched sample) or Cy5 (MRL non-ear-punched sample) was synthesized using the Superscript II reverse transcription kit (Gibco-BRL). 0.6μg of mRNA was mixed with 2μg of 20-mer oligo dT primer in a total volume of 14.2 μl, heated to 70°C for 6 min and immediately chilled on ice water. To this sample, 6 μl of 5x reverse transcriptase buffer, 0.8 μl of dNTPs (25 mM each of dA, dG, dC, and 10 mM of dT), 3 μl of 0.1 M DTT, 1 μl of RNasin, 3 μl of Cy-dUTP and 2μl of SuperScript II reverse transcription (400 units) were added. After a 2-hour incubation at 42°C, the mRNA was degraded by adding 1.5 μl of 1 M NaOH and incubating at 70°C for 10 min, followed by adding 1.5 μl of 1 M HCl to neutralize the sample. The probe was purified by centrifugation in a Centricon-30 micro-concentrator (Amicon, MA). The Cy3 and Cy5 probes were then combined, brought to volume of 500 μl with TE, and concentrated to a volume of 10μl. One μl of mouse COT-1 DNA (10μg/μl), 1 μl of Poly dA (10μg/μl), 2.6 μl of 20 X SSC (3.5 X final), and 0.45 μl of 10% SDS (0.3% final) were added to the probes. The sample was denatured by placing the tube in a 100°C water bath for 1 min and then cooled at room temperature for at least 10 min. The hybridization solution was centrifuged for 5 min at 14,000g to pellet any

particulate matter and then placed onto the center of the array. After carefully applying a cover slip over the probe, the slide was placed in a hybridization chamber and incubated at 65°C Oven for 16 hrs. In the next morning, the slide was submerged in a washing solution (2 X SSC and 0.1% SDS) until the coverslip came off, and then washed for 1 min in 1 X SSC, and 1 min in 0.2 X SSC.

The slide was immediately scanned using a ScanArray 4000 scanner (GSI Lumonics). Separate images for Cy3 and Cy5 were acquired using ScanArray software (version 2.0) and date were analyzed using QuantArray software (version 2.0). Net signal was determined by subtraction of the local background from the average intensity for each spot. Spots deemed unsuitable for accurate quantitation because of array artifacts were excluded for further analysis. Signal intensities between the Cy3 and Cy5 were normalized using the public domain EST (accession number: AA021858) as a control target element because we knew that the expression of this gene did not respond to ear punch in MRL mice.

Results

Ear-healing profile in MRL and B6 strain of mice. Figure 1 shows overall wound repair profiles in MRL and B6 strains that consist of three healing stages: a) slow initiation stage (day 0 to day 5) where there was no significant difference in wound closure between MRL and B6 mice; b) fast-healing stage where two strains achieved their maximal wound closure (day 5 to day 20) and exhibited a markedly different healing rate; c) stabilizing stage where strains had no or limited healing. Thirty days after ear punch,

MRL completely healed the hole with normal tissue architecture reminiscent of regeneration, while B6 healed only 45% of the hole with obvious scar formation (Fig. 2).

Analysis of genes related to the inflammatory stage of repair. We first examined the signal values of non-ear-punched control tissues in MRL and B6 to evaluate gene expression levels in accordance with our existing knowledge (Fig. 3). Structural genes, such as procollagen type I, elongation factor-1-alpha, and procollegan type III, generally have a high expression level. In contrast, the regulatory genes, such as interleukin 4 receptor and zinc finger protein 147, have a low expression level. Overall gene expression detected by the hybridization is consistent with the functional requirement in the cells.

A comparison of gene expression profile from the ear-punched and non-ear-punched control tissue revealed that the inflammatory stage of repair is associated with the altered mRNA expression of 2.5% genes analyzed in both strains. Of the 8734 mouse cDNA clones surveyed in the GEM1 microarray, 54 (0.6%) exhibited a greater than two-fold increase in expression levels in both MRL and B6 mice, 113 (1.3%) in MRL mice only, and 50 (0.6%) in B6 mice only.

The up-regulated genes after ear punch in both strains fall into 4 main categories (Table 1). The first category (class I) contains genes that are involved in inflammatory response, including lipocalin 2, hemoglobin α, and glycoprotein 49B. Eight of the genes are known to or suspected to fall into this category. The largest differential expression between the non-ear punched and ear punched tissue (10.1-fold in MRL and 11.6-fold in B6) in this category was observed for the gene encoding calgranulin A. This is consistent

with our previous protein expression study using surface-enhanced laser desorption and ionization (SELDI) ProteinChip technology in which we also detected that the calgranulin A protein level increased by 4-fold 24 hours after ear punch in both MRL and B6 mice (manuscript submitted to BBA for publication). The second category (class II) contains genes that are involved in wound repair. The gene products in this category represent primarily the basic components for tissue re-growth, such as laminin γ 2, keratin complex 2 gene 6A, and small proline-rich protein 1A. The third category (class III) includes genes that have unknown function or the genes whose known functions are not obviously related to wound repair. The last category (class IV), also the largest category, contains ESTs, accounting for 57% of the genes displayed a greater than two-fold increase in expression in both strains.

Comparison of gene expression profiles between the MRL and B6 mice. A baseline comparison of non-ear-punched tissues showed that only 11 genes or ESTs displayed a more than two-fold difference in expression between the MRL and B6 mice. In response to the ear punch, none of these 11 genes/ESTs exhibited a greater than two-fold change in expression in either MRL or B6 mice. In order to study the genetic basis for difference in wound healing between the MRL and B6 strains, we identified the genes in which expression level increased by more than two-fold after ear punch in one of the strains but not in the other. Table 2 shows the genes that displayed a greater than two-fold increase in expression in MRL mice only. Of the 21 known genes, 10 (48%) are known to or are most likely to be directly involved in the repair process, such as small proline rich protein 2A (construction of cell envelop) and formin binding protein 21 (reorganization of

cytoskeleton), three of the known genes are related to the inflammatory response, and the rest can not be unambiguously classified into either of the groups based on our current knowledge, although some of them seem to have an indirect involvement in wound repair such as mCDC47 (DNA.replication) and phosphorylase kinase alpha 1 (regulator of glycogenolysis). Thus, the expression profile 24 hours after ear punch in MRL was dominated by induction of the genes involved in the second phase of wound repair – tissue rebuilding.

Ear punch in B6 induced a transcriptional profile which was different from that of MRL. Of the greater than two-fold induction in expression of 18 known genes (Table 3), 10 (56%) are related to inflammation, such as heparin cofactor II (thrombin inhibition), tissue factor pathway inhibitor (regulation of blood coagulation), and secretory leukoprotease inhibitor (regulation of inflammation), whereas only 3 are associated with tissue rebuilding, and the rest have an unknown function in the wound-repair process. In comparison to MRL mice, B6 mice appear to exhibit an excessive response to inflammation and a slow response to tissue repair.

Fifteen genes or ESTs displayed a greater than two-fold decrease in expression in MRL mice, but none of the genes decreased more than two-fold in B6 (Table 4). Among these genes, the most substantial suppression of gene expression by ear punch was selenoprotein P, whose function is still not completely understood, although a function in the immune response seems most probable. Ear punch in MRL also decreased the expression level of procollagen type I and type III (2.4-fold in both cases), the basic components of extracellular matrix.

Validation of Incyte data with in-house microarray hybridization To investigate the reliability of Incyte expression data, we measured the differential expression of 10 cDNA clones in response to ear punch of MRL mice using our in-house microarray facilities with a different batch of mRNA samples, and compared the fold changes with those obtained from the Incyte hybridization. Table 5 shows that the differential expression of 9 out of the 10 genes (hybridization signal from one gene was not suitable for accurate quantitation and was eliminated from data analysis) as determined by the in-house hybridization was similar to that observed with the Incyte hybridization. The correlation coefficient between the two data sets (fold change) is 0.95 ($p<0.01$).

Another line of evidence to support that the Incyte hybridization data make biological sense is that many of the differentially expressed genes are localized to the wound healing QTL regions identified by McBrearty et al. (1998). These genes include esterase 1, deubiquitinating enxyme, eIF-1A, keratin complex 2 gene 6A, lymphocyte antigen 6C, metallothionein 1 and 2.

Discussion

What molecular mechanisms underlie changes in the rate and quality of wound repair, and how these processes can be manipulated by therapeutic intervention represent the key questions in the field of mammalian wound repair. Our study was aimed to address the first of these questions by examining the gene expression changes during the inflammatory stage of repair in two inbred strains of mice with extreme differences in wound-healing capacity. Because of the logical connection between the function of a

gene and its pattern of expression, examination of the gene expression change can infer its potential function in wound repair process.

The first phase of wound healing is the inflammatory phase, which is characterized by the hemostasis and initial clean-up (Kunimoto 1999). We chose this stage (24 hours after injury) for the gene expression study for our first analysis (studies on other stages of wound repair are in progress using our in-house microarray facility) because fundamental to our understanding of wound healing mechanisms is a knowledge of the signals that trigger cell lineage to proliferate at the wound margin (Martin 1997). It is the inflammatory stage of repair that initiates the signaling cascade to start the healing process. In addition, reepithelialization of wounds begins within hours after injury, and epidermal cells at the wound margin begin to proliferate behind the actively migrating cells one day after injury (Singer et al. 1999). Examination of expression profile 24 hours after ear punch could reveal the genes involved in early signaling for the release of proinflammatory cytokines, and subsequent inflammatory response as well as actual repair process. Previous studies have shown that the initial cell response to the injury at this stage is crucial to the rate and quality of the overall healing (Shan et al. 1994, 1995).

Of the 54 genes that exhibited a greater than two-fold increase in expression after ear punch in both MRL and B6, 15 (28%) could be assigned to wound repairing pathways based on previously known functions, whereas 39 (72%) have no previously recognized roles in wound repair and include genes with known function in other pathways and the genes with unknown function or ESTs. The identification of more genes with previously unknown function than the genes with known function in wound repair (72% unknown vs 28% known) suggests that the molecular basis of wound repair may be much more

complex than we currently understand. Further studies are needed to establish the causal relationship between the changes in mRNA levels of these novel genes and rapid wound repair.

With the qualification that many wound healing genes are yet to be identified, the most significant observation of this study was the dramatic shift of transcription programming from inflammation to repairing at 1 day post-ear punch in MRL mice. A comparison of gene expression profiles between MRL and B6 mice (Table 2 and Table 3) revealed that the transcriptional events in B6 mice were dominated by expression of inflammation-related molecules, indicating a prolonged inflammatory period and delayed repairing. In contrast, MRL mice had a repairing molecule-dominated expression profile at the same period of time, suggesting a low inflammatory response and an enhanced repairing activity. The current study revealed that differential expression occurred as early as one day post-ear punch between MRL and B6, if not earlier. The shift of expression profile toward the actual repair process in MRL could be primarily responsible for its rapid healing phenotype. The key genes regulating this transcriptional shift are yet to be determined, although one can speculate on the candidate genes based on our previous knowledge. One such a candidate gene is deubiquitinating enzyme (2.5-fold increase in expression in MRL only), which has been shown to be involved in the control of many intracellular processes, including cell cycle progression, transcriptional activation, and signal transduction (D'Andrea 1998). Conjugation to the small eukaryotic protein ubiquitin can target protein for degradation, and removal of the ubiquitin modification performed by deubiquitinating enzymes can reverse this process. Therefore, deubiquitination is an important mechanism regulating the protein ubiquitination

pathway. Increased production of deubiquitinating enzyme (UBH1) could change the ubiquitination state of an unknown growth regulatory factor, resulting in an increased cell growth response.

Little is known about the genes regulating mammalian tissue regeneration. The findings of this study along with previously published observations provide some clues that could explain the high quality of healing in MRL mice. A previous study (Abbott et al. 1998) showed that the quality of wound healing is closely correlated to the degree of inflammatory response. Tight regulation of inflammation is necessary to prevent impaired healing during early tissue repair. Thus, the low inflammatory response as suggested by decreased expression of inflammatory genes in MRL mice could contribute to a better healing quality. Another line of evidence supporting this view is that embryonic/fetal wound healing is a kind of regeneration where the inflammation response is almost absent in contrast to adult wound healing (Martin 1997). The high quality of healing in MRL mice could also be related to its tight regulation of extracellular matrix deposition immediately after injury. Shah et al. (1994, 1995) have demonstrated that the exogenous addition of neutralizing antibody to TGF-β_1 or TGF-β_2 to incisional wounds at the time of wounding or soon thereafter reduced the extracellular matrix deposition (collagen type I and III) in the early stages of wound healing, resulting in less scar formation and improved quality of healing. Consistent with this result, we have observed down-regulation of procollagen type I and III by 2.4-fold in response to ear punch in MRL mice only. If the mechanisms underlying the association between the reduced extracellular matrix deposition immediately after injury and improved quality of

healing could be established, the genetic manipulation of the extracellular matrix deposition should provide a potential tool in the treatment of wound repair.

We recognize that this study may underestimate the number of genes involved in tissue repair for the following reasons: 1), we only examined one time point in the inflammatory stage, and some changes in expression may occur at an earlier or a later stage of the repair process; 2), we used a threshold of > two-fold change in data analysis, and some genes that had a small change in expression, such as transcription factors, could have a big impact on the downstream reactions; 3), we surveyed 8734 genes in this study, representing 8-12% of the mouse genome. However, the expression data presented here have been verified by examining representative clones using our in-house microarray facilities. The differential expression profiles have provided a logical explanation for the difference in wound healing between MRL and B6 mice. Additional genes related to wound repair may be discovered by the development of higher density mouse DNA microarrays with multiple replicates of each clone on the chip and by the examination of gene expression at multiple-time points.

In summary, although a large number of differentially expressed genes identified in this study are ESTs that are not informative in elucidating the molecular mechanisms of wound repair in this instance, the data derived from the genes that have a known function suggest that the expression profile in MRL mice exhibited a metabolic shift toward a lower inflammatory response and an enhanced tissue repair compared to that in B6 mice. The trigger for this shift may be pivotal for understanding rapid wound repair/regeneration in the MRL strain of mice.

Acknowledgements. This work was supported by Assistance Award No. DAMD17-99-1-9571. The U.S. Army Medical Research Acquisition Activity, 820 Chandler Street, Fort Detrick MD 21702-5014, is the awarding and administering acquisition office. The information contained in this publication does not necessarily reflect the position or the policy of the Government and no official endorsement should be inferred. The authors would like to thank Melanie Hamilton-Ulland and Mary Stover for their excellent technical support.

References

Abbott RE, Corral CJ, MacIvor DM, Lin X, Ley TJ et al. (1998) Augmented inflammatory responses and altered wound healing in cathepsin G-deficient mice. Arch Surg 133,1002-1006

Adachi O, Kawai T, Takeda K, Matsumoto M, Tsutsui H et al. (1998) Targeted disruption of the MyD88 gene results in loss of IL-1- and IL-18-mediated function. Immunity 9, 143-150

Agarwal A, Nick HS (2000) Renal response to tissue injury: lessons from heme oxygenase-1 gene ablation and expression. J Am Soc Nephrol 11, 965-973

Anwaar I, Gottsater A, Ohlsson K, Mattiasson I, Lindgarde F (1998) Increasing levels of leukocyte-derived inflammatory mediators in plasma and cAMP in platelets during follow-up after acute cerebral ischemia. Cerebrovasc Dis 8, 310-317

Bauman SJ, Church FC (1999) Enhancement of heparin cofactor II anticoagulant activity. J Biol Chem 274, 34556-34565

Berry MD, Boulton AA (2000) Glyceraldehyde-3-phosphate dehydrogenase and apoptosis. J Neurosci Res 60, 150-154

Caslini C, Shilatifard A, Yang L, Hess JL (2000) The amino terminus of the mixed lineage leukemia protein (MLL) promotes cell cycle arrest and monocytic differentiation. PNAS 97, 2797-2802

Chaudhuri J, Chowdhury D, Maitra U (1999) Distinct functions of eukaryotic translation initiation factors eIF1A and eIF3 in the formation of the 40S ribosomal preinitiation complex. J Biol Chem 274, 17975-17980

Clark LD, Clark RK, Heber-Katz E (1998) A new murine model for mammalian wound repair and regeneration. Clin Immunol Immunopathol 88, 35-45

Cui X, De Vivo I, Slany R, Miyamoto A, Firestein R et al. (1998) Association of SET domain and myotubularin-related proteins modulates growth control. Nat Genet 18, 331-337

D'Andrea A, Pellman D (1998) Deubiquitinating enzymes: a new class of biological regulators. Crit Rev Biochem Mol Biol 33, 337-352

Dib K (2000) BETA 2 integrin signaling in leukocytes. Front Biosci 5, 438-451

Ebert-Dumig R, Seufert J, Schneider D, Kohrle J, Schutze N et al. (1999) Expression of selenoproteins in monocytes and macrophages-implications for the immune system. Med Klin 94, 29-34

Ekblom M, Falk M, Salmivirta K, Durbeej M, Ekblom P (1998) Laminin isoforms and epithelial development. Ann N Y Acad Sci 857, 194-211

English JM, Pearson G, Hockenberry T, Shivakumar L, White MA (1999) Contribution of the ERK5/MEK5 pathway to Ras/Raf signaling and growth control. J Biol Chem 274, 31588-31592

Fedorov AA, Fedorov E, Gertler F, Almo SC (1999) Structure of EVH1, a novel proline-rich ligand-binding module involved in cytoskeletal dynamics and neural function. Nat Struct Biol 6, 661-665

Fuchs SY, Tappin I, Ronai Z (2000) Stability of the ATF2 transcription factor is regulated by phosphorylation and dephosphorylation. J Biol Chem 275, 12560-12564

Gessner A, Rollinghoff M (2000) Biologic functions and signaling of the interleukin-4 receptor complexes. Immunobiology 201, 285-307

Gopalkrishnan RV, Lam EWF, Kedinger C (1998) The p53 tumor suppressor inhibits transcrition of the TATA-less mouse DP1 promoter. J Biol Chem 273, 10972-10978

Gregory CD (2000) CD14-dependent clearence of apoptotic cells: relevance to the immune system. Curr Opin Immunol 12, 27-34

Hanninen A, Jaakkola I, Salmi M, Simell O, Jalkanen S (1997) Ly-6C regulates endothelial adhesion and homing of CD8(+) T cells by activating integrin-dependent adhesion pathways. PNAS 94, 6898-6903

Ho G, Narita M, Broze GJ Jr, Schwartz AL (2000) Recombinant full-length tissue factor pathway inhibitor fails to bind to the cell surface: implications for catabolism in vitro and in vivo. Blood 95, 1973-1978

Hochman A, Liang H, Offen D, Melamed E, Sternin H (2000) Developmental changes in antioxidant enzymes and oxidative damage in kidneys, liver and brain of bcl-2 knochout mice. Cell Mol Biol 46, 41-52

Holzinger I, de Baey A, Messer G, Kick G, Zwierzina H et al. (1995) Cloning and genomic characterization of LST1: a new gene in the human TNF region. Immunogenetics 42, 315-322

Huovila APJ, Almeida EA, White JM (1996) ADAMs and cell fusion. Curr Opin Cell Biol 8, 692-699

Inouye C, Remondelli P, Karin M, Elledge S (1994) Isolation of a cDNA encoding a metal response element binding protein using a novel expression cloning procedure: the one hybrid system. DNA Cell Biol 13, 731-742

Introna M, Alles VV, Castellano M, Picardi G, De Gioia L (1996) Cloning of mouse ptx3, a new member of the pentraxin gene family expressed at extrahepatic sites. Blood 87, 1862-1872

Iyer VR, Eisen MB, Ross DT, Schuler G, Moore T et al. (1999) The transcriptional program in the response of human fibroblasts to serum. Science 283, 83-87

Jindal HK, Chaney WG, Anderson CW, Davis RG, Vishwanatha JK (1991) The protein-tyrosine kinase substrate, calpactin I heavy chain (p36), is part of the primer recognition protein complex that interacts with DNA polymerase alpha. J Biol Chem 266, 5169-5176

Jones MH, Bachant JB, Castillo AR, Giddings TH Jr, Winey M (1999) Yeast Dam1p is required to maintain spindle integrity during mitosis and interacts with the Mps1p kinase. Mol Biol Cell 10, 2377-2391

Kartasova T, Darwiche N, Kohno Y, Koizumi H, Osada S (1996) Sequence and expression patterns of mouse SPR1: Correlation of expression with epithelial function. J Invest Dermatol 106, 294-304

Kelly SE, Jones DB, Fleming S (1989) Calgranulin expression in inflammatory dermatoses. J Pathol 159, 17-21

Kimura H, Ohtomo T, Yamaguchi M, Ishii A, Sugimoto K (1996) Mouse MCM proteins: complex of formation and transportation to the nucleus. Genes Cells 1, 977-993

Kunimoto BT (1999) Growth factors in wound healing: the next great innovation? Ostomy/Wound Management 45, 56-64

Kuziel WA, Morgan SJ, Dawson TC, Griffin S, Smithies O et al. (1997) Severe reduction in leukocyte adhesion and monocyte extravasation in mice deficient in CC chemokine receptor 2. PNAS 94, 12053-12058

Lind T, Falk E, Hjertson E, Kusche-Gullberg M, Lidholt K (1999) cDNA cloning and expression of UDP-glucose dehydrogenase from bovine kidney. Glycobiology 9, 595-600

Liu H, Nakagawa T, Kanematsu T, Uchida T, Tsuji S (1999) Isolation of 10 differentially expressed cDNAs in differentiated Neuro2a cells induced through controlled expression of the GD3 synthase gene. J Neurochem 72, 1781-1790

Mackie EJ (1997) Molecules in focus: tenascin-C. Int J Biochem Cell Biol 29, 1133-1137

Martin P (1997) Wound healing-aiming for perfect skin regeneration. Science 276, 75-81

Matsumoto Y, Handa S, Taki T (1997) gp49B1, an inhibitory signaling receptor gene of hematopoietic cells, is induced by leukemia inhibitory factor in the uterine endometrium just before implantation. Dev Growth Differ 39, 591-597

McBrearty BA, Clark LD, Zhang XM, Blankenhorn EP, Heber-Katz E (1998) Genetic analysis of a mammalian wound-healing trait. PNAS 95, 11792-11797

McFaul SJ, Bowman PD, Villa VM (2000) Hemoglobin stimulates the release of proinflammatory cytokines from leukocytes in whole blood. J Lab Clin Med 135, 263-269

Miyagishi M, Nakajima T, Fukamizu A (2000) Molecular characterization of mesoderm-restricted basic helix-loop-helix protein, POD-1/Capsulin. Int J Mol Med 5, 27-31

Nadeau OW, Traxler KW, Fee LR, Baldwin BA, Carlson GM (1999) Activators of phosphorylase kinase alter the cross-linking of its catalytic subunit to the C-terminal one-sixth of its regulatory alpha subunit. Biochemistry 38, 2551-2559

Nguyen H, Teskey L, Lin R, Hiscott J (1999) Identification of the secretory leukocyte protease inhibitor (SLPI) as a target of IRF-1 regulation. Oncogene 18, 5455-5463

Ohta Y, Okamura K, McKinney EC, Bartl S, Hashimoto K et al. (2000) Primitive synteny of vertebrate major histocompatibility complex class I and class II genes. PNAS 97, 4712-4717

Okochi H, Kato M, Nashiro K, Yoshie O, Miyazono K et al. (1997) expression of tetra-spans transmembrane family (CD9, CD37, CD53, CD63, CD81 and CD82) in normal and neoplastic human keratinocytes: an association of CD9 with alpha 3 beta 1 integrin. Br J Dermatol 137, 856-863

Rajaram S, Baylink DJ, Mohan S (1997) Insulin-like growth factor-binding proteins in serum and other biological fluids: regulation and functions. Endocrine Reviews 18, 801-831

Ramirez A, Vidal M, Bravo A, Jorcano JL (1998) Analysis of sequence controlling tissue-specific and hyperproliferation-related keratin 6 gene expression in transgenic mice. DNA Cell Biol 17, 177-185

Rankin CT, Bunton T, Lawler AM, Lee SJ (2000) Regulation of left-right patterning in mice by growth/differentiation factor-1. Nat Genet 24, 262-265

Rothe MJ, Falanga V (1992) Growth factors and wound healing. Clinics in Dermatol 9, 553-559

Schena M, Shalon D, Davis RW, Brown PO (1995) Quantitative monitoring of gene expression patterns with a complementary DNA microarray. Science 270, 467-470

Shan M, Foreman DM, Ferguson MWJ (1994) Neutralising antibody to TGF-$\beta_{1,2}$ reduces cutaneous scarring in adult rodents. J Cell Sci 107, 1137-1157

Shan M, Foreman DM, Ferguson MWJ (1995) Neutralisation of TGF-β_1 and TGF-β_2 or exogenous addition of TGF-β_3 to cutaneous rat wounds reduces scarring. J Cell Sci 108, 985-1002

Singer AJ, Clark RAF (1999) Cutaneous wound healing. The New England J Med 341, 738-746

Siomi MC, Zhang Y, Siomi H, Dreyfuss G (1996) Specific sequences in the fragile X syndrome protein FMR1 and the FXR proteins mediate their binding to 60S ribosomal subunits and the interactions among them. Mol Cell Biol 16, 3825-3832

Song HJ, Poy G, Darwiche N, Lichti U, Kuroki T et al. (1999) Mouse Sprr2 genes: a clustered family of genes showing differential expression in epithelial tissues. Genomics 55, 28-42

Stevens RL, Austen KF (1989) Recent advances in the cellular and molecular biology of mast cells. Immunol Today 10, 381-386

Stromberg H, Svensson SP, Hermanson O (2000) Distribution of the transcription factor signal transducer and activator of transcription 3 in the rat central nervous system and dorsal root ganglia. Brain Res 853, 105-114

Tamatani T, Kitamura F, Kuida K, Shirao M, Mochizuki M et al. (1993) Characterization of rat LECAM-1 (L-selectin) by the use of monoclonal antibodies and evidence for the presence of soluble LECAM-1 in rat sera. Eur J Immunol 23, 2181-2188

Tanaka K (2000) Formin family proteins in cytoskeletal control. Biochem Biophys Res Commun 267, 479-481

Trowbridge HO, Emling RC (1997) Inflammation: a review of the process, 5th ed. (Quintessence Publishing Co, Inc)

Uphoff CC, Gignac SM, Metge K, Zschunke F, Radzun HJ, Drexler HG (1993) Expression of the monocyte-specific esterase gene in leukemia-lymphoma cell lines. Leukemia 7, 58-62

Uratani Y, Takiguchi-Hayashi K, Miyasaka N, Sato M, Jin MH et al. (2000) Latexin, a carboxypeptidase A inhibitor, is expressed in rat peritoneal mast cells and is associated with granular structures distinct from secretory granules and lysosomes. Biochem J 346, 817-826

Van Lookeren CM, Thibodeaux H, Van Bruggen N, Cairns B, Gerlai R et al. (1999) Evidence of a protective role of metallothionein-1 in focal cerbral ischemia. PNAS 96, 12870-12875

Vasak M, Hasler DW (2000) Metallothioneins: new functional and structural insights. Curr Opin Chem 4, 177-183

Villasante A, Wang D, Dobner P, Dolph P, Lewis SA et al. (1986) Six mouse alpha-tubulin mRNAs encode five distinct isotypes: testis-specific expression of two sister gene. Mol Cell Biol 6, 2409-2419

White KP, Rifkin SA, Hurban P, Hogness DS (1999) Microarray analysis of Drosophila development during metamorphosis. Science 286, 2179-2184

Zhu Y, Carroll M, Papa FR, Hochstrasser M, D'Andrea AD (1996) DUB-1, a deubiquitinating enzyme with growth-suppressing activity. PNAS 93, 3275-3279

Figure legends:

Fig. 1. Ear healing profile of a 2 mm hole in MRL and B6 inbred strains of mice. The healing process can be divided into three phases: initiation phase (I), rapid healing phase (II), and stabilizing phase (III).

Fig. 2. Comparisons of ear-healing rate and quality in MRL and B6 strains of mice. In panel A (MRL) and C (B6), photographs were taken immediately after ear punch. In panel B (MRL) and D (B6), photographs were taken 30 days after ear punch when MRL completely healed the 2 mm hole with normal tissue, while B6 healed 45% of the hole with scar tissue.

Fig. 3. Non-ear-punched signal value plot. Each black circle in the plot represents one of the 8734 cDNA elements. Each gray circle represents control element that was used to monitor the quality of hybridization. Structural genes tend to have a high signal value while regulatory genes tend to have a low signal value.

Table 1. Genes in which expression level increased by more than two-fold after ear punch in MRL and B6 mice

Class[a]	Gene	ID#	Increase (fold) MRL	Increase (fold) B6	Proposed function	References
I	Calgranulin A	669813	10.1	11.6	Inflammatory cytokine	Kelly et al. (1989)
I	Hemoglobin α	571819	3.9	3.4	Regulating proinflammatory cytokines	McFaul et al. (2000)
I	Lipocalin 2	493658	3.7	4.1	Inflammatory mediator	Anwaar et al. (1998)
I	Glycoprotein 49B	820498	3.3	3.1	Immunoreceptor	Matsumoto et al. (1997)
I	Metallothionein 1	480068	2.5	3.3	Cellular defense	Van et al. (1999)
I	Pentaxin related gene	354318	2.5	2.2	Indicator of inflammatory reactions	Introna et al. (1996)
I	Major histocompatibility gene	329741	2.3	2.8	Immune response	Ohta et al. (2000)
I	Chemokine receptor 2	749361	2.1	2.3	Regulator of macrophage trafficking	Kuziel et al. (1997)
II	Keratin complex 2, gene 6A	335736	4.3	6.2	Filament protein in stratified epithelia	Ramirez et al. (1998)
II	CD53	576862	2.8	2.4	Epidermal differentiation	Okochi et al. (1997)
II	Laminin gamma 2	315993	2.8	3.7	Epithelial morphogenesis	Ekblom et al. (1998)
II	Lymphocyte antigen 6C	425855	2.5	2.4	Endothelial adhesion	Hanninen et al. (1997)
II	L-selectin precursor	621878	2.3	2.4	Intercellular adhesion	Tamatani et al. (1993)
II	Tubulin β-5 chain	333325	2.2	2.2	Component of microtubules	Villasante et al. (1986)
II	Small proline-rich protein 1A	672405	2.1	3.0	Construction of cell envelopes	Kartasova et al. (1996)
III	Small inducible cytokine A6	575397	3.0	2.8	Unknown	Not available
III	GAPDH	579715	2.4	2.7	Glycolysis	Berry et al. (2000)
III	Secreted phosphoprotein 1	571759	2.3	2.4	Unknown	Not available
III	Erythrocyte protein band 7.2	481880	2.2	2.1	Unknown	Not available
III	Calpactin I heavy chain	420429	2.2	2.2	Stimulate activity of DNA polymerase	Jindal HK et al. (1991)
III	MPS1 gene	747364	2.1	2.6	Spindle assembly	Jones et al. (1999)
III	Small inducible cytokine A4	621095	2.1	2.1	Unknown	Not available
III	Thymus cell antigen 1	316409	2.1	2.1	Unknown	Not available
IV	**31 ESTs[b]**					

[a] Class I contains genes involved in the inflammatory response. Those that trigger the release of proinflammatory cytokines, regulate macrophage, or that are related to hemostasis and immune response are classified into this group. Class II includes genes directly involved in tissue re-growth. Those that make the basic components of the cells, extracellular matrix, or that regulate cell differentiation and growth are grouped into this class. The genes that do not obviously belong to these two classes are placed in Class III. Class IV contains ESTs. These assignment criteria apply to all four tables. [b] Average increase (fold) for MRL: 3 ± 1.40; for B6: 3.2 ± 1.47. Data are expressed as mean ± SD.

Table 2. Genes in which expression level increased by more than two-fold after ear punch in MRL but not in B6 mice

Class	Gene	ID#	Increase (fold)	Proposed function	References
I	Heme oxygenase 1	677499	2.2	Anti-inflammation	Agarwal et al. (2000)
I	Leucocyte specific transcript 1	846366	2.2	Immune response	Holzinger et al. (1995)
I	Integrin beta 2	808785	2.1	Signaling receptor	Dib (2000)
II	Small proline rich protein 2A	888512	11.8	Component of cell envelope	Song et al. (1999)
II	Secretory granule proteoglycan protein	445929	2.5	Regulating extra-cellular matrix	Stevens et al. (1989)
II	Deubiquitinating enzyme	443554	2.5	Cellular growth regulator	Zhu et al. (1996)
II	IGFBP1	404595	2.2	Growth regulation	Rajaram et al. (1997)
II	ERK5	751560	2.1	Signaling and growth control	English et al. (1999)
II	Formin binding protein 21	658427	2.1	Reorganization of cytoskeleton	Tanaka (2000)
II	Transcription factor Dp1	765649	2.1	Cell cycle regulation	Gopalkrishnan (1998)
II	GDF-1	386194	2.1	Cell growth and differentiation	Rankin et al. (2000)
II	Myotubularin	765871	2.1	Cell growth and differentiation	Cui et al. (1998)
II	GDAP 10	423021	2.1	Cell differentiation	Liu et al. (1999)
III	mCDC47	480852	2.7	DNA replication	Kimura et al. (1996)
III	EMAPI	669969	2.4	Unknown	Not available
III	Small inducible cytokine A12	777824	2.4	Unknown	Not available
III	DNA-binding protein M96	779876	2.2	Activation of MT genes	Inouye et al. (1994)
III	Basic helix-loop-helix	419138	2.2	Transcription factor	Miyagishi et al. (2000)
III	Phosphorylase kinase alpha 1	749428	2.1	Regulator of glycogenolysis	Nadeau et al. (1999)
III	Hemopoietic cell kinase	638455	2.1	Unknown	Not available
III	Fragile X MRS 1 homolog	638257	2.1	Translation or mRNA stability	Siomi et al (1996)
IV	92 ESTs[a]		2.3 ± 0.74		

[a] Data are expressed as mean ± SD

Table 3. Genes in which expression level increased by more than two-fold after ear punch in B6 but not in MRL mice

Class	gene	ID#	Increase (fold)	Proposed function	References
I	Heparin cofactor II	693170	11.3	Thrombin inhibition	Bauman et al. (1999)
I	SLPI	638243	7.7	Regulation of inflammation	Nguyen et al. (1999)
I	Glutathione-S-transferase	367627	5.7	Antioxidant	Hochman et al. (2000)
I	CD14 antigen	751756	4.7	Pro-inflammatory responses	Gregory (2000)
I	Tissue factor pathway inhibitor	445829	4.4	Regulation of blood coagulation	Ho et al. (2000)
I	Histidine decarboxylase	573039	2.8	Synthesizing inflammatory mediator	Trowbridge et al. (1997)
I	Mixed-lineage leukemia	617388	2.6	Macrophage differentiation	Caslini et al. (2000)
I	MyD 88	572317	2.3	Adaptor for proinflammatory cytokine	Adachi et al. (1998)
I	IL-4	635530	2.2	Immune response	Gessner et al. (2000)
I	ATF-2	778942	2.2	Stress response	Fuchs et al. (2000)
II	Ena-VASP like protein	477177	3.7	Cytoskeletal reorganization	Fedorov et al. (1999)
II	Tenascin C	736372	2.7	Cell differentiation	Mackie (1997)
II	GDAP2	524541	2.4	Cell differentiation	Liu et al. (1999)
III	UDP-glucose dehydrogenase	523796	6.5	Glucose metabolism	Lind et al. (1999)
III	Esterase 1	643854	2.7	A serine hydrolase	Uphoff et al. (1993)
III	eIF-1A	351631	2.4	Translation initiation	Chaudhuri et al. (1999)
III	STAT3	440571	2.2	Intracellular signaling molecule	Stromberg et al. (2000)
III	ADAM 8	582054	2.1	Cell-cell fusion	Huovila et al. (1996)
IV	**33 ESTs**[a]		3 ± 1.31		

[a] Data are expressed as mean ± SD

Table 4. Genes in which expression level decreased by more than two-fold after ear punch in MRL but not in B6 mice

Class	Gene	ID#	Decrease (fold)	Proposed function	References
I	Selenoprotein P	777018	2.5	Immune response	Ebert-Dumig et al. (1999)
II	Procollagen, type I	536306	2.4	Component of extracellular matrix	Shah et al. (1995)
II	Procollagen, type III	420322	2.4	Component of extracellular matrix	Shah et al. (1995)
III	Metallothionein 2	643725	2.3	Metal homeostasis	Vasak et al. (2000)
III	Latexin	476369	2.1	Carboxypeptidase A inhibitor	Uratani et al. (2000)
IV	10 ESTs[a]		2.2 ± 0.09		

[a] Data are expressed as mean ± SD

Table 5. Comparison of differential gene expression (MRL ear-punched vs MRL non-ear-punched) between the Incyte hybridization and in-house hybridization

Gene	ID#	Fold change	
		Incyte	In-house (mean±SD)[a]
Procollagen, type I	536306	-2.4	-3.2±0.67
Procollagen, type III	420322	-2.4	-2.8±0.72
Selenoprotein P	777018	-2.5	-3±0.63
Metallothionein 2	643725	-2.3	-1.5±0.27
Public domain	637305	-2.2	-1.4±0.4
Small proline-rich protein 2A	888512	11.8	5.9±2.3
EST	404198	8.5	5±2.1
Secretory granule proteoglycan protein	445929	2.5	3.3±0.9
EST	480697	3	2.2±1.0

[a] Means were calculated from 7 to 10 replicates

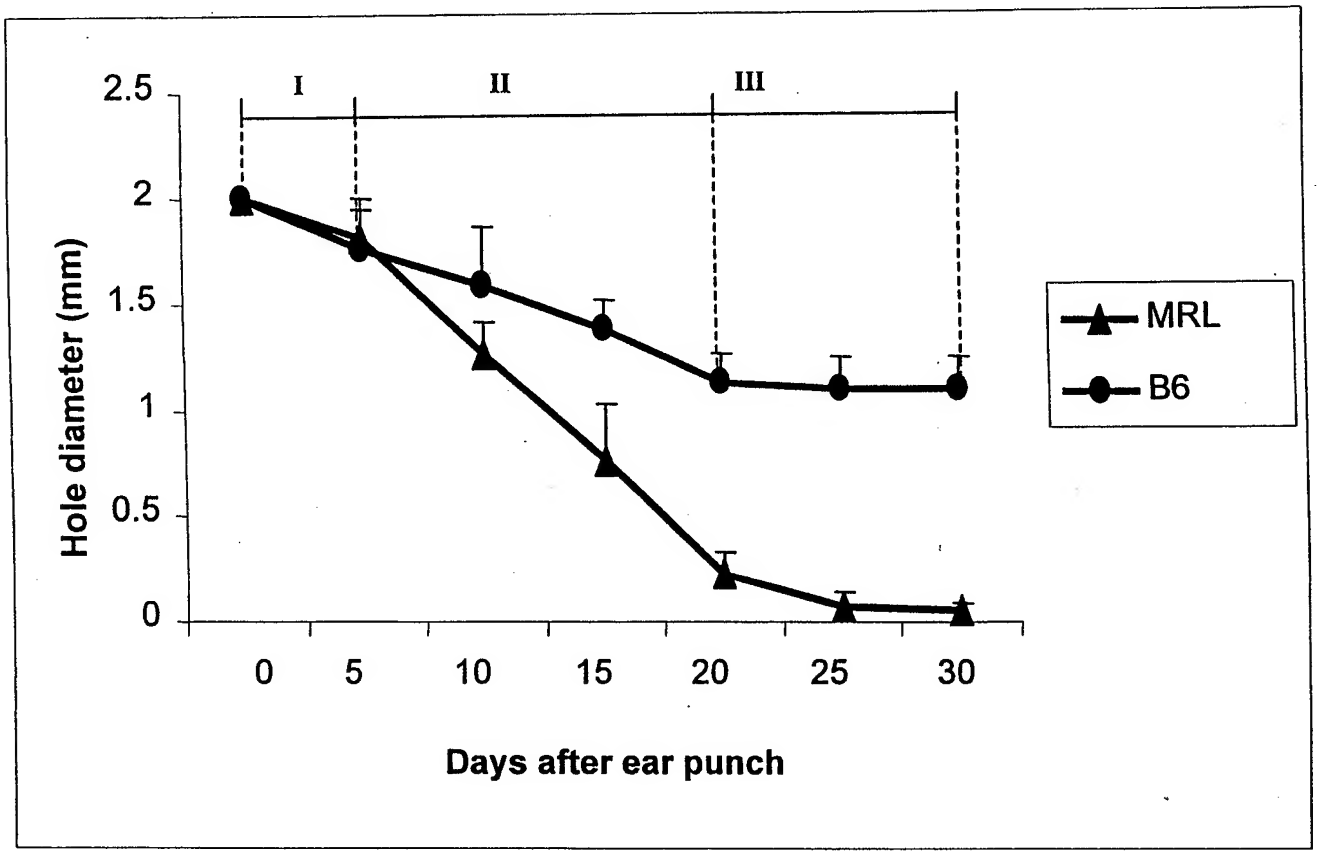
I
II
III
2.5
2
1.5
1
0.5
0
Hole diameter (mm)
0
5
10
15
20
25
30
Days after ear punch
MRL
B6

A
B
C
D

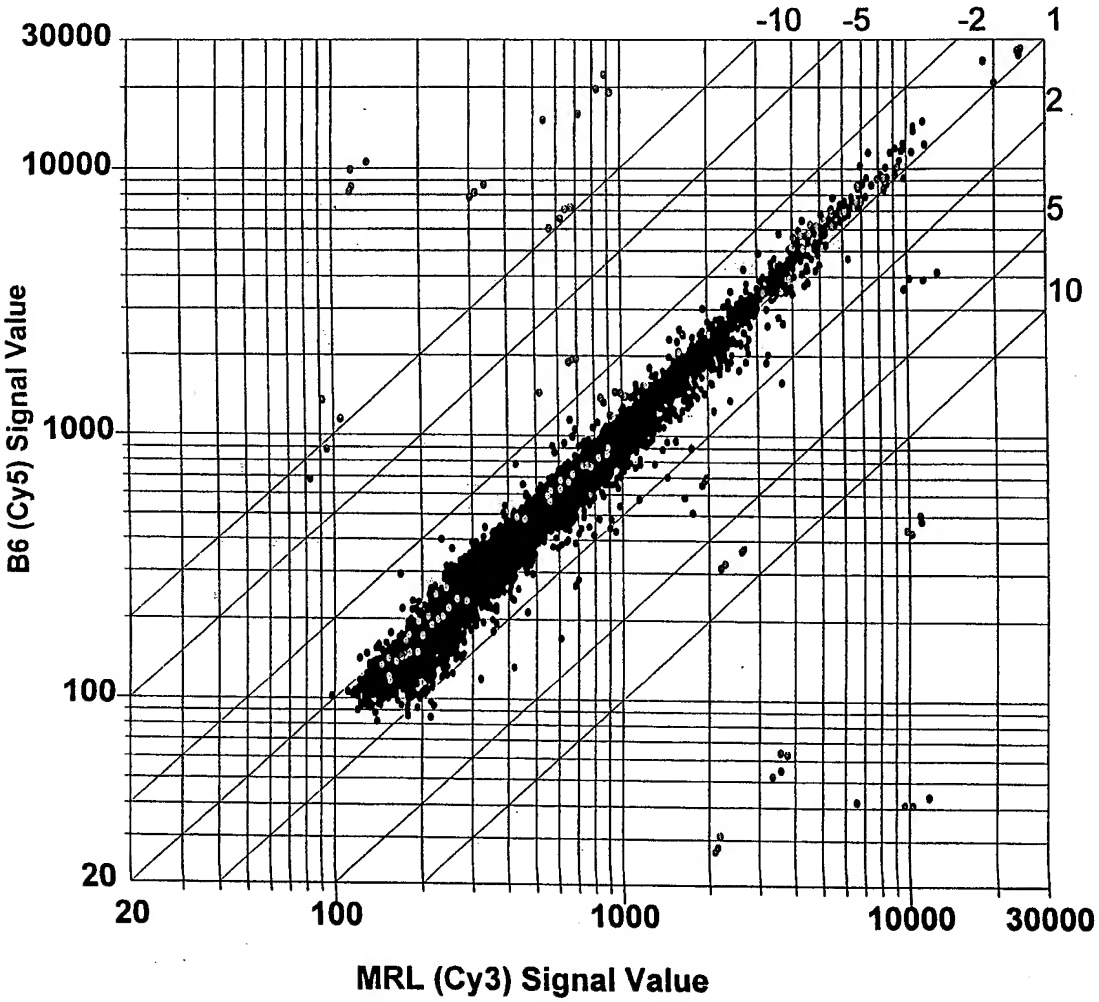
-10
-5
-2
1
2
5
10
30000
10000
1000
100
20
B6 (Cy5) Signal Value
20
100
1000
10000
30000
MRL (Cy3) Signal Value

Differential protein profile in the ear-punched tissue of regeneration and non-regeneration strains of mice: a novel approach to explore the candidate genes for soft-tissue regeneration

X. Li, S. Mohan, W. Gu, N. Miyakoshi and D.J. Baylink

Musculoskeletal Disease Center, JL Pettis VA Medical Center and Loma Linda University, Loma Linda, CA

Keywords: wound repair; regeneration; SELDI ProteinChip; microarray; protein profile.

Corresponding author: David Baylink, MD., Musculoskeletal Disease Center, JL Pettis VA Medical Center, 11201 Benton Street (151), Loma Linda, CA 92357.

Tel: (909) 422-3101

Fax: (909) 796-1680

E-mail: David.Baylink@med.va.gov

Summary

Wound repair/regeneration is a genetically controlled, complex process. In order to identify candidate genes regulating fast wound repair/regeneration in soft-tissue, the temporal protein profile of the soft-tissue healing process was analyzed in the ear-punched tissue of regeneration strain MRL/MpJ-Fas^{lpr} (MRL) mice and non-regeneration strain C57BL/6J(B6) mice using surface-enhanced laser desorption and ionization (SELDI) ProteinChip technology. Five candidate proteins were identified in which responses of MRL to the ear-punch were 2-4 fold different compared to that of B6. Their corresponding genes were predicted using an antigen-antibody assay validated mass-based approach. Most of the predicted genes are known to play a role or are likely to play a role in the wound repair/regeneration. Of the five candidate proteins, the amount of the 23560 Dalton protein in the ear-punched tissue was significantly correlated with the rate of ear healing in six representative strains of mice, making it a good candidate for fast wound repair/regeneration. We speculate that the increased concentration of the 23560 Dalton protein in the wound tissue could stimulate the expression of various growth-promoting proteins and consequently speed up the wound repair/regeneration processes. Here, we have shown that examination of protein expression profile using SELDI technology, coupled with database search, is an alternative approach to search for candidate genes for wound repair/regeneration. This novel approach can be implemented in a variety of biological applications.

1. Introduction

It has been suggested that regeneration in amphibians is a fundamental property of vertebrate ancestors related to embryogenesis, which has been apparently lost in most vertebrate species [1-3]. Given the fact that urodeles have retained this ancestral property, it is possible that some of the mammalian species might retain the potential for tissue regeneration. The possibility has been strengthened by a recent report that MRL/MpJ-Fas^{lpr} (MRL) mouse, unlike all other strains of mice tested including C57BL/6 (B6), displays a remarkable capacity for rapid and complete ear wound closure that resembles regeneration [4]. The regeneration of ear tissue, which consists of several major cell types including chondrocyte, chondroblasts, dermal cells, and fiberblasts in MRL mice was indicated by the presence of normal dermal regrowth with organized extracellular matrix deposition, normal vasculature, and cartilage regrowth, and absence of scar formation. In contrast, the 2 mm ear hole in B6 mice only healed about 50% with disorganized extracellular matrix deposition, obvious scar formation, and without cartilage regeneration. Further studies have shown that the healing capacity of MRL is a heritable quantitative trait and genes regulating the phenotype are mapped to five quantitative trait loci (QTL) regions [5]. The remarkable capacity for ear tissue regeneration of MRL mice makes them ideal models to study the molecular mechanisms that underlie tissue regeneration and to explore the potential of genetically manipulating regeneration in mammalian tissue that do not naturally regenerate.

Many traditional methods such as differential screening, differential display, subtraction hybridization, sodium dodecyl sulfate polyacrylamide gel electrophoresis (SDS-PAGE), and two dimensional gel electrophoresis have been used to study the molecular basis of the tissue regeneration/wound repair [1, 6-7]. However, due to the sensitivity of the assay, the scale of the analysis, and the amount of effort involved, power of these methods is limited. A more efficient and comprehensive approach is needed to broaden and complement our limited knowledge on the molecular basis underlying the wound repair/regeneration in this newly identified murine model.

One powerful approach is the recently developed cDNA microarray technology which has been successfully used to study global changes in gene expression in response to a variety of physiological and pathological perturbation (8). Proteins translate mRNA sequence information into function, enabling biological processes. As a complementary approach to gene expression profiling on cDNA microarray, in this study we employed the SELDI ProteinChip technology to determine the differential protein expression profile between MRL and B6, the strains with extreme phenotype in the capacity for wound repair/regeneration. The SELDI ProteinChip array (Ciphergen Biosystems, Palo Alto, CA, USA) is able to determine molecular mass with deviations of less then 0.2% (200 ppm), to detect a few femtomoles of protein, and to estimate the amount of hundreds of proteins simultaneously [9-13]. These features have made it feasible to examine the protein profile from the crude protein extract in response to ear-punch between MRL and B6. Here, we will report the differential protein expression profile between the two strains and describe the candidate gene selections with the aid of database search. This

survey provides insight not only into a general picture of wound healing process in MRL and B6 strains, but also provides several specific target genes that merit further investigation.

2. Materials and methods

2.1. Animals

Four-week old MRL/MpJ-Fas^{lpr} and C57BL/6 female mice were obtained from the Jackson Laboratories (Bar Harbor, ME) and housed at the Animal Reserach Facility, Pettis VA Medical Center, Loma Linda, CA under conditions of 14 h light, 10 h darkness, ambient temperature of 20^0 C, and relative humidity of 30-60%. Experimental animal procedures performed in this study have been approved by the Jerry L Pettis Memorial VA Medical Center, Loma Linda, CA.

2.2. Ear punch, tissue collection and protein extraction

Experimental procedures used in this study are outlined in Figure 1. Briefly, one week after animals arrived, three 2 mm through-and-through holes in diameter were made in both ears of mice using a metal ear punch (Fisher Scientific, Pittsburgh, Catalog No. 01-337B). A 4 mm square disc of ear tissue which contained the punched hole was isolated using scissors 1 day, 5 days, 10 days, or 20 days after ear punch. The equivalent amount of ear tissue was also isolated from the non-ear-punched control mice. The tissue

was immediately put into liquid nitrogen until use. Total proteins were extracted in a buffer containing 50mM Tris, 5% glycerol, 100mM KCl, 1% Triton X-100, 2μg/ml leupeptin, 10μg/ml aprotinin, 10μg/ml soybean trypsin inhibitor, and 7μl/ml β-ME. Total protein concentration was determined at OD_{595} using Bio-Rad Protein Assay reagent (Bio-RAD, Cat# 500-0006).

2.3. SELDI ProteinChip analysis

H4 (aliphatic hydrophobic), NP (normal phase), SAX2 (strong anion exchange), IMAC3 (immobilized metal affinity chromatography), and WCX2 (weak cation exchange) ProteinChip arrays were used for the analysis (each kind of chip has a unique property to bind to a certain group of proteins. The combination of data from several chips is necessary for generating a comprehensive protein profile). Detailed protocol for individual arrays was based on the manufacturer's instruction (Ciphergen Biosystems, Inc. Palo Alto, CA). Below is a general procedures for chip analysis: (1) wash the chip with a proper buffer just before use; (2) remove excess buffer from spots; (3) load 1μg total protein (1μg/μl), containing 200pg myoglobin and 200pg β-lactoglobulin H as an internal control, onto the chip; (4) incubate in a moist chamber and shake at room temperature for 1h; (5) wash each spot with 5μl of buffer, followed by a water wash. Wipe dry around spots; (6) add 0.5μl of energy absorbing molecules, either CHCA (α-cyano-4-hydroxy cinnamic acid) or SPA (sinapinic acid) prepared in an aqueous solution containing 50% acetonitrile and 0.5% trifluroacetic acid to each spot. Air dry; (7) analyze chip using SELDI ProteinChip System (PBS-I, Ciphergen). Data were collected using

laser intensity 15%, 30% and 80%; (8) normalize data and calibrate mass with internal standards before making a comparison between spots.

2.4. Antibody-antigen assay

The monoclonal antibody Mac 387 (DAKO, Denmark) was concentrated to 0.4mg/ml using Centricon YM-30 (Millipore) and equilibrated with 1 X PBS. 2µl of Mac 387 or anti-osteocalcin control antibody was added to the spots of a pre-activated PS-1 chip and incubated in a humidity chamber for 2 hrs at room temperature. The residual active sites on the spots were blocked by incubating with 4 µl of 1 M ethanolamine (pH 8) in 1 X PBS for 30 min, followed by washing the entire chip with 0.05% Triton X-100 in PBS for 5 min, 0.5 M NaCl in 0.1 M sodium acetate (pH 4.5) for 10 min, and 0.5 M NaCl in 0.1 M Tris (pH 8) for 10 min (12, 13). After rinsing the chip with 1 X PBS, 2 µl of ear-punched protein extract was added to the spots containing the covalently bound antibody, and incubation continued for 1 hr at room temperature in the humidity chamber. The chip was then washed with 0.05% of Triton X-100 in PBS for 5 minutes, 1% of Triton X-100 in PBS for another 5 minutes, and finally rinsed with water before adding the energy absorbing molecule CHCA to read the array.

3. Results

3.1. Precision of SELDI ProteinChip analysis

Because the SELDI ProteinChip array is a new technology, we first tested the precision of the measurements (protein mass and concentration) to determine its suitability for the proposed study. Eight major proteins within the 20,000 Dalton range were used to evaluate average measured mass and their coefficient of variation over 8 spots on IMAC3 array. Table 1 shows that the coefficient of variation for protein mass varied from 0.05% to 0.4%. The average CV for eight proteins analyzed is 0.17%. This precision makes it possible to pick up a single amino acid difference or post-translational modification, such as phosphorylation, glycosylation or methylation, depending on the total mass of the measured protein. Variation for peak height, representing the amount of protein, ranged from 4% to 20%. The average CV is 14%. This parameter has been used as a threshold in the data analysis. Potential variation in the precision of the measurements between the different arrays was also tested. Of the five major proteins detected within the 20,000 Dalton range on H4 arrays, CV for protein mass varied from 0.1% to 0.4% (average 0.18%), CV for protein concentration varied from 10% to 20% (average 16%). Therefore, the precision for the measurements between the IMAC3 and H4 arrays was similar.

3.2. Differential protein expression profiling in the MRL and B6 strains of mice

Based on the wound healing process, the comparison was made at five time points: day 0 (before ear punch), day 1 (inflammatory phase), days 5 & 10 (proliferative phase), and day 20 (matrix remodeling phase). Due to the limited tissue from an individual mouse, proteins were pooled from the same strains after we confirmed that the

variation in protein profile between the mice was within the range of the precision of the SELDI measurement (data not shown).

Figure 2 shows the comparison of protein profiling between the day 1 ear-punched tissue and non-ear-punched control (data were combined from the different chips of MRL and B6). Of the 219 proteins detected within the range from 5kDa to 20kDa, 29 proteins (13%) were suppressed and 21 proteins (9%) were stimulated in response to the ear punch. The dramatic change in protein profile after ear punch is in agreement with our understanding that the healing of a wound requires the collaborative efforts of many different tissues and cell lineages.

The comparison of protein profiling between B6 and MRL mice revealed that at least five proteins exhibited more than two-fold changes in expression (Figure 3). Of the five proteins, the expression level of 4 proteins at day 1 increased while one decreased compared to day 0 in both strains. However, the magnitude of change was greater in MRL for three proteins (panel C, D, E). At day 5, three of the proteins returned to base line in MRL, still suppressed or stimulated in B6 (panel A, B, and C). If these proteins were stress-related, this would suggest that MRL is more stress-resistant than B6. Two of the five proteins (panel D and E) were expressed at a higher level in MRL over all time points after ear punch compared to B6, suggesting that they may be functionally related to the ear regeneration phenotype.

3.3. Candidate gene selections based on the mass of differentially expressed proteins

The SELDI system (PBS-1) is able to determine molecular mass with deviations of less than 0.2% (200 ppm). With further calibration using internal protein standards, we can determine the mass of a given protein with reasonably high accuracy. Based on the precision of mass determinations, the TagIdent tool was used to search for proteins that match the measured molecular mass with a variation of 0.175% (This was the average CV for protein mass analyzed in this experiment) of the five interesting proteins (Figure 3) that have shown differential expression between MRL and B6. Seven mouse proteins were identified and their corresponding genes and chromosomal locations were summarized in Table 2. Of the five proteins, the 14300 Dalton protein did not match any known mouse protein. This could be a novel protein yet to be identified or a known protein with post-translational modifications specific for the wound repair process. The 23560 Dalton protein matched 3 known proteins, one of which interestingly, RAS-related protein RAB-8, is localized to the soft-tissue regeneration QTL region (5).

3.4. Antigen-antibody assay to validate the predicted calgranulin A

The 10170 Dalton protein was predicted to represent calgranulin A. An anti-calgranulin A monoclonal antibody (Mac 387) was immobilized covalently on the surface of the PS-1 ProteinChip array and used to test if the 10170 Dalton protein could be captured on the array (Our choice for calgranulin A was based on the availability of the monoclonal antibody for this protein). Figure 4 shows that the 10170 Dalton protein

was absent before ear punch in MRL strain of mice (Fig 4A), stimulated one day after ear punch (Fig 4B), and captured on the anti-calgranulin A-PS1 surface (Fig 4C). One additional protein with molecular mass of 13089 Dalton was also detected on the anti-calgranulin A-PS1 surface, the identity of which is unknown. When the irrelevant anti-osteocalcin antibody was applied to the PS1 surface, no predominant capture was observed (Fig 4D). These results strengthen the suitability of the mass-based gene prediction approach.

3.5. The amount of 23560 Dalton protein was associated with the rate of ear healing

The 23560 Dalton protein was expressed in non-ear-punched tissue at a low level in both MRL and B6. After ear-punch, the relative concentration of this protein was dramatically increased and maintained at a high level over 10 days in MRL mice. However, expression in B6 was increased to a lesser extent and returned to the base line much quicker than MRL. As shown in Table 3, the level of 23560 Dalton protein in MRL was twice as much in B6 before ear-punch, and was four-fold higher 10 days after ear-punch as determined by peak area.

We further investigated the functional significance of 23560 Dalton protein by testing the relationship between the amount of this protein and the rate of ear healing in six strains of mice that represent a wide range of ear healing capacity. Results showed that the good healers consistently had a higher concentration of the 23560 Dalton protein in the ear punched tissue compared to the poor healers (Table 4). The correlation

coefficient between the size of the residual hole and the amount of this protein is –0.85 ($P<0.01$). Furthermore, the differences in the level of 23560 Dalton protein between MRL and B6 mice over the time course were closely correlated with the differences in the healing rate at the early time points. The correlation coefficient between the ratio of this protein level (MRL/B6) and the ratio of the hole size (MRL/B6) is –0.94 ($P<0.01$).

4. Discussion

To examine the molecular events associated with the ear tissue repair/regeneration and identify candidate genes responsible for fast wound repair/regeneration in MRL mice, we used the SELDI technology to define the translational response to ear punch in MRL and B6 mice. Our choice of the technology was guided by the facts that 1) protein is the final functional unit, not the mRNA; 2) SELDI is able to perform differential protein profiling with high sensitivity. Our choice of the mouse strains was based on the fact that the MRL and B6 exhibited large differences in the rate and quality of the ear wound healing (see introduction) and were used for the QTL mapping of soft-tissue regeneration. Thus, examining the physical positions of candidate genes, using the information provided by the QTL mapping, can further strengthen the candidacy selected by the differential protein expression.

We have now shown that the substantial number of proteins responded to the ear punch after 24 hrs of injury and the response eased to a great extent five days later (data not shown). One day after ear punch represents the inflammatory phase of wound

healing, which is characterized by the processes of hemostasis and initial clean-up. Proteins active at this stage are likely involved in inflammation as well as the early stage of wound healing process (6). Dramatic alterations in protein levels one day after ear punch support the histological observation that wounding healing is a dynamic and interactive process [14].

In addition to identifying large number of genes that responded to the initiation of wound healing, we also identified a small subset of genes that comprise a highly specific molecular response related to fast wound repair/regeneration in MRL mice. Five proteins were expressed at a greater than two-fold difference between the 2 strains of mice five days after ear punch. This time point represents the early stage of the second phase of the wound healing process where cells actively rebuild the injured tissue by way of formation of granulation tissue, movement of macrophage, fibroblasts and blood vessels into the wound space (6). The difference in amount of these proteins at this stage could result in a functional alteration in wound repair/regeneration. A small number of differentially expressed proteins indicate that a better healing capacity of MRL is unlikely to be due to large, wide-spread alterations in protein expression.

We developed a protein mass-based, and database search-mediated approach to predict the candidate genes of those differentially expressed proteins. The feasibility of this candidate gene selection approach was strengthened by the antigen-antibody assay in which 10170 Dalton protein, predicted to be calgranulin A, was captured on the anti-calgranulin A-PS1 array. Review of the possible function of the predicted genes suggests

that most of the genes play or have the potential to play a role in the wound healing process. The assignment of the identified, unknown proteins, that are most likely controlling fast wound repair/regeneration, to candidate gene/genes could facilitate the evaluation of these differentially expressed proteins.

The differentially expressed protein that has a molecular mass of 23560 Dalton is particularly interesting. Presence of this protein at low level before ear punch and up-regulation over ten days after ear punch strongly suggest that this is not a stress induced protein. We speculate that this protein may play an important role in wound repair/regeneration based on following: 1) the expression level of the 23560 Dalton protein was stimulated 7 times one day after ear punch in MRL and was 4 times higher in MRL than in B6 at day 10; 2) one of the three predicted genes for the 23560 Dalton protein (based on mass) was the RAS-related protein RAB-8 which was localized in the soft-tissue regeneration QTL region. Furthermore, it is well documented that the RAS-related proteins play an important role in the control of cellular proliferation and coordinate multiple growth-promoting proteins [15-17]; 3) and more importantly, the expression level of the 23560 Dalton protein was functionally correlated with the rate of ear healing in six representative strains of mice. If the 23560 Dalton protein does represent the RAS-related protein RAB-8, it is possible that the increased concentration of RAB-8 in the wound tissue would trigger expression of various growth-promoting proteins and consequently speed up the wound repair/regeneration processes in MRL mice.

The data presented here provide the first "global" assessment of the wound healing process at protein level. However, it is important to point out that the SELDI ProteinChip system has its limitations. First, abundantly expressed proteins are more likely to bind to the surfaces. Some of the regeneration/wound repair proteins are expressed at a low level, and could not be identified in the assay or could not be confidently analyzed due to the instrument's precision in determining quantity (CV=14%). Secondly, the system can detect small proteins more efficiently than large proteins. Most proteins analyzed in this study ranged between 10kDa to 30kDa, which represent only a small fraction of total proteins in the cells. This could be due to a number of possibilities, including the limitation in detecting larger proteins, the procedure used for protein extraction (availability of extractable proteins), and solubility of proteins in the assay buffer. In future experiment, prefractionation of the tissue extracts should be considered to reduce the complexity of the samples so that more proteins could be detected from the ProteinChip surfaces. Additional proteins/genes involved in wound repair/regeneration would be discovered with the development of new ProteinChip array with higher binding capacity, sensitivity, and selectivity. In situ (on the array surface) evaluation of the identity of the differentially expressed proteins is a major task still ahead for this assay. However, its ability to determine protein mass and to quantify the hundreds of proteins simultaneously offers a powerful tool to examine differential protein profile with greater precision and less effort compared to other traditional methods.

Acknowledgements

This work was supported by Assistance Award No. DAMD17-99-1-9571. The U.S. Army Medical Research Acquisition Activity, 820 Chandler Street, Fort Detrick MD 21702-5014, is the awarding and administering acquisition office. The information contained in this publication does not necessarily reflect the position or the policy of the Government and no official endorsement should be inferred. The authors would like to thank Melanie Hamilton-Ulland and Mary Stover for their excellent technical support, to James LeBlanc, Ph.D (Ciphergen Biosystems) for his technical advice and critical comments on the manuscript.

References

[1] R.J. Goss, Getting to mammalian wound repair and amphibian limb regeneration: a mechanistic link in the early events, Wound Rep. Reg. 4 (1996) 190-202.

[2] R.J. Goss, Why mammals do not regenerate – or do they? News in Physiol. Sci. 2 (1987) 112-115.

[3] R.J. Goss, The evolution of regeneration. Adaptive or inherent? J. Theor. Biol. 159 (1992) 241-260.

[4] L.D. Clark, R.K. Clark, E. Heber-Katz, A new murine model for mammalian wound repair and regeneration, Clin. Immunol. Immunopathol. 88 (1998) 35-45.

[5] B.A. McBrearty, L.D. Clark, X.M. Zhang, E.P. Blankenhorn, E. Heber-Katz, Genetic analysis of a mammalian wound-healing trait, PNAS 95 (1998) 11792-11797.

[6] B.T. Kunimoto, Growth factors in wound healing: the next great innovation? Ostomy/Wound Management. 45 (1999) 56-64.

[7] D.L. Stocum, Tissue restoration: approaches and prospects, Wound Rep. Reg. 4 (1996) 3-15.

[8] P.O. Brown, D. Botstein, Exploring the new world of the genome with DNA microarrays, Nature Genetics 21 (1999) 33-37.

[9] H. Kuwata, T.T. Yip, M. Tomita, T.W. Hutchens, Direct evidence of the generation in human stomach of an antimicrobial peptide domain (lactoferricin) from ingested lactoferrin, Biochim Biophys Acta 1429 (1998) 129-41.

[10] H. Kuwata, T.T. Yip, C.l. Yip, M. Tomita, T.W. Hutchens, Direct detection and quantitative determination of bovine lactoferricin and lactoferrin fragments in human gastric contents by affinity mass spectrometry, Adv Exp Med Biol. 443 (1998) 23-32.

[11] H. Kuwata, T.T. Yip, C.L. Yip, M. Tomita, T.W. Hutchens, Bactericidal domain of lactoferrin: detection, quantitation, and characterization of lactoferricin in serum by SELDI affinity mass spectrometry, Biochem Biophys Res Commun. 245 (1998) 764-73.

[12] E.R. Frears, D.J. Stephens, C.E. Walters, H. Davies, B.M. Austen, The role of cholesterol in the biosynthesis of beta-amyloid, Neuroreport 10 (1999) 1699-705.

[13] H. Davies, L. Lomas, B. Austen, Profiling of amyloid β peptide variants using SELDI ProteinChip arrays, BioTechniques 27 (1999) 1258-1261.

[14] A.J. Singer, R.A.F. Clark, Cutaneous wound healing, The New England Journal of Medicine 341 (1999) 738-746.

[15] M.V. Blagosklonny, A node between proliferation, apoptosis, and growth arrest, Bioessays 21 (1999) 704-709.

[16] F. McCormick, Ras-related proteins in signal transduction and growth control, Mol. Reprod. Dev. 42 (1995) 500-506.

[17] A. Wittinghofer, N. Nassar, How Ras-related proteins talk to their effectors, Trends in Biochemical Sciences 21 (1996) 488-491.

Figure legends

Fig.1. Diagram of experimental procedures (for details, see methods).

Fig. 2. Comparison of protein profiling between non-ear-punched and ear-punched tissues. The numbers on the X axis indicate protein mass and on the Y axis indicate peak height (percent of full scale) representing the protein concentration. Diamonds on the X axis indicate that there is more than one protein located at this position, which were automatically determined by the ProteinChip™ software (Version 2.0, Ciphergen). Vertical lines in the field represent individual proteins. Top panel: combined protein profiles of non-punched MRL and B6 mice; Middle panel: combined protein profiles of MRL and B6 one day after ear punching; Bottom panel: the upper part represents the proteins only present in the combined non-punched control compared to the ear-punched tissue, the lower part indicates the proteins only present in the combined tissues one day after ear punch compared to the non-punched control (the negative values on the Y axis only indicate direction and do not mean down regulation).

Fig. 3. Temporal expression profiles of five selected proteins in MRL and B6 mice. X axis indicates the time after ear punch (day 0 designates the time point before ear punch) and Y axis indicates the peak height (percent of full scale), which represents protein concentration.

Fig. 4. Calgranulin A from the extract of ear-punched tissue captured by the monoclonal antibody Mac 387 covalently bound to pre-activated ProteinChip array. The numbers next to the peak indicate the molecular mass of that protein. A: protein profile from the non-ear-punched MRL control extract on IMAC3 array in which the 10170 Dalton protein was not detectable; B: protein profile from the MRL extract 1 day after ear punch on IMAC3 array in which the 10170 Dalton protein was present; C: protein profile from the MRL extract 1 day after ear punch on the anti-calgranulin A PS1 chip in which the 10170 Dalton protein was captured by monoclonal antibody MAC 387. The 13089 Dalton protein appears to cross-react with monoclonal antibody MAC 387 used in this study; D: protein profile from the MRL extract 1 day after ear punch on the anti-osteocalcin PS1 chip in which neither the 10170 nor 13089 Dalton protein was captured.

5-week old MRL or B6 female mice

Punch three 2 mm holes on each ear

Non-ear-punched control

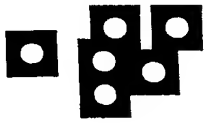

Collect ear-punched tissues and age-matched non-ear-punched control tissues at different time points

Protein extraction and SELDI analysis

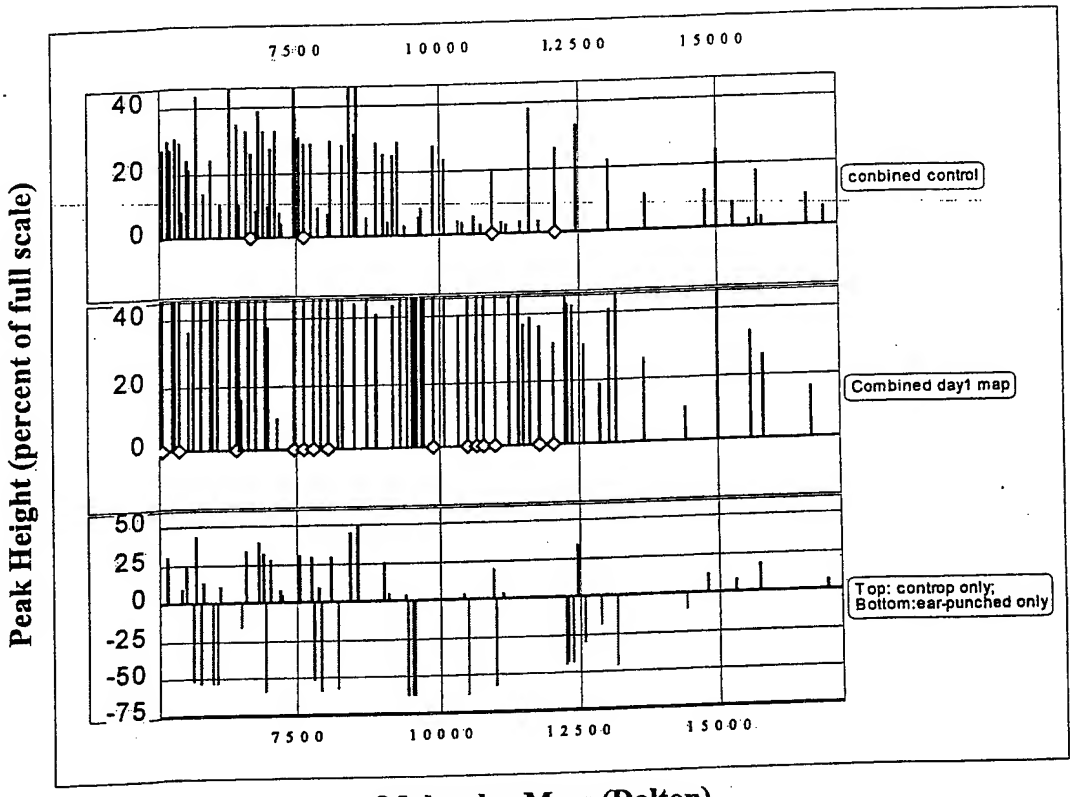
7500
10000
12500
15000
40
20
0
conbined control
40
20
0
Combined day1 map
50
25
0
-25
-50
-75
Top: controp only;
Bottom:ear-punched only
7500
10000
12500
15000
Peak Height (percent of full scale)
Molecular Mass (Dalton)

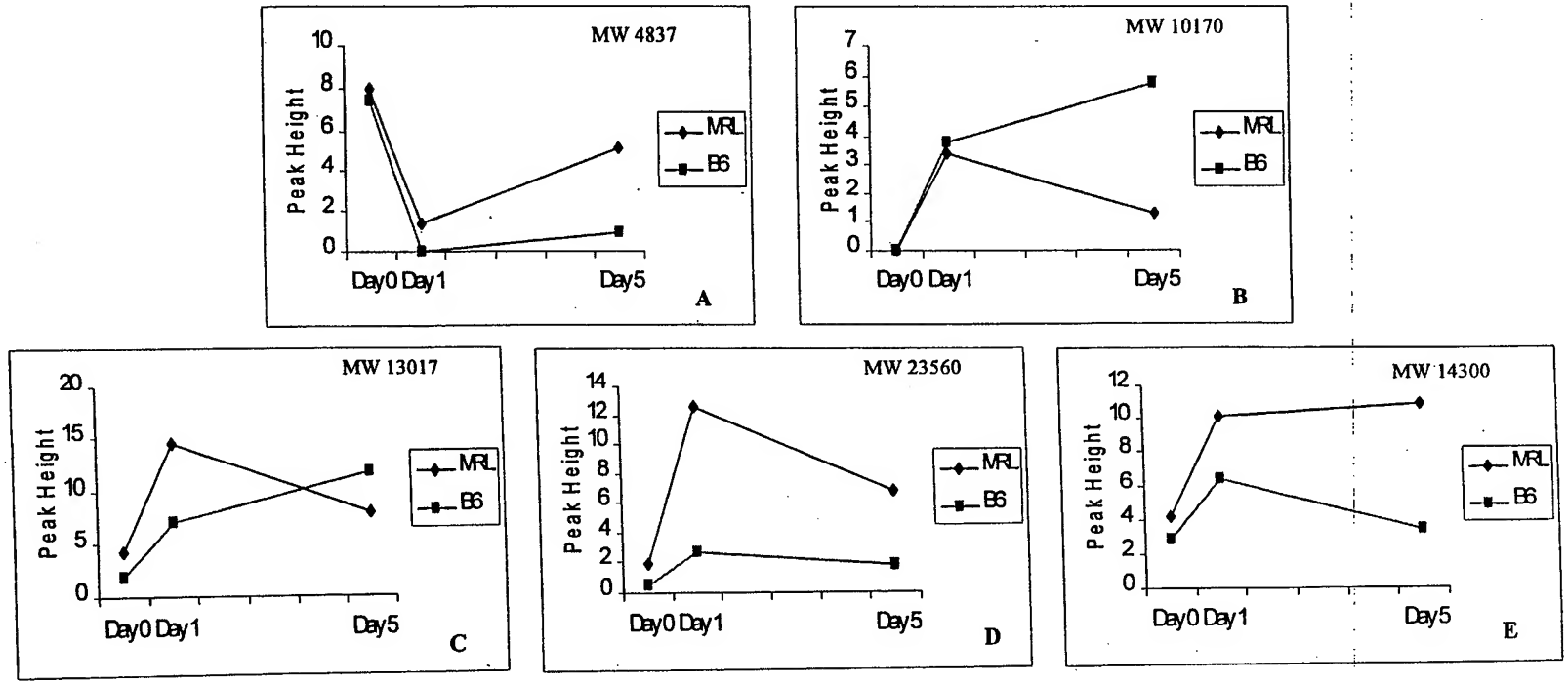
MW 4837
Peak Height
10
8
6
4
2
0
Day0 Day1
Day5
MRL
B6
A
MW 10170
Peak Height
7
6
5
4
3
2
1
0
Day0 Day1
Day5
MRL
B6
B
MW 13017
Peak Height
20
15
10
5
0
Day0 Day1
Day5
MRL
B6
C
MW 23560
Peak Height
14
12
10
8
6
4
2
0
Day0 Day1
Day5
MRL
B6
D
MW 14300
Peak Height
12
10
8
6
4
2
0
Day0 Day1
Day5
MRL
B6
E

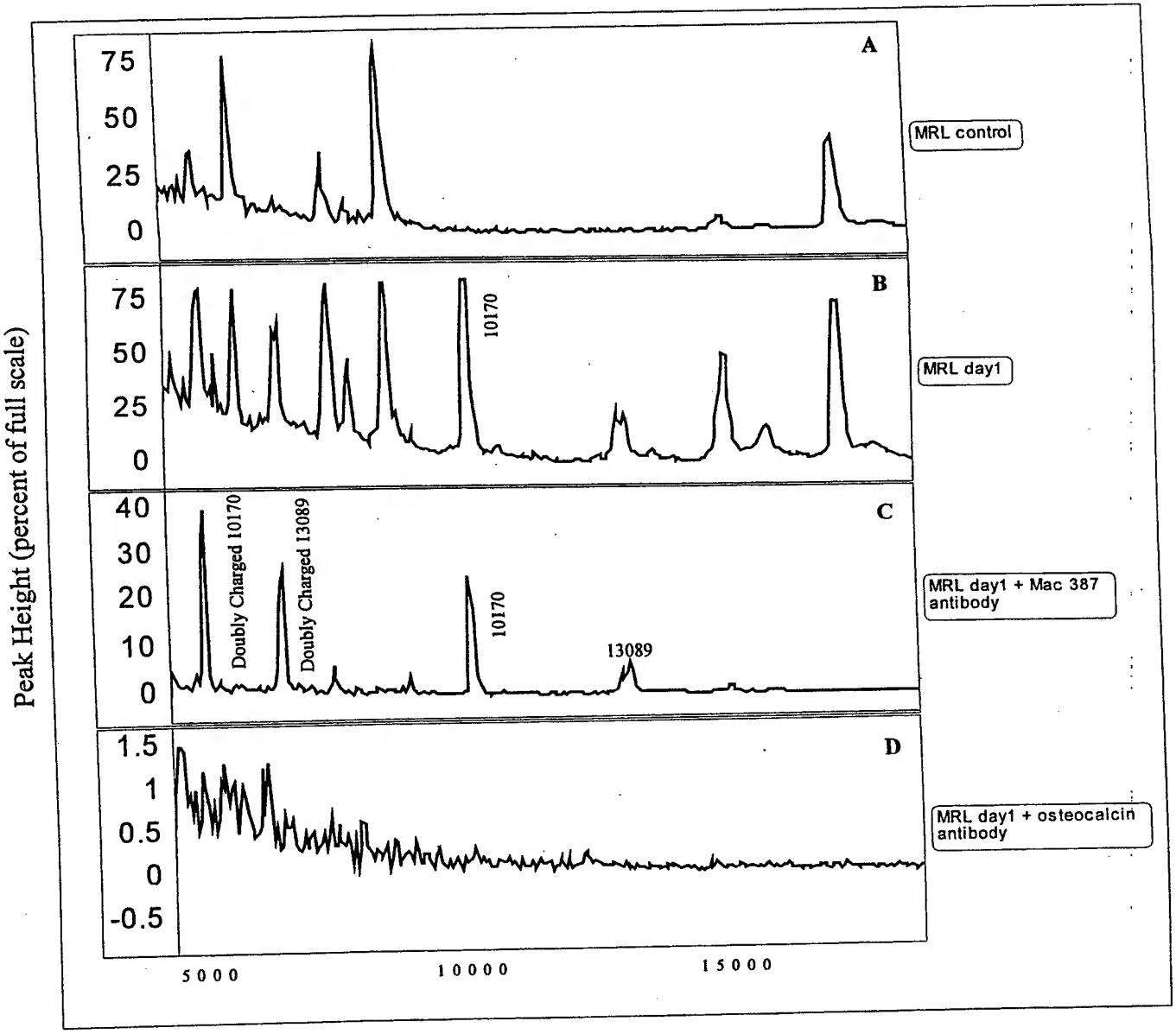
A
75
50
25
0
MRL control
B
75
50
25
0
10170
MRL day1
C
40
30
20
10
0
Doubly Charged 10170
Doubly Charged 13089
10170
13089
MRL day1 + Mac 387 antibody
D
1.5
1
0.5
0
-0.5
MRL day1 + osteocalcin antibody
5000
10000
15000
Peak Height (percent of full scale)
Molecular Mass (Dalton)

Table 1
The precision of the SELDI instrument for measurement of protein mass and concentration. 1 μg of total protein (24h after ear punch) from CBA strain of mice was loaded onto each of eight spots of IMAC3 protein chip. Major proteins between 5000 Daltons and 20000 Daltons were selected for measurement of average protein mass and concentration. Myoglobin was used as an internal control. Peak height represents the amount of protein retained on the chip.

Protein	Mass (Daltons)	CV%	Concentration (peak height)	CV%
1	5062 ± 23	0.4	76 ± 10	14
2	7482 ± 15	0.2	78 ± 13	16
3	9332 ± 20	0.2	41 ± 5	14
4	10163 ± 23	0.2	55 ± 2	4
5	13086 ± 18	0.1	59 ± 12	20
6	15053 ± 29	0.1	72 ± 7	9
7	15824 ± 24	0.1	46 ± 9	19
Internal control	17136 ± 10	0.05	54 ± 10	19

Values are mean ± SD (n=8)

Table 2
Candidate gene selections based on the predicted protein mass. Bolded gene is localized in the soft-tissue regeneration QTL region.

Protein Mass (Dalton)	Predicted genes	Chromosomal location	
		Chromosome #	cM Position
4837	Neuronatin	2	88
10170	Calgranulin A	3	Syntenic to human 1q21
	Lymphocyte Antigen 6, locus F	Unkown	
13017	Growth Differentiation factor 3	6	58
14300	N/A		
23560	**Ras-related Protein RAB-8**	**8**	**33**
	Mad4	5	20
	Ras-related Protein RAB-7	6	37

Table 3
The relative concentration of the 23560 Dalton protein at different time points after ear punch in MRL and B6 mice, determined by peak area and peak height.

Time point	Relative Protein Concentration					
	MRL		B6		MRL/B6	
	Peak Area	Peak Height	Peak Area	Peak Height	Peak Area	Peak Height
Day 0	2403	1.9	1177	0.6	2	3.1
Day 1	16260	12.5	7389	2.7	2.2	4.6
Day 5	9290	6.8	2713	1.8	3.4	3.7
Day 10	6985	5.1	1834	1.3	3.8	3.9

Table 4

The relationship between the concentration of 23560 Dalton protein and the rate of ear healing in six representative strains of mice. The concentration, as measured by peak height, was determined one day after ear punch and ear hole size was measured 20 days after ear punch.

Strain	*MRL*	*CBA*	*C3*	*SJL*	*Balb/c*	*B6*
Hole Size (mm)	0.025	0.358	0.81	1.49	1.6	1.04
Peak Height	10	3.5	1.3	0.4	0.5	2.2

Quantitative assessment of forearm muscle size, forelimb grip strength, forearm bone mineral density and forearm bone size in determining humerus breaking strength in ten inbred strains of mice

X. Li, S. Mohan, W. Gu, J. Wergedal and D.J. Baylink

Molecular Genetics Division, Musculoskeletal Disease Center, JL Pettis VA Medical Center and Loma Linda University, Loma Linda, CA 92357, USA

Running title: Determinants of humerus breaking strength in mice

Corresponding author: David Baylink, MD., Musculoskeletal Disease Center, JL Pettis VA Medical Center, 11201 Benton Street (151), Loma Linda, CA 92357, USA

Tel: (909) 422-3101

Fax: (909) 796-1680

E-mail: baylid@lom.med.va.gov

Abstract. Bone strength is an important clinical endpoint of osteoporosis research. The evaluation of the relative importance of bone and muscle components to bone strength has widespread implications for the understanding and prevention of osteoporosis. The objectives of this study were to understand the inter-relationship between the different components of the muscular skeletal system and to determine the effect of forearm muscle size, forelimb grip strength, forearm bone mineral density (BMD), and forearm bone size on the humerus breaking strength among 10 inbred strains of mice. The forearm muscle size was measured using a peripheral quantitative computed tomography (pQCT). The forearm BMD and forearm bone size were measured using a PIXIMUS™ Densitometer. The forelimb grip strength and humerus breaking strength were measured using an Instron Mechanical Tester. Significant correlations were found among the five regional phenotypes. All variables have a moderately high genetic component with heritability estimates of 0.83 for forelimb grip strength, 0.76 for forearm muscle size, 0.6 for forearm BMD, 0.63 for forearm bone size, and 0.68 for humerus breaking strength. Forward stepwise multi-regression analysis showed that the forearm, forelimb grip strength, and forearm bone size were three major determinants to bone strength and explained 61% of variation in bone breaking strength. These data suggest that evaluation of these three parameters together, rather than BMD alone, is a more effective, noninvasive approach for predicting fracture risk.

Key words: Muscle size – Muscle strength – Bone density – Bone strength – Bone size

Introduction

A relationship between muscle and bone systems in humans has been extensively studied in an attempt to find theoretical grounds for the treatment and prevention of osteoporosis [1-8]. However, in the analyses of human subjects, a direct measure of bone breaking strength is not feasible. This has posed a technical difficulty to quantitatively evaluate the relative importance of bone and muscle components in affecting bone strength, an ultimate predictor of the risk of osteoporosis.

It is now widely recognized that many human diseases can be modeled in mouse. Studies have been carried out in mice to examine the relationship between bone density and grip strength, muscle size, and bone strength [9, 10]. These analyses mainly focused on bone density as a primary parameter. The knowledge on the relative importance of regional bone- and muscle-related parameters to bone strength is limited.

In this study, we used five regional bone and muscle phenotypes, including forearm muscle size, forelimb grip strength, forearm bone mineral density (BMD), forearm bone size, and humerus breaking strength, to evaluate the fundamental relationship between bone and muscle systems and to determine the quantitative effect of these regional phenotypes on bone strength among 10 inbred strain of mice. We hypothesized that other regional phenotypes, such as muscle size and muscle strength, would have considerable contribution to bone strength in addition to bone size and bone density.

Materials and methods

Animals

Ten inbred strains of mice (129J, CBA/J, FVB/NJ, LG/J, LP/J, NZB/BINJ, RIIIS/J, SENCAR/PtJ, SJL/J, SWR/J,) were selected from subgroups of the major inbred strains representing as diversified genetic origin as possible. Three female mice of each strain were obtained from The Jackson Laboratory (Bar Harbor, ME). The animals were housed at the Animal Research Facility, VA Medical Center, Loma Linda under conditions of 14 h light, 10 h darkness, ambient temperature of 20^0 C, and relative humidity of 30-60%. The animals were six months old when the experiment was carried out. Experimental animal procedures performed in this study have been approved by the Animal Studies Subcommittee of the Jerry L. Pettis Memorial VA Medical Center, Loma Linda, CA.

Forelimb grip strength

An Instron DynaMight Low-Force Testing System (Instron Corporation, Canton, MA) was used to measure the forelimb grip strength *in vivo*. A metal bar (2mm in diameter and 8 cm in length) was attached to the Instron machine force transducer. The mouse was grasped at the base of the tail and lowered vertically toward the bar. When two paws were grasping the bar, the mouse was pulled slightly backwards from the tail (very gently). This triggered a "counter-pull" from the mouse. A computer recorded grasping

force in gram at 0.01-second intervals. The maximum force (gram) exerted by the mouse as it resisted being pulled off the bar was identified and taken as the measure of forelimb grip strength. All mice were tested twice a day (about 10am and 3pm) for 4 consecutive days. No significant difference was found between the morning and afternoon measurement or between the consecutive days. Mean of measurements for each mouse was used.

Humerus breaking strength

Both humeri were dissected, cleaned and then subjected to strength measurement by three point bending using an Instron Mechanical Tester with a constant span length of 2 mm and a constant speed of 10mm/min. The press head, as well as the two support points, was rounded to avoid shear load and cutting. The bone was positioned horizontally with the anterior surface upwards, centered on the supports, and the pressing head was directed vertically to the midshaft of the bone. Humerus strength was defined as the maximum force (Newton) at failure. A computer automatically recorded the breaking force profile and the maximum force was used for data analysis.

Forearm BMD

A PIXIMUS™ Densitometer (LUNAR Corporation, Madison, WI) was used for the measurement of forearm BMD. It is a rapid (5-minute image acquisition) and very precise small animal densitometer with the precision of 1% CV for total skeletal BMD,

and 1.5% CV for femur region of interest (ROI) BMD. Routine calibration was performed daily with a defined standard (phantom). Before measurement, mice were anesthetized using an IP dose of 50/10 mg/kg Ketamine/xylazine solution and then placed on a specimen tray (the head was to the left) and put in the PIXI imaging area for analysis. After a measurement was completed, ROI rectangle was moved and resized to cover a portion of left forearm. The PIXI software automatically calculated the forearm bone density and recorded the data as Microsoft Excel files.

Muscle size

Forearm cross-section muscle size was measured with a peripheral quantitative computed tomography (pQCT) system Stratec XCT Research M^{TM} (Norland Medical Systems, Fort Atkinson, WI). The most important part of the procedure is to determine the scan site where the forearm muscle is the largest. By choosing the range color scale that included density values down to minus 300mg/ccm, which made the muscle visible, we experimentally determined that the 30% of the forearm length from the humerus joint would be an ideal site for mouse forearm muscle scan. An additional two slices (0.5mm above and below the center scan) were scanned. The forearm muscle size was defined as the average of these three scans.

Statistical analysis

Results are reported as mean ± SD for 3 animals per strain. ANOVA, correlation analysis, and forward stepwise regression analysis were performed using commercially available statistical software (STATISTICA, StatSoft Inc., Tulsa, OK). Results were considered significantly different for $P<0.05$. Heritability was estimated from the analysis of variance. We used a one-way ANOVA with strains treated as groups. Three individuals were measured within each inbred strain. The mean square within strains (MS_W) reflects the environmental variance (σ_W^2), while the mean square between strains (MS_B) is determined by both the genetic variance between strains (σ_B^2) and the environmental variance. The expectations of MS_W and MS_B are $E(MS_W) = \sigma_W^2$ and $E(MS_B) = \sigma_W^2 + r\sigma_B^2$, respectively, where $r = 3$ is the replicate within each strain. Letting the expected mean squares equal the observed mean squares, we get the estimated broad-sense heritability as:

$$\hat{H}^2 = \frac{\hat{\sigma}_B^2}{\hat{\sigma}_B^2 + \hat{\sigma}_W^2} = \frac{MS_B - MS_W}{MS_B + (r-1)MS_W}$$

Results

Measurement values

Table 1 showed the measurements of bone and muscle-related phenotypes in the forelimb of ten inbred strains of mice. Although the variations of the phenotypes among strains were all significant at $P<0.0001$, forearm muscle size was the most variable (CV=26%) and forearm bone mineral density was the least variable trait (CV=11%) among strains.

Humerus breaking strength was the second most variable trait (CV=20%) in which a 1.8-fold difference between the highest (LG/J) and lowest (SWR/J) strain was observed. Heritability indices showed that the muscle-related phenotypes had a higher heritability estimate compared to the bone-related phenotypes (Table 2).

Correlations

A significant, positive correlation was found among all six phenotypes (Table 3. Above the diagonal). In the five forelimb-related phenotypes, forearm bone mineral density had the highest correlation coefficient with humerus breaking strength (r=0.69). The second highest correlation was observed between bone breaking strength and forelimb grip strength (r=0.63). The forearm muscle size was also highly correlated with forelimb grip strength (r=0.62). After adjusting with body weight (Table 3. Below the diagonal), overall correlations were not significantly changed.

Partial correlation and multi-regression analysis

To further evaluate the correlation between the regional phenotypes and humerus breaking strength and the relative importance of these phenotypes in determining the humerus breaking strength, the partial correlation of regional phenotypes with humerus breaking strength was estimated. Table 4 showed that BMD had the highest partial correlation with bone strength (R_p=0.42) among the regional phenotypes. Grip strength was the second (R_p=0.31) and then bone size (R_p=0.0.26). Muscle size (R_p=0.11) had

very little influence on bone strength. As tolerance indicated, 70% will be redundant if muscle size is included in the multi-regression analysis equation. Consistent with the partial correlation results, the forward stepwise multi-regression analysis (Figure 1) indicated that the order of importance of regional phenotypes in determining humerus breaking strength was forearm BMD (β coefficient was 0.37) > forelimb grip strength (β=0.31) > forearm bone size (β=0.26). Three parameters had a multi-correlation coefficient, r=0.78, and explained 61% of variation in humerus breaking strength. Muscle size and body weight were eliminated in stepwise regression analysis.

Discussion

The aims of this study were to investigate the fundamental relationship between the muscle and bone systems and then evaluate the relative contribution of forelimb grip strength, forearm muscle size, forearm BMD, and forearm bone size to the humerus breaking strength. We selected five site-specific phenotypes from the forelimb based on the fact that the effects on bone strength are likely to be regional. A similar highly specific regional quantitative study has not been previously carried out in either humans or mice.

Humerus breaking strength has not been previously compared among the inbred strains of mice. Our study showed that it had a considerable variation among the strains tested (the second largest CV in the five regional phenotypes). The large divergence provides the opportunity to search for quantitative trait loci that regulate the humerus breaking

strength, which may be more relevant to osteoporosis research compared to bone density QTLs.

We observed a significant correlation between all five regional phenotypes. One might expect to find a positive correlation between the size of the muscle and the performance of the muscle or between the strength of the bone and density or size of the bone. The most striking observation in this study was the strong association between the *in vivo* muscle strength and *in vitro* bone strength (the forelimb grip strength had the second highest correlation with bone strength among all correlations in five regional phenotypes and was identified as one of the three main determinants to bone strength). There are several possibilities that could explain this seemly interesting association. In general, the more the muscle loading is, the more the bone loading will be. The largest voluntary loads on bones come from muscles. To adapt bone strength to the loads, special strain threshold ranges determine where modeling adds and strengthens bone, and where remodeling conserves or removes it [11]. Thus, there are adaptive mechanisms that regulate an interaction between the muscle and bone. Another possibility is that muscle strength could influence bone strength by improving bone quality. It is generally believed that bone density, bone size and bone quality are key determinants to bone strength [12], although little is known on the relative contributions of these three variables. In the forward stepwise multi-regression analysis, the tolerance for grip strength was 0.69 (data not shown), which indicated that the grip strength was not redundant in the regression equation in relation to bone density and bone size. A tentative explanation is that the grip strength complemented the bone quality, which we did not measure in this experiment.

At the molecular level, we speculate the third possibility that the strong association between the two traits may be mediated by common genes regulating both bone and muscle systems or mediated by the gene interaction between the two systems. This suggestion is in agreement with a monozygotic and dizygotic twin study [13] where the authors concluded that more than half the covariance in BMD of the femoral neck and lean body mass was attributed to the same genetic factors and also a parent-offspring study [14] in which data suggested that a general association between bone mass, lean body mass and muscle strength was mediated by some genes influencing these parameters by affecting size during late puberty in boys.

Regression analysis showed that BMD is the most important determinant to bone strength, but muscle strength and bone size also play a fundamental role. There are rich literatures in which bone density has been widely treated as a reliable predictor for bone strength [12, 15-16]. Current studies suggest that the prediction could be substantially improved by the combination of bone size, muscle strength and bone density. Three parameters explained 61% of variation in humerus breaking strength. Forelimb grip strength and bone size played a role equivalent to 84% and 70% of bone density's contribution to bone strength, respectively, based on the estimate of β coefficient.

A limitation in this study was the number of animals (n=30. Data from one animal was lost due to a technical difficulty) used for the analysis, which could have potentially biased our estimate. However, the animals used in this study were all inbred strains. There was a relatively small variation between animals of the same strain and a large

variation between the different strains of mice. Overall estimates should not be significantly inflated.

In conclusion, the present study has suggested that the strong association between bone and muscle systems could be contributed to adaptive mechanisms and mediated by common genes or gene interaction between the two systems. The relative importance of four regional phenotypes in determining humerus breaking strength is: forearm BMD > forelimb grip strength > forearm bone size > forearm muscle size. Our data have also demonstrated that using the combination of bone density, muscle strength and bone size in contrast to using bone density alone can substantially increase the power for the prediction of bone breaking strength. The identification of forelimb grip strength as the second most important determinant to bone breaking strength has suggested that therapeutic strategies that have targeted to increase muscle strength should have an effect on the treatment and prevention of osteoporosis fracture.

Acknowledgements. This work was supported by Assistance Award No. DAMD17-99-1-9571. The U.S. Army Medical Research Acquisition Activity, 820 Chandler Street, Fort Detrick MD 21702-5014, is the awarding and administering acquisition office. The information contained in this publication does not necessarily reflect the position or the policy of the Government and no official endorsement should be inferred. The authors would like to thank Mary Stover and Melanie Hamilton-Ulland for their excellent technical support.

References

1. Rhodes EC, Martin AD, Taunton JE, Donnelly M, Warren J, Elliot J (2000) Effects of one year of resistance training on the relation between muscular strength and bone density in elderly women. Br J Sports Med 34: 18-22
2. Osei-Hyiaman D, Ueji M, Toyokawa S, Takahashi H, Kano K (1999) Influence of grip strength on metacarpal bone mineral density in postmenopausal Japanese women: a cross-sectional study. Calcif Tissue Int 64: 263-266
3. Hakkinen A, Sokka T, Kotaniemi A, Kautiainen H, Jappinen I, Laitinen L, Hannonen P (1999) Dynamic strength training in patients with early rheumatoid arthritis increases muscle strength but not bone mineral density. J Rheumatol 26: 1257-1263
4. Pocock N, Eisman J, Gwinn T, Sambrook P, Kelly P, Freund J, Yeates M (1989) Muscle strength, physical fitness, and weight but not age predict femoral neck bone mass. J Bone Miner Res 4: 441-447
5. Arden NK, Spector TD (1997) Genetic influences on muscle strength, lean body mass, and bone mineral density: a twin study. J Bone Miner Res 12: 2076-2081
6. Bevier WC, Wiswell RA, Pyka G, Kozak KC, Newhall KM, Marcus R (1989) Relationship of body composition, muscle strength, and aerobic capacity to bone mineral density in older men and women. J Bone Miner Res 4: 421-432
7. Snow-Harter C, Bouxsein M, Lewis B, Charette S, Weinstein P, Marcus R (1990) Muscle strength as a predictor of bone mineral density in young women. J Bone Miner Res 5: 589-595

8. Henderson NK, Price RI, Cole JH, Gutteridge DH, Bhagat CI (1995) Bone density in young women is associated with body weight and muscle strength but not dietary intakes. J Bone Miner Res 10: 384-393
9. Kaye M, Kusy RP. (1995) Genetic lineage, bone mass, and physical activity in mice. Bone 17: 131-135.
10. Jamsa T, Jalovaara P, Peng Z, Vaananen HK, Tuukkanen J (1998) Comparison of three-point bending test and peripheral quantitative computed tomography analysis in the evaluation of the strength of mouse femur and tibia. Bone 23: 155-161
11. Schiessl H, Frost HM, Jee WSS (1998) Estrogen and bone-muscle strength and mass relationships. Bone 22: 1-6
12. Weinstein RS (2000) True strength. J Bone Miner Res 15: 621-625
13. Seeman E, Hopper J, Young N, Formica C, Goss P, Tsalamandris C (1996) Do genetic factors explain associations between muscle strength, lean mass, and bone density? A twin study. Am J Physiol 270: 320-327
14. Nordstrom P, Lorentzon R (1999) Influence of heredity and environment on bone density in adolescent boys: a parent-offspring study. Osteopros Int 10: 271-277
15. Carter DR, Hayes WC (1977) The compressive behavior of bone as a two-phase porous structure. J Bone Joint Surg Am 59: 954-962
16. Jiang C, Giger ML, Kwak SM, Chinander MR, Martell JM, Favus MJ (2000) Normalized BMD as a predictor of bone strength. Acad Radiol 7: 33-39

Figure legend

Fig 1. Illustration of the relative importance of the forearm bone mineral density, forelimb grip strength, forearm bone size to humerus breaking strength. β: β coefficient that is a standardized regression coefficient and represents relative contribution of cause factor to effect factor. Different form regression coefficient, β coefficients are directly comparable to each other. R: correlation coefficient. * $P < 0.05$. [a] forward stepwise multi-regression formula.

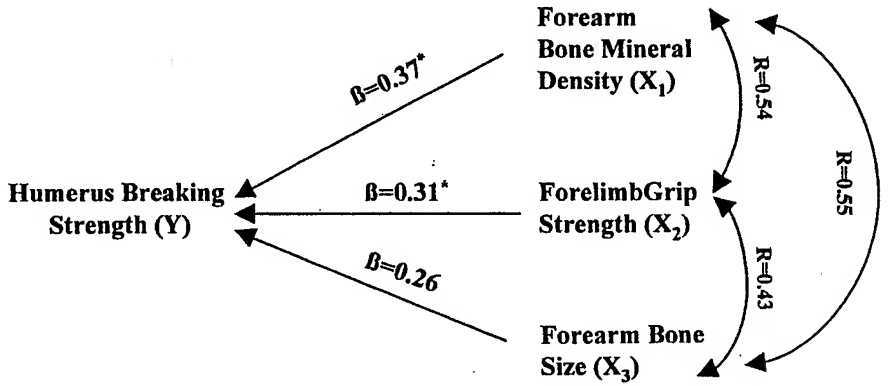

$$Y^a = -17 + 458.7^* X_1 + 0.101^* X_2 + 15.9 X_3$$

Table 1. Measurements of bone and muscle-related phenotypes in the forelimb of ten inbred strains of mice[a]

Strains	BMD (g/cm^2)	Breaking strength (N)	Bone size (cm^2)	Grip strength (g)	Muscle size (mm^2)	Body weight (g)
129/J	0.03843 ± 0.002205	20.16 ± 2.12	0.4867 ± 0.0404	104.1 ± 3.75	8.29 ± 0.44	24.00 ± 2.93
Sencar/PtJ	0.04333 ± 0.005750	22.89 ± 2.24	0.5133 ± 0.0702	142.6 ± 12.20	13.52 ± 2.07	39.57 ± 3.91
C57BL/6J	0.03393 ± 0.000153	18.96 ± 0.22	0.4467 ± 0.0252	108.1 ± 11.21	8.18 ± 1.14	23.43 ± 0.80
CBA/J	0.03917 ± 0.001069	19.53 ± 0.78	0.5400 ± 0.0173	117.4 ± 1.42	10.12 ± 0.43	24.63 ± 1.17
FVB/NJ	0.03697 ± 0.001443	18.11 ± 2.75	0.4567 ± 0.0231	122.3 ± 2.12	7.66 ± 0.35	23.63 ± 1.72
NZB/BINJ	0.03397 ± 0.003453	14.62 ± 1.49	0.4467 ± 0.0416	96.4 ± 1.21	8.10 ± 0.51	25.63 ± 0.51
RIIIS/J	0.03363 ± 0.000777	16.47 ± 1.54	0.3900 ± 0.0265	110.6 ± 0.75	8.00 ± 1.10	18.20 ± 0.76
LP/J	0.03837 ± 0.001457	21.45 ± 3.18	0.4633 ± 0.0208	119.5 ± 3.90	7.46 ± 1.32	20.30 ± 0.52
LG/J	0.04137 ± 0.000404	24.72 ± 3.11	0.5333 ± 0.0289	126.1 ± 2.43	12.05 ± 1.34	34.87 ± 0.51
SWR/J	0.03350 ± 0.001552	13.43 ± 1.64	0.4133 ± 0.0058	99.7 ± 1.59	6.54 ± 1.20	22.03 ± 1.36
All strains	0.03727 ±0.003916	19.04 ± 3.84	0.4690 ± 0.0555	114.7 ± 14.17	8.99 ± 2.33	25.63 ± 6.51
CV%	11	20	12	12	26	25
F value	6.24	8.40	6.23	17.96	11.77	40.42
P	<0.001	<0.0001	<0.001	<0.0001	<0.0001	<0.0001

[a] Data are presented as mean ± SD.

Table 2. Heritability estimates of bone and muscle-related phenotypes in the forelimb of ten inbred strains of mice

Traits	Heritability
BMD (g/cm^2)	0.60
Breaking strength (N)	0.68
Bone size (cm^2)	0.63
Grip strength (g)	0.83
Muscle size (mm^2)	0.76
Body weight (g)	0.52

Table 3. Correlations among the muscle and bone related phenotypes in 10 inbred strains of mice[d]

Variable	Grip Strength	Muscle Size	Bone Density	Bone Size	Breaking Strength	Body Weight
Grip Strength	1	0.62[a]	0.54[b]	0.43[c]	0.63[a]	0.48[b]
Muscle Size	0.53[b]	1	0.50[b]	0.61[a]	0.58[b]	0.78[a]
Bone Density	0.89[a]	0.42[c]	1	0.55[b]	0.69[a]	0.50[b]
Bone Size	0.79[a]	0.41[c]	0.85[a]	1	0.60[b]	0.72[a]
Breaking Strength	0.70[a]	0.39[c]	0.70[a]	0.69[a]	1	0.5227[b]
Body Weight	-0.81[a]	-0.31	-0.88[a]	-0.80[a]	-0.50[b]	1

[a] $P < 0.001$; [b] $P < 0.01$; [c] $P < 0.05$; [d] Below the diagonal, the correlation was adjusted by body weight.

Table 4. Partial correlation of regional phenotypes with humerus breaking strength

Traits	Partial correlation	Tolerance[a]	p-level
Bone density	0.42	0.58	0.039
Grip strength	0.31	0.54	0.131
Bone size	0.26	0.43	0.205
Muscle size	0.11	0.31	0.590
Body weight	-0.07	0.30	0.742

[a] The tolerance of a variable is defined as 1 minus the squared multiple correlation of this variable with all other independent variables in the regression equation. Therefore, the smaller the tolerance of a variable, the more redundant is its contribution to the regression (i.e., it is redundant with the contribution of other independent variables). If the tolerance of a variable is 0.01, it means that this variable is 99% redundant with the variables already in the equation.

ELSEVIER

Development and Evaluation of C-telopeptide Enzyme-linked Immunoassay for Measurement of Bone Resorption in Mouse Serum

A. K. SRIVASTAVA, S. BHATTACHARYYA, G. CASTILLO, N. MIYAKOSHI, S. MOHAN, and D. J. BAYLINK

Musculoskeletal Disease Center, Jerry L. Pettis VA Medical Center and Loma Linda University, Loma Linda, CA, USA

Fn1 **The mouse is increasingly being used as an animal model for the study of skeletal phenotypes in humans, mainly because of the ease of genetic manipulation. Biochemical markers of bone metabolism provide a valuable parameter for the assessment of skeletal metabolism. In the mouse model, assays for bone formation have been available for long time; however, little is known about bone resorption markers. The present study describes the development of a serum C-telopeptide enzyme-linked immunoassay (ELISA), which measures degradation products of type I collagen that are generated by osteoclastic bone resorption. The C-telopeptide ELISA uses affinity-purified antibodies generated against human sequence DFSFLPQPPQEKAHDGGR. The epitope involves an amino acid sequence, which is identical in the mouse and human C-terminal peptide of type I collagen (α1 chain). Sensitivity of the ELISA used was <0.1 ng/mL. The average intra- (n = 10) and interassay (n = 8) coefficient of variation for two controls was <12%. The average dilution and spike recovery rates were 98% and 97%, respectively. Application of the ELISA to measure C-telopeptide in 3–4-week postovariectomized (ovx) C57BL/6J (B6) mice (n = 9 or 10) showed a 45% higher C-telopeptide concentration than the sham-operated mice. Treatment of ovx mice with estradiol (400 μg/kg body weight) or alendronate (1.0 mg/kg body weight) resulted in a 20%–50% decrease in C-telopeptide levels compared to the vehicle-treated ovx group. In addition, B6 mice fed a calcium-deficient diet (0.01% calcium) showed a 50% higher C-telopeptide concentration compared to the B6 mice receiving a normal diet (0.6% calcium). In conclusion, the C-telopeptide ELISA exhibited acceptable analytical performance and sufficient discriminatory power to show expected directional changes in the rate of bone resorption following ovariectomy, ovx plus estradiol or alendronate** AQ: 1 **treatment, and administration of a calcium-deficient diet. Therefore, the ELISA developed in this study could be used for measuring bone resorption in the mouse model. (Bone 27: 000–000; 2000)**

Address for correspondence and reprints: David J. Baylink, M.D., Musculoskeletal Disease Center, Jerry L. Pettis VA Medical Center, 11201 Benton Street, Loma Linda, CA 92357. E-mail: baylid@lom.med.va.gov

Key Words: C-telopeptide; Resorption; Enzyme-linked immunoassay (ELISA); Mouse; Ovariectomy (ovx); Alendronate.

Introduction

The mouse is being used more than ever as an animal model to study skeletal remodeling mechanisms relevant to humans. The popularity of the mouse as an animal model is largely because of its utility in genetic studies, such as mapping of quantitative trait loci (QTL)[1] and transgenic and knockout studies,[4–7] all of which AQ: 2 are frequently relevant to human biology. The skeletal remodeling process is reflected in the blood circulation by the presence of various biomolecules derived from either the bone matrix or the cells actively involved in bone formation or resorption. Application of these markers as accurate, noninvasive, and relatively simple tests provides a unique means to assess bone turnover and its components, bone formation and resorption, in humans as well as in animals.[2,6,7]

In the mouse model, formation markers such as osteocalcin or alkaline phosphatase have long been available; however, little is known about bone resorption markers. Biochemical evaluation of bone resorption in the mouse model has been performed by high-performance liquid chromatography (HPLC) determination of pyridinium cross-links[2,6] in urine. Urinary markers show a relatively high variation, in part because of a need to calculate excretion of cross-links as a ratio of creatinine. In addition, collections of timed urine samples from mice have been associated with practical difficulties. A serum assay, therefore, offers potential advantages in terms of decreased variability and ease of sample collection. In this study, we describe the development of a C-telopeptide enzyme-linked immunoassay (ELISA) for the measurement of bone resorption in mouse serum. The ELISA developed herein measures degradation products of type I collagen (α1 chains) that are released into the circulation during osteoclastic resorption of bone matrix. This ELISA utilizes a polyclonal antiserum that was developed against a human C-telopeptide sequence,[13] but binds to an epitope that is identical in the human and mouse C-telopeptide sequence. The in vivo efficacy of the ELISA was evaluated by measuring the C-telopeptide concentration in conditions known to modulate bone resorption in the mouse model. Three perturbations known to influence bone resorption by different mechanisms were studied: (1) an increase in bone resorption in mice following cessation of ovarian function and subsequent reversal of elevated bone resorption by treatment with either estradiol[10] or bisphosphonate[3];

8756-3282/00/$20.00
PII S8756-3282(00)00356-2

Orig. Op.	OPERATOR:	Session	PROOF:	PE's:	AA's:	COMMENTS	ARTNO:
1st mke, 2nd scw	trumans	5					5842

zjs=Original articles zjss=Original articles

Bone Vol. 27, No. 4
October 2000:000–000

(2) an increase in bone resorption in response to a calcium-deficient diet[11]; and (3) an increase in bone resorption induced by administration of high doses of parathyroid hormone(1–34) [PTH(1–34)].[9,10]

Materials and Methods

Materials

Peptides NH_2—CDFSFLPQPPQEKAHDGGR—COOH (human C-telopeptide), and NH_2—CDFSFLPQPPQEKSQDGGR—COOH (rat C-telopeptide)[3] were synthesized commercially (SynPep, Dublin, CA) and were of 95%–99% purity, as determined by HPLC and mass spectrometry. Eight-well Maxisorp strips were purchased from Nunc (Switzerland). Maliemide-activated horseradish peroxidase (HRP) and keyhole limpet hemocyanin (KLH) were purchased from Pierce (Rockford, IL) and coupled to synthetic C-telopeptide containing N-terminal cysteine, according to the manufacturer's directions. Avidin and biotin-hydrazide were also purchased from Pierce. Tetramethylbenzidine (TMB) substrate for HRP was purchased from Biotech Laboratories (Houston, TX) and stored at 4°C. 17β-estradiol (tissue-culture grade) was purchased from Sigma Co. (St. Louis, MO). Alendronate was a gift from Merck (West Point, PA).

AQ:3

Animals and Treatment

All animal protocols used in this study had prior approval of the animal studies subcommittee of this research institution.

Treatment of Ovariectomized C57BL/6N Mice With Estradiol

A group of 7–8-week-old female C57BL/6N mice were ovariectomized (ovx) or sham operated at Hilltop Lab Animals, (Scottsdale, PA). The mice were housed on a 12 h light/dark cycle, fed standard rodent diet and water, and randomly divided into the following groups of 9 or 10 animals each: (1) sham; (2) ovx; or (3) ovx + estradiol. Sham and ovx groups were given weekly subcutaneous injections of vehicle for 3 weeks. At the end of the 3 week period, the mice were killed, blood was collected, and bones were processed for peripheral quantitative computed tomography (pQCT). The ovx + estradiol group received weekly subcutaneous injections of 400 μg/kg of estradiol for 3 weeks. Blood and bone specimens were collected for C-telopeptide and pQCT measurements, respectively.

Treatment of Ovx C57BL/6J Mice With Alendronate

Ovariectomized or sham-operated 8–9-week-old C57BL/6J mice were purchased from Harlan-Teklad (Madison, WI). The mice were acclimatized for 1 week and assigned to one of the following three groups (n = 10): (1) sham; (2) ovx; or (3) ovx + alendronate (ALN). The sham and one ovx group received daily subcutaneous injections of vehicle (phosphate-buffered saline [PBS]) for 2 weeks. The remaining ovx (ovx + ALN) group received daily subcutaneous injections of ALN (1.0 mg/kg body weight) for 2 weeks. At the end of the 2 week period, blood was collected for C-telopeptide measurements.

C57BL/6J Mice Receiving Low Calcium Diet

A group of 3–4-week-old female C57BL/6J mice was purchased from Jackson Labs (Bar Harbor, ME), acclimatized as described earlier for 1 week, and randomly assigned to one of two groups: one group (n = 13) was fed a 0.01% calcium-deficient diet (TD 95027, Harlan-Teklad) for 2 weeks; and a control group (n = 12) of C57BL/6J mice received a normal diet of 0.6% calcium (TD 97191, Harlan-Teklad) for 2 weeks. At the end of the 2 week period, blood was collected for C-telopeptide analysis.

For all studies, serum was separated within 1 h of blood collection and stored at −70°C until assays were performed. The right femurs were cleaned and stored frozen in 0.05 mol/L phosphate buffer at −20°C until bone density measurements were performed by pQCT.

C-telopeptide Antiserum

Antiserum used for the development of C-telopeptide ELISA was provided by DiaSorin Inc. (Stillwater, MN). Production of C-telopeptide antiserum against a human C-telopeptide sequence corresponding to amino acids 1197–1214 of type I collagen (α1 chains) has been described elsewhere.[13] The C-telopeptide-specific antibodies were purified by affinity chromatography using synthetic C-telopeptide peptide coupled to a SulfoLink column (Pierce). Affinity-purified goat anti-C-telopeptide antibodies were biotinylated by using biotin-hydrazide as per the manufacturer's specifications. Biotinylated antibodies were purified on a size-exclusion column and stored at 4°C at a concentration of >2 mg/mL until being used.

C-telopeptide ELISA

Avidin was immobilized on eight-well Maxisorb (Nunc) strips by overnight incubation in 200 μL of avidin solution (1 μg/mL in 0.05 mol/L sodium carbonate buffer, pH 9.6) at 4°C. After antibody coating, nonspecific sites were blocked by incubation with a 1% solution of bovine serum albumin (BSA), D-mannitol, and glycine for 2 h at room temperature (RT). Avidin-coated strips were freeze-dried and stored at 4°C in vapor-sealed pouches with silica gel desiccant. Under these conditions, avidin-coated strips were stable for >6 months without significant loss of immunoreactivity. A synthetic peptide corresponding to amino acids 1197–1214 of the rat type I collagen (α1) sequence was used as a calibrator. The ELISA was initiated by incubation with 200 μL of biotinylated C-telopeptide antibodies for 1 h at 25°C. After washing twice with a wash solution (0.05 mol/L PBS containing 0.05% Tween-20), 100 μL of C-telopeptide/HRP conjugate and 100 μL of C-telopeptide calibrator or diluted serum samples (0.01 mol/L Tris-HCl buffer containing 0.1% BSA and 0.1% thimerosal, pH 7.0) was added to the antibody-coated strips. The ELISA plate was incubated for 2 h at RT with continuous stirring (800 rpm). The ELISA plate was then washed with an automatic strip washer. Color reaction was initiated by adding 200 μL of TMB substrate (OneBlue, Biotex Laboratories, Houston, TX) and incubating the plate with constant stirring for 30 min at RT. The color reaction was stopped by the addition of 100 μL 4 mol/L sulfuric acid, and optical densities were recorded at 450 nm using a plate reader (Tecan SLT Spectra, Research Triangle Park, NC). Unknown values were calculated by using a four-parameter curve-fitting procedure.

Bone Mineral Density Measurements

Bone mineral density (BMD) of the excised distal femurs was measured by a pQCT (XCT Research M, Norland Medical Systems). BMD measurements were performed only in the estradiol repletion study. Quadruplicate determination of five different femurs showed a coefficient of variation of <3.0%.

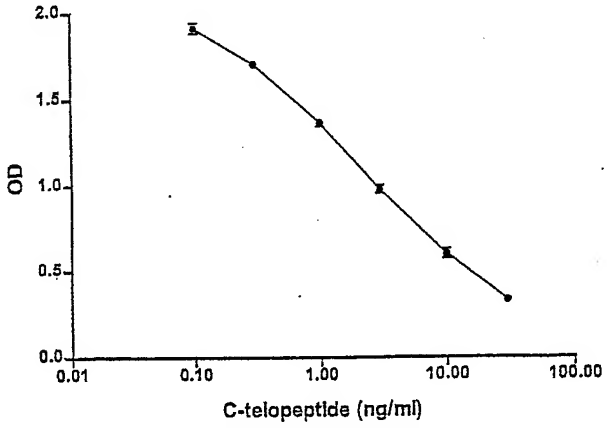

Figure 1. Standard curve of C-telopeptide ELISA.

Statistics

All comparisons of results of the different groups were performed using the Mann–Whitney *U*-test, with $p < 0.05$ (two-tailed) considered statistically significant. All bar diagrams show the mean values, and error bars represent standard error of the mean (SEM).

Results

Analytical Performance of C-telopeptide ELISA

F1 **Figure 1** shows the calibration curve determined. The calibration range of the C-telopeptide measurements was 0.1–30 ng/mL of synthetic peptide. Sensitivity of the ELISA, defined as a value 2 SD (n = 20) below the zero binding value, was <0.1 ng/mL. The reproducibility of the C-telopeptide measurements in mouse T1 serum is summarized in **Table 1.** The averaged intra-assay coefficient of variation (CV) evaluated by measuring ten replicates of two mouse serum control samples was CV <9%, whereas interassay CV measured in eight different runs was <12%.

The effect of the serum matrix dilution on the performance of C-telopeptide ELISA was evaluated in three different mouse serum samples diluted 75%, 50%, and 25% with the assay buffer. The undiluted serum sample values, as determined in the assay, were used to establish the expected values for subsequent dilution. Recoveries were calculated as the measured concentrations divided by the expected concentrations and expressed as percentages. Dilution recoveries ranged between 88% and 110% (**Table** T2 **2**). Spike recoveries were performed by mixing C-telopeptide AQ: 4 ELISA calibrator with three different mouse serum samples. The spiked samples were evaluated as unknown within a single run. The values of serum samples mixed with buffer were used to determine the recovered C-telopeptide concentrations. Spike recoveries, calculated as observed concentration divided by expected concentration, and expressed as percentages, ranged between 77% and 109% (**Table 3**). T3

Table 1. Intra- and interassay coefficient of variation (CV) in the measurements of two mice serum control samples by enzyme-linked immunoassay (ELISA)

	Within-assay precision (n = 10)			Between-assay precision (n = 8)		
Serum control	Mean (ng/mL)	SD	% CV	Mean (ng/mL)	SD	% CV
Low	9.2	0.8	8.2	9.5	1.1	11.6
High	21.6	1.8	8.3	20.7	2.3	11.1

Table 2. Effect of sample dilution on determination of mouse C-telopeptide

Sample no.	Sample dilution (serum volume)	Theoretical value (ng/mL)	Measured value (ng/mL)	Recovery (%)
1	100% (20 µL)	5.3		
	75% (15 µL)	4.0	3.5	88.1
	50% (10 µL)	2.6	2.7	101.9
	25% (5 µL)	1.3	1.3	98.1
2	100% (20 µL)	14.1		
	75% (15 µL)	10.6	11.4	94.5
	50% (10 µL)	7.1	7.6	95.8
	25% (5 µL)	3.5	3.9	92.1
3	100% (20 µL)	7.9		
	75% (15 µL)	5.9	6.1	105.2
	50% (10 µL)	3.9	4.1	104.4
	25% (5 µL)	2.0	2.2	109.7

Effect of Ovx and Estrogen Treatment on C-telopeptide Levels in Mouse Serum

Figure 2 shows the C-telopeptide levels in sham or ovx mice F2 receiving vehicle or 400 µg/kg (body weight) of estradiol. The C-telopeptide levels were approximately 45% higher in ovx mice compared to the sham group. Treatment of ovx mice with estradiol resulted in approximately 20% decreases in C-telopeptide levels compared to ovx mice receiving vehicle. However, the decrease in C-telopeptide concentration did not reach statistical significance by the criteria used (two-tailed Mann–Whitney *U*-test) in this study.

Effect of Ovx and Alendronate Treatment on C-telopeptide Levels in Mouse Serum

Figure 3 shows C-telopeptide levels in sham, ovx, and ovx mice F3 treated with alendronate (1.0 mg/kg). There was a 50% increase in C-telopeptide concentration between sham and ovx mice. Treatment with alendronate resulted in a 50% drop in C-telopeptide levels compared to the ovx group. C-telopeptide concentration in the alendronate-treated ovx group was indistinguishable from the vehicle-treated sham group ($p = 0.883$).

Measurement of C-telopeptide Levels in C57BL/6J Mice Treated With Low Calcium Diet

C-telopeptide concentration in mice receiving a low calcium diet showed 40% higher values compared to the control group, which received a normal diet (**Figure 4**). The body weights in the F4 control and calcium-deficient groups were similar ($p > 0.5$) at the beginning (12.6 ± 1.2 g in controls vs. 12.6 ± 1.4 g in the calcium-deficient group) and at the end (17.8 ± 1.4 g in controls vs. 17.7 ± 1.4 g in the calcium-deficient group) of the experiment. Therefore, the growth rates of these mice were not affected by the low calcium diet.

Table 3. Recovery of exogenously added C-telopeptide calibrator to pooled mouse serum as determined by enzyme-linked immunoassay (ELISA)

Sample number	C-telopeptide added (ng/mL)	C-telopeptide expected (ng/mL)	C-telopeptide observed (ng/mL)	Percent recovery
1	0	6.6		
	1.0	7.6	7.3	96.4
	3.0	9.6	8.3	85.8
	10.0	16.6	12.9	77.4
2	0	9.6		
	1.0	10.6	11.5	108.8
	3.0	12.6	12.0	95.2
	10.0	19.6	17.5	89.6
3	0	12.1		
	1.0	13.1	12.4	94.1
	3.0	16.1	14.7	96.9
	10.0	22.1	23.0	104.1

Effect of Ovx on Trabecular BMD of Distal Femur

Total BMD at the distal femur showed a significant loss in the ovx group (363.9 ± 2.7, $p < 0.001$) compared to the sham group (411.6 ± 5.5). Treatment with estradiol partially prevented bone loss (386.3 ± 6.3, $p < 0.05$ vs. ovx group).

AQ: 5

Discussion

In the mouse model, formation markers have been available for several years. However, use of resorption markers has been limited to highly complex HPLC measurement of pyridinium cross-links or hydroxyproline in urine. To overcome the complexities associated with urinary markers and urine collection in mice, we have developed a serum C-telopeptide ELISA that can be applied to measure bone resorption. High crossreactivity of an antihuman C-telopeptide polyclonal antiserum toward mouse serum prompted us to develop this ELISA. The epitope of the affinity-purified antibodies was determined by examining the crossreactivity of the ELISA with several synthetic peptides of six to eight amino acids in length. Only peptide with amino acids—DFSFLPQ—showed crossreactivity.[13] The sequence—DFSFLPQ—is identical in human, rat, and mouse type I collagen

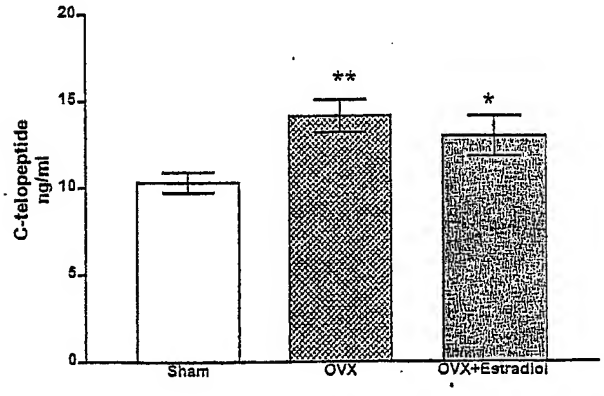

Figure 2. Effect of ovariectomy and estradiol treatment of ovariectomized mice on serum levels of C-telopeptide as determined by ELISA. Values represent mean ± SE (n = 9). *p = 0.0947 vs. ovx and p = 0.1333 vs. sham group, **$p < 0.05$ vs. sham.

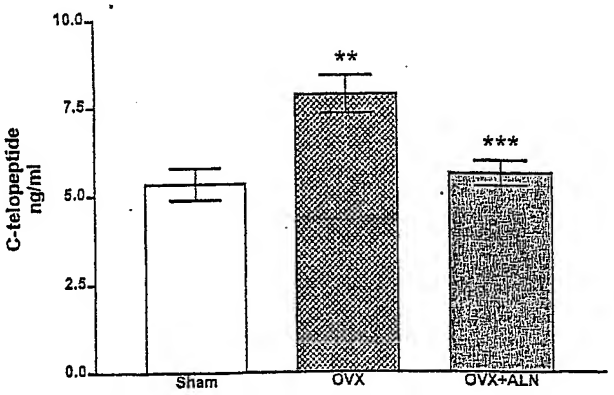

Figure 3. Effect of ovariectomy and alendronate treatment on the serum levels of C-telopeptide as determined by ELISA. Results expressed as mean ± SE (n = 9 or 10). **$p < 0.05$ vs. sham; ***$p < 0.01$ vs. ovx and $p = 0.883$ vs. sham group.

C-telopeptide, which provided the rationale for using a C-telopeptide antiserum developed against the human sequence for developing ELISA for the rodent model. However, our epitope determination does not rule out measurement of type I chains only, in which case C-telopeptide measured by the current ELISA may also reflect synthesis or metabolism of collagen in addition to bone resorption, because some of the newly synthesized collagen can be degraded and released into circulation before it can be deposited in bone. It remains to be verified if the circulating moiety measured by the current antibody contains a pyridinium cross-link, in which case it would support the view that this assay measures collagen degradation and not synthesis of collagen. Previously, we described a rat C-telopeptide ELISA[13] using the same antibody and found approximately 65% higher C-telopeptide levels in ovx rats compared to the sham group and a complete reversal in C-telopeptide levels in ovx rats treated with estradiol (40 μg/kg, 14 days). In this study, we modified the rat C-telopeptide ELISA to enable it to measure bone resorption in mouse serum. The mouse C-telopeptide ELISA utilizes biotinylated antibodies and avidin-coated plates. The biotinylated antibodies were introduced in the new ELISA format to overcome a nonspecific interference caused by the crossreactivity of capture antibodies (rabbit antigoat immunoglobulin G) toward mouse serum proteins. A preincubation of biotinylated antibodies with avidin-coated plates and a subsequent wash cycle resulted in improved sensitivity (0.1 ng/mL) of

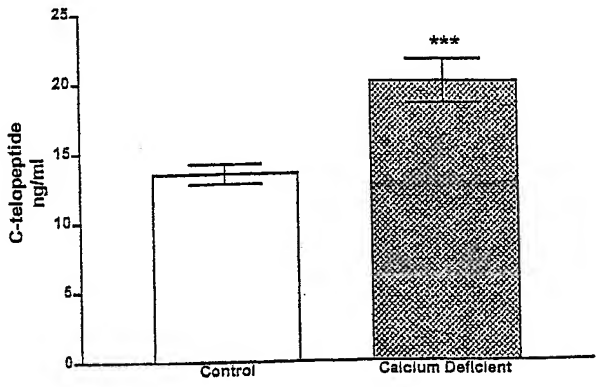

Figure 4. Effect of calcium-deficient diet on serum levels of C-telopeptide as determined by ELISA. Results expressed as mean ± SE (n = 12 or 13). ***$p < 0.01$.

the ELISA, which allowed us to reliably measure C-telopeptide levels with small amounts (0.010–0.020 mL) of mouse serum.

The serum C-telopeptide ELISA described in this study is a new assay, and therefore required a comprehensive in vivo evaluation of its efficacy to measure bone resorption in a mouse model. Consequently, we included several skeletal perturbations known to influence bone resorption in a mouse model to evaluate the effectiveness of the C-telopeptide ELISA. The ovx mouse model mimics some of the changes in bone metabolism observed in postmenopausal osteoporosis.[7] Biochemical markers are elevated after the ovariectomy and return to low levels after treatment with estradiol or other antiresorptive agents.[12,14] Therefore, the ovx mouse provides a good model to study changes in biochemical markers associated with skeletal remodeling. In addition, a low calcium diet and administration of PTH(1–34)[9] are also known to increase bone resorption in the mouse model. We used these conditions to further evaluate the in vivo efficacy of C-telopeptide ELISA.

In the evaluation of the ovx model, there was a 45% increase in serum C-telopeptide concentrations in ovx mice compared to sham-operated mice at 3–4 weeks post-ovx. Estradiol treatment (400 μg/kg) resulted in a moderate decline in C-telopeptide levels in the ovx mice (Figure 2). The decrease in C-telopeptide levels did not reach statistical significance ($p = 0.093$) compared to the ovx group. Nonetheless, changes in C-telopeptide levels were consistent with changes in BMD measured in the distal femur by pQCT. Our results suggest that a longer treatment time or higher estradiol dose may be required to revert C-telopeptide concentration to that of the vehicle-treated sham group. As expected, treatment of ovx mice with alendronate (1 mg/kg) resulted in a complete reversal of C-telopeptide levels to those of sham-operated mice receiving vehicle (Figure 3). This is consistent with previous observations that alendronate inhibits the activity of the mature osteoclast[14] as well as the formation of osteoclasts from bone marrow-derived precursor cells, resulting in a rapid decline in markers of bone resorption. The absolute concentrations of C-telopeptide in mice obtained in estradiol and alendronate studies were significantly different. There could be three possible explanations for this finding: (1) the age of mice in two groups was slightly different; (2) the two groups of mice were obtained from different sources (NIH and Jackson Labs); and (3) C-telopeptide levels follow a circadian rhythm. A combination of all these factors may have contributed to the difference in absolute values observed in the two studies.

Other perturbations, namely a low calcium diet and PTH administration, both of which are known to increase bone resorption in mice,[9,10] also increased serum C-telopeptide levels. Our data show that C-telopeptide levels were approximately 50% higher (Figure 4) in mice fed a low calcium diet, as compared to mice fed a normal diet. In addition, administration of PTH(1–34) (80 μg/kg per day) to mice for 22 weeks caused a significant increase in serum C-telopeptide levels compared to vehicle-treated control mice (S. Mohan, personal communication). There are indications by other investigators[10] that long-term treatment with PTH(1–34) increases resorption in mice, and findings from this study are consistent with our earlier findings[9] of increased tartrate-resistant acid phosphatase activity in femurs of mice treated with PTH(1–34).

In conclusion, the C-telopeptide ELISA developed in this study demonstrated adequate analytical sensitivity, accuracy, and reproducibility. The changes observed in biochemical parameters and BMD coincide with those in previous work. The C-telopeptide ELISA demonstrated sufficient discriminatory power to detect changes in bone resorption as a result of: ovariectomy, estradiol, or bisphosphonate treatment of ovx mice; a calcium-deficient diet; and administration of PTH(1–34). Hence, this ELISA could be a useful tool for the study of bone resorption in mice. Additional studies may be required to further establish the efficacy of this marker in the measurement of bone resorption.

Acknowledgments: The study supported in part by DiaSorin, Stillwater, MN.

References

1. Beamer, W. G., Donahue, L. R., Rosen, C. J., and Baylink, D. J. Genetic variability in adult bone density among inbred strains of mice. Bone 18(5):397–403; 1996.
2. Blanque, R., Cottereaux, C., and Gardener, C. R. Increase in osteocalcin after ovariectomy are amplified by LPS injection: Strain differences in bone remodeling. Gen Pharmacol 30(1):51–56; 1998.
3. Brandsten, C., Lundmark, C., Christersson, C., Hammarstorm, L., and Wurtz, T. Expression of collagen alpha 1 (I) mRNA variants during tooth and bone formation in rats. J Dent Res 78(1):11–19; 1999.
4. Clemens, T. L., Tang, H., Maeda, S., Kesterson, R. A., Demayo, F., Pike, J. W., and Gundberg, C. M. Analysis of osteocalcin expression in transgenic mice reveals a species difference in vitamin D regulation of mouse and human osteocalcin genes. J Bone Miner Res 12(10):1570–1576; 1997.
5. Clement, L. P., Ormandy, C., Lepescheux, L., Ammann, P., Damotte, D., Goffin, V., Bouchard, B., Amling, M., Gaillard, K. M., Binart, N., Baron, R., and Kelly, P. A. Osteoblasts are a new target for prolactin receptor knockout mice. Endocrinology 140(1):96–105; 1999.
6. Corral, D. A., Amling, M., Priemel, M., Loyar, E., Fuchs, S., Ducy, P., Baron, R., and Karsenty, G. Dissociation between bone resorption and bone formation in osteopenic transgenic mice. Proc Natl Acad Sci 95:13835–13840; 1998.
7. Ducy, P., Desbois, C., Boyce, B., Pinero, G., Story, B., Dunstan, C., Smith, E., Bonadio, J., Goldstein, S., Gundberg, C., Bradley, A., and Karsenty, G. Increased bone formation in osteocalcin-deficient mice. Nature 382(6590): 448–452; 1996.
8. Kalu, D. N. and Chen, C. Ovariectomized murine model of postmenopausal calcium malabsorption. J Bone Miner Res 14(4):593–601; 1999.
9. Mohan, S., Kutilek, C., Zhang, C., Shen, H. G., Kodama, Y., Srivastava, A. K., and Baylink, D. J. Evidence that PTH effects on bone formation may involve modulation of PKA pathway while its effect on bone resorption may involve modulation of PKC pathway in a mouse model. Bone 23(5)(Suppl.):S449; 1998.
10. Most, W., Schot, L., Ederveen, A., van der Wee-Pals, L., Papapoulos, S., and Lowik, C. In vitro and ex vivo evidence that estrogen suppress increased bone resorption induced by ovariectomy or PTH stimulation through an effect on osteoclastogenesis. J Bone Miner Res 10(10):1523–1530; 1995.
11. Murray, E. J., Song, M. K., Laird, E. C., and Murray, S. S. Strain-dependent differences in vertebral bone mass, serum osteocalcin, and calcitonin in calcium-replete and -deficient mice. Proc Soc Exp Biol Med 203(1):64–73; 1993.
12. Seedor, J. G., Gentile, M. A., Pennypacker, B. L., Rodan, G. A., and Kimmel, D. B. Bone mineral density (BMD) and uterine weight response to estrogen in ovariectomized (OVX) C57BL/6J mice. J Bone Miner Res 14(Suppl. 1): SU405; 1999.
13. Srivastava, A. K., Bhattacharyya, S., Castillo, G., Wergedal, J., Mohan, S., and Baylink, D. J. Development and application of a serum C-telopeptide and osteocalcin assay to measure bone turnover in ovariectomized rat model. Calcif Tissue Int. In press. AQ: 7
14. Van, B. E., Lowik, C. W. G. M., and Papapoulos, S. E. Effect of alendronate treatment on the osteoclastogenic potential of bone marrow cells in mice. Bone 20(4):335–340; 1997.

Date Received: January 11, 2000
Date Revised: May 16, 2000
Date Accepted: May 31, 2000

Calcif Tissue Int (2000) 67:000–000

Calcified Tissue International

Development and Application of a Synthetic Peptide-Based Osteocalcin Assay for the Measurement of Bone Formation in Mouse Serum

A. K. Srivastava, G. Castillo, J. E. Wergedal, S. Mohan, D. J. Baylink

Musculoskeletal Disease Center, Jerry L. Pettis VA Medical Center, 11201 Benton Street, and Loma Linda University, Loma Linda, California, USA

Received: 29 October 1999 / Accepted: 1 March 2000

Abstract. The mouse is frequently used as an animal model to study skeletal mechanisms relevant to humans. Biochemical markers of bone formation and resorption provide one of the key parameters for assessing skeletal metabolism. One biochemical marker that has proven to be useful in the studies of mouse skeletal metabolism is osteocalcin. Assay for osteocalcin is available in the mouse. The present study describes development of an osteocalcin radioimmunoassay (RIA) using a synthetic peptide. Intact osteocalcin purified from mouse bone extracts shows parallel displacement with synthetic peptide. Sensitivity of the RIA was 19 ng/ml. The average (n = 9) intra- and interassay coefficient of variation for two controls was less than 10%; the averaged recoveries were 106%. The osteocalcin concentration measured by peptide RIA shows a high correlation ($r = 0.88$, $n = 188$, $P < 0.0001$) with an intact osteocalcin assay. In addition, when the intact assay and peptide assays were applied to evaluate skeletal perturbation, similar results were obtained. Accordingly, osteocalcin levels measured by both intact and peptide-based RIA in 8-week C57BL/6J (n = 8) mice treated with PTH 1-34 were twofold higher compared with the vehicle-treated control group. Further studies of the application of the peptide-based RIA for osteocalcin revealed that osteocalcin levels in 4-week postovariectomized (OVX) C57BL/6N mice (n = 10) were 80% higher than the sham-operated (n = 10) mice receiving vehicle. OVX mice receiving weekly injections of estradiol (400 μg/kg body weight) were 38% lower compared with the OVX group treated with vehicle. In conclusion, the peptide-based RIA has analytical and a discriminative power similar to that of the intact osteocalcin assay but the advantage that the resources for this assay are much easier to accrue.

Key words: Osteocalcin — Radioimmunoassay — Mouse — Ovariectomy.

With increasing frequency, the mouse is being used as an animal model to study skeletal mechanisms relevant to humans [1]. The particular popularity of the mouse as a model is largely because of its utility in genetic studies, such as QTL studies [2] and knockout studies [3–6, 10], both of which are relevant to human biology. In skeletal metabolism, one of the key parameters relevant to human diseases is bone density. Bone density is readily measured in the mouse with new technologies. However, changes in bone density take some time to become measurable whereas biochemical markers, which measure the determinants of bone density, namely, bone formation and bone resorption, can provide more accurate information with respect to skeletal metabolism. One of the biochemical markers that have proven to be useful in the studies of human skeletal metabolism is osteocalcin.

Osteocalcin is a bone-specific protein that is secreted by osteoblasts. A fraction of newly synthesized osteocalcin is released into the bloodstream, where its concentration correlates with the indices of osteoblastic activity and bone formation rate [8]. In humans, changes in circulating osteocalcin levels have been associated with metabolic bone diseases such as osteoporosis and hyperparathyroidism [9]. In the mouse model, measurements of osteocalcin have been used to study the rate of bone formation in several studies including (1) hypophosphatemic (hyp) mouse as a human model of familial hypophosphatemic rickets [8, 10, 11]; (2) osteopenic transgenic mice [6]; (3) osteocalcin-deficient transgenic mice [3]; and (4) ovariectomized (OVX) mice in testing the effect of lipopolysaccharide on bone remodeling [12].

Measurements of mouse osteocalcin have been performed by radioimmunoassay (RIA) using antibodies generated against intact native mouse osteocalcin isolated from bone. The present study was undertaken to develop synthetic osteocalcin peptide-based antibodies that bind to amino acids 29–46. Accordingly, we describe production of polyclonal anti-mouse osteocalcin antibodies using synthetic peptide, and development of a RIA procedure using synthetic peptide as a tracer and calibrator. The in vivo usefulness of the RIA was evaluated by assessing the biological response of (1) C57BL/6J mice treated with PTH 1-34 and (2) OVX C57BL/6N mice treated with estradiol. Both of these treatments are known to modulate the bone formation in the mouse model [6, 13]. In addition, changes in biochemical markers were compared with changes in bone mineral density as measured by peripheral quantitative computed tomography (pQCT).

Materials and Methods

Osteocalcin peptide (NH_2-CSDQYGLKTAYKRIYGITI-COOH) was synthesized commercially and was 99% pure, as determined by HPLC and mass chromatography. Maliemide-activated keyhole-lympet-hemocyanin (KLH) was purchased from Pierce (Rockford, IL) and coupled to osteocalcin peptide containing N-terminal cysteine according to the manufacturer's directions. Nor-

Correspondence to: D. J. Baylink, Musculoskeletal Disease Center

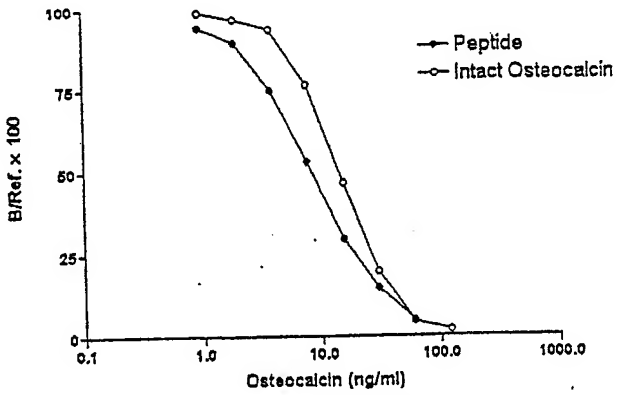

Fig. 1. Standard curve of mouse osteocalcin using synthetic peptide (●) and intact mouse osteocalcin (O). 'B' represents CPM bound in the presence of osteocalcin standard; 'Ref' represents CPM bound in the presence of zero standard.

mal rabbit serum and goat anti-rabbit antiserum were purchased from Chemicon (Temecula, CA). Radioactive sodium iodide was purchased from NEN™ Life Science Products (Boston, MA), and iodination of synthetic osteocalcin peptide fragment was performed by the standard Chloramine-T method.

Animals and Treatment

Treatment of C57BL/6J Mice with PTH 1-34. All animal protocols used in this study were approved by the Animal Studies Subcommittee of our institution. Normal female, 8-week-old C57BL/6J (B6) mice were purchased from The Jackson Laboratory (Bar Harbor, MN) and randomly divided into two groups of 8 mice each. A control group received daily subcutaneous injections of 50 µl phosphate-buffered saline (PBS), and the other group of mice received 80 µg/kg of parathyroid hormone (PTH) 1-34 (synthetic peptide from SynPep Corp., CA) for 9 days. On day 10, the animals were sacrificed, and blood was collected and used for serum osteocalcin determination.

Treatment of Ovariectomized C57BL/6J Mice with Estradiol. Eight-week-old OVX or sham-operated C57BL/6N mice were from Hilltop Lab Animals, Inc., (Scottsdale, PA), and randomly divided into the following groups of 10 animals each: (1) sham-1W; (2) OVX-1W; (3) sham-4W; (4) OVX-4W; (5) OVX/40 E2; and (6) OVX/400 E2. Sham-1W and OVX-1W groups were sacrificed 1 week after the OVX or sham operation and blood was collected. One week after the OVX or sham operation, sham-4W and OVX-4W groups were given weekly subcutaneous injections of vehicle (corn oil) for 3 weeks. At the end of the 3-week period, blood was collected and bones were processed for pQCT. OVX/40 E2 and OVX/400 E2 groups received weekly subcutaneous injections of 40 µg/kg and 400 µg/kg of estradiol for 3 weeks, respectively. Blood and bone specimens were collected as described above for the sham group of animals.

Serum was separated within 1 hour of blood collection and stored at −70°C until analyzed. The right femurs were cleaned and stored frozen in 0.05 M phosphate buffer at −20°C until bone density measurements were made by pQCT.

Osteocalcin antiserum. Antibodies against osteocalcin were generated in White New Zealand rabbits. Initial immunization was performed by 20–30 intradermal injections of 100 µg of conjugate emulsified with Freund's adjuvant. A booster was given 45 days after initial immunization and thereafter every 30 days. Blood was collected 15 days after the booster injection and serum was separated and stored in small aliquots at −70°C.

Osteocalcin RIA. To develop RIA, 2.0 µg of osteocalcin peptide was labeled with ^{125}I by the Chloramine-T method using 2.0 mCi of ^{125}I-sodium iodide and purified on a Sep-Pak C-18 cartridge. The RIA procedure is initiated by mixing 100 µl of tracer prepared in assay buffer (diluted in 0.05 M citrate buffer, pH 7.0, containing 0.1% BSA and 0.15 M sodium chloride, and 0.1% sodium azide), 100 µl of antiserum (final diluted of 1:10,000 in assay buffer), and 100 µl of peptide standard or mouse serum sample (5 µl of mouse serum diluted 1:20 with assay buffer) in polypropylene tubes and incubated at room temperature (RT) for 2 hours. The bound radioactivity is separated by the addition of 500 µl of secondary antibody mixture (containing goat anti-rabbit IgG antiserum and normal rabbit serum) and 200 µl of 8% (w/v) polyethylene glycol followed by incubation at RT for 2 hours. Tubes were centrifuged at 2000 *g* for 20 minutes and the supernatant was discarded. Precipitate was counted on a Micromedic 4600 Plus Automatic Gamma Counter (ICN, CostaMesa, CA), and unknown values were calculated by comparison with a standard curve constructed by weighted regression using Logit-log curve fitting.

Table 1. Intra- and interassay CV of the osteocalcin measurements of two serum control samples by RIA

	Within-assay precision (n = 10)			Between-assay precision (n = 9)		
Serum control	Mean (ng/ml)	SD	%CV	Mean (ng/ml)	SD	%CV
Low	108.5	5.4	5.0	112.1	10.8	9.6
High	239.5	16.1	6.7	232.6	18.6	8.0

Table 2. Effect of sample dilution on mouse osteocalcin determination

Sample no.	Sample dilution (%)	Theoretical value (ng/ml)	Measured value (ng/ml)	Recovery (%)
1.	100	1076.5		
	75	806.2	638.4	79.2
	50	540.6	461.3	85.3
	25	270.3	256.3	94.8
2.	100	1029.9		
	75	768.9	713.0	92.7
	50	512.6	466.0	90.9
	25	256.3	256.3	100
3.	100	1006.6		
	75	754.9	638.4	84.6
	50	503.3	433.4	86.1
	25	251.6	279.6	111.1

Bone Mineral Density Measurements

The bone mineral density of excised femurs was measured by a pQCT (XCT Research M system, Norland Medical Systems, Inc., WI). Bone density was measured at the distal femur. Quadruplicate determination of five different femurs showed a CV of the measurement of less than 4.0%.

Statistics

Results of the different groups were compared by using the Mann Whitney test, with $P < 0.05$ accepted as significant difference. All bar diagrams represent mean values, and error bars represent standard error of mean.

Table 3. Recovery of the exogenously added mouse osteocalcin in RIA

Sample no.	Osteocalcin concentration (ng/ml)	Osteocalcin added (ng/ml)	Expected (ng/ml)	Observed (ng/ml)	% recovery
1	233.7	178.6	412.3	472.9	114.7
	233.7	238.1	471.8	455.7	96.6
	233.7	267.9	501.6	485.1	96.7
2	205.7	274.9	480.6	456.1	94.9
	205.7	366.6	572.3	486.5	85.0
	205.7	412.4	618.1	557.8	90.2
3	354.9	245.8	600.7	552.7	92.0
	354.9	327.8	682.7	660.9	96.8
	354.9	368.7	723.6	681.4	94.2

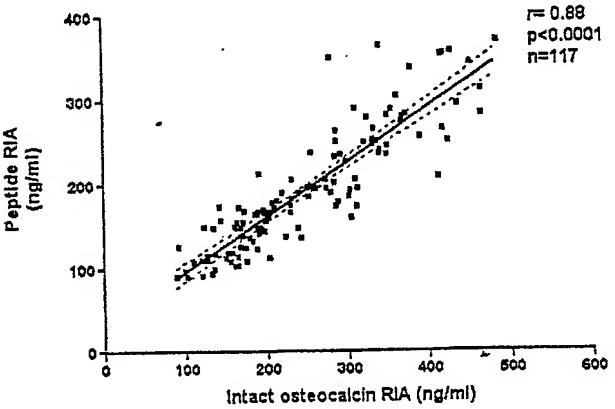

Fig. 2. Correlation between osteocalcin levels in mice serum as determined by the peptide RIA and a commercial RIA that measures intact osteocalcin.

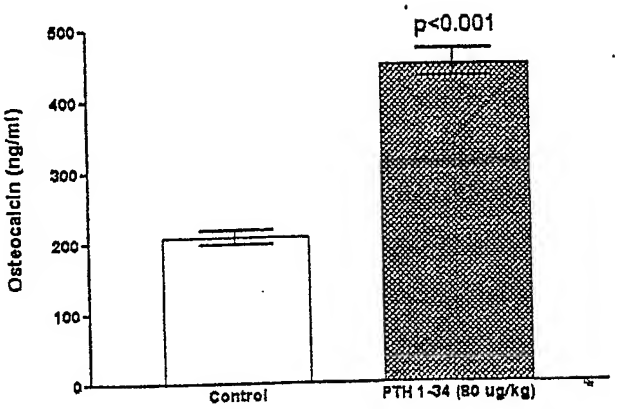

Fig. 3. Osteocalcin concentration in C57BL/6J mice treated with PTH 1-34 compared with control group of mice treated with vehicle. Values represent mean ± SE.

Results

Standard Curve Range and Sensitivity

Figure 1 shows the binding of ^{125}I-labeled osteocalcin peptide to anti-mouse osteocalcin antibodies and displacement with peptide calibrator and intact osteocalcin calibrator, extracted from mouse bone. The calibration range for the osteocalcin assay was 0.9–80 ng/ml. Sensitivity of the RIA, defined as value greater than 2 SD (n = 20) below the zero binding value, was 0.9 ng/ml.

Assay Variability

Reproducibility of osteocalcin measurements in mouse serum is summarized in Table 1. The averaged intraassay CV, evaluated by measuring 10 replicates of two mouse serum samples, had a CV of less than 7%, and the interassay CV, measured in nine different runs, was <10%.

Dilution Effect

The effect of serum matrix dilution on the performance of osteocalcin RIA was evaluated in three different mouse serum samples diluted at 75%, 50%, and 25% in the assay buffer. The undiluted serum sample values, as determined in the RIA, were used to establish the expected values for subsequent dilution. Recoveries were calculated as the measured concentrations divided by the expected concentrations and expressed as percentages. Dilution recoveries were between 81 and 111% (Table 2).

Analytical Recovery

Supplementation and recovery study was performed by mixing different proportions of samples with high osteocalcin concentration with serum samples of low osteocalcin concentrations. The values of samples without mixing were used to determine the expected values. Analytical recoveries were calculated as described for dilution recoveries and ranged between 85 and 115% (Table 3).

Correlation Between Peptide RIA and Intact Osteocalcin RIA

Osteocalcin levels in mice serum determined by peptide RIA showed a high correlation ($r = 0.88$, $P < 0.001$, $n = 117$) with a commercial RIA (Biomedical Technologies Inc., Stoughton, MA) that utilizes intact osteocalcin as tracer and calibrator (Fig. 2).

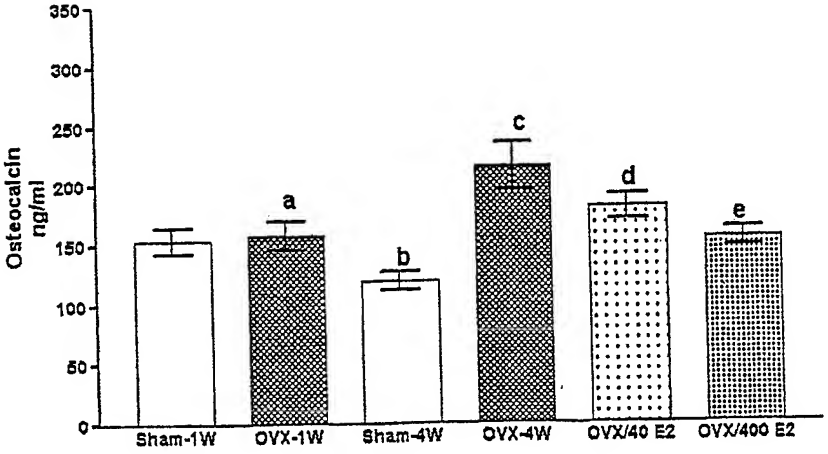

Fig. 4. Effect of ovariectomy and estrogen repletion of OVX mice on the osteocalcin levels as determined by peptide RIA. Values represent mean ± SE.

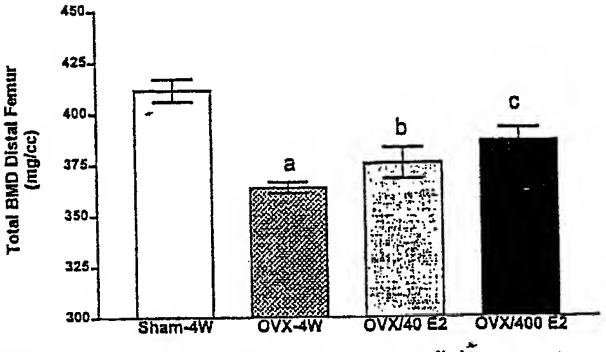

Fig. 5. Effect of ovariectomy and the estradiol treatment on the total bone density of the distal femur of C57BL/6J mice as measured by pQCT. Results are shown as mean ± SE (n = 10).

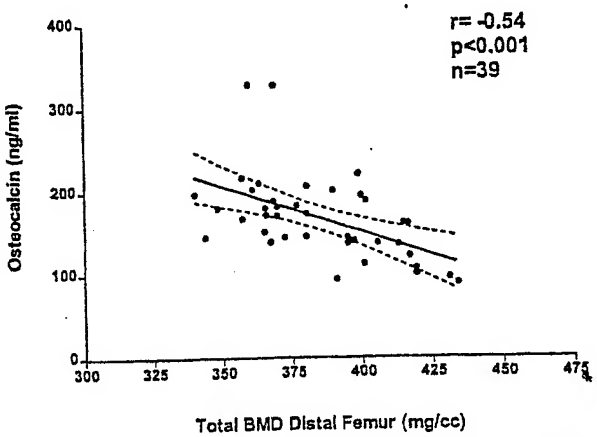

Fig. 6. Correlation between serum levels of osteocalcin measured by RIA and total bone density measured by pQCT (n = 39). Significance (p) value was calculated from linear regression analysis (continuous line). Dotted lines represents 95% confidence intervals.

Measurement of Mouse Osteocalcin Levels in C57BL/6J Mice Treated with PTH 1-34

Osteocalcin concentrations in C57BL/6J mice treated with PTH 1-34 were twofold higher compared with the control group treated with vehicle (Fig. 3). Measurements of these samples with an intact osteocalcin RIA showed similar changes between the control and PTH 1-34-treated group (228 ± 33 ng/ml versus 480 ± 43 ng/ml, $P < 0.001$).

Effect of OVX and Estrogen Treatment on the Osteocalcin Levels in Mouse Serum

Figure 4 shows the osteocalcin levels in sham and OVX mice receiving either 40 or 400 μg/kg (body weight) of estradiol. Four weeks after the OVX, the osteocalcin levels were approximately 80% higher in OVX mice compared with the sham group receiving vehicle. Treatment of OVX mice with estradiol resulted in significant decreases in osteocalcin levels compared with OVX mice receiving vehicle.

Effect of OVX on the Total Bone Mineral Density of Rat Femur

Bone density measurements on the distal femurs of various groups are shown in Figure 5. The distal femur, a region rich with cancellous bone, showed a significant loss of bone density in the OVX group. Estrogen repletion at the 400 μg/kg dose partially prevented the bone loss ($P < 0.001$ versus OVX group), which was statistically different from the OVX group receiving the vehicle.

Correlation Between Total Bone Mineral Density and Osteocalcin Concentration

Figure 6 shows the correlation between the osteocalcin concentration and total BMD measurements performed by pQCT in OVX and estradiol-treated OVX C57BL/6N mice. Statistical analysis performed by excluding the two outliers did not significantly change the correlation coefficient or significance levels ($r = -0.54$, $P < 0.001$).

Discussion

We have developed a synthetic peptide-based osteocalcin RIA to measure rate of bone formation in mouse serum. The synthetic peptide was used for antibody production for making the tracer and calibrator. The osteocalcin antiserum, which was generated against a synthetic linear peptide, showed parallel displacement with intact osteocalcin purified from mouse bone albeit with slightly lower affinity. Nonetheless, the RIA exhibited acceptable analytical per-

formance in terms of sensitivity, reproducibility, and analytical recoveries. In addition, the peptide RIA showed high correlation ($r = 0.88$, $n = 117$, $P < 0.001$) with a commercial assay (BTI, Stoughton, MA), which utilizes intact osteocalcin as tracer and standard (Fig. 2). Owing to the difference in the affinity of osteocalcin antibodies towards synthetic peptide and the intact osteocalcin extracted from bone, the absolute concentrations determined by the peptide RIA were, on an average, 20% lower than that obtained by an RIA utilizing intact osteocalcin. Notwithstanding these differences in absolute levels of osteocalcin measured by peptide or intact osteocalcin RIA, we found that discriminative power to differentiate C57BL/6J mice treated with PTH 1-34 and control group treated with vehicle was identical for both assays.

In the OVX mouse model, previous studies have mainly used histological analysis of bone formation and bone resorption [14–16] as efficacy parameters to study the effect of therapeutic agents used for the prevention of osteoporosis. Histological analyses are invasive, time consuming, and yield information only on restricted areas of bone. It is widely believed that the use of biochemical tests for measuring bone turnover would aid preclinical trials of pharmaceutical agents in the mouse model. In this regard, a recent study has suggested usefulness of osteocalcin measurements to study bone remodeling in OVX C57BL/6J mice [12]. This study compared osteocalcin levels in OVX C57BL/6J and Balb/c mice and found higher increases in osteocalcin levels in C57BL/6J mice compared with Balb/c mice due to ovariectomy.

However, use of osteocalcin to determine the efficacy of estrogen treatment in the OVX mice model has not been investigated so far. Our study is the first to describe changes in osteocalcin levels in response to estrogen repletion in OVX C57BL/6N mice. We measured osteocalcin levels in C57BL/6N mice 7 and 28 days postovariectomy to determine the sensitivity of the peptide RIA to detect early changes in bone formation following ovariectomy. Osteocalcin levels were only marginally higher in the 7-day post-OVX group compared with the sham group. In 28-day post-OVX mice, as expected, the osteocalcin levels were 80% higher than the sham group treated with vehicle.

The magnitude of change in serum osteocalcin after OVX is comparable with that seen using intact assay [12]. Estradiol repletion of OVX mice resulted in significantly lower osteocalcin levels compared with the vehicle-treated OVX group. Unexpectedly, osteocalcin levels were significantly higher in the OVX/E400 group compared with the sham group receiving the vehicle. Perhaps a longer treatment time may be required to revert the osteocalcin concentration to that of the vehicle-treated sham group. In any case, the changes in osteocalcin levels were consistent with the changes in total bone density measured at the distal femur by pQCT. Furthermore, the osteocalcin levels in sham and all OVX groups of mice showed a highly significant and negative correlation with total BMD ($r = -0.54$, $P < 0.001$, $n = 39$).

In conclusion, we have developed an RIA that shows acceptable analytical performance in terms of sensitivity, reproducibility, and accuracy. In addition, the peptide-based osteocalcin RIA shows discriminatory power similar to the intact osteocalcin assay to detect changes in bone turnover observed after (1) treatment with an anabolic agent (PTH 1-34), and (2) the ovariectomy and estrogen repletion of OVX mice. Furthermore, the advantage of RIA is that it is peptide based, and, thus the resources for this assay are much easier to accrue.

Acknowledgment. This study was partially supported by a Merit Review Grant from the Veterans Administration.

References

1. Van BE, Lowik C, van DP, Papapoulos S (1999) The role of geranylgeranylation in bone resorption and its suppression by bisphosphonates in fetal bone explants in vitro: a clue to the mechanism of action of nitrogen-containing bisphosphonates. J Bone Miner Res 14(5):722–729
2. Beamer WG, Donahue LR, Rosen CJ, Baylink DJ (1996) Genetic variability in adult bone density among inbred strains of mice. Bone 18(5):397–403
3. Ducy P, Desbois C, Boyce B, Pinero G, Story B, Dunstan C, Smith E, Bonadio J, Goldstein S, Gundberg C, Bradley A, Karsenty G (1996) Increased bone formation in osteocalcin-deficient mice. Nature 382(6590):448–452
4. Clemens TL, Tang H, Maeda S, Kesterson RA, Demayo F, Pike JW, Gundberg CM (1997) Analysis of osteocalcin expression in transgenic mice reveals a species difference in vitamin D regulation of mouse and human osteocalcin genes. J Bone Miner Res 12(10):1570–1576
5. Clement LP, Ormandy C, Lepescheux L, Ammann P, Damotte D, Goffin V, Bouchard B, Amling M, Gaillard KM, Binart N, Baron R, Kelly PA (1999) Osteoblasts are a new target for prolactin receptor knockout mice. Endocrinology 140(1):96–105
6. Corral DA, Amling M, Priemel M, Loyar E, Fuchs S, Ducy P, Baron R, Karsenty G (1998) Dissociation between bone resorption and bone formation in osteopenic transgenic mice. Proc Natl Acad Sci 95:13835–13840
7. Kalu DN, Chen C (1999) Ovariectomized murine model of postmenopausal calcium malabsorption. J Bone Miner Res 14(4):593–601
8. Gundberg CM, Clough ME, Carpenter TO (1992) Development and validation of a radioimmunoassay for mouse osteocalcin: paradoxical response in the Hyp mouse. Endocrinology 130(4):1909–1915
9. Minisola S, Pacitti MT, Romagnoli E, Rosso R, Carnevale V, Carnevella P, Scillitani A, Dicembrino F (1999) Clinical validation of a new immunoradiometric assay for intact human osteocalcin. Calcif Tissue Int 64(5):365–369
10. Carpenter TO, Moltz KC, Ellis B, Andreoli M, McCarthy TL, Centrella M, Bryan D, Gundberg CM (1998) Osteocalcin production in primary osteoblast cultures derived from normal and Hyp mice. Endocrinology 139(1):35–43
11. Tsuji H, Cawthorn C, Ecarot B (1996) Abnormal modulation of serum osteocalcin by dietary phosphate and 1,25-dihydroxyvitamin D3 in the hypophosphatemic mouse. J Bone Miner Res 11(9):1234–1240
12. Blanque R, Cottereaux C, Gardener CR (1998) Increases in osteocalcin after ovariectomy are amplified by LPS injection: strain differences in bone remodeling. Gen Pharmacol 30(1): 51–56
13. Mohan S, Kutilek C, Zhang C, Shen HG, Kodama Y, Srivastava AK, Baylink DJ (1998) Evidence that PTH effects on bone formation may involve modulation of PKA pathway while its effect on bone resorption may involve modulation of PKC pathway in a mouse model. Bone 23(5)(suppl):S449
14. Edwards MW, Bain SD, Bailey MC, Lantry MM, Howard GA (1992) 17β estradiol stimulation of endosteal bone formation in the ovariectomized mouse: an animal model for the evaluation of bone-targeted estrogens. Bone 13:29–34
15. Bain SD, Bailey MC, Edwards MW (1992) The anabolic effect of estrogen on endosteal bone formation in the mouse is attenuated by ovariohysterectomy: a role for the uterus in the skeletal response to estrogen. Calcif Tissue Int 51:223–228
16. Most W, Schot L, Ederveen A, van der Wee-Pals L, Papapoulos S, Lowik C (1995) In vitro and ex vivo evidence that estrogen suppresses increased bone resorption induced by ovariectomy or PTH stimulation through an effect on osteoclastogenesis. J Bone Miner Res 10(10):1523–1530
17. Breen SA, Loveday BE, Millest AJ, Waterton JC (1998) Stimulation of bone formation: use of peripheral quantitative tomography in the mouse in vivo. Lab Anim 32(4):467–476

Circadian and Longitudinal Variation of Serum C-telopeptide, Osteocalcin, and Skeletal Alkaline Phosphatase in C3H/HeJ Mice

A. K. SRIVASTAVA, S. BHATTACHARYYA, X. LI, S. MOHAN AND D. J. BAYLINK

Musculoskeletal Disease Center, Jerry L. Pettis VA Medical Center & Loma Linda University, Loma Linda, CA.

Running title: Biological variation of bone markers in C3H/HeJ mice.

Address for correspondence:

David J. Baylink, M.D.

Musculoskeletal Disease Center (151)

Jerry L. Pettis VA Medical Center

11201 Benton Street

Loma Linda, CA 92357

(909) 422-3101; FAX: (909) 796-1680

E-mail: baylid@lom.med.va.gov

Abstract

Over the past several years, the popularity of inbred strains of mice as an animal model to investigate skeletal disorders relevant to humans has increased, as evidenced by the fact that these animals are frequently used for genetic studies and for gene over-expression or gene knockout studies. In the bone field, one of the most convenient endpoints for evaluating genetic, physiological or pharmaceutical perturbations is the use of biochemical markers. In order to apply biochemical markers in an effective manner, it is of key importance to establish the biological variation and appropriate sampling time. In this study, we have evaluated two components - namely circadian changes and longitudinal variation for three serum markers, osteocalcin, C-telopeptide, and skeletal alkaline phosphatase (sALP) - using C3H/HeJ (C3H) mice. To study circadian rhythms, six-week-old female and male C3H mice were randomly divided into 8 groups of 15 mice each. Blood was collected at 3-hour intervals, starting at 9:00 AM and continuing until 6:00 AM the next day, with minimum disturbances in day/night light cycle. To determine whether the circadian rhythm is intrinsically regulated or influenced by restricted food intake, circadian rhythm was also studied in male and female C3H mice by collecting blood after a 12-hour fasting period. Serum osteocalcin and C-telopeptide levels were measured by ELISA methods. Skeletal alkaline phosphatase was measured by a kinetic assay. The present investigation demonstrated significant circadian variations in osteocalcin and C-telopeptide levels with a peak value between 0900 and 1200 hours during daytime and a nadir between 1500 and 1800 hours. The peak levels of C-telopeptide and osteocalcin were 26% to 66% higher as compared to

the 24-hour mean values. The pattern of the circadian variation of C-telopeptide and osteocalcin was similar in female and male animals and was not significantly affected by restricted food intake. The sALP levels were only marginally affected by the circadian rhythm. To study within-subject and between-subject variation, two studies were performed: 1) blood samples were collected in the morning on day 1, day 3, and day 7; 2) blood samples were collected as described in study one but in the afternoon. The longitudinal variation expressed as coefficient of variance (CV) in osteocalcin, C-telopeptide, and sALP concentrations were 17%, 14%, and 16%, respectively. The longitudinal variations were not significantly influenced by the time of blood collection in sALP and osteocalcin levels, whereas C-telopeptide levels showed significantly higher within-subject day-to-day variation in morning samples. Notably, average population variance was also significantly higher for C-telopeptide concentration in morning samples as compared to afternoon samples. The results highlight the importance of: 1) the timing of sample collection for appropriate interpretation of the bone marker data; and 2) using the appropriate number of samples based on the variance obtained herein.

Key Words

Circadian Rhythm – biological variation – C-telopeptide – Osteocalcin – Skeletal Alkaline Phosphatase - mouse

Introduction

The mouse is the best-developed vertebrate genetic model organism for which there is a rich collection of well-characterized, naturally occurring mutations, and genes of interest have been experimentally manipulated. Several genetic tools that are currently being developed, such as the complete mouse genome sequence, large collections of new mutations, phenotypic characterization of common laboratory strains, and techniques for regionally and temporally specific gene targeting[2,4-6], will increase utility of the mouse as an animal model to study skeletal disorders relevant to humans. The skeletal remodeling process is reflected in the blood circulation by the presence of various bio-molecules derived from either the bone matrix or the cells actively involved in bone formation or resorption. Measurements of these molecules of bone resorption or formation provides an accurate, noninvasive and relatively simple means to assess bone turnover in humans[5,8], as well as in animals[16-18]. In humans, it has been well-documented[3,8,9,14,15,19] that biochemical markers of bone metabolism show a circadian rhythm over a 24-hour period. Therefore, it is of key importance to establish the appropriate sampling time for optimal use of biochemical markers to reflect bone turnover changes.

Osteocalcin, a marker for osteoblastic activity and bone formation, shows a circadian rhythm[14,15] in humans with a high during the night and a low in the afternoon. Another marker of bone formation, carboxyl-terminal pro-collagen peptide (PICP) exhibits a circadian rhythm[15] comparable to that of osteocalcin. Similarly, urinary concentration of free and peptide bound pyridinium crosslinks, which are markers of bone resorption, show a circadian rhythm[19] with highs during the night and lows during the afternoon.

Serum carboxy-terminal and amino-terminal telopeptide of type-I collagen[8] also shows this type of circadian periodicity. Circadian rhythmicity of bone cell metabolic activity[1,16,17,20,25] has been documented in both rats and mice. In addition, rhythmicity of hormones[12-13,27] has been well established in rodents, which also have an important influence on bone metabolism. Diurnal rhythm of skeletal alkaline phosphatase[28] has been described in rat serum and mouse duodenum extracts[10]; however, little is known about the circadian rhythm of other biochemical markers of bone metabolism in the mouse model. In addition, a systematic study of within- and between-subject variation has not been performed in the mouse model.

The present study examines the diurnal variation, within-subject day-to-day biological variability, and between-subject variability in C3H/HeJ (C3H) mice. We selected C3H/HeJ mice for our studies on biological variation because this strain of mice is being used in our chemical mutagenesis (ethylnitrosourea) studies to screen for skeletal mutants of interest. Reference values for markers are required to identify abnormal values. However, the utility of these conventional population-based values will remain unknown unless the data on biological variation are available and the factors affecting biological variations are minimized. In addition, data on biological variation can provide valuable information necessary for calculation of power and, therefore, the number of animals required for studies using biochemical markers. In this study, we evaluated the circadian changes and longitudinal variation for three mouse bone turnover assays, namely osteocalcin, C-telopeptide (Type-I collagen alpha-1 chain), and skeletal alkaline

phosphatase. The diurnal variation was studied over a 24-hour period and longitudinal variation was studied over a 7-day period. The assays used in this study and their *in-vivo* efficacy in the mouse model has been described[23,24] earlier.

Materials and Methods

The Experimental Protocol

All animal protocols used in this study had prior approval of the Animal Studies Sub-committee of this research institution.

Circadian rhythm study

Male and female 5-week-old C3H/HeJ mice were purchased from The Jackson Laboratory (Bar Harbor, ME). The mice were housed on a 12-hour light/dark cycle, fed standard rodent diet and water, allowed to acclimatize for one week, and randomly divided into four groups of 120 mice each. Group 1 consisted of female mice with a normal diet. Group 2 consisted of female mice with food withdrawn 12 hours before the blood collection. Group 3 consisted of male mice with a normal diet. Group 4 consisted of male mice with food withdrawn 12-hours before the blood collection. Each group of animals was further divided into 8 groups of 15 animals. A group of 15 animals was euthanized every three hours starting at 0900 hours, and this continued until 0600 hours the next day. Blood was collected by decapitation, serum was separated within 1 hour of blood collection and stored at –70°C until assays were performed.

Longitudinal Variation Study

To study the effect of diurnal variation (or sampling time) on within- and between-individual differences in biochemical markers of bone, we collected blood samples from 6-week old male and female groups of mice at two different times of the day. Male and female 5-week-old C3H/HeJ mice were purchased from The Jackson Laboratory (Bar Harbor, ME) and allowed to acclimatize for one week as described above for the circadian rhythm study. Male and female mice were randomly divided into two groups of 6 mice each. From one group of mice, blood samples were collected between 9-10 AM and from the second group, samples were collected between 3-4 PM. Blood (50-60 µl) was collected alternatively from each eye by retro-orbital sinus puncture under inhalation anesthesia (Halothane) on day 1, and day 3. On day 7, the animals were euthanized and maximum amounts of blood collected. Blood was processed as described earlier for the circadian rhythm study.

Biochemical Measurements

Mouse C-telopeptide ELISA

The C-telopeptide measurements were performed by a mouse C-telopeptide ELISA described[24] earlier. The average within-assay variation was coefficient of variation (CV) <7%; the average between-assay variation was CV<14%.

Mouse Osteocalcin ELISA

The osteocalcin measurements were performed by a modified mouse osteocalcin assay described[23] earlier. In brief, the synthetic osteocalcin peptide was biotinylated by using iodoacetyl derivative of Biotin (Pierce, Rockford, IL) as per manufacturer's procedure.

The assay was initiated by incubation of 0.05 ml synthetic osteocalcin peptide calibrator made in assay buffer (0.05 M Tris buffer with 0.15M sodium chloride, 5mM EDTA, 0.05% thimersol, 0.05% casein, and 0.1% bovine serum albumin, pH 7.0), 0.05 ml mouse serum (diluted 1:5 in assay buffer), 0.1 ml affinity purified osteocalcin antibodies (approximately 0.5 ng/well) in 8-well strips (Nunc, Rocksdile, Denmark) coated with anti-rabbit goat IgG (1 μg/ml) for 2 hours at 25°C. Strips were washed three times with 0.01M phosphate buffer (containing 0.05% Tween-20 and 0.15M sodium chloride) using an automated ELISA plate washer. A solution of peroxidase-streptavidin conjugate (Poly-HRP 40, Research Diagnostics Inc., Minneapolis, MN) (1:7000 dilution made in assay buffer) was added to all wells and strips were further incubated for 1 hour at 25°C. All strips were washed three times as described earlier, and 0.2 ml TMB substrate (One-Blue, Biotex Laboratories, Houston, TX) was added to all wells. After a brief incubation time (20 minutes), color reaction was stopped by the addition of 0.1 ml of 4 M sulfuric acid, and optical densities were recorded at 450 nm using a Tecan Spectra plate reader (Research Triangle Park, NC). Unknown values were calculated by using a four-parameter curve-fitting procedure. Analytical and clinical performance of the modified assay was identical with earlier mouse osteocalcin radioimmunoassay. The average within assay coefficient of variation (CV) was <10%; the average between-assay variation was CV<15%.

Skeletal Alkaline Phosphatase Assay

Alkaline phosphatase was measured in serum by the kinetic method[7] using p-nitro-

phenylphosphate (PNPP) as substrate. In the mouse, the major isoform of alkaline phosphatase (ALP) that may interfere in the serum measurements of sALP is the intestinal alkaline phosphatase. However, activity of this intestinal isoenzyme is more sensitive to inhibition by L-phenylalanine. By the addition of 15 mM L-phenylalanine, up to 90% of intestinal alkaline phosphatase can be inhibited without significantly affecting the skeletal isoenzyme activity. The L-phenylalanine inhibition assay exhibited intra-assay (n=10) and inter-assay (n=8) variation (CV) between 1.9% and 3.8%. The assay can detect <10 mU/ml of alkaline phosphatase in mouse serum.

Statistical Analysis

Comparison of markers between different groups was performed by the Mann-Whitney test, with $p<0.05$ (two-tailed) accepted as the significant difference. All bar diagrams represent mean values, and error bars represent standard error of mean. Power calculations to calculate the number of animals required for means of each group to be statistically significant was calculated by using statistical software (GraphPad Software, Inc., San Diego, CA). Rhythms of biochemical markers were analyzed by software for the analysis of biological rhythms using Non-Linear Multi-Oscillator Cosinor Modeling[26] (CirceSoft Inc., Waltham, MA). In this analysis, a predetermined period (24-hour) was fitted to cosine curves and their significance was evaluated by the least square method. The analysis yields three main parameters: mesor (arithmetic mean value of the fitted cosine curve), acrophase (occurrence of maxima in hours, which may not be at time where maximum concentration was observed), and amplitude (one half of the difference

between the highest and lowest point of the fitted cosine curve). Correlation coefficient constant and mean square error determines the goodness of the cosine curve.

Results

Circadian Variation

The serum levels of skeletal alkaline phosphatase, C-telopeptide, and osteocalcin in female and male C3H/HeJ mice, determined at 8 different time intervals spread over a 24-hour period, are shown in **Figures 1-6**. The rhythm parameters of C-telopeptide, osteocalcin, and skeletal alkaline phosphatase in male and female mice are summarized in **Tables 1- 3**.

Skeletal alkaline phosphatase activity showed little or no change during the 24-hour cycle, while C-telopeptide and osteocalcin exhibited a significant 24-hour rhythm. The C-telopeptide and osteocalcin levels demonstrated a peak concentration between 0900-1200 hours and a nadir between 1500-2400 hours (**Figures 1 & 2**). The peak C-telopeptide levels in female and male mice were 28-35% and 39-43% higher, respectively, compared to 24-hour mean values. The mesor and the amplitude for the fasting group of mice were slightly lower in both female and male mice; however, these differences were not statistically significant. The peak C-telopeptide levels in fasting and non-fasting male C3H mice (19.9±2.5 and 20.2±3.2 ng/ml, mean±SD) were significantly higher ($p<0.01$) as compared to that of the corresponding groups of female mice (13±1.3 and 14.8±1.1 ng/ml, mean±SD).

The highest and lowest concentrations of osteocalcin in both female and male mice (**Figures 3 & 4**) were observed at 9000 hours and 1500 hours, respectively. The peak osteocalcin concentrations in fasting and non-fasting female mice were 40% and 42% higher, respectively, than the 24-hour mean values. The peak concentrations in male fasting and non-fasting mice were 25% and 47%, higher respectively, than the 24-hour mean value. Although the effect of fasting on osteocalcin levels was more pronounced between 3000 hours and 1200 hours in both the fasting and non-fasting group (**Figures 3 & 4**). However, the differences in amplitude between fasting and non-fasting groups did not reach statistical significance (Table 2), perhaps due to a relatively large variation. Moreover, these differences were not consistent, and male and female groups showed contrasting effects. The peak osteocalcin concentration for fasting male (324±37.4 ng/ml, mean±SD) mice was significantly higher ($p<0.05$) than the fasting female (261.9±30.1 ng/ml, mean±SD) group. The difference between non-fasting male and corresponding female mice was not statistically significant.

The sALP activity showed little or no change during the 24-hour period (**Figures 5 & 6**). Only the non-fasting female group provided a significant cosine fit for circadian rhythm with correlation coefficient $r=0.62$ ($p>0.05$). In this group, the sALP levels were significantly higher for the 0900-hour samples ($p<0.05$) compared to all other time points. The other groups showed a poor fit (for frequencies of one as well as two cycles per day) with r-values <0.55 ($p>0.05$). In addition, the amplitudes of 24-hour

sALP activity were low (<4% of mesor) making it difficult to define peak (**Table 3**). These data indicated non-existence of a definite 24-hour rhythm in serum activity of sALP. Notably, fasting significantly reduced the sALP activity in the male group throughout the 24-hour period, as compared to the non-fasting male group. On the other hand, fasting had no significant effect on sALP levels of female mice.

Longitudinal variation

To assess the impact of sampling time on longitudinal and population variation in biochemical bone markers, we measured markers in serial blood samples collected from male and female groups of C3H mice at two different times of the day as described in the Methods section. Average day-to-day variations of all three markers studied are shown in **Figure 7**. The absolute concentrations of C-telopeptide and osteocalcin were 25-40% higher ($p<0.01$) in morning blood collection compared to afternoon samples, while sALP concentrations were similar. This was consistent with what was observed in the circadian variation study for these three markers. Day-to-day variation in C-telopeptide concentration over a period of 7 days, expressed as coefficient of variance (CV), was 15.3±2.6% (mean±SEM) and 9.5±1.5% (mean±SEM), respectively, for samples collected in the morning and in the afternoon. Day-to-day variations in C-telopeptide levels were most affected by the sampling time, showing significantly higher ($p<0.05$) longitudinal variation for samples collected in the morning compared to those collected in the afternoon. Average day-to-day variations in alkaline phosphatase and osteocalcin levels were 15% and 12%, respectively, and were not significantly affected by sampling time.

The day-to-day variations observed in this study suggest that, in an individual animal, about 40% change in biochemical marker levels will be required in response to a skeletal perturbation to be seen as a statistically significant change [reference change value = $1.96 \times \sqrt{2} \times \sqrt{(CV_i)^2+(CV_a)^2}$, where CV_i is day-to-day variation and CV_a is analytical variation].

Population Variation

Between-subject variations were calculated from samples collected on three different days, and mean value of population CV (from three days) is shown in **Figure 8**. The average between-subject (n=12) CV for C-telopeptide was 60% higher for morning blood collection as compared to afternoon samples ($p<0.05$). The differences in population CV of sALP and osteocalcin levels for morning and afternoon blood collection were statistically not significant.

Comparison of power of bone markers using test-of-significance calculations

In a rodent model, one of the important utilities of the data on biological variation of bone markers is to calculate sample size for experiments designed to achieve statistically significant difference between mean of (marker levels) two groups of animals. **Table 4** shows the approximate number of animals required for the mean of two groups to be significantly different, which is calculated from the biological variation obtained in this study. In addition, we also calculated the signal (to a skeletal perturbation) to noise (between-individual variance) ratio

using published[24] changes in markers in response to ovariectomy. The C-telopeptide levels were 48% higher in ovariectomized (OVX) mice[24] as compared to sham group of mice and the corresponding values for osteocalcin and sALP concentrations (unpublished observation) were 47% and 31% (higher values in OVX mice respectively, as compared to sham group of mice).

Because the C-telopeptide levels showed higher variance in blood samples collected between 0900-1200 hours, it follows that higher number of animals would be required in response to a skeletal perturbation to be seen as a statistically significant change when the samples were collected between 0900-1000 hours, as compared to samples collected between 1500-1600 hours. In case of sALP, the overall variance was low yet a higher number of animals would be required to detect a similar change in skeletal perturbation because the magnitude of change in sALP levels was smaller (31% vs 47% in C-telopeptide or osteocalcin) in response to OVX.

Discussion

To our knowledge, this is the first study to assess the circadian and longitudinal variation of blood-based biochemical markers of bone metabolism in the mouse model. The results of the present investigation showed that sALP activities were only marginally affected by diurnal variation, which was further evident from the low amplitudes of sALP activity in all groups of C3H mice, making it difficult to accurately determine the timing of peak activity. In contrast, the pattern of circadian variation of C-telopeptide and osteocalcin were clearly characterized by high concentrations during

0900-1200 hours and low concentrations during late afternoon or evening (1500-2100 hours). In terms of percent differences from 24-hour mean levels, the lowest and highest concentration varied between 67% to 110% for C-telopeptide and osteocalcin. Notably, the amplitude of osteocalcin rhythm was similar to that of C-telopeptide in C3H mice, which is in contrast to previously reported[3,18] studies in humans where osteocalcin and other formation markers have been shown to exhibit significantly less amplitude than the resorption markers. The C-telopeptide levels showed a sharp decline (25-30%) between 0900 hours and 1200 hours, whereas osteocalcin levels remained high until 1200 hours and then decreased sharply. This resulted in acrophase of C-telopeptide precede that of osteocalcin by approximately two hours. Further studies are needed to establish that the observed circadian changes in biochemical markers are unique to C3H mice or similar circadian pattern exists for the other strains of mice.

Food intake has been shown to affect diurnal rhythm of bone resorption[20,21] in rats. In this study, restricted food intake slightly reduced the amplitude of the C-telopeptide rhythm in both male and female C3H mice. The effect of fasting on osteocalcin levels was inconsistent between female and male groups. These findings were somewhat consistent with recent observations in humans where fasting appears to reduce the amplitude of the circadian rhythm in C-telopeptide levels[3], while it had no significant effect on osteocalcin levels. The reasons for the effect of fasting on circadian variations are currently unknown.

Circadian rhythmicity of bone marrow cells, hormones, and some enzymes that play important roles in bone formation and bone resorption have been demonstrated in earlier studies in rat model. Some of these studies, which used radiotracer kinetics to measure rate of bone formation and resorption, indicated that there was increased bone formation and resorption during the inactive (light) period[11,16,21,25] in rats. Our findings on circadian changes of C3H mice are similar to what has been reported in rats, thus suggesting that rhythmicity of biochemical markers may be regulated by similar mechanisms in rats and mice. The small differences in acrophase of C-telopeptide and osteocalcin may reflect differences in metabolic disposition of these two molecules rather than the bone formation or resorption activity of the bone tissue. Our findings demonstrated that the C-telopeptide and osteocalcin levels were relatively constant between afternoon and early morning periods, and the peak levels and the nadir of these markers were separated by only 3-6 hours. The sharp decline (of 25-30%) in bone markers between 0900 and 1500 hours was the most noteworthy difference between the diurnal rhythms of bone markers in mice and humans, where peak levels are separated from nadir by an approximate 12-hour period. We cannot rule out that time of peak and nadir (in the present investigation) are approximate, as blood samples or values are not available for every hour for the 24-hour period studied due to the study design and assay variations. It may be possible that longer collection intervals used in this study may flatten the changes between collections and may not detect the full amplitude. Nevertheless, the results of the present investigation agree with earlier reports on the diurnal rhythm in bone formation and resorption in the rodent model.

In the mouse model, significant variations in diurnal rhythmicity of several hormones and proteins have been reported in different strains of mice. Circadian variations in some steroids have been shown to exhibit contrasting rhythm parameters (such as acrophase) in different strains of mice. These differences in rhythm parameters in different strains are equated with the individual differences observed in the degree of circadian rhythmicity of biochemical markers in humans. In addition, circadian rhythms in different strains are partially affected by slight differences in sensitivity to some environmental stimulus, such as light, temperature or differences in internal capacity to respond with cyclic variation. Consequently, results of the present study must be interpreted carefully and may not be applicable to other strains of mice.

One of the most prevalent methods to minimize the effect of diurnal variation in bone markers is to collect blood samples at the same time of day, because circadian intra-individual variations for a number of metabolites is considered to be stable enough to be measured any time of day. However, no systematic studies have been performed in the mouse model to ascertain whether samples collected during a particular time of the 24-hour period can influence day-to-day or between-individual variation in bone markers. To explore the effect of time of blood collections on longitudinal and population variation in bone markers, we selected two time points, one in the late morning where all markers peaked and variation among markers was high. The other sampling time was in the afternoon when most markers show decreased concentrations. The within-individual day-to-day variation was higher in C-telopeptide

levels when measured in the morning blood collection. The sALP and osteocalcin day-to-day CVs were not significantly influenced by the time of blood collection. The between-individual CV data presented in this study, though limited by the number of animals used in this study, was significantly higher for C-telopeptide when samples were collected in the morning, while CV for sALP and osteocalcin were unaffected. It is not clear what causes higher day-to-day variation in C-telopeptide as compared to osteocalcin, which shows similar diurnal rhythmicity. In any case, biological variation data does allow for the setup of strictly controlled sampling protocols for minimizing the effect of biological variation for more accurate interpretation of bone marker measurement data.

The present investigation was designed to study biological variation of three bone markers using the same set of serum samples. In addition, we have earlier reported[24] the magnitude of change in bone markers in response to ovariectomy. Therefore, it was plausible to use the results of this study, in conjunction with earlier data on skeletal perturbation in the mouse model, to compare the effectiveness of each marker as a predictor of biological response for a given skeletal perturbation. A brief comparison of biological variance data of all three markers indicates that sALP measurement may offer some superiority over other markers because it showed the lowest analytical variation, and its concentrations appear to be least affected by diurnal variation. However, the day-to-day variation and population variances were not significantly different for the three assays when the samples were collected between 1500-1600 hours. Consequently, if we calculate the power of assay in view of change in marker

values in response to a skeletal perturbation, the C-telopeptide and osteocalcin were equally well or slightly superior to sALP. This indicates it is essential that both magnitude of change for each assay (to a given skeletal perturbation) and biological variance should be taken into account to determine if one marker is superior to the other bone turnover marker (**Table 4**).

In conclusion, our findings demonstrated significant diurnal variation that has a practical implication for bone marker measurements in the mouse model. In addition, the present study provides data on within-subject and between-subject variation in markers necessary for calculating the number of animals required for studies employing markers to detect changes in skeletal metabolism. Furthermore, findings from this study suggest that optimization of the sample collection period is critical for the valid use of biochemical marker data to reflect changes in bone metabolism.

Acknowledgment

This work was supported by Assistance Award No. DAMD17-99-1-9571. The U.S. Army Medical Research Acquisition Activity, 820 Chandler Street, Fort Detrick MD 21702-5014 is the awarding and administering acquisition office. The information contained in this publication does not necessarily reflect the position or the policy of the Government, and no official endorsement should be inferred.

References

1. Aardal, N.P., and Laerum, O.D. Circadian variation in mouse bone marrow. Exp Hematol 11(9): 792-801; 1983.

2. Beamer, W. G., Donahue, L. R., Rosen, C. J. and Baylink, D. J. Genetic variability in adult bone density among inbred strains of mice. Bone 18(5):397-403; 1996.

3. Christgau, S., Bitsch-Jenson, O., Bjarnason, N.H., Henriksen, E. G., Qvist, P., Alexandersen, P., and Henriksen, D.B. Serum Crosslaps for monitoring the response in individuals undergoing antiresorptive therapy. Bone 26(5): 505-511; 2000.

4. Clement, L. P., Ormandy, C., Lepescheux, L., Ammann, P., Damotte, D., Goffin, V., Bouchard, B., Amling, M., Gaillard, K. M., Binart, N., Baron, R. and Kelly, P. A. Osteoblasts are a new target for prolactin receptor knockout mice. Endocrinology 140(1):96-105; 1999.

5. Corral, D. A., Amling, M., Priemel, M., Loyar, E., Fuchs, S., Ducy, P., Baron, R. and Karsenty, G. Dissociation between bone resorption and bone formation in osteopenic transgenic mice. Proc Natl Acad Sci 95:13835-13840; 1998.

6. Ducy, P., Desbois, C., Boyce, B., Pinero, G., Story, B., Dunstan, C., Smith, E., Bonadio, J., Goldstein, S., Gundberg, C., Bradley, A. and Karsenty, G. Increased bone formation in osteocalcin-deficient mice. Nature 382(6590):448-52; 1996.

7. Farley, J.R., Hall, S.L., Herring, S., and Tarbaux, N.M. Two biochemical indices of mouse bone formation are increased, in vivo, in response to calcitonin. Calcif Tissue Int 50(1):67-73; 1992.

8. Gertz, B.J., Clemens, D.J., Holland, S.D., Yuan, W., and Greenspan S. Application of a new serum assay for type-I collagen cross-linked N-telopeptide: assessment of diurnal changes in bone turnover with and without Alendronate treatment. Calcif Tissue Int 63:102-106; 1998.

9. Hassager, C., Resteli, J., Resteli, L., Jensen, S. B., and Christiansen, C. Diurnal variation in serum markers of type I collagen synthesis and degradation in healthy premenopausal women. J Bone Miner Res 7 (11): 1307-1311; 1992.

10. Hugon, J.S., Charuel, Cl., and Laurendean, D. Circadian rhythm of alkaline phosphatase activity in the golgi zone of mouse duodenal enterocytes. Histochemie 35:263-272; 1973.

11. Igarashi, K., Miyoshi, K., Shinoda, H., Saeki, S., and Mitani, H. Diurnal variation in tooth movement in response to orthodontic force in rats. Am J Orthod Dentofacial Orthop 114 (1): 8-14; 1998.

12. Keating, R. J., and Tcholakian R. K. In vivo patterns of circulating steroids in adult male rats. I. Variations in testosterone during 24- and 48-hour standard and reverse light/dark cycles. Endocrinology 104(1):184-188; 1979.

13. Lucas L. A., and Eleftherlou B.E. Circadian variation in concentrations of testosterone in the plasma of male mice: a difference between Balb/c and C57BL/6By inbred strains. J Endocr 87: 37-46; 1980.

14. Nielsen H.K. Circadian and circatrigintan changes in osteoblast activity assessed by serum osteocalcin. Physiological and methodological aspects. Dan Med Bull 41(2): 216-227; 1994.

15. Nielsen, H. K., Brixen, K., and Mosekilde, L. Diurnal rhythm in serum activity of wheat-germ lectin-precipitable alkaline phosphatase: temporal relationships with the diurnal rhythm of serum osteocalcin. Scand J Clin Lab Invest 50(8): 851-856; 1990.

16. Ohtsuka, M., Saeki, S., Igarashi, K., and Shinoda H. Circadian rhythms in the incorporation and secretion of 3H-proline by odontoblasts in relation to incremental lines in rat dentine. J Dental Res 77(11):1889-95; 1998.

17. Saito, M., and Bray, G.A. Diurnal rhythm for corticosterone in obese (ob/ob) diabetes (db/db) and gold-thioglucose-induced obesity in mice. Endocrinology 113(6): 2181-2185; 1983.

18. Schlemmer, A., Hassager, C., Alexandersen, P., Fledelius, C., Pedersen, B. J., Kristensen, I. O., and Christiansen C. Circadian variation in bone resorption is not related to serum cortisol. Bone 21(1): 83-88; 1997.

19. Schlemmer, A., Hassager, C., Pedersen, B. J., and Christiansen C. Posture, age, menopause, and osteopenia do not influence the circadian variation in the urinary excretion of pyridinium crosslinks. J Bone & Miner Res 9: 1883-1888; 1994.

20. Simmons DJ, Nichols G. Diurnal periodicity in the metabolic activiuty of bone tissue. Am J Physiol 210: 411-418; 1966.

21. Shinoda H., and Seto H. Diurnal rhythms in calcium and phosphate metabolism in rodents and their relations to lighting and feeding schedules. Mineral & Electrolyte Metabolism 11(3):158-166; 1985.

22. Srivastava, A. K., Bhattacharyya, S., Castillo, G., Wergedal, J., Mohan, S. and Baylink, D. J. Development and application of a serum C-telopeptide and

osteocalcin assay to measure bone turnover in ovariectomized rat model. Calcif Tissue Int 60:435-442; 2000.

23. Srivastava, A. K., Castillo, G., Wergedal, J. E., Mohan, S. and Baylink, D. J. Development and application of a synthetic peptide-based osteocalcin assay for the measurement of bone formation in mouse serum. Calcif Tissue Int 66:2000 (In press).

24. Srivastava, A. K., Bhattacharyya, S., Castillo, G., N. Miyakoshi, Mohan, S. and Baylink, D. J. Development and evaluation of C-telopeptide enzyme-linked immunoassay for measurement of bone resorption in mouse serum. Bone 27(4): 2000 (In press).

25. Stevenson, S., Hunziker, E. B., Herrman, W., and Shenk R. K. Is longitudinal bone growth influenced by diurnal variation in the mitotic activity of chondrocytes of the growth plate. J Orthop Res 8 (1): 132-135; 1990.

26. Teicher, M.H., and Barber, N.I. COSIFIT: An interactive program for simultaneous multioscillator cosinor analysis of time-series data. Computers & Biomedical Research 23:283-295; 1990.

27. Wong C, Dohler K., Atkinson, M.J., Geerlings, H., Hesch, R., and Muhlen A.V,Z. Influence of age, strain, and season on diurnal periodicity of thyroid stimulating

hormone, thyroxine, triiodothyronine and parathyroid hormone in the serum of male laboratory rats. Acta Endocrinologica 102:377-385; 1983.

28. Yosipovitch G, Yosipovitch Z, Harell D, Ashkenazi I, and Erman A. Diurnal rhythm of postanoid secretion from bone/marrow organ in the rat. Bone 17(1): 79-83; 1995.

Table 1. Rhythm parameters of C-telopeptide

		Mesor (ng/ml)	Amplitude (ng/ml)	Acrophase (Hours)	Nadir/Peak (%)
Fasting	Female	10.5±0.6[a]	2.0±0.8[a,c]	0623[a]	67.3
	Male	14.2±0.8	3.8±1.2[c]	0613	75.3
Non-fasting	Female	10.3±0.7[b]	2.7±1.0[b]	0710[b]	105.4
	Male	14.7±1.0	5.0±1.4	0659	109.2

a= $p<0.02$ vs fasting male group, b= $p<0.02$ vs non-fasting male group, c= p=NS vs corresponding non-fasting group

Table 2. Rhythm parameters of osteocalcin

		Mesor (ng/ml)	Amplitude (ng/ml)	Acrophase (Hours)	Nadir/Peak (%)
Fasting	Female	184.3±10.7	49±15.7	0918	84.5
	Male	226.5±12.3	69.3±18.4[a]	0844	69.3
Non-fasting	Female	195.3±10.4	61.5±14.7	0839	80.8
	Male	188.2±15.6	38.3±19.2	0956	77

a= p=0.0700 vs non-fasting male group

Table 3. Rhythm parameters of skeletal alkaline phosphatase

		Mesor (U/L)	Amplitude (U/L)	Acrophase (Hours)	Nadir/Peak (%)
Fasting	Female[b]	272.6±7.12	8±6.9	2320	12
	Male[b]	245.8±3.3[a]	4.5±4.6	0408	14.1
Non-fasting	Female	264.7±5	8.4±5.7	1030	15
	Male[b]	277.1±3.4	8.5±5	1847	9.6

a= $p<0.001$ vs.. non-fasting male group, b= groups did not show a definite circadian rhythm

Table 4. Power calculations for biochemical markers for a given skeletal perturbation and biological variance

Biochemical marker	% Change in markers due to ovariectomy	Between-individual variance (CV)	Sample size#	Signal to noise ratio
C-telopeptide	47.8	20.6 (9-10 AM sample)	10	2.3
		12.9 (3-4 PM sample)	5	3.7
Osteocalcin	47.1	16.4 (9-10 AM sample)	7	2.9
		13.3 (3-4 PM sample)	5	3.5
Skeletal Alkaline Phosphatase	31.5	12.9 (9-10 AM sample)	10	2.4
		12.6 (3-4 PM sample)	10	2.5

#Sample size for means of two groups to be statistically different (for p-value less than 0.01, two-tailed)

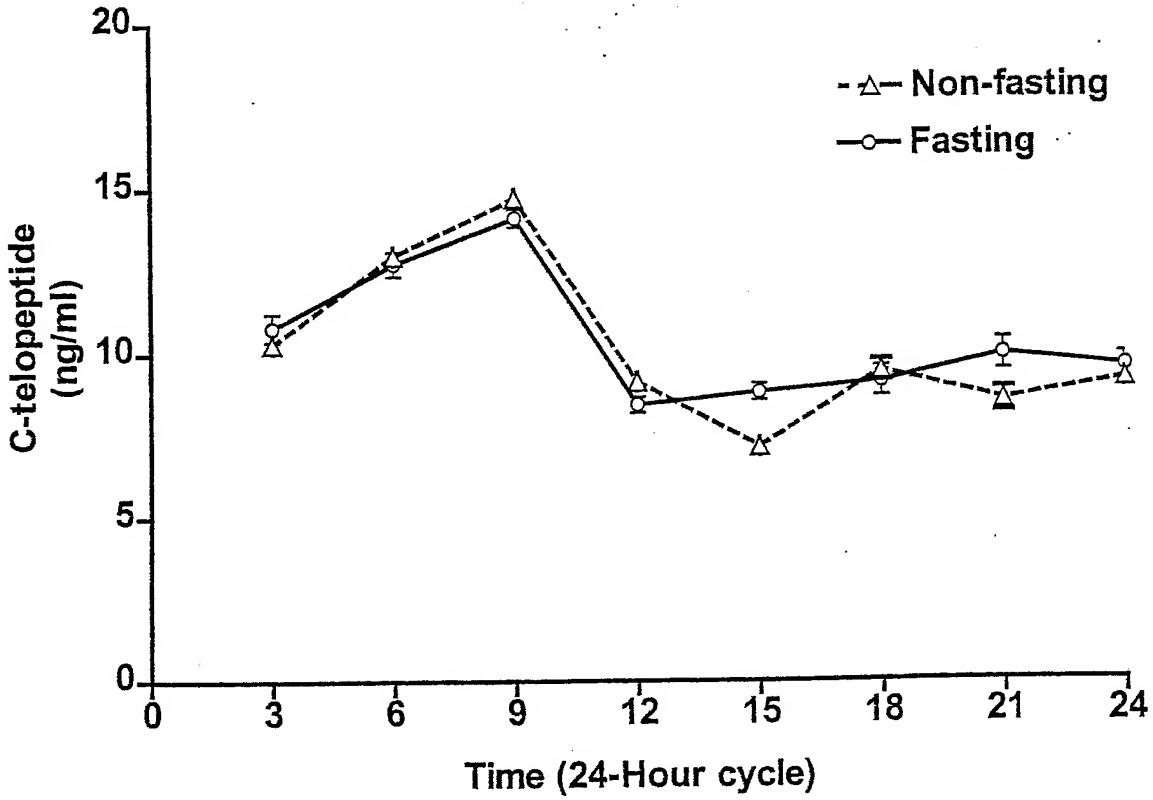
20
15
10
5
0
C-telopeptide (ng/ml)
Non-fasting
Fasting
0
3
6
9
12
15
18
21
24
Time (24-Hour cycle)

Figure 1

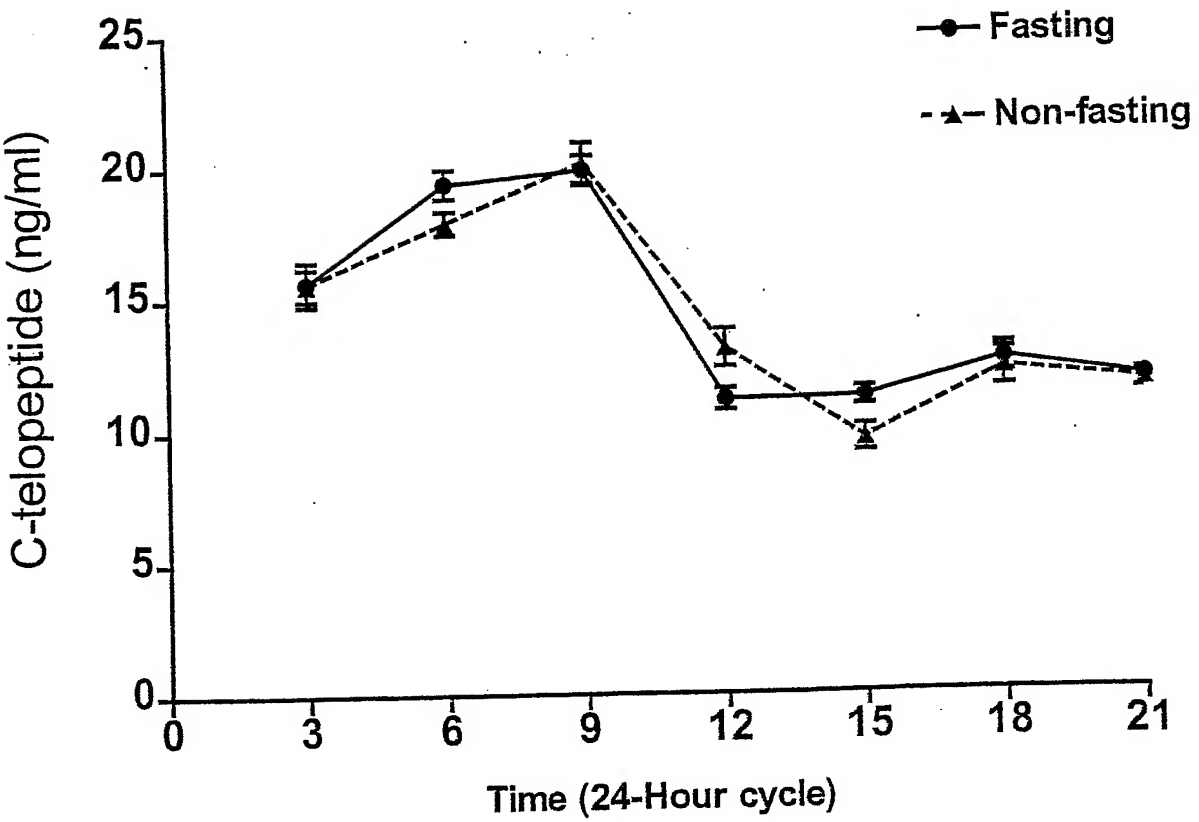
Fasting
Non-fasting
C-telopeptide (ng/ml)
25
20
15
10
5
0
0
3
6
9
12
15
18
21
Time (24-Hour cycle)

Figure 2

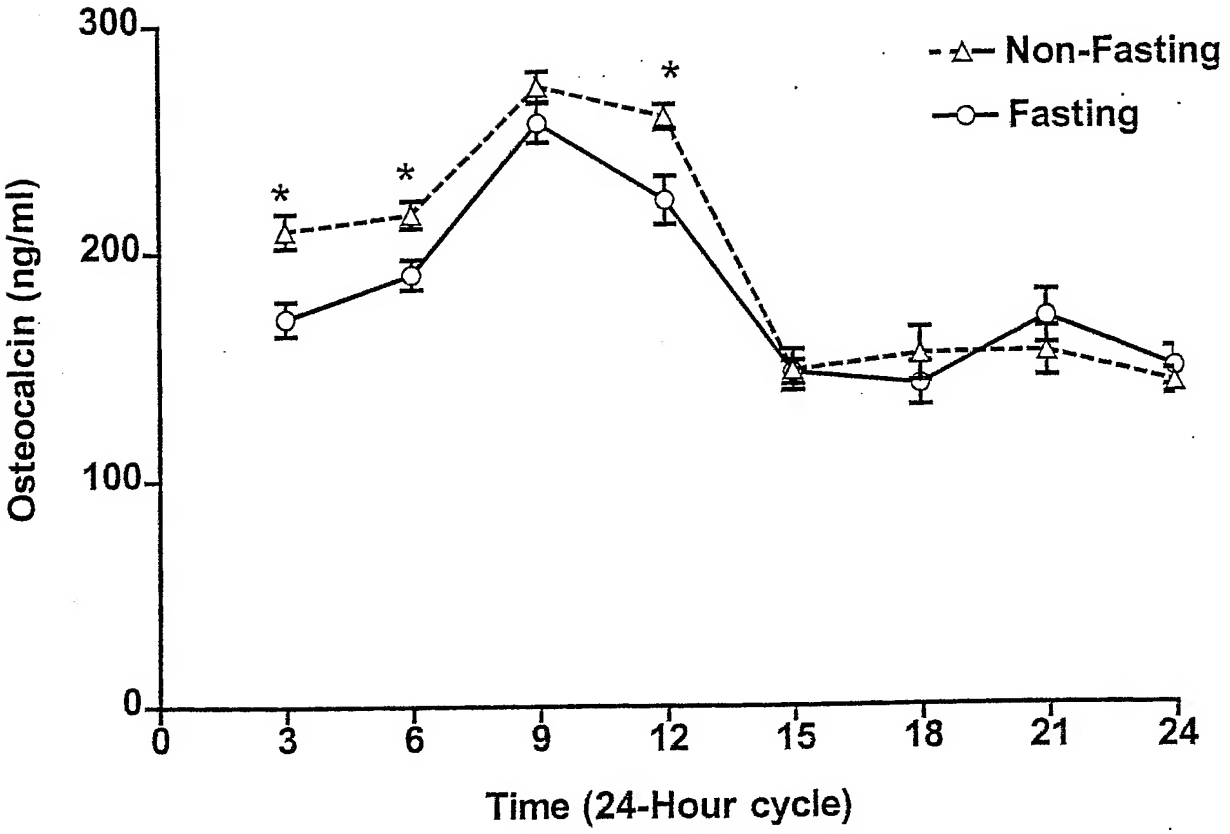
300
200
100
0
Osteocalcin (ng/ml)
Non-Fasting
Fasting
*
*
*
0
3
6
9
12
15
18
21
24
Time (24-Hour cycle)

Figure 3

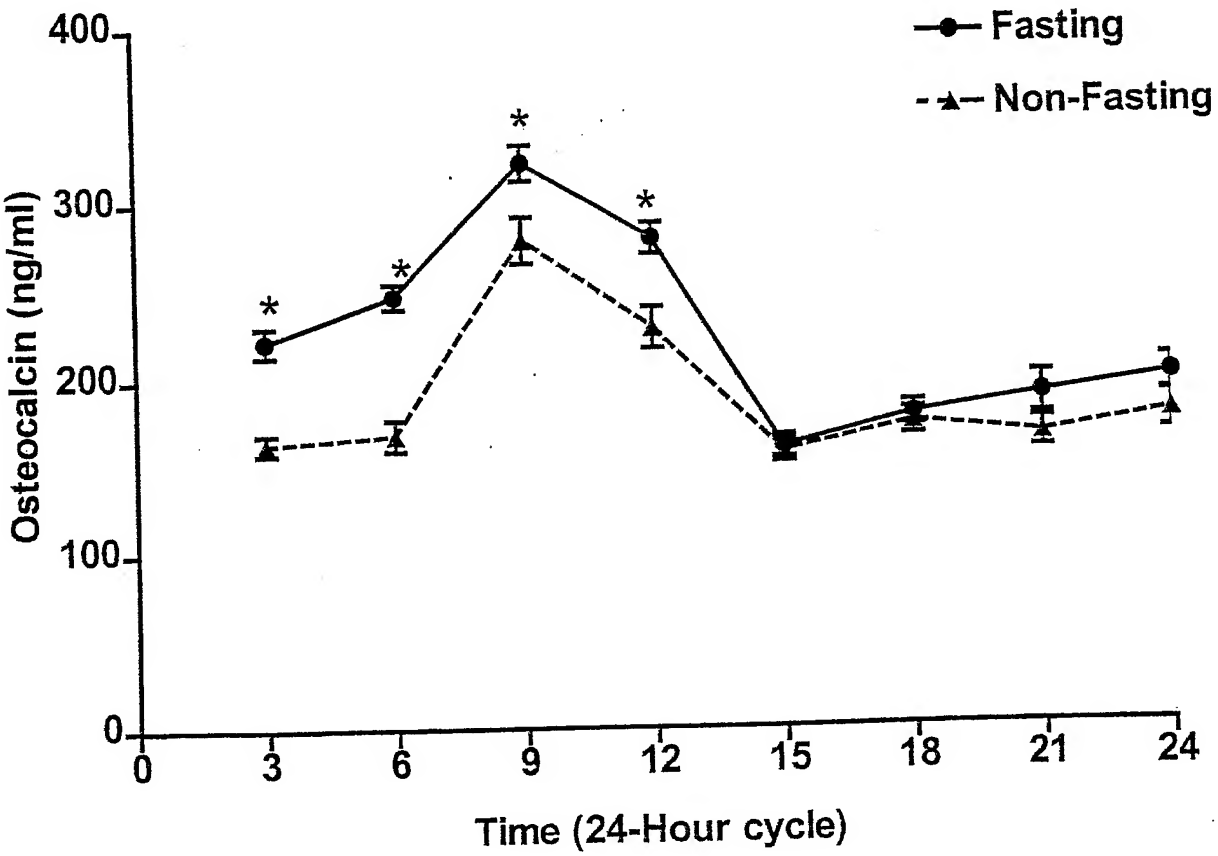
Fasting
Non-Fasting
Osteocalcin (ng/ml)
400
300
200
100
0
0
3
6
9
12
15
18
21
24
Time (24-Hour cycle)
*
*
*
*

Figure 4

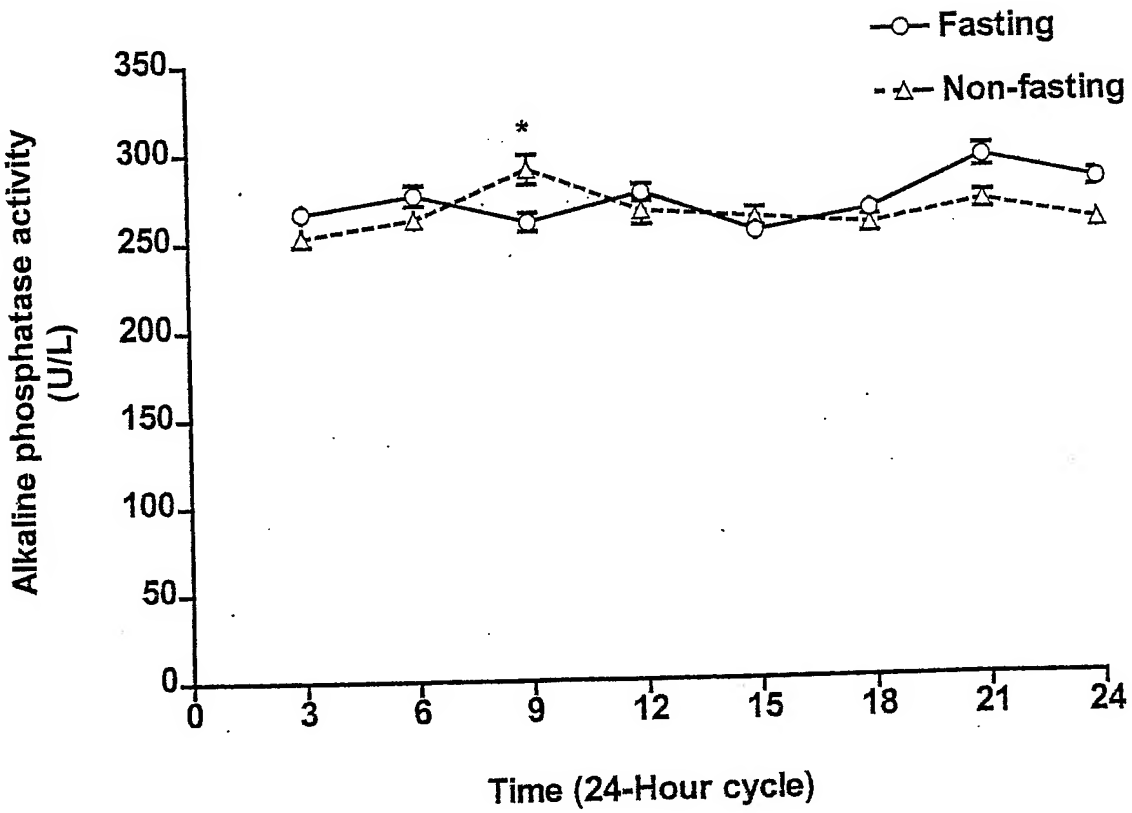
Fasting
Non-fasting
Alkaline phosphatase activity (U/L)
350
300
250
200
150
100
50
0
*
0
3
6
9
12
15
18
21
24
Time (24-Hour cycle)

Figure 5

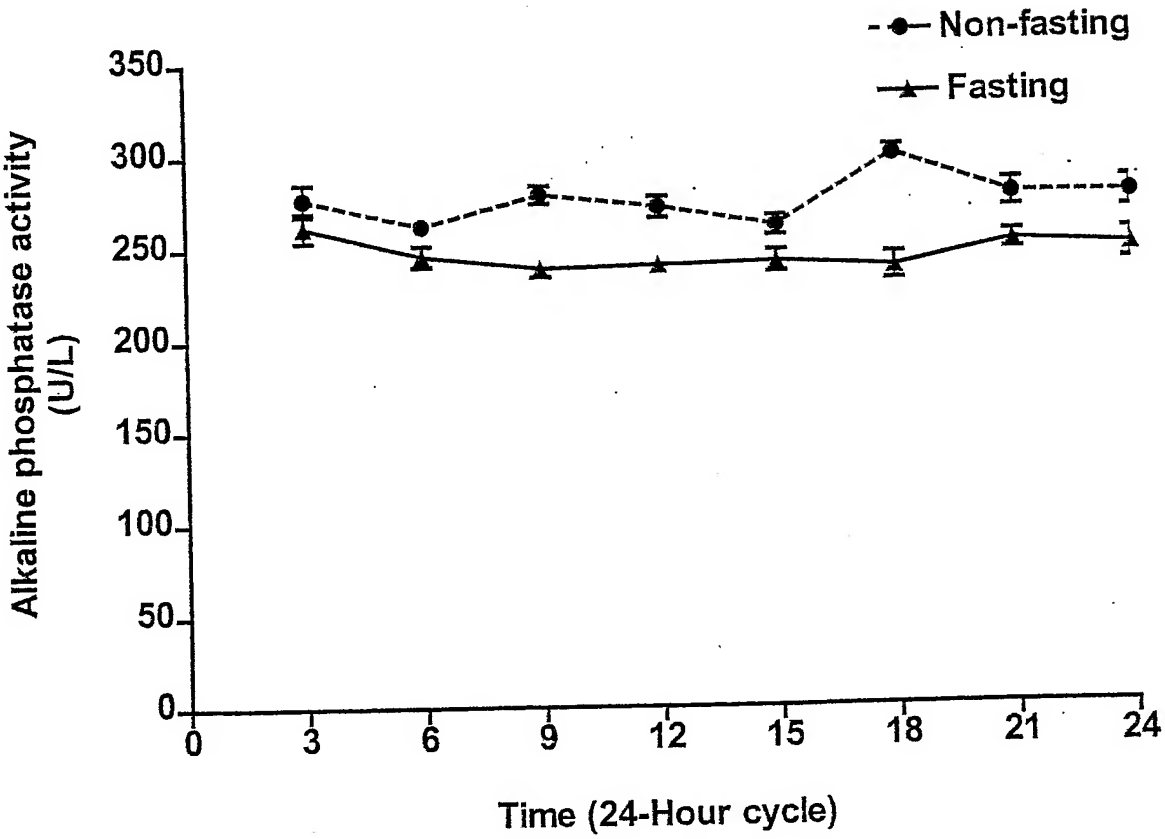
Non-fasting
Fasting
Alkaline phosphatase activity (U/L)
350
300
250
200
150
100
50
0
0
3
6
9
12
15
18
21
24
Time (24-Hour cycle)

Figure 6

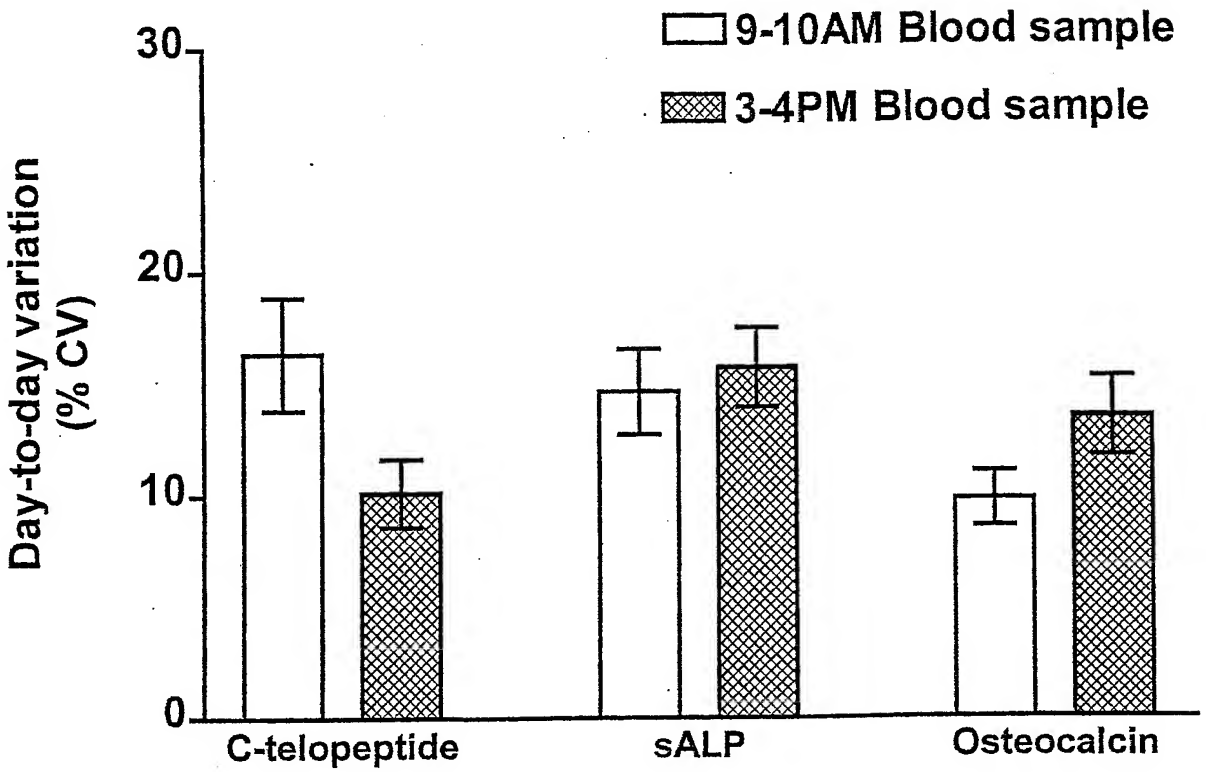
9-10AM Blood sample
3-4PM Blood sample
Day-to-day variation (% CV)
30
20
10
0
C-telopeptide
sALP
Osteocalcin

Figure 7

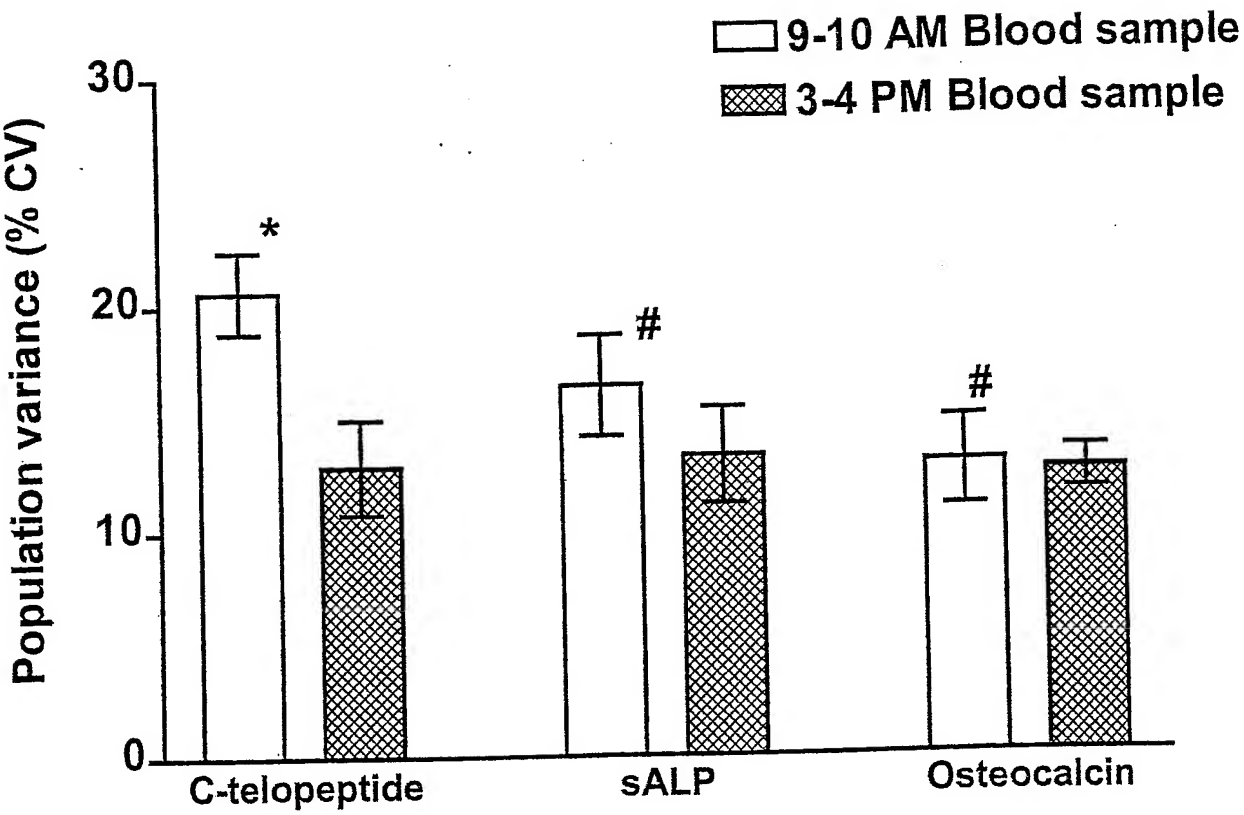
9-10 AM Blood sample
3-4 PM Blood sample
Population variance (% CV)
30
20
10
0
*
#
#
C-telopeptide
sALP
Osteocalcin

Figure 8

Legends

Figure 1. Circadian variation in serum C-telopeptide levels of fasting and non-fasting 6-week old female C3H/HeJ mice. Each data point represents mean±SEM (n=13-15). Both fasting and non-fasting groups showed significant circadian rhythm. The C-telopeptide levels at 0900 hours are significantly ($p<0.05$) higher than 0300, 1200-2400 hour samples by ANOVA.

Figure 2. Circadian variation in serum C-telopeptide levels of fasting and non-fasting 6-week old male C3H/HeJ mice. For details see Figure 3. The C-telopeptide levels at 0900 hours are significantly ($p<0.05$) higher than 0300, 1200-2400 hour samples by ANOVA.

Figure 3. Circadian variation in osteocalcin levels in 6-week old fasting and non-fasting female C3H/HeJ mice. Each data point represents mean±SEM of 13-15 mice. Both fasting and non-fasting groups showed significant circadian rhythm. The osteocalcin levels at 0900 and 1200 hours were significantly ($p<0.05$) higher than all other time points by ANOVA. *$p<0.05$ vs fasting group.

Figure 4. Circadian variation in osteocalcin levels in 6-week old fasting and non-fasting male C3H/HeJ mice. For details see Figure 5. The osteocalcin levels at 0900 and 1200 hours were significantly ($p<0.05$) higher than all other time points by ANOVA. *$p<0.05$ vs non-fasting group.

Figure 5. Circadian variation in serum skeletal alkaline phosphatase (sALP) activity of 6-week old female C3H/HeJ mice. Serum samples were collected at 3-hour intervals over a 24-hour period. In one part of the experiment, mice fasted for 12 hours before blood collection. Each data point represents mean±SEM of 15 mice and expressed in units/L. *$p<0.05$ vs than all other time points.

Figure 6. Circadian variation in serum skeletal alkaline phosphatase levels (sALP) of 6-week old male C3H/HeJ mice. For details see Figure 1. The sALP activity of the fasting group was significantly lower compared to that of the non-fasting group.

Figure 7. Day-to-day variation in bone markers calculated from three serial blood samples collected from 6 female and 6 male C3H/HeJ mice over a period of 7 days. In one study, samples were collected between 0900 – 1000 hours while in other study samples were collected between 1500 – 1600 hours. Each bar represents mean coefficient of variation (CV) of three samples from 12 mice (data from male and female mice were combined) and error bars represent standard error of mean (SE). The differences between morning (0900-1000 hours) and afternoon (1500-1800 hours) blood samples were not statistically significant.

Figure 8. Between-subject variation of bone markers in 6-week old male and female C3H/HeJ mice (n=12). Each bar represents mean of three measurements performed on samples collected at three different days (for details see Figure 7). *$p<0.05$, #p=NS.

M293

Comparison of an Automated C-Telopeptide Assay on the Elecsys 2010 with Six Serum and Urine Bone Resorption Markers in Microtiter Assay Format. E. T. Leary,[1] M. K. McLaughlin,*[1] D. Swezey,*[1] T. H. Carlson,*[1] A. P. Foster.*[2] [1]Pacific Biometrics, Inc., Seattle, WA, USA, [2]Roche Diagnostics Corporation, Indianapolis, IN, USA.

Degradation products of type I collagen have shown promise as bone resorption markers. Recently introduced resorption marker assays have primarily been microtiter plate-based. We evaluated a fully automated assay for C-terminal telopeptide (β -CrossLaps/serum; β -CTx) in serum on the Elecsys 2010 (Roche Diagnostics). Elecsys β -CTx assay results, which are based on the CrossLaps™ antibody (Osteometer BioTech A/S) and an electrochemiluminescence detection principle, were compared with six serum and urine bone resorption marker assays using paired urine and serum samples from 220 clinically documented individuals (62 healthy males, 42 premenopausal females, 41 postmenopausal females, 55 osteoporotics and 20 Paget's). The microtiter plate-based comparison assays were serum and urinary N-telopeptides (NTx; Osteomark® , Ostex International, Inc.), serum and urinary C-telopeptides (CTx, CrossLaps, Osteometer BioTech A/S) and urinary pyridinoline and deoxypyridinoline (PYD, DPD; Pyrilinks® and Pyrilinks-D® , Metra Biosystems).

The linearity of Elecsys β -CTx was demonstrated from 0.02 to 6.0 ng/mL. Intra-run CVs were 2.5%, 2.9% and 2.5% at 3.20, 0.82 and 0.13 ng/mL respectively. Among-run CVs (from 37 to 52 test runs over 3 months) using fresh frozen serum pools were 5.5% and 8.1% at 1.14 and 0.21 ng/mL respectively and 3.7%, 4.4 % and 14.9 % at 3.04, 0.79 and 0.12 ng/mL respectively using lyophilized controls. Similar recoveries were observed for 22 paired sets of serum, EDTA and heparinized plasma samples with values ranging from 0.03 and 3.5 ng/mL. Correlation coefficients (r) among the serum resorption markers based on all 220 patients ranged from 0.735 to 0.898. The r-values for serum and urine marker correlation ranged from 0.547 to 0.908. The correlations were lower between serum and urine markers, especially between telopeptides and pyridinium crosslinks in patient categories with lower marker concentrations. Ten of the urine samples (4.5%) were below the low-end detection limit of the urine CTx method, and one serum sample interfered with the serum CTx ELISA method.

In summary, the various marker assays differed in format and design, which impact laboratory performance and logistics. All the serum and urine resorption markers discriminated among the different patient categories, but they need to be further investigated for clinical utility. The fully automated β -CTx on the Elecsys analyzer was precise, convenient and robust, and is suitable for use in the routine laboratory.

Work supported by Roche Diagnostics Corporation.

M294

Assessment of Bone Resorption Marker Assays in Thoroughbred Horses. P. L. Kellerhouse,* C. Brown,* K. Newhall,* K. Judd,* D. Thompson. MRL, Merck Research Laboratories, Somerville, NJ, USA.

Commercial assays are available in human medicine which allow monitoring of bone resorption by the detection of collagen breakdown products in serum or urine. In clinical veterinary medicine there are few species specific assays to detect bone resorption but the conserved nature of these markers has led to their experimental use in animals.

A preliminary study was conducted in Thoroughbred horses to compare the assay Pyrilinks -D (Metra Biosystems, CA, USA) which detects urinary deoxypyridinoline (Dpd) with one which detects serum C-telopeptides (Ctx) serum (CrossLaps™, Osteometer Biotech, Denmark). Based on these results a second study was conducted to determine the effect on bone resorption as measured by serum Crosslaps assay when Thoroughbred horses were confined to complete stall rest.

The first study monitored collagen breakdown products in 12 horses over 56 days by taking concurrent weekly urine and serum samples which were processed and submitted for their respective assays. Urine was also assayed for creatinine, and Dpd was expressed as nM Dpd/mM creatinine to normalize urine for variations in concentration. A correlation coefficient of 0.4 was determined for the urine and serum levels of Dpd and Ctx respectively, with a p value of <0.001 indicating that there is a modest association between the two assays. Since it is much easier to obtain a timely serum sample than a urine specimen from a horse (and the serum assay does not require a creatinine correction) the Crosslaps assay offers some advantages in monitoring bone resorption in horses.

In the second study 12 adult Thoroughbred horses which had been at pasture for at least 3 months were placed on a minimal exercise program consisting of 15 minutes of lunging 5 days per week for 3 weeks. At that time baseline Ctx levels were determined (the mean of 3 samples taken from each horse) and the group was divided randomly into 6 horses which continued the exercise regiment and the other 6 which were confined to complete stall rest. Serum samples were collected over the next 42 days and submitted to the Crosslaps assay. The results demonstrated that Ctx levels rose to 45% above baseline level 7 days after stall rest and remained elevated for the duration of the experiment.

In conclusion, available commercial human assays for markers of bone resorption may be useful to monitor metabolic bone disorders in horses. The serum assay has some procedural advantages in specimen collection and does not require a creatinine test. Finally we have shown that serum bone resorption markers are elevated above baseline in horses which are confined to stall rest.

M295

Circadian Rhythms of Serum C-telopeptide, Osteocalcin, and Skeletal Alkaline Phosphatase in C3H/HeJ Mice. A. K. Srivastava, S. Bhattacharyya,* G. Castillo,* X. Li, D. J. Baylink. Musculoskeletal Disease Center, JL Pettis Memorial VAMC & Loma Linda University, Loma Linda, CA, USA.

The popularity of inbred strains of mice as an animal model has increased over the past several years, as evidenced by the fact that these animals are frequently used for genetic studies, for the production of transgenic and knockout mice, etc. In bone field, one of the most convenient endpoints for evaluating genetic, physiological or pharmaceutical perturbations is serum and urine biochemical markers. In order to apply such markers in an effective manner given the long-term biological variation in biochemical markers, it is of key importance to establish the appropriate sampling time. Because most markers undergo circadian rhythms, this study was undertaken to evaluate the circadian rhythm of three serum markers in mice. We compared changes in osteocalcin, C-telopeptide, and skeletal alkaline phosphatase (sALP) concentration over a 24-hour period in the C3H/HeJ (C3H) mice. Six-week-old female and male C3H mice were randomly divided into 8 groups of 15 mice each. Blood was collected at 3-hourly intervals, starting at 9:00 AM and continuing until 6:00 AM next day, with minimum disturbances in day/night light cycle. Serum osteocalcin and C-telopeptide levels were measured by an RIA and ELISA, respectively. Skeletal alkaline phosphatase was measured by a kinetic assay. Data were analyzed by non-linear regression analysis. Changes in biochemical markers over a 24-hour period were calculated as percent of 24-hour mean value and are shown in the figure (Mean± SD). The present investigation demonstrated significant circadian variations in osteocalcin and C-telopeptide levels with a peak value between 0900 and 1200 during daytime and a nadir between 2100 and 0300 at night. The amplitude of variation was between 20% to 25% of the 24-hour mean (mesor) value. The pattern of the circadian variation of C-telopeptide and osteocalcin was similar in female and male animals. The sALP levels were only marginally affected by the circadian rhythm. In conclusion, both C-telopeptide and osteocalcin levels follow a marked circadian rhythm in C3H/HeJ mice with the peak values an average of 25% higher than the 24-hour mean value. The results highlight the importance of the timing of sample collection for appropriate interpretation of the results.

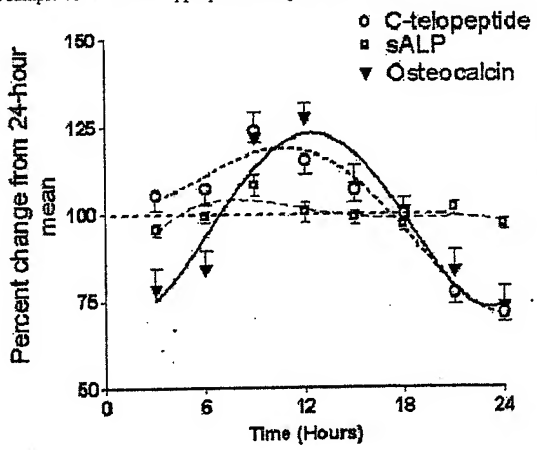

M296

Relationship between Calcaneal Stiffness Index and Hip Bone Density in Older Men and Women. M. G. Bemben,* D. A. Bemben, R. Munde,* S. Brickman.* Health and Sport Sciences, University of Oklahoma, Norman, OK, USA.

The purpose of this study was to examine the relationships between the stiffness index of the heel and bone mineral density (BMD) of the hip sites in men (n=41) and women (n=52), 60-70 years of age. Subjects were not excluded for estrogen or other anti-resorptive drug use. None of the subjects had a history of hip fracture. BMD of the left proximal femur (neck, Ward's area, trochanter, total hip) was measured using DXA (Lunar DPX-IQ, version 4.1). The Achilles+ Ultrasonometer (Lunar Corporation) was used to obtain the stiffness index of the left os calcis. There were no significant (p>.05) gender differences in stiffness index (Men 87±3; Women 81±2). The hip BMD sites were similar for men and women, except for the trochanter which was significantly higher (p<.01) for men (.839±.023 g/cm^2 vs. .743±.017 g/cm^2). Based on the WHO criteria, 79% of the women and 76% of the men were osteopenic, whereas only 2% of the women and 10% of the men were osteoporotic. There were significant differences in stiffness index based on bone status for both men and women with stiffness index decreasing from the normal (107±5 men; 91±6 women) to osteopenic (85±3 men; 79±2 women) categories. Stiffness index showed moderate positive relationships with the hip BMD sites in men and it was a significant predictor of femoral neck BMD. In women, correlations between stiffness index and hip BMD sites were lower than those observed in men. Although stiffness index was a significant

Gender	Stiffness vs. Neck BMD	Stiffness vs. Ward's Area BMD	Stiffness vs. Trochanter BMD	Stiffness vs. Total Hip BMD
Men	r=.58**	r=.51**	r=.62**	r=.63**
Women	r=.44**	r=.47**	r=.50**	r=.49**

**p<.01